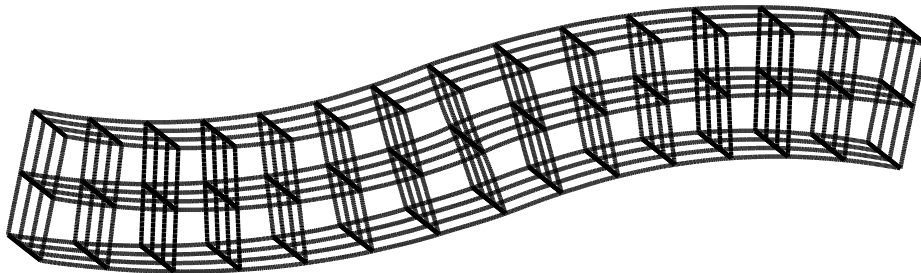


Fast multiscale methods for lattice equations

Per-Gunnar Martinsson



*Doctoral thesis written under the supervision of Professors Ivo Babuška and Gregory Rodin.
Approved by the committee members, Professors Jerry Bona, Mark Mear and J. Tinsley Oden on June 12th, 2002.
Texas Institute for Computational and Applied Mathematics, The University of Texas at Austin.*

ABSTRACT

The thesis concerns multi-scale analysis of equations defined on very large lattices. A new method for model reduction that allows the resolution scale to vary with spatial position is presented. It leads to fast numerical implementations and comes with strict error bounds. This is obtained by incorporating the averaging of the micro-structure directly into a solver that is based on hierarchical data structures, such as the Fast Multipole Method. For boundary value problems, a lattice analogue of the boundary element method is used.

Homogenized equations of arbitrary order are derived and strict error bounds are proved. For mechanical lattice structures, special attention is paid to the question of non-degeneracy and whether rotational degrees of freedom should be incorporated. A computer program that automatically derives the homogenized equations was developed. For any lattice geometry, the lattice Green's function is determined and its asymptotic expansion in rational poly-harmonic functions is derived.

The presented results have applications in many areas of physics and engineering but particular attention is paid to how they can be used to design composite materials with high stiffness-to-weight ratios and prescribed wave-propagation modes. In particular, it is shown how to design materials that have phononic bandgaps, in other words, they block mechanical waves of certain frequencies.

THANKS

Ivo Babuška and Greg Rodin have gone far beyond the call of duty as thesis advisors. The thesis could certainly not have been written without them and I sometimes doubt whether the other vicissitudes of graduate school would have been overcome either.

Jerry Bona has throughout my years at UT-Austin been generous with his time and offered advice on mathematics and the workings of the academy. His most valuable contribution to the present work was in telling me, with very little ambiguity indeed, what he thought of my attempt at a thesis proposal.

Vidar Thomée supervised my *licentiate* thesis. Much of what I know about PDEs, numerical methods and the art of mathematical writing, I have learnt from him.

Mark Mear and Tinsley Oden have, as committee members, given me valuable advice.

Alex Movchan contributed greatly to the investigation of dynamic properties of lattices. He has also been most helpful during my job-search during the last year.

Stefan Sauter has been involved with the lattice project all along. He developed some of the notation used and inspired many of the results presented.

Jonathan Priluck at Jonathan Aerospace Materials Corporation in Massachusetts has been very supportive throughout and once hosted me on a very inspirational visit.

Lorna Gibson, Benqui Guo, Mike Marder, Valdimir Rokhlin, Jinchao Xu and many others have shared their knowledge and provided valuable insights.

Holly I owe more than I can describe. Although she is infinitely more precious to me than the LaTeX file I am currently editing, this has for the last year been much less obvious than I could have wished.

Mom and Dad, I owe them everything.

Johan Ivarsson, Jonas Larsson, Mats Larsson and Martin Nilsson have remained close friends during the numerous years I have spent as a student. Their support and inspiration have been, and continue to be, very important to me.

Patience Henson, Levi Larkey and Joel Tropp have shared my office and hence the joys and frustrations of grad school. I would not have traded them for anything.

Contents

Chapter 1. Introduction	1
1. Lattice equations	1
2. Applications of lattice models	2
3. Mathematical analysis of multiscale problems and lattice equations	5
4. Computational techniques for multiscale problems	6
5. A chapter by chapter description of the presented results	7
Chapter 2. Basic properties of static lattice equations	13
1. Introduction	13
2. Preliminaries	14
3. Fourier analysis	19
4. Well-posedness of the lattice equations	25
Chapter 3. Homogenization	29
1. Introduction	29
2. Scaled lattices and function spaces	30
3. Projection operators	31
4. Homogenization of conduction problems on mono-atomic lattices	33
5. Homogenization of conduction problems on multi-atomic lattices	40
6. Homogenization of mechanical lattices	43
Chapter 4. The lattice Green's function	45
1. Introduction	45
2. Mono-atomic lattices in three dimensions	46
3. Mono-atomic lattices in dimensions other than three	48
4. Multi-atomic lattices	50
5. A numerical example	52
Chapter 5. Fast summation methods for poly-harmonic kernels	55
1. Introduction	55
2. Multipole expansions of poly-harmonic functions	56
3. Convergence of the new multipole expansions	60
4. Numerical experiments	63
Chapter 6. Boundary equation methods for problems on finite domains	65
1. Introduction	65
2. Indirect formulations of the Dirichlet problem	65

CONTENTS

3. Inclusions	67
4. Partial summation and direct formulations	68
5. Conditioning of the boundary equations	70
Chapter 7. Vibrations of lattices and acoustic bandgaps	77
1. Introduction.	77
2. Two examples of mechanical lattices	82
3. Periodic structures of general geometry	86
4. Designing lattices with prescribed bandgaps	89
5. Conclusions	91
Chapter 8. Concluding remarks	93
Appendix A. The stiffness matrix of a slender beam	95
Appendix B. Examples of lattices	97
1. Introduction	97
2. Simple square and cubic lattices	97
3. Body-centered lattices	100
4. Triangular and hexagonal lattices	102
Appendix C. A derivation of the multipole expansion of a poly-harmonic function using Laurent series	107
Appendix D. Numerical evaluation of the lattice Green's function	109
Appendix E. Notes on Chapter 7	111
1. Derivation of the second dispersion equation in section 1.2	111
2. Derivation of the stiffness matrix for a square framed structure	112
Bibliography	115
Vita	119

CHAPTER 1

Introduction

1. Lattice equations

A lattice equation relates an unknown function defined on an integer lattice (either \mathbb{Z}^d or a subset thereof) to some given data function. Such equations occur naturally in the study of atomic crystals and materials with periodic micro-structures. They also appear when continuum problems are discretized using regular meshes. In this thesis, we present new mathematical results regarding the asymptotic behavior of such lattice equations as the lattice cell size tends to zero. Using these results, we construct a numerical method for solving lattice equations that has a much better asymptotic work estimate than previously known methods. The existence of such a method will dramatically increase the range of lattice problems that can be solved using brute force. Finally, we discuss how problems outside this range can be handled using model reduction techniques based on local averaging.

In this introductory chapter, we describe in Section 2 some applications where lattice models arise. In Section 3 we describe the new mathematical results regarding stability and asymptotic behavior of lattice equations and put them in context. In Section 4 we do the same thing for the new numerical methods. Finally, in Section 5 we summarize the results of each subsequent chapter individually. Before proceeding to the more detailed descriptions of the new results and their relation to the existing literature, we will introduce some main concepts in an informal manner by discussing a concrete example.

Consider the mechanical structure in Figure 1.1. It is loaded by a known external load and we are given the task of determining the deflections and stresses in the structure. Using classical techniques of structural mechanics, we can form a system of linear equations that relate the nodal deflections, \mathbf{u} , to the applied load \mathbf{f} . Upon labeling the nodes using integer coordinates so that $\mathbf{u} = \mathbf{u}(m)$ and $\mathbf{f} = \mathbf{f}(m)$ for $m \in \mathbb{Z}^2$, this system takes the form

$$(1.1) \quad \begin{cases} [\mathfrak{A}\mathbf{u}](m) = \mathbf{f}(m), & \forall m \in \Omega, \\ [\partial_\nu \mathbf{u}](m) = 0, & \forall m \in \Gamma_N, \\ \mathbf{u}(m) = 0, & \forall m \in \Gamma_D, \end{cases}$$

where $\Omega \subset \mathbb{Z}^2$ is the set of interior nodes and $\Gamma_N, \Gamma_D \subset \mathbb{Z}^2$ are sets containing the boundary nodes at which Neumann and Dirichlet data are pre-scribed. The operator \mathfrak{A} is a finite difference operator that qualitatively behaves very much like a good discretization of the partial differential operator that governs linear (continuum) elasticity. Known solution techniques for such problems can roughly be organized into three distinct categories, depending on the number of nodes, N .

Brute force solution: If N is not too large, then fast numerical methods such as FFT or multigrid can be used to solve equation (1.1) in $O(N)$ operations.

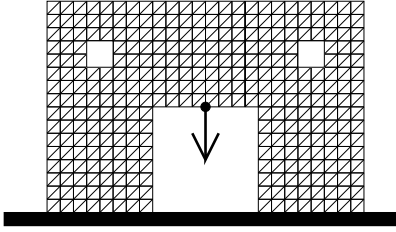


FIGURE 1.1. A loaded mechanical structure.

Homogenization: If N is very large (or equivalently, if the size of the micro-structure is much smaller than the macro-structure) then it is possible to average out the contributions of the microstructure and replace equation (1.1) by an analogous partial differential equation with constant coefficients. This continuum equation can then be solved using, *e.g.*, a finite element method. Unless the domain is very regular and the load is smooth, a large modelling error may be incurred.

Multiscale methods: These methods were developed for situations where N is so large that brute force calculations are impossible and local irregularities prohibit the use of homogenization. By representing \mathbf{u} and \mathbf{f} in some wavelet basis the resolution scale can change with spatial position. In such a basis, \mathfrak{A} can be approximated by a sparse matrix and then an iterative solver is used to solve (1.1) in $O(n)$ operations, where n is the number of coefficients needed to represent \mathbf{u} and \mathbf{f} .

In this thesis, we present a brute force method that can solve (1.1) using roughly $O(N_B + N_F)$ operations, where N_B is the number of nodes at which boundary conditions are specified and N_F is the number of nodes that are externally loaded (note that N_F is typically very small and that $N_B \sim N^{1/2}$ in two dimensions and $N_B \sim N^{2/3}$ in three dimensions). In order to achieve this, (1.1) is reformulated as a discrete boundary equation which can then be solved with iterative methods using a fast summation technique for lattice sums that is based on the Fast Multipole Method by Rokhlin and Greengard. Furthermore, we argue that the new method can be extended to a multiscale method that solves (1.1) using $O(n_F + n_B)$ operations, where n_F and n_B are the number of coefficients required to capture the body load and a (fictitious) boundary potential in a hierarchical data representation.

2. Applications of lattice models

Of the many areas where lattice models appear naturally, we will focus on two.

Mechanics of structures and composites: The connection between lattice models and the mechanics of solids dates back at least to Navier, who derived continuum governing equations by considering a solid as an aggregate of a vast number of atoms connected by linear springs, see Timoshenko [63]. Later, Hrennikoff [36] and McHenry [44] turned the tables and showed how to obtain an approximate solution of the equations of elasticity by replacing the continuum structure by an artificial spring-mass system (with cell-sizes several orders of magnitudes larger than the atomic scale). These investigations later led to the development of the finite difference and finite element methods. The lattice method of discretizing continuum media is still used to investigate crack propagation since it provides a clean way of avoiding the problem of singular stress concentrations present in continuum models, Grah *et al* [30].

Lattice models are particularly useful for modeling structures that can in a natural fashion be viewed as periodic arrays of structural elements with some simple interaction mechanism. Examples include large truss systems, Noor [50], honeycombs and materials with periodically distributed inclusions, Gibson and Ashby [27], as illustrated in Figure 1.2. For a recent survey on the use of lattice models in mechanics, see Ostoja-Starzewski [52].

Much of the literature in this field concerns methods for deriving equivalent continuum models for lattice structures. This is usually done by first postulating that the continuum model should be a PDE of a given form, then a periodic boundary value problem is solved on the unit cell, the energy is computed and coefficients are identified to ensure that the energy is the same in the lattice structure as for the continuum model (this Ansatz is sometimes referred to as the *Cauchy-Born* postulate). In this thesis, we present an analytical framework that obviates the need to postulate a continuum model in advance. Given any lattice geometry and any node-to-node interaction mechanism (*e.g.* axial springs, Euler beams, Timoschenko beams), a continuum model can automatically be determined through a limit process that is systematic enough that it can be carried out by symbolic algebra software (Maple subroutines are provided). The user can specify the desired level of accuracy/complexity so that, *e.g.*, a square frame structure such as the one illustrated in Figure 1.1, can yield either a classical elasticity model (simple, less accurate) or a full micro-polar model (complicated, more accurate). This is discussed in Chapter 3 and specific examples are given in Appendix B.

Very recently, lattice models have received substantial attention as the primary modeling tool in the study of a new class of ultra light weight materials with a truss-like micro-structure called *lattice materials*, illustrated to the left in Figure 1.2, see Evans, Hutchinson and Ashby [22], Wallace and Gibson [67], Deshpande, Fleck and Ashby [16], Wicks and Hutchinson [69] and Thompson and Renaud [62]. These materials are attractive alternatives to fiber composites since they offer more design flexibility and may be cheaper to manufacture. An important engineering problem is to determine the local stresses and displacements in a piece of lattice material that is subjected to an external load. The challenge lies in that the piece of material may contain a very large number of structural members, easily in the billions, so that the micro-structure cannot be fully resolved numerically; but due to the presence of boundaries, inclusions and concentrated loads, classical averaging methods do not work. We present new numerical algorithms that are ideally suited for such problems since they can selectively resolve exactly those length-scales needed.

Using emerging manufacturing methods (*e.g.* sand casting, injection moulding, solid free-form fabrication), lattice materials can be manufactured out of several base materials (metals, plastic, rubber) and a wide spectrum of micro-structural geometries can be realized. This opens up the possibility of tailoring materials that fit very specific design criteria. As an example, we will demonstrate how materials can be designed that block mechanical waves in certain frequency intervals, see Chapter 7. The methods presented there can equally well be used to design materials with high resistance to micro-buckling.

Physics of atomic crystals: Lattice models very naturally appear in the study of atomic crystals and much effort has been spent determining properties of the lattice Green's function (defined as the solution of (1.1) when \mathbf{f} is a point load) with the purpose of gaining understanding about, among other things, imperfections and inclusions in the lattice, see Maradudin [42], Economou [21], Glasser [29] and Joyce [39].

In this thesis, we construct the asymptotic expansion of the lattice Green's function for an arbitrary lattice. The construction is again fully automated so that once a lattice geometry has been specified, symbolic algebra software can be used to compute the expansions. We have verified the process by checking that the results are in agreement with expansions that have been computed for specific lattice geometries by Duffin [19, 20] and Cserti [15]. We found in this investigation that the (matrix-valued) Green's function for any multi-atomic lattice can be determined by computing the asymptotic expansion of the Green's function for an associated (fictitious) mono-atomic lattice. For instance, the Green's function for the honeycomb lattice labeled D in Figure 1.3 has essentially the same expansion as its associated lattice, which is lattice C rotated 30° .

Lattice models have recently been used to quantitatively study dynamic magnetization of very small ferro-magnets, an application with immediate relevance to the design of magnetic storage devices such as hard-drives, Fidler and Schrefl [23]. Here the nodes in the lattice model represent clusters of roundabouts $10 \times 10 \times 10$ atoms in a ferro-magnetic crystal (by clustering, quantum mechanical effects can be neglected). The governing equation, the Landau-Lifshitz-Gilbert equation, involves a term representing interactions between the magnetization vector of a node and the field generated by all the other nodes. Evaluation of this term typically constitutes the most expensive part of a numerical calculation. We believe that the fast summation methods presented here can very advantageously be used to speed up these calculations. Some results using early incarnations of the Fast Multipole Method are given by Brown *et al* [12].



FIGURE 1.2. Structures naturally modeled as periodic lattices.

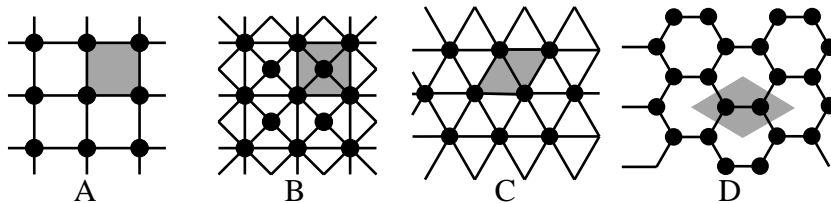


FIGURE 1.3. Examples of lattices. An irreducible unit cell is shaded.

3. Mathematical analysis of multiscale problems and lattice equations

A strict mathematical theory for how to derive averaged, or *homogenized*, equations for a media with micro-structure was developed in the sixties and seventies by Bensoussan, Lions, Papanicolaou [6] and others. Among the rich literature on the subject, we will mention only work that more or less directly relates to our investigation. For a general reference to homogenization in relation to composite media, see Sánchez and Palencia, [57]. More specifically, Cioranescu and Vanninathan treat the case of homogenization of low-porosity, periodic structures similar to ours in [13]. Homogenization of networks was considered by Vogelius [66] and Bonnetier [9].

In this thesis we derive the homogenized equations for lattice problems associated with any lattice geometry and several local models (conduction problems, mechanical truss and frame structures). As described in section 2, this derivation can be fully automated. First we consider conduction problems and prove convergence of the lattice equations to the homogenized equation as the lattice cell size tends to zero. The results cover homogenizations of arbitrary order on infinite domains. Usually, high-order models do not receive much attention due to the severe regularity requirements they come with but we study them here for the specific purpose that they help understanding the fast numerical methods that we present. Our analysis is based on Fourier transforms and was inspired by earlier work by Babuška and Morgan [5, 46, 47, 48].

The homogenization results are then extended to cover two mechanical models, a “truss” model where the bars are considered as axial springs that are pin-jointed at the nodes and a “frame” model where the bars are considered to be general elastic objects that are rigidly connected at the nodes. Truss problems are more difficult than conduction problems in that the lattice equation loses coercivity for many lattice geometries (such as geometries A and D in Figure 1.3). We resolve this question by giving a computable condition that can be used to prove that a given lattice structure is non-degenerate. This condition is considerably weaker than other conditions given in the literature, *cf.* [52]. For the frame model, such degeneracy is not an issue (connectivity is a sufficient requirement on the lattice geometry), but in this case, both translational and rotational degrees of freedom must be incorporated in the model. These variables enter the homogenized equations in fundamentally different ways and we demonstrate that the influence of a torque load decays faster than a linear force load. The results presented can be used to quantitatively determine whether a micro-polar or a classical elasticity model is better suited for a particular application.

We also provide some new mathematical results regarding asymptotic expansions of Green’s functions. These results extend earlier work on the cubic lattices by Duffin [19, 20] to general lattices in two and three dimensions. Casting the analysis in a modern framework of tempered distributions, we obtain formulas that are systematic enough that any asymptotic expansion can be computed using symbolic algebra software.

For multi-atomic lattices, we demonstrate that by a simple algebraic procedure, it is possible to construct an associated (fictitious) mono-atomic lattice with the property that to lowest order, it has the same homogenized equation as the original lattice (for mechanical frame structures, this is true only in the absence of torque loads). Moreover, the asymptotic expansion of the lattice Green’s function for a multi-atomic lattice is given as a small perturbation of the asymptotic expansion of the Green’s function for the associated mono-atomic lattice.

4. Computational techniques for multiscale problems

For many problems, the micro-structure can be fully resolved in a brute force computation using fast algorithms such as FFT or multigrid for which the computational cost scales linearly with the problem size. As an example, Jinchao Xu and co-workers at Penn State have recently developed a multigrid algorithm capable of solving problems on mechanical structures with up to ten million structural elements. For problems where there is a clear separation of length-scales and the geometry is benign, the averaging methods described earlier can be used to remove the micro-scale entirely. This reduces the problem to that of solving a partial differential equation with constant (or slowly varying) coefficients. Hybrid methods that use averaging in certain parts of the domain, resolve the micro-structure in problem regions (such as corners and crack-tips) and then paste the models together are commonly used. Recent work combining this idea with adaptivity and à posteriori error estimation is described by Oden and Vemaganti [51]. Another approach based on combining local and global computations with error estimation is given by Hou *et al* [35].

The investigation underlying this thesis was strongly influenced by the recent development of numerical methods based on multiresolution (wavelet) techniques by Beylkin, Coifman, Rokhlin and others [3, 7, 10], Engquist and co-workers [1, 17] and Gilbert [28]. The advantage of using multiresolution bases to represent the relevant data is that functions can be represented with different frequency resolution in different parts of the spatial domain. In other words, the micro-structure can be fully resolved in certain regions, very coarsely averaged in others, and resolved at a number of intermediate resolution depths in between. A fundamental observation underlying the work mentioned above is that if the bases are selected appropriately, then in the new coordinate system, the operator \mathfrak{A} is numerically very close to a sparse operator, which means that iterative methods may be employed to solve the equilibrium equation. The remaining difficulty is that \mathfrak{A} is typically very poorly conditioned, but the authors show that in many situations, good preconditioners are available.

The methods presented here share with the wavelet methods the basic goal of allowing the resolution depth to change with spatial position, dependent upon the local regularity of the solutions that should be represented. The main difference is that our methods represent functions using multipole moments rather than wavelets. It is then possible to use a variation of the Fast Multipole Method by Rokhlin and Greengard [31, 32] to very quickly compute convolutions of the form $\mathfrak{G} * \mathfrak{f}$ where \mathfrak{G} is the lattice Green's function and \mathfrak{f} is a load vector. This straight-forwardly provides a solution method for equation (1.1) for the case that $\Omega = \mathbb{Z}^d$ since in this case $\mathbf{u} = \mathfrak{G} * \mathfrak{f}$. When boundary conditions are present, the convolution is used to determine a particular solution to take care of the body load, then a boundary equation with \mathfrak{G} as the kernel is used to account for the finite domain. The boundary equations that we present are well-conditioned and since we know how to compute $\mathfrak{G} * \mathfrak{f}$ fast, an iterative solver can be used to determine the solution. The relative merit of this multipole algorithm as compared with the multiresolution algorithms described above has not yet been assessed but we believe that it will be competitive due to increased stability gained by approximating \mathfrak{A}^{-1} rather than \mathfrak{A} , and better ability to handle complicated domains.

Note that even without the use of local averaging, the new numerical method represents an improvement upon earlier solvers in that unloaded internal loads are completely eliminated from the computation. This reduces the computational cost from $O(N)$, where N is the total number of nodes, to $O(N_F + N_B)$, where N_F is the number of loaded internal nodes and N_B is the number of nodes at which boundary conditions are prescribed.

We present the following technical results that are needed to realize the new method:

- We show how to determine a rational poly-harmonic function G_P that approximates \mathfrak{G} at long distances. Specifically, $\mathfrak{G}(m) = G_P(m) + O(|m|^{-2P-d})$, see Chapter 4.
- We extend the FMM to cover poly-harmonic kernels to obtain a fast method for computing the convolution $G_P * \mathfrak{f}$, see Chapter 5.
- We derive well-conditioned discrete equivalents of boundary integral equations with single and double layer potentials, see Chapter 6.

The function G_P is actually the fundamental solution of the $O(\varepsilon^{2P+2})$ homogenized equation. Thus, one can view the fast algorithm that we present as a stable method to use high order homogenized equations without enforcing global regularity requirements.

5. A chapter by chapter description of the presented results

The findings of the thesis could be presented in different styles, and with different emphases, depending on the targeted audience. For the most part, we have chosen a presentation that is aimed at applied mathematicians interested in continuum and multiscale problems. Chapters 2, 3 and 4 in particular, rely on advanced tools of mathematical analysis. Chapters 5 and 6 are aimed at numerical analysts and assume familiarity with the fast multipole and boundary element methods. Chapter 7 is aimed at researchers in applied areas and does not contain advanced mathematics.

Chapter 2 — *Basic properties of static lattice equations:* In this chapter we set up a mathematical framework for analysis of general lattice problems. We prove that under (very weak) regularity requirements on the lattice geometry, the operator \mathfrak{A} satisfies certain coercivity properties. The analysis gets somewhat involved since the operator frequently has a non-trivial nullset. For instance, for mechanical problems, the rigid body motions should not cause any internal stresses in a structure. Once the coercivity results have been established, we apply them to prove well-posedness and stability for the equation (1.1).

We will illustrate some of the analysis presented in Chapter 2 by showing how it applies to heat conduction on the cubic lattice \mathbb{Z}^3 , a model that has been studied extensively in the literature [14, 15, 19, 29, 39, 42, 53]. Each node is connected to its six closest neighbors by links of conductivity 1. Let $\mathbf{u}(m)$ denote the temperature of node $m \in \mathbb{Z}^3$ and let $\mathfrak{f}(m)$ denote an external heat source. In equilibrium, these are related by

$$(1.2) \quad [\mathfrak{A}\mathbf{u}](m) = \mathfrak{f}(m), \quad \forall m \in \mathbb{Z}^3,$$

where

$$(1.3) \quad \begin{aligned} [\mathfrak{A}\mathbf{u}](m) = & \left[-\mathbf{u}(m_1 - 1, m_2, m_3) + 2\mathbf{u}(m_1, m_2, m_3) - \mathbf{u}(m_1 + 1, m_2, m_3) \right. \\ & - \mathbf{u}(m_1, m_2 - 1, m_3) + 2\mathbf{u}(m_1, m_2, m_3) - \mathbf{u}(m_1, m_2 + 1, m_3) \\ & \left. - \mathbf{u}(m_1, m_2, m_3 - 1) + 2\mathbf{u}(m_1, m_2, m_3) - \mathbf{u}(m_1, m_2, m_3 + 1) \right]. \end{aligned}$$

Since (1.2) is a convolution equation it can be diagonalized by the discrete Fourier transform,

$$(1.4) \quad \tilde{\mathbf{u}}(\xi) = [\mathfrak{F}\mathbf{u}](\xi) := \sum_{m \in \mathbb{Z}^3} e^{im \cdot \xi} \mathbf{u}(m), \quad \text{for } \xi \in (-\pi, \pi)^3 =: I^3.$$

Applying this transform to both sides of (1.2) we obtain

$$\sigma(\xi)\tilde{\mathbf{u}}(\xi) = \tilde{\mathfrak{f}}(\xi), \quad \forall \xi \in I^3$$

where $\sigma(\xi)$ is the Fourier representation, or *symbol*, of \mathfrak{A} ,

$$\sigma(\xi) = \mathfrak{F} \mathfrak{A} \mathfrak{F}^{-1} = \sum_{j=1}^3 (-e^{i\xi_j} + 2 - e^{-i\xi_j}) = \sum_{j=1}^3 4 \sin^2 \frac{\xi_j}{2}.$$

Applying the Fourier inversion formula we easily obtain a representation for the solution of (1.2),

$$(1.5) \quad \mathbf{u}(m) = \mathfrak{F}^{-1} \left[[\sigma]^{-1} \tilde{\mathbf{f}} \right] (m) = \frac{1}{(2\pi)^3} \int_{I^3} e^{-im \cdot \xi} [\sigma(\xi)]^{-1} \tilde{\mathbf{f}}(\xi) d\xi.$$

The Fourier transform \mathfrak{F} is an isometric isomorphism from $l^2(\mathbb{Z}^3)$ to $L^2(I^3)$ that maps the convolution operator \mathfrak{A} to the multiplicative operator σ . This means that when we seek to prove that \mathfrak{A} satisfies some property, it is sufficient (and usually easier) to prove that σ satisfies that property. For instance, we trivially see that \mathfrak{A} is self-adjoint since σ is real and that $\|\mathfrak{A}\|_{l^2} = (2\pi)^{-3} \sup_{\xi} |\sigma(\xi)| = 3/(2\pi^3)$. Coercivity is a more delicate question; since a constant temperature field does not cause internal flows, it follows that $\sigma(0) = 0$ and that σ^{-1} is unbounded near the origin. Therefore, the stability results that we give rely only on the bounds $\sigma(\xi) \geq c|\xi|^2$ and $|\sigma(\xi)^{-1}| \leq C|\xi|^{-2}$. The real difficulty enters the picture when we consider multi-atomic lattices since then σ is a matrix. A central result of Chapter 2 is a proof that $\det \sigma(\xi) \geq c|\xi|^2$ if and only if a lattice is connected. This fact leads to the remarkable result that all entries of $\sigma^{-1}(\xi)$ have the same singularity at the origin, in other words, there exist a constant c_0 and a positive definite matrix M such that $[\sigma(\xi)^{-1}]_{ij} = c_0(\xi \cdot M\xi)^{-1} + O(|\xi|^{-1})$. These results concerning the singular structure of $\sigma(\xi)^{-1}$ at the origin underlie most subsequent results presented in Chapters 3 and 4.

We will also consider two different models for mechanical lattices. Any mechanical lattice can be modeled as a system of beams with both bending and axial stiffnesses that are rigidly connected at the nodes, a so called “frame” model. However, this is quite a complicated model that involves keeping track of both translational and rotational degrees of freedom. It is therefore useful to consider a simplified model, the “truss” model, in which the bending stiffness is neglected (for a slender element, it is much lower than the axial stiffness) and the links are treated as axial springs that are pin-jointed at the nodes, a model that requires us to handle translational variables only. Such a model works well for lattice geometries like B and C in Figure 1.3 but does not work at all for the geometries A and D. Mathematically, we will prove that for the frame model, connectivity implies that $\det \sigma(\xi) \geq c|\xi|^{2d}$, where d is the dimension, that $|\sigma(\xi)^{-1}| \leq C|\xi|^{-2}$ and that all *blocks* of $\sigma(\xi)^{-1}$ have the same leading order singularity at the origin. For the truss model, we will show that the same results hold true for geometries that satisfy a certain non-degeneracy condition (devised to rule out geometries such as A and D).

Chapter 3 — Homogenization: In this chapter, we will show that when the lattice cell size tends to zero, then the solution to the lattice equation (1.1) approaches the solution of a constant coefficient differential equation. We illustrate the concept by using the simple cubic lattice considered in the previous subsection. When the lattice cell size is ε , we let $\mathbf{u}^{(\varepsilon)}$ and $\mathbf{f}^{(\varepsilon)}$ denote the temperature and the load, and introduce a scaled Fourier transform,

$$\tilde{\mathbf{u}}^{(\varepsilon)}(\xi) = [\mathfrak{F}_{\varepsilon} \mathbf{u}^{(\varepsilon)}](\xi) = \varepsilon^3 \sum_{m \in \mathbb{Z}^3} e^{i(\varepsilon m) \cdot \xi} \mathbf{u}^{(\varepsilon)}(m), \quad \text{and} \quad \mathbf{u}^{(\varepsilon)}(m) = \frac{1}{(2\pi)^3} \int_{I_{\varepsilon}^3} e^{-i(\varepsilon m) \cdot \xi} \tilde{\mathbf{u}}^{(\varepsilon)}(\xi) d\xi.$$

The scaled symbol, $\sigma^{(\varepsilon)}$, takes the form

$$\sigma^{(\varepsilon)}(\xi) = \frac{1}{\varepsilon^2} \left(4 \sin^2 \frac{\varepsilon \xi}{2} + 4 \sin^2 \frac{\varepsilon \xi}{2} + 4 \sin^2 \frac{\varepsilon \xi}{2} \right).$$

As $\varepsilon \rightarrow 0$ we see that $\sigma^{(\varepsilon)}(\xi) \rightarrow |\xi|^2$. Thus, if the sequence of loads $\{\mathfrak{f}^{(\varepsilon)}\}_\varepsilon$ has the property that

$$(1.6) \quad \tilde{\mathfrak{f}}^{(\varepsilon)}(\xi) \rightarrow \hat{f}(\xi) := \int_{\mathbb{R}^3} e^{i\mathbf{x} \cdot \xi} f(x) dx,$$

then we find that formally, as $\varepsilon \rightarrow 0$ and $m \rightarrow \infty$ in such a way that $\varepsilon m \equiv x$,

$$\mathbf{u}^{(\varepsilon)}(m) = \frac{1}{(2\pi)^3} \int_{I_\varepsilon^3} e^{-i(\varepsilon m) \cdot \xi} \frac{\tilde{\mathfrak{f}}^{(\varepsilon)}(\xi)}{\sigma^{(\varepsilon)}(\xi)} d\xi \rightarrow \frac{1}{(2\pi)^3} \int_{\mathbb{R}^3} e^{-i\mathbf{x} \cdot \xi} \frac{\hat{f}(\xi)}{|\xi|^2} d\xi =: u^{(0)}(x),$$

where $u^{(0)}$ solves Poisson's equation

$$(1.7) \quad -\Delta u^{(0)} = f, \quad \text{on } \mathbb{R}^3.$$

The operator \mathfrak{A} is in fact a well-known discretization of the Laplace operator and in the numerical analysis literature, it is well-established that if f is sufficiently regular, then $\mathbf{u} = u^{(0)} + O(\varepsilon^2)$. It is also known how to construct difference operators that approximate (1.7) to an arbitrary degree of accuracy. Here, we are interested in going in the opposite direction: Given a difference operator, how can a series of *continuum* equations with increasing order of approximation be constructed? The answer is given by the series expansion of the singularity of $\sigma^{(\varepsilon)}(\xi)^{-1}$. Thus, using that

$$(1.8) \quad \left[\sigma^{(\varepsilon)}(\xi) \right]^{-1} = \frac{1}{|\xi|^2} + \varepsilon^2 \frac{1}{12} \frac{\xi_1^4 + \xi_2^4 + \xi_3^4}{|\xi|^4} + \varepsilon^2 O(|\varepsilon \xi|^2),$$

we can write down a high order averaged, or "homogenized", equation

$$(1.9) \quad (-\Delta)^2 u^{(\varepsilon,1)} = (-\Delta) f + \varepsilon^2 \frac{1}{12} \left(\frac{\partial^4 f}{\partial \xi_1^4} + \frac{\partial^4 f}{\partial \xi_2^4} + \frac{\partial^4 f}{\partial \xi_3^4} \right).$$

If f is (very) regular, then $u^{(\varepsilon,1)}$ will be an $O(\varepsilon^4)$ approximation of $\mathbf{u}^{(\varepsilon)}$.

In Chapter 3 we construct homogenized equations of arbitrary order of accuracy for conduction problems on any lattice geometry, either mono- or multi-atomic. We prove convergence in both pointwise and Sobolev norms and consider scalar conduction problems as well as mechanical lattices of both frame and truss type. A technical difficulty in this analysis is how, given a load f , to construct a sequence $\mathfrak{f}^{(\varepsilon)}$ such that $\tilde{\mathfrak{f}}^{(\varepsilon)}(\xi) = \hat{f}(\xi) + O(|\varepsilon \xi|^p)$ for some integer p . In this, we were much guided by prior work by Babuška [4] and Fix and Strang [24, 25].

Chapter 4 — Lattice Green's functions: Recall that the solution of the basic lattice equation (1.2) is given by $\mathbf{u} = \mathfrak{F}^{-1}[\sigma^{-1} \tilde{\mathfrak{f}}]$. Since multiplication in Fourier space corresponds to convolution in physical space, we can rewrite the representation as $\mathbf{u} = \mathfrak{F}^{-1}[\sigma^{-1}] * \mathfrak{f}$. Thus, setting

$$(1.10) \quad \mathfrak{G}(m) := [\mathfrak{F}^{-1} \sigma^{-1}](m) = \frac{1}{(2\pi)^3} \int_{I^3} e^{-im \cdot \xi} \sigma(\xi)^{-1} d\xi,$$

we obtain a representation for the solution in physical space as follows

$$\mathbf{u}^{(\varepsilon)}(m) = [\mathfrak{G} * \mathfrak{f}](m) = \sum_{n \in \mathbb{Z}^3} \mathfrak{G}(m - n) \mathfrak{f}(n).$$

In Chapter 4 we derive Green's functions of this form for a wide category of lattice problems and study the asymptotic behavior of $\mathfrak{G}(m)$ as $|m| \rightarrow \infty$. It turns out that the long-range character of \mathfrak{G} is entirely determined by the $O(|\xi|^{-2})$ singularity of $\sigma(\xi)^{-1}$ at the origin (to see this, note that the integrand in the Fourier integral (1.10) is analytic away from the origin, which means that those parts of the integral decay faster than any inverse polynomial). Using again the cubic lattice as an illustration, our analysis will show that, *cf.* (1.8)

$$\mathfrak{G}(m) = \mathcal{F}^{-1} \left[\frac{1}{|\xi|^2} \right] (m) + \mathcal{F}^{-1} \left[\frac{1}{12} \frac{\xi_1^4 + \xi_2^4 + \xi_3^4}{|\xi|^4} \right] (m) + O(|m|^{-5}).$$

Here, the inverse continuous Fourier transform is defined by

$$[\mathcal{F}^{-1}\varphi](x) = \frac{1}{(2\pi)^3} \int_{\mathbb{R}^3} e^{-ix \cdot \xi} \varphi(\xi) d\xi,$$

for $\varphi \in L^1$, and then extended to tempered distributions in the standard fashion (see Chapter 4 for details). Evaluating the Fourier transforms, we find that

$$(1.11) \quad \mathfrak{G}(m) = \frac{1}{4\pi|m|} + \frac{1}{48\pi} \frac{m_1^4 + m_2^4 + m_3^4 - 3m_1^2m_2^2 - 3m_2^2m_3^2 - 3m_3^2m_1^2}{|m|^7} + O(|m|^{-5}).$$

Note that to lowest order, $\mathfrak{G}(m)$ behaves like the fundamental solution of $-\Delta$, and, not unexpectedly, the two rational terms together form the fundamental solution of (1.9) for $\varepsilon = 1$. More generally, we will for conduction problems on any lattice with a lattice Green's function \mathfrak{G} and any positive integer P , derive a rational function G_P such that $|\mathfrak{G}(m) - G_P(m)| \leq C|m|^{-(2P+d)}$, where $C = C(P)$. These functions will be poly-harmonic, $(-\Delta)^{P+1}G_P(x) = 0$, for $x \neq 0$. Some explicit examples are given in Appendix B.

Early work on lattice Green's functions using Fourier methods was performed by McCrea and Whipple [43] and Watson [68]. Much work has been spent determining exact values of the integral (1.10). Some results that are useful for small m are given for simple lattice models by Joyce and co-workers [37, 38, 39], Glasser and Boersma [29] and others. The asymptotic behavior was touched upon by McCrea and Whipple [43], and later elaborated by Duffin [19] and Duffin and Shelly [20] who derived the expansion (1.11) and the corresponding expansion for two-dimensional cubic lattices. Since then, the first few terms of the asymptotic expansions of the lattice Green's functions for a number of common lattices have been derived, see Cserti [15] and references therein.

Chapter 5 — Fast summation methods: In this chapter we present fast methods for evaluation of convolution sums of the form

$$(1.12) \quad u(m) := \sum_{n \in \Omega} \mathfrak{G}(m-n)q_n,$$

where \mathfrak{G} is the lattice Green's function. If the kernel in the sum had been the standard harmonic kernel $\Phi(m) = -(4\pi|m|)^{-1}$ (in two dimensions, $\Phi(m) = -(2\pi)^{-1} \log|m|$), then a fast method would have been provided by the Fast Multipole Method (FMM) by Rokhlin and Greengard, [31, 32]. For the present case, we first replace \mathfrak{G} by the poly-harmonic approximation G_P when evaluating the long-range interactions. Then an extended version of the FMM is used to compute a convolution with G_P as the kernel. To obtain this extension, we have determined:

- (1) How to expand a poly-harmonic function in a multipole expansions.
- (2) How to shift the origin in the new expansions.

(3) How to bound the truncation error.

The first of these items has previously been solved by Vekua [64, 65], Sobolev, [61], and Kounchev [41]. We derive the representation in a different fashion, essentially by “culling” a Taylor expansion of the kernel. We doubt that this idea is new, but we have not found it in the literature. It leads to general statements about a wide class of kernels (in particular, non-isotropic problems are treated as easily as isotropic) and it greatly simplifies the derivation of the shift formalæ in item (2).

Chapter 6 — *Boundary equation methods for problems on finite domains:* In this chapter we demonstrate that the summation methods derived in Chapter 5 can be used to obtain fast solvers for lattice equations on finite domains. The results presented extend to lattice problems a set of techniques for continuous boundary value problems that have been derived by Rokhlin [56], Hackbusch [33], McLean [45] and others. In order to illustrate the main concepts we will show how they apply to a homogeneous Dirichlet problem,

$$(1.13) \quad \begin{cases} -\Delta u = 0, & \text{on } \Omega, \\ u = g, & \text{on } \Gamma = \partial\Omega. \end{cases}$$

The idea is to look for a solution in the form of a double layer potential

$$(1.14) \quad u(x) = \int_{\Gamma} \frac{\partial G(x-y)}{\partial \nu_y} \phi(y) dy,$$

where ν_y is the outward normal of Γ at y , and ϕ is some unknown potential. By investigating the limit of (1.14) as $x \rightarrow \Gamma$, it can be shown that ϕ satisfies a second kind Fredholm equation,

$$(1.15) \quad -\frac{1}{2}\phi(x) - \int_{\Gamma} \frac{\partial G}{\partial n_y}(x-y)\phi(y) dy = g(x). \quad \forall x \in \Gamma.$$

For many boundaries Γ , the integral operator is compact. It is then possible to discretise (1.15) in such a way that the resulting matrix is well conditioned and therefore, an iterative solver will converge very fast. The difficulty of this approach is that each step of the iteration requires a matrix-vector multiplication which could potentially be very expensive since the matrix is in this case dense. This problem has been overcome by the development of fast solvers by Rokhlin [8, 56], Hackbusch [33] and others. The method that results by combining a good boundary integral formulation with a fast summation method is very fast indeed, see Helsing and Peters [34] and Fu, Rodin and Overfelt [26].

In order to solve discrete boundary value problems with the methods described, we derived discrete analogues of both single and double layer boundary integral equations valid for general lattices. The derivation is an analogue of what is known as a “direct” method in the classical theory but we also show for a special case how a discrete Green’s identity can be derived and used for an “indirect” derivation of the boundary equations. We demonstrate how to handle cases where inclusions and voids in the lattice destroy the periodicity of the equilibrium operator. We prove that the new boundary equations are non-singular, and demonstrate through several numerical examples that the condition numbers are typically small, especially for the double layer formulation.

When an iterative method is used to solve the new boundary equations, the matrix-vector multiplication that occurs is very similar to the convolution (1.12) discussed in Chapter 5. The fast summation methods that we derived can therefore be used to obtain very fast solvers for discrete lattice equations. This formulation is also primed for the use of multi-scale homogenization methods

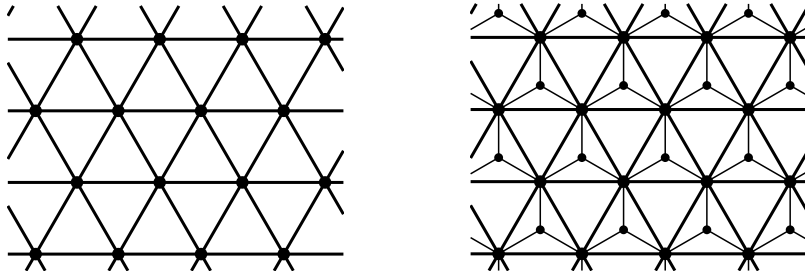


FIGURE 1.4. A triangular lattice without (left) and with (right) an oscillator.

that can speed up the computation further in cases where only averaged properties of the solution are sought in smooth regions of the domain. This is discussed further in Chapter 8.

Chapter 7 — *Lattice vibrations and phononic bandgaps:* In this chapter we study harmonic vibrations of lattices, with an emphasis on mechanical lattices. The governing equation is then the Helmholtz equation

$$(1.16) \quad (\mathfrak{A} - \omega^2 I)u = 0,$$

where ω is the frequency of the vibration. Upon Fourier transformation, (1.16) takes the form

$$(\sigma(\xi) - \omega^2 I)\tilde{u}(\xi) = 0,$$

which is now an algebraic equation. What makes this exciting is that with the lattice models, we can capture much of the qualitative behavior of vibrations in continuous media with a periodic micro-structure, but without having to solve the (sometimes quite complicated) local problems that arise in the latter case, see Movchan and Zalipaev [49].

One particularly interesting feature of materials with micro-structure is that oftentimes, there will be intervals of frequencies for which there are no propagating modes. Such an interval is called a photonic bandgap if the underlying equation is a conduction equation and a phononic bandgap if the underlying equation is a mechanical equation. It is possible to take advantage of such phenomena in order to create highly efficient bandpass filters and virtually loss-free wave-guides.

For lattices, a bandgap is easily characterised as an interval in which there is no solution to the “dispersion” equation

$$\det(\sigma(\xi) - \omega^2 I) = 0,$$

which is in this case a trigonometric equation. Taking advantage of the simplicity of this formulation, we could determine a simple mechanism for designing lattice structures that have prescribed bandgaps. Very roughly speaking, the idea is that given a lattice structure such as the one illustrated to the left in Figure 1.4, that does not have any bandgaps, a bandgap can be created by introducing an oscillator, as shown to the right in the figure. The location of the bandgap can be tuned by adjusting the properties of the introduced oscillator.

Since the material of Chapter 7 stands somewhat apart from the rest of the thesis (in that it deals with dynamic rather than static properties) we present the material in that section as a self-contained exposition, with a minimum amount of references to the rest of the thesis.

CHAPTER 2

Basic properties of static lattice equations

1. Introduction

In this chapter we set up a mathematical framework for analysis of the equations associated with linear and static problems on periodic lattices. Letting \mathbf{u} denote the unknown “potential” (a temperature, a displacement) and \mathbf{f} the “load” (a heat source, a force), we write the basic lattice equation in the form

$$(2.1) \quad [\mathfrak{A}\mathbf{u}](m) = \mathbf{f}(m), \quad \forall m \in \mathbb{Z}^d,$$

where the lattice operator \mathfrak{A} is a constant coefficient convolution operator

$$[\mathfrak{A}\mathbf{u}](m) = \sum_{n \in \mathbb{B}} A^{(n)} \mathbf{u}(m - n),$$

for a finite index set \mathbb{B} and some local matrices $A^{(n)}$. This general framework can be used to model a wide range of problems but we will focus on conduction problems, mechanical truss problems and mechanical frame problems. We treat both mono-atomic and multi-atomic lattices, in fact, the only restrictions on lattice geometries are the minimal requirements needed to avoid degeneracy of the equations (for instance, that the lattice must be connected).

The core mathematical results of this chapter are a number of coercivity results concerning \mathfrak{A} . Once these are established, it is a simple matter to prove existence, uniqueness and stability results for the basic lattice equation (2.1). Additionally, the coercivity results form the foundation of the asymptotic analysis in subsequent chapters.

The coercivity question is somewhat delicate because for each of the models that we study, there will be a non-trivial set \mathcal{N} of potentials that do not cause any internal loads in the lattice. For instance, when studying heat conduction, we expect that a potential that is constant from node to node should not cause any internal flows. Likewise, in the study of mechanical problems, we do not expect rigid body motions to cause any internal forces. For conduction problems and mechanical frames, we will prove that for any connected lattice, the operator \mathfrak{A} is coercive “modulo \mathcal{N} ”, which is the best that could be hoped for. For the mechanical truss model (axial springs that are connected by pin-joints at the nodes), additional assumptions on the lattice geometry are needed. We will provide a condition that is simple to verify and that is sufficient to ascertain “coercivity modulo rigid body motions”. We do not know whether it is necessary.

The chapter is structured as follows: In section 2 we construct a notational framework, specify function spaces, derive the mathematical models for the three problems that we consider (conduction, trusses and frames) and specify non-degeneracy conditions on the lattice geometry that imply a certain coercivity property of the lattice operator. In section 3 we introduce the Fourier transform and prove various properties of the symbol $\sigma(\xi)$, which is the Fourier representation of the lattice

operator \mathfrak{A} . These results about the symbol provide quantitative coercivity results on the operator \mathfrak{A} that are used in section 4 to prove that the lattice equation is well-posed.

2. Preliminaries

2.1. Notation: For a d -dimensional lattice with q nodes in the unit cell, we use $m \in \mathbb{Z}^d$ to label the different cells and $\kappa \in \{1, \dots, q\} = \mathbb{N}_q$ to label the different nodes in a cell. Thus, $(m, \kappa) \in \mathbb{Z}^d \times \mathbb{N}_q =: \Omega$ uniquely labels a node. Let $X(m, \kappa) \in \mathbb{R}^d$ denote the coordinates of node (m, κ) . Since the lattice is periodic, there exists a matrix T such that $X(m, \kappa) = X(0, \kappa) + Tm$. Finally, define for non-negative integers J , the sub-lattices $\Omega_J := \{(m, \kappa) \in \Omega : |m| \leq J\}$.

Since the lattice is periodic, we can describe all links by describing only those originating in the zero-cell, Ω_0 . A link from the node $(0, \kappa)$ to the node (n, λ) is represented by the triple (κ, n, λ) . All such triples are collected in the set \mathbb{B}_+ .

Example: For the lattice in Figure 2.1; $q = 2$, $T = I$, $X(0, 1) = (0, 0)^t$, $X(0, 2) = (1/2, 1/2)^t$, and $\mathbb{B}_+ = \{ (1, [1, 0], 1), (1, [0, 1], 1), (1, [0, 0], 2), (2, [1, 0], 1), (2, [1, 1], 1) \}$. \square

For the most part, we will suppose that the reference cell is a hypercube (rather than a parallelepiped), so that the lattice matrix T equals the identity matrix I . This considerably simplifies notation and entails no loss of generality since any lattice can be affinely mapped to one for which $T = I$, as illustrated in Figure 2.2. On occasion, the use of such a map has non-obvious practical implications, but we try to clarify such points when they arise.

2.2. Lattice equations and function spaces. With each node $(m, \kappa) \in \Omega$ we associate a potential $\mathbf{u}(m, \kappa) \in \mathbb{C}^p$. Depending on the application, this “potential” will represent a quantity such as a temperature or a displacement. We let \mathcal{V} represent the set of all functions $\mathbf{u} : \Omega \rightarrow \mathbb{C}^p$, and let $V := l^2(\Omega, \mathbb{C}^p)$, denote the subset of square summable functions. This is a Hilbert space with inner product

$$\langle \mathbf{u}, \mathbf{v} \rangle_V = \langle \mathbf{u}, \mathbf{v} \rangle := \sum_{(m, \kappa) \in \Omega} \overline{\mathbf{u}(m, \kappa)} \cdot \mathbf{v}(m, \kappa).$$

Similarly, we let $V_J := l^2(\Omega_J, \mathbb{C}^p)$ denote the functions in \mathcal{V} that are supported in Ω_J , and define P_J as the canonical projection $\mathcal{V} \rightarrow V_J$.

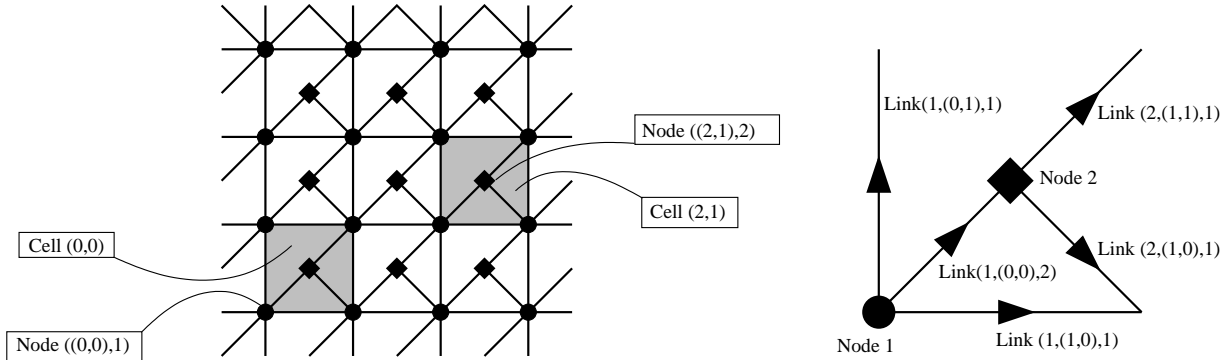


FIGURE 2.1. Lattice notation. Circles denote nodes of type 1 and diamonds nodes of type 2. The unit cell is depicted on the right.

Next, we will derive the equilibrium equation that relates the potential \mathbf{u} to an applied load $\mathbf{f} \in \mathcal{V}$. Consider the link (κ, n, λ) that links the node $(0, \kappa)$ to the node (m, λ) . If the two ends are given potentials $u, v \in \mathbb{C}^p$, then the loads $f, g \in \mathbb{C}^p$ that need to be applied to the two ends to keep the link in equilibrium are specified by the Hermitian matrix $A^{(\kappa, n, \lambda)} \in \mathbb{C}^{p \times p}$,

$$(2.2) \quad A^{(\kappa, n, \lambda)} \begin{bmatrix} u \\ v \end{bmatrix} = \begin{bmatrix} f \\ g \end{bmatrix}, \quad \text{where} \quad A^{(\kappa, n, \lambda)} = \begin{bmatrix} B^{(\kappa, n, \lambda)} & C^{(\kappa, n, \lambda)} \\ (C^{(\kappa, n, \lambda)})^t & D^{(\kappa, n, \lambda)} \end{bmatrix}.$$

We then define an operator $\mathfrak{A}^{(\kappa, n, \lambda)}$ acting on the global potential \mathbf{u} by

$$(2.3) \quad \begin{aligned} [\mathfrak{A}^{(\kappa, n, \lambda)} \mathbf{u}](0, \kappa) &= B^{(\kappa, n, \lambda)} \mathbf{u}(0, \kappa) + C^{(\kappa, n, \lambda)} \mathbf{u}(n, \lambda) \\ [\mathfrak{A}^{(\kappa, n, \lambda)} \mathbf{u}](n, \lambda) &= (C^{(\kappa, n, \lambda)})^t \mathbf{u}(0, \kappa) + D^{(\kappa, n, \lambda)} \mathbf{u}(n, \lambda), \end{aligned}$$

and $[\mathfrak{A}^{(\kappa, n, \lambda)} \mathbf{u}](l, \mu) = 0$, for all other nodes (l, μ) . The operator that represents the connection between the nodes (m, κ) and $(m + n, \lambda)$ is then given by $\tau_{-m} \mathfrak{A}^{(\kappa, n, \lambda)} \tau_m$, where for $m \in \mathbb{Z}^d$ the translation operator $\tau_m : \mathcal{V} \rightarrow \mathcal{V}$ is defined by

$$(2.4) \quad [\tau_m \mathbf{u}](l) := \mathbf{u}(l - m).$$

Thus, the operator $\mathfrak{A} : \mathcal{V} \rightarrow \mathcal{V}$ that accounts for all links is given by

$$(2.5) \quad \mathfrak{A} := \sum_{m \in \mathbb{Z}^d} \sum_{(\kappa, n, \lambda) \in \mathbb{B}_+} \tau_{-m} \mathfrak{A}^{(\kappa, n, \lambda)} \tau_m,$$

whence we obtain the global equilibrium equation

$$[\mathfrak{A} \mathbf{u}](m, \kappa) = \mathbf{f}(m, \kappa), \quad \forall (m, \kappa) \in \Omega.$$

Lemma 2.1: *The operator $\mathfrak{A} : V \rightarrow V$ is bounded, self-adjoint and positive semi-definite.*

Proof: The fact that \mathfrak{A} is bounded is a direct consequence of the facts that every term in (2.5) is bounded and that \mathbb{B}_+ is finite. Similarly, the self-adjointness and semi-definiteness of \mathfrak{A} are inherited from the corresponding properties of each $\mathfrak{A}^{(\kappa, m, \lambda)}$. \square

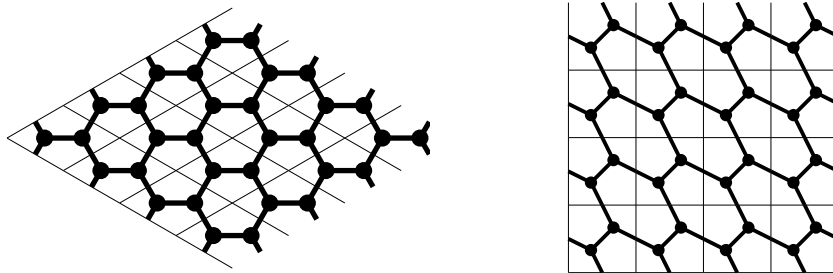


FIGURE 2.2. Using an affine transformation, the honeycomb lattice to the left can be transformed to one that has a square irreducible cell, shown to the right.

Given a potential field \mathbf{u} , we say that the quantity $\langle \tau_m \mathbf{u}, \mathfrak{A}^{(\kappa, n, \lambda)} \tau_m \mathbf{u} \rangle$ is the “energy” stored in the link connecting the node (m, κ) to the node $(m + n, \lambda)$. We then define

$$(2.6) \quad W[\mathbf{u}](m) := \sum_{(\kappa, n, \lambda) \in \mathbb{B}_+} \langle \tau_m \mathbf{u}, \mathfrak{A}^{(\kappa, n, \lambda)} \tau_m \mathbf{u} \rangle$$

as the energy of the bars originating in the node m and let

$$\|\mathbf{u}\|_{\mathfrak{A}}^2 := \lim_{J \rightarrow \infty} \sum_{|m| \leq J} W[\mathbf{u}](m) = \sum_{m \in \mathbb{Z}^d} \sum_{(\kappa, n, \lambda) \in \mathbb{B}_+} \left[\frac{\overline{\mathbf{u}(m, \kappa)}}{\mathbf{u}(m + n, \lambda)} \right] A^{(\kappa, n, \lambda)} \begin{bmatrix} \mathbf{u}(m, \kappa) \\ \mathbf{u}(m + n, \lambda) \end{bmatrix}$$

define the global energy semi-norm. When $\|\mathbf{u}\|_{\mathfrak{A}} < \infty$, we have

$$\|\mathbf{u}\|_{\mathfrak{A}}^2 = \langle \mathbf{u}, \mathfrak{A} \mathbf{u} \rangle =: \langle \mathbf{u}, \mathfrak{A} \mathbf{u} \rangle.$$

Note that for many potentials $\mathbf{u} \in \mathcal{V}$ such that $\mathfrak{A} \mathbf{u} = 0$, we have $\|\mathbf{u}\|_{\mathfrak{A}} = \infty$.

The conduction problem: Suppose that we wish to model heat conduction on a lattice. Then the “potential” of a node represents its temperature, and a “load” is a heat flow. If two nodes of potentials u and v are connected by a link of conductivity α , then in equilibrium, the flows at the two ends are given by $f = \alpha(u - v)$ and $g = \alpha(v - u)$. Thus, for some $\alpha^{(\kappa, n, \lambda)} > 0$,

$$A^{(\kappa, n, \lambda)} = \alpha^{(\kappa, n, \lambda)} \begin{bmatrix} 1 & -1 \\ -1 & 1 \end{bmatrix}.$$

Mechanical trusses: A common model for a mechanical structure with a geometry such as the lattices B or C in Figure 1.3 is to consider the links as axial springs that are pin-jointed at the nodes. In this case, the “potential” of a node is its physical displacement, so $p = d$, and a “load” is a physical force. Thus, if two ends of a bar with an axial stiffness α that is directed along the unit vector $e \in \mathbb{R}^d$ are displaced by u and v , then the forces needed to keep the bar in equilibrium are $f = \alpha e (e \cdot (u - v))$ and $g = \alpha e (e \cdot (v - u))$. Thus, the local stiffness matrix takes the form

$$A^{(\kappa, n, \lambda)} = \alpha^{(\kappa, n, \lambda)} \begin{bmatrix} e^{(\kappa, n, \lambda)} [e^{(\kappa, n, \lambda)}]^t & -e^{(\kappa, n, \lambda)} [e^{(\kappa, n, \lambda)}]^t \\ -e^{(\kappa, n, \lambda)} [e^{(\kappa, n, \lambda)}]^t & e^{(\kappa, n, \lambda)} [e^{(\kappa, n, \lambda)}]^t \end{bmatrix}.$$

where $e^{(\kappa, n, \lambda)}$ is the orientation vector of the link,

$$e^{(\kappa, n, \lambda)} := \frac{X(n, \lambda) - X(0, \kappa)}{|X(n, \lambda) - X(0, \kappa)|} \in S_{d-1}.$$

Mechanical frames: When modeling structures with a geometry such as lattices A or D in Figure 1.3 we include the bending stiffness of the links in the model. One must then include rotational degrees of freedom in the nodal potential so that $p = d(d + 1)/2$. The “load” will in this case represent both forces and torques. The local matrices are rank p matrices of the general form

$$A^{(\kappa, n, \lambda)} = \begin{bmatrix} B^{(\kappa, n, \lambda)} & C^{(\kappa, n, \lambda)} \\ (C^{(\kappa, n, \lambda)})^t & D^{(\kappa, n, \lambda)} \end{bmatrix}.$$

By Castigliano’s theorem, the matrix $A^{(\kappa, n, \lambda)}$ must be symmetric, but it is in general *not* the case that $C^{(\kappa, n, \lambda)} = -B^{(\kappa, n, \lambda)}$ or that $D^{(\kappa, n, \lambda)} = A^{(\kappa, n, \lambda)}$. See Appendix A for details.

A comparison of the different models is given in Table 2.1. For concrete illustrations of how to derive the lattice equations given a lattice model and a geometry, see Appendix B.

Remark: It is worth commenting on how the truss and frame models relate to one another. Given a mechanical lattice of arbitrary geometry (as long as it is connected), it is *always* possible to model it as a frame. As we shall see, such a model is always coercive “modulo rigid body motions”. However, we know that for a slender bar, the bending stiffness is lower than the axial stiffness by roughly a factor of β^2 , where β is the slenderness ratio. This means that when $\beta \ll 1$, the lattice operator decouples into two parts of different magnitudes (see Appendix A),

$$(2.7) \quad \mathfrak{A} = \mathfrak{A}^{\text{axial}} + \beta^2 \mathfrak{A}^{\text{bending}}.$$

Moreover, if we split the potential and the load into translational and rotational components $\mathbf{u} = \mathbf{u}_t \oplus \mathbf{u}_r$, and $\mathbf{f} = \mathbf{f}_t \oplus \mathbf{f}_r$ (note that \mathbf{f}_t represents forces acting at the nodes and \mathbf{f}_r represents torques), then \mathfrak{A} splits further into

$$(2.8) \quad \left(\begin{bmatrix} \mathfrak{A}_{tt}^{\text{axial}} & 0 \\ 0 & 0 \end{bmatrix} + \beta^2 \begin{bmatrix} \mathfrak{A}_{tt}^{\text{bending}} & \mathfrak{A}_{tr}^{\text{bending}} \\ \mathfrak{A}_{rt}^{\text{bending}} & \mathfrak{A}_{rr}^{\text{bending}} \end{bmatrix} \right) \begin{bmatrix} \mathbf{u}_t \\ \mathbf{u}_r \end{bmatrix} = \begin{bmatrix} \mathbf{f}_t \\ \mathbf{f}_r \end{bmatrix}.$$

Now, for lattice geometries such as B or C in Figure 1.3, the operator $\mathfrak{A}_{tt}^{\text{axial}}$ is coercive (modulo rigid body motions). Thus, if there is no torque loading, $\mathbf{f}_r = 0$, which is usually the case, we are justified in making the following approximation,

$$\mathbf{u}_t = \left[\mathfrak{A}_{tt}^{\text{axial}} + \beta^2 \mathfrak{A}_{tt}^{\text{bending}} - \beta^2 \mathfrak{A}_{tr}^{\text{bending}} (\mathfrak{A}_{rr}^{\text{bending}})^{-1} \mathfrak{A}_{rt}^{\text{bending}} \right]^{-1} \mathbf{f}_t \approx \left[\mathfrak{A}_{tt}^{\text{axial}} \right]^{-1} \mathbf{f}_t.$$

since $\beta^2 \ll 1$. However, if $\mathfrak{A}_{tt}^{\text{axial}}$ is *not* coercive, then the full equations must be used. In the next section considerable effort is spent constructing an easily verified criteria that picks out those geometries for which the truss approximation is valid. \square

2.3. Coercivity. We mentioned in the introduction that some combinations of lattice geometries and node-to-node interaction mechanisms produce degenerate models. An extreme example occurs when not all nodes of a lattice are connected; a more subtle type of degeneracy occurs when a mechanical truss turns into a “mechanism”, meaning that the lattice can deform without incurring any internal forces, like lattices A and D in Figure 1.3. In this section we seek to formulate some readily verifiable “coercivity” requirement that disqualifies such degenerate lattices.

First we specify a subspace $\mathcal{N} \subset \mathcal{V}$ of potentials that we expect to cause no internal energy, in the sense that $\|\mathbf{v}\|_{\mathfrak{A}} = 0$ for $\mathbf{v} \in \mathcal{N}$. We ask that such a subspace satisfy:

- (1) \mathcal{N} is translation invariant, $\tau_m \mathcal{N} = \mathcal{N}$, for any $m \in \mathbb{Z}^d$.
- (2) There exists an integer k such that any $\mathbf{v} \in \mathcal{N}$ is uniquely determined by $P_k \mathbf{v}$.

Examples: For conduction problems, \mathcal{N} is the set of constants and $k = 0$. For mechanical problems, \mathcal{N} is the space of rigid body motions. For truss problems, $k = 1$, meaning that a rigid body motion is uniquely determined by the displacements of the nodes in Ω_1 . For frames, information about rotational displacements are included in the nodal potential and thus any rigid body motion is uniquely determined by its value at any node, and $k = 0$. \square

The space \mathcal{N} must clearly satisfy $\mathcal{N} \subset \text{Null}(\mathfrak{A}^{(\kappa, n, \lambda)})$ for all links (κ, n, λ) , so that automatically $\mathcal{N} \subseteq \text{Null}(\|\cdot\|_{\mathfrak{A}})$. Our goal is to formulate conditions that guarantee that $\mathcal{N} = \text{Null}(\|\cdot\|_{\mathfrak{A}})$. We remark at this point that it would be very practical if we could perform a split “ $\mathcal{N} = \mathcal{N} \oplus \mathcal{N}^\perp$ ”,

where $\mathcal{N} = \text{Null}(\mathfrak{A})$ and ask that \mathfrak{A} be coercive when restricted to “ \mathcal{N}^\perp ”. Unfortunately, \mathcal{V} is not a Hilbert space, and such an approach does not seem to be feasible.

Definition: Say that \mathfrak{A} is \mathcal{N} -coercive if $\text{Null}(\|\cdot\|_{\mathfrak{A}}) = \mathcal{N}$.

It is not easy to verify whether \mathfrak{A} is \mathcal{N} -coercive for a given lattice. We will therefore give a stronger, local condition that is simple to verify and that implies \mathcal{N} -coercivity. The idea is to look at the finite sub-lattices created by removing all links that do not originate in the finite set Ω_J . Such a sub-lattice is governed by the operator

$$\mathfrak{A}_J := \sum_{|m| \leq J} \sum_{(\kappa, n, \lambda) \in \mathbb{B}_+} \tau_{-m} \mathfrak{A}^{(\kappa, n, \lambda)} \tau_m.$$

Clearly $\mathcal{N} \subset \text{Null}(\mathfrak{A}_J)$. Now, if we can find a finite J such that for the nodes at the center of the sub-lattice, the *only* displacement fields that are energy free are those in \mathcal{N} , then we may be able to use the translation invariance to prove global \mathcal{N} -coercivity. It turns out that if we can “lock” the nodes (modulo \mathcal{N}) in the set Ω_{k+1} , then \mathcal{N} -coercivity follows.

Definition: \mathfrak{A} is locally \mathcal{N} -coercive if there exists a finite J such that $P_{\Omega_{k+1}} \text{Null}(\mathfrak{A}_J) = P_{\Omega_{k+1}} \mathcal{N}$.

Lemma 2.2: *If \mathfrak{A} is locally \mathcal{N} -coercive, then it is \mathcal{N} -coercive.*

Proof: Fixing a $\mathbf{v} \in \text{Null}(\|\cdot\|_{\mathfrak{A}})$ we will prove that $\mathbf{v} \in \mathcal{N}$.

A simple calculation shows that

$$(2.9) \quad P_{\Omega_{k+1}} \mathbf{v} \in P_{\Omega_{k+1}} \text{Null}(\|\cdot\|_{\mathfrak{A}}) \subset P_{\Omega_{k+1}} \text{Null}(\|\cdot\|_{\mathfrak{A}_J}) = P_{\Omega_{k+1}} \text{Null}(\mathfrak{A}_J) = P_{\Omega_{k+1}} \mathcal{N}.$$

Thus there exists a unique $\mathbf{v}' \in \mathcal{N}$ such that $P_{\Omega_{k+1}} \mathbf{v} = P_{\Omega_{k+1}} \mathbf{v}'$.

Next we will show that $\mathbf{v}' = \mathbf{v}$ on all of Ω . Let $m \in \mathbb{Z}^d$ be any vector such that $|m|_\infty = 1$. Since $\tau_m \mathbf{v} \in \text{Null}(\mathfrak{A})$, the calculation (2.9) can be used to find a unique $\mathbf{v}'' \in \mathcal{N}$ that equals \mathbf{v} in $\tau_m \Omega_{k+1}$. Now use that $P_{\Omega_k} \mathbf{v}'' = P_{\Omega_k} \mathbf{v}'$ to deduce that $\mathbf{v}'' = \mathbf{v}'$. Since m was arbitrary, this shows that $\mathbf{v}(n) = \mathbf{v}'(n)$ for $|n|_\infty \leq k+2$. This process can be continued to cover all of Ω . \square

We provide a condition that can often be used to assert local \mathcal{N} -coercivity.

Definition: We say that a link (κ, n, λ) is \mathcal{N} -coercive if for any $\varphi \in \mathbb{C}^p$, there exists a unique $\mathbf{v} \in \mathcal{N}$ such that $\mathbf{v}(0, \kappa) = \varphi$ and $\mathfrak{A}^{(\kappa, n, \lambda)} \mathbf{v} = 0$.

Of the models that we have discussed, the conduction model and the mechanical frame model have \mathcal{N} -coercive links but the mechanical truss model does not.

Lemma 2.3: *Suppose that all links are \mathcal{N} -coercive. Then if a lattice is connected, it is locally \mathcal{N} -coercive (and hence \mathcal{N} -coercive).*

Proof: Let J be large enough that every node in Ω_{k+1} is connected to the node $(0, 1)$ through a path entirely contained within Ω_J . Fixing a $\mathbf{v} \in \text{Null}(\mathfrak{A}_J)$ we need to show that there exists a $\mathbf{v}' \in \mathcal{N}$ such that $P_{\Omega_{k+1}} \mathbf{v} = P_{\Omega_{k+1}} \mathbf{v}'$.

Due to the symmetry and the positive semi-definiteness of all the local bars we know that $\tau_{-m} \mathfrak{A}^{(\kappa, n, \lambda)} \tau_m \mathbf{v} = 0$ for all $|m| \leq J$. Thus, given any link $(1, n, \lambda)$, there exists a unique $\mathbf{v}' \in \mathcal{N}$ such that $\mathbf{v}(0, 1) = \mathbf{v}'(0, 1)$ and $\mathbf{v}(n, \lambda) = \mathbf{v}'(n, \lambda)$.

Given any node $(l, \mu) \in \Omega_{k+1}$ choose a path that connects $(0, 1)$ to (l, μ) . Since $\mathfrak{A}_J \mathbf{v}' = 0$ and $\mathbf{v}'(0, 1) = \mathbf{v}(0, 1)$ it then follows from the \mathcal{N} -coercivity of all the links in the path that $\mathbf{v}'(l, \mu) = \mathbf{v}(l, \mu)$. Thus $P_{\Omega_{k+1}} \mathbf{v} = P_{\Omega_{k+1}} \mathbf{v}'$, which concludes the proof. \square

Model	Potential	Load	p	$\text{Rank}(A^{(\kappa,n,\lambda)})$	\mathcal{N}
Conduction	Temperature	Heat source/sink	1	1	Constants
Mech. truss	Displacement	Force	d	1	Rigid body mot.
Mech. frame	Displ. + rot.	Force + torque	$d(d+1)/2$	$d(d+1)/2$	Rigid body mot.

TABLE 2.1. Table comparing the conduction problem to two mechanical problems. The truss model is the only one that does not have \mathcal{N} -coercive links.

3. Fourier analysis

3.1. Introduction. The operator \mathfrak{A} is a constant coefficient convolution operator that can be diagonalized by a Fourier transform. Noting that we can identify $V = l^2(\mathbb{Z}^d \times \mathbb{N}_q, \mathbb{C}^p)$ by $l^2(\mathbb{Z}^d, \mathbb{C}^{pq})$, we use the well-known isometric isomorphism

$$\mathcal{F} : l^2(\mathbb{Z}^d, \mathbb{C}^{pq}) \rightarrow L^2(I^d, \mathbb{C}^{pq}) : \mathbf{u} \mapsto \tilde{\mathbf{u}}(\xi) = \sum_{m \in \mathbb{Z}^d} e^{im \cdot \xi} \mathbf{u}(m), \quad \text{where } I^d := (-\pi, \pi)^d,$$

to obtain the diagonalization

$$[\mathcal{F}[\mathfrak{A}\mathbf{u}]](\xi) = \left[\sum_{(\kappa,n,\lambda) \in \mathbb{B}_+} \Upsilon^{(\kappa,n,\lambda)}(\xi) \right] \tilde{\mathbf{u}}(\xi),$$

where each matrix $\Upsilon^{(\kappa,n,\lambda)}(\xi)$ consists of $q \times q$ blocks, each of size $p \times p$. The four non-zero blocks are located at the intersections of the κ, λ -rows and columns,

$$(2.10) \quad \Upsilon^{(\kappa,n,\lambda)}(\xi) := \begin{bmatrix} & \vdots & & \vdots & \\ \dots & B^{(\kappa,n,\lambda)} & \dots & e^{im \cdot \xi} C^{(\kappa,n,\lambda)} & \dots \\ & \vdots & & \vdots & \\ \dots & e^{-im \cdot \xi} (C^{(\kappa,n,\lambda)})^t & \dots & D^{(\kappa,n,\lambda)} & \dots \\ & \vdots & & \vdots & \end{bmatrix}.$$

We introduce the symbol $\sigma(\xi) \in \mathbb{C}^{pq \times pq}$ as the Fourier representation of \mathfrak{A} ,

$$(2.11) \quad \sigma(\xi) := \sum_{(\kappa,n,\lambda) \in \mathbb{B}_+} \Upsilon^{(\kappa,n,\lambda)}(\xi).$$

Lemma 2.4: *The symbol $\sigma(\xi)$ is a uniformly bounded Hermitian positive semi-definite matrix.*

The claims of the lemma follow from Lemma 2.1 since $\sigma = \mathcal{F}\mathfrak{A}\mathcal{F}^{-1}$, and \mathcal{F} is an isometric operator. Another consequence of this is that one can easily determine the spectrum of \mathfrak{A} by determining the eigenvalues of $\sigma(\xi)$ for $\xi \in I^d$. In particular, this gives a simple method for computing $\|\mathfrak{A}\|_{\mathcal{L}(V,V)}$ accurately.

We will next show that the quadratic form on \mathbb{C}^{pq} induced by $\sigma(\xi)$, namely

$$\varphi \mapsto \langle \varphi, \sigma(\xi), \varphi \rangle := \bar{\varphi} \cdot [\sigma(\xi)\varphi],$$

is related to the energy of the periodic potential field $\mathbf{u}(m, \kappa) = \varphi(\kappa)e^{-im \cdot \xi}$. To this end, recall that $W[\mathbf{u}](m)$ denotes the energy of the links originating in the cell m under the potential \mathbf{u} , cf. (2.6).

Lemma 2.5: *Set $\mathbf{u}(m, \kappa) = \varphi(\kappa)e^{-im \cdot \xi}$. Then $W[\mathbf{u}](m) = \langle \varphi, \sigma(\xi), \varphi \rangle$.*

Proof: Inserting the expression for \mathbf{u} in the definition of W , we get

$$W[\mathbf{u}](m) = \sum_{(\kappa, n, \lambda) \in \mathbb{B}_+} e^{im \cdot \xi} \begin{bmatrix} \overline{\varphi(\kappa)} \\ e^{in \cdot \xi} \varphi(\lambda) \end{bmatrix} \cdot A^{(\kappa, n, \lambda)} e^{-im \cdot \xi} \begin{bmatrix} \varphi(\kappa) \\ e^{-in \cdot \xi} \varphi(\lambda) \end{bmatrix} = \sum_{(\kappa, n, \lambda) \in \mathbb{B}_+} \overline{\varphi} \cdot [\Upsilon^{(\kappa, n, \lambda)}(\xi) \varphi],$$

which equals $\overline{\varphi} \cdot [\sigma(\xi) \varphi]$ by the definitions (2.10) and (2.11). \square

Lemma (2.5) can be combined with knowledge of the null-spaces \mathcal{N} , discussed in section 2.3, to obtain upper and, more importantly, *lower* bounds for $\varphi \mapsto \langle \varphi, \sigma(\xi), \varphi \rangle$.

Lemma 2.6: *Let M be the length of the longest link, $M := \max\{|n|_\infty : (\kappa, n, \lambda) \in \mathbb{B}_+\}$. Then there exists a constant C such that, with $\mathbf{u}(m, \kappa) = \varphi(\kappa) e^{-im \cdot \xi}$,*

$$\langle \varphi, \sigma(\xi), \varphi \rangle \leq C \inf_{\mathbf{v} \in \mathcal{N}} \|\mathbf{u} - \mathbf{v}\|_{V_M}^2.$$

Proof: Fix any $\mathbf{v} \in \mathcal{N}$ and invoke Lemma 2.5 to obtain that $\langle \varphi, \sigma(\xi), \varphi \rangle = W[\mathbf{u}](0) = W[\mathbf{u} - \mathbf{v}](0)$. Since all links originating in Ω_0 are wholly contained in Ω_M , we know that $W[\mathbf{u} - \mathbf{v}](0) \leq \|\mathfrak{A}\|_V \|\mathbf{u} - \mathbf{v}\|_{V_M}^2$, and the claim follows from the boundedness of \mathfrak{A} . \square

Lemma 2.7: *If a lattice is locally \mathcal{N} -coercive, then there exists a positive constant c such that, with $\mathbf{u}(m, \kappa) = \varphi(\kappa) e^{-im \cdot \xi}$,*

$$\langle \varphi, \sigma(\xi), \varphi \rangle \geq c \inf_{\mathbf{v} \in \mathcal{N}} \|\mathbf{u} - \mathbf{v}\|_{V_{k+1}}^2.$$

Proof: We use Lemma 2.5 to ascertain that $\langle \varphi, \sigma(\xi), \varphi \rangle = (2J+1)^{-d} \langle \mathbf{u}, \mathfrak{A}_J, \mathbf{u} \rangle$. Next we will show that there exists a $c > 0$ such that $\langle \mathbf{u}, \mathfrak{A}_J, \mathbf{u} \rangle \geq c \|Q\mathbf{u}\|^2$, where Q denotes the projection onto the orthogonal complement of \mathcal{N} in V_{k+1} (so that $\inf_{\mathbf{v} \in \mathcal{N}} \|\mathbf{u} - \mathbf{v}\|_{V_{k+1}} = \|Q\mathbf{u}\|$). Set

$$c := \inf_{\mathbf{u} \in \mathcal{V}} \frac{\langle \mathbf{u}, \mathfrak{A}_J, \mathbf{u} \rangle}{\|Q\mathbf{u}\|^2}.$$

Now note that the infimum can be restricted to the compact set $\{\mathbf{u} \in V_{J+M} : \|\mathbf{u}\| = 1\}$, with the M defined in Lemma 2.6. Since the infimum is taken over a compact set, we know that if $c = 0$, then there must exist a minimizer \mathbf{u}' such that $\|Q\mathbf{u}'\| \neq 0$ and $\langle \mathbf{u}', \mathfrak{A}_J, \mathbf{u}' \rangle = 0$, but this contradicts the assumption of local \mathcal{N} -coercivity. Thus $c > 0$ which proves the claim. \square

In sections 3.2 – 3.4, we will study each of the lattice models in Table 2.1 and prove coercivity results for the symbol $\sigma(\xi)$ but first we review some general results for Hermitian positive matrices.

Definition: If X and Y are Hermitian positive definite (HPD) matrices, such that $\langle \varphi, X, \varphi \rangle \leq \langle \varphi, Y, \varphi \rangle$ for every φ , then we say that $X \leq Y$. If there are positive constants a and b , such that $aX \leq Y \leq bX$, then we say that $X \sim Y$. \square

Lemma 2.8: *If X and Y are HPD and $X \leq Y$, then $\det X \leq \det Y$ and $Y^{-1} \leq X^{-1}$.*

Proof: Note that since X is HPD, it has a well-defined non-singular square root. To prove the first statement, set $\psi = X^{1/2} \varphi$ and write the condition as $|\psi|^2 \leq \psi \cdot (X^{-1/2} Y X^{-1/2} \psi)$. This implies that $1 \leq \det(X^{-1/2} Y X^{-1/2}) = \det Y / \det X$.

The second inequality is similarly obtained by setting $\varphi = Y^{-1/2} [Y^{-1/2} X Y^{-1/2}]^{-1/2} Y^{-1/2} \psi$. \square

3.2. The conduction problem. The results we are about to present are technical in nature but are absolutely central in that (1) they form a pattern for how to study other lattice models and (2) they will be invoked in almost every subsequent result presented in this chapter (well-posedness of the lattice equations, homogenization, lattice Green's functions). The core result is that if a vector $\varphi \in \mathbb{C}^q$ is split into a local average and a deviation from the average, $\varphi = \varphi_A \oplus \varphi_D$, then

$$(2.12) \quad c (|\xi|^2 |\varphi_A|^2 + |\varphi_D|^2) \leq \langle \varphi, \sigma(\xi), \varphi \rangle \leq C (|\xi|^2 |\varphi_A|^2 + |\varphi_D|^2),$$

for some positive constants c and C that do not depend on ξ . The significance of this result is that it leads to a fairly complete description of the action of \mathfrak{A} in physical space; if a potential \mathbf{u} is split into a *cell-wise* average \mathbf{u}_A , and a local deviation \mathbf{u}_D , so that $\mathbf{u} = \mathbf{u}_A \oplus \mathbf{u}_D$, then

$$c (\langle \mathbf{u}_A, \mathfrak{A}_\circ, \mathbf{u}_A \rangle + \|\mathbf{u}_D\|^2) \leq \langle \mathbf{u}, \mathfrak{A}, \mathbf{u} \rangle \leq C (\langle \mathbf{u}_A, \mathfrak{A}_\circ, \mathbf{u}_A \rangle + \|\mathbf{u}_D\|^2),$$

where \mathfrak{A}_\circ is the discrete Laplace operator, *cf.* (2.25). The result (2.12) can also be used to show that to lowest order, all elements of $\sigma(\xi)^{-1}$ are identical, meaning that there exists a constant c_0 and a symmetric positive definite matrix $M \in \mathbb{R}^{d \times d}$ such that

$$(2.13) \quad [\sigma(\xi)^{-1}]_{\kappa\lambda} = \frac{c_0}{\xi \cdot (M\xi)} + O(|\xi|^{-1}),$$

for all $\kappa, \lambda \in \mathbb{N}_q$. This result has important ramifications to the nature of the homogenized equations and the lattice Green's functions.

In order to define the projection operators, we set $\psi_1 := q^{-1/2}[1, \dots, 1]^t \in \mathbb{R}^q$ and define for $j = 2, \dots, q$, vectors $\psi_j \in \mathbb{R}^q$ such that $\Psi = [\psi_1, \psi_2, \dots, \psi_q]$ is a unitary matrix. We split Ψ into two sub-matrices $\Psi = [\psi_1, 0, \dots, 0] + [0, \psi_2, \dots, \psi_q] =: \Psi_A + \Psi_D$ so that any vector $\varphi \in \mathbb{C}^q$ can be split into orthogonal components $\Psi^t \varphi = \Psi_A^t \varphi \oplus \Psi_D^t \varphi =: \varphi_A \oplus \varphi_D$. For $\mathbf{v} \in \mathcal{V}$, we set $\mathbf{v} = \mathbf{v}_A \oplus \mathbf{v}_D$, where $\mathbf{v}_A(m) = \Psi_A^t \mathbf{v}(m)$, and $\mathbf{v}_D(m) = \Psi_D^t \mathbf{v}(m)$. Finally, we set $L(\xi) = \text{diag}(|\xi|^2, 1, \dots, 1)$, and formulate the result (2.12) as follows.

Theorem 2.9: *For the conduction problem on a connected lattice, $\sigma(\xi) \sim \Psi L(\xi) \Psi^t$.*

Proof: First note that since the links are \mathcal{N} -coercive, the connectivity assumption implies local \mathcal{N} -coercivity for the lattice. Thus Lemmas 2.6 and 2.7 apply, with $\mathbf{u}(m, \kappa) := \varphi(\kappa) e^{-im \cdot \xi}$.

To prove the upper bound in (2.12), use Lemma 2.6 with the choice $\mathbf{v}(m, \kappa) := \varphi_A$ to get

$$\begin{aligned} \langle \varphi, \sigma(\xi), \varphi \rangle &\leq C (\|\mathbf{u}_A - \mathbf{v}\|_{V_M}^2 + \|\mathbf{u}_D\|_{V_M}^2) \\ &= C \sum_{|m| \leq M} (|\varphi_A e^{-im \cdot \xi} - \varphi_A|^2 + |\varphi_D e^{-im \cdot \xi}|^2) \leq C (|\xi|^2 |\varphi_A|^2 + |\varphi_D|^2). \end{aligned}$$

Next we prove the lower bound in (2.12) using Lemma 2.7. Set

$$(2.14) \quad l_A(\xi) := \inf_{\varphi \in \mathbb{C}^q} \frac{1}{2} \frac{\langle \varphi, \sigma(\xi), \varphi \rangle}{|\varphi_A|^2}, \quad \text{and} \quad l_D(\xi) := \inf_{\varphi \in \mathbb{C}^q} \frac{1}{2} \frac{\langle \varphi, \sigma(\xi), \varphi \rangle}{|\varphi_D|^2},$$

so that

$$\langle \varphi, \sigma(\xi), \varphi \rangle \geq l_A(\xi) |\varphi_A|^2 + l_D(\xi) |\varphi_D|^2.$$

First note that the infimum can be restricted to the unit ball in \mathbb{C}^q , which is a compact set. Then, since $\mathbf{u} \notin \mathcal{N}$ for $\xi \neq 0$, Lemma 2.7 immediately tells us that both $l_A(\xi)$ and $l_D(\xi)$ are positive for $\xi \neq 0$. It remains to investigate their behavior near the origin.

To prove that $l_D(0) > 0$, we note that for $\xi = 0$, the minimizer in Lemma 2.7 is \mathbf{u}_A , so that

$$\langle \varphi, \sigma(0), \varphi \rangle \geq c \|\mathbf{u} - \mathbf{u}_A\|_{V_1}^2 = c \|\mathbf{u}_D\|_{V_1}^2 = c 3^d |\varphi_D|^2.$$

In order to prove that $l_A(\xi) \geq c|\xi|^2$, we first use that

$$\langle \varphi, \sigma(\xi), \varphi \rangle \geq c \inf_{\mathbf{v} \in \mathcal{N}} \|\mathbf{u} - \mathbf{v}\|_{V_1}^2 \geq c \inf_{\mathbf{v} \in \mathcal{N}} \|\mathbf{u}_A - \mathbf{v}_A\|_{V_1}^2 = c \inf_{z \in \mathbb{C}} \sum_{|m| \leq 1} |\varphi_A e^{-im \cdot \xi} - z|^2.$$

The minimizer is

$$z^{(\min)} = \frac{1}{3^d} \sum_{|m| \leq 1} \varphi_A e^{-im \cdot \xi} = \varphi_A \prod_{j=1}^d \sum_{m_j=-1}^1 \frac{e^{-im_j \xi_j}}{3} = \varphi_A \prod_{j=1}^d \left(1 - \frac{4}{3} \sin^2 \frac{\xi_j}{2} \right) =: \varphi_A (1 + r_d(\xi)),$$

where $r_d(\xi)$ satisfies $|r_d(\xi)| \leq C|\xi|^2$. Thus, using that $|a + b|^2 \geq |a|^2 - |b|^2$ we find that

$$\begin{aligned} \langle \varphi, \sigma(\xi), \varphi \rangle &\geq c \sum_{|m| \leq 1} |\varphi_A e^{-im \cdot \xi} - \varphi_A - \varphi_A r_d(\xi)|^2 \\ &\geq c |\varphi_A|^2 \sum_{|m| \leq 1} \left(|e^{-im \cdot \xi} - 1|^2 - |r_d(\xi)|^2 \right) \geq c |\varphi_A|^2 (|\xi|^2 - |\xi|^4) \geq c |\varphi_A|^2 |\xi|^2, \end{aligned}$$

which proves that $l_A(\xi) \geq c|\xi|^2$. \square

Corollary 2.10: *For the conduction problem on a connected lattice there exists a positive definite matrix M such that $\det \sigma(\xi) = \xi \cdot (M\xi) + O(|\xi|^4)$.*

Proof: First note that $\det \sigma(\xi)$ is a trigonometric polynomial, and hence an entire function with an everywhere convergent power series. Next note that $\det \sigma(0) = 0$, and that by combining Theorem 2.9 and Lemma 2.8 we know that $\det \sigma(\xi) \geq c \det L(\xi) = c|\xi|^2$. Together, these statements prove the corollary. \square

Corollary 2.11: *For the conduction problem on a connected lattice, $\sigma(\xi)^{-1} \sim \Psi L(\xi)^{-1} \Psi^t$.*

Proof: Combine Theorem 2.9 and Lemma 2.8. \square

The last corollary can be used to prove the identity (2.13). For $\alpha, \beta \in \{A, D\}$, set $\sigma_{\alpha\beta}(\xi) := \Psi_\alpha^t \sigma(\xi) \Psi_\beta$ and $S_{\alpha\beta}(\xi) := \Psi_\alpha^t \sigma(\xi)^{-1} \Psi_\beta$ so that

$$\Psi^t \sigma(\xi) \Psi = \begin{bmatrix} \sigma_{AA}(\xi) & \sigma_{AD}(\xi) \\ \sigma_{DA}(\xi) & \sigma_{DD}(\xi) \end{bmatrix}, \quad \text{and} \quad \Psi^t \sigma(\xi)^{-1} \Psi = \begin{bmatrix} S_{AA}(\xi) & S_{AD}(\xi) \\ S_{DA}(\xi) & S_{DD}(\xi) \end{bmatrix}.$$

where the $S_{\alpha\beta}$ can be computed from the $\sigma_{\alpha\beta}$ through the relations

$$\begin{aligned} S_{AA}(\xi) &= [\sigma_{AA}(\xi) - \sigma_{AD}(\xi) \sigma_{DD}^{-1}(\xi) \sigma_{DA}(\xi)]^{-1}, \\ S_{AD}(\xi) &= [S_{DA}(\xi)]^* = -[\sigma_{AA}(\xi) - \sigma_{AD}(\xi) \sigma_{DD}^{-1}(\xi) \sigma_{DA}(\xi)]^{-1} \sigma_{AD}(\xi) \sigma_{DD}^{-1}(\xi) \\ S_{DD}(\xi) &= [\sigma_{DD}(\xi) - \sigma_{DA}(\xi) \sigma_{AA}^{-1}(\xi) \sigma_{AD}(\xi)]^{-1}. \end{aligned}$$

By Theorem 2.9 and Corollary 2.11 we know that

$$\sigma_{AA}(\xi) \sim |\xi|^2, \quad \sigma_{DD}(\xi) \sim I, \quad S_{AA}(\xi) \sim |\xi|^{-2}, \quad \text{and} \quad S_{DD}(\xi) \sim I,$$

from which it follows that $|S_{AD}(\xi)| \leq C|\xi|^{-1}$. Thus, to lowest order, we have

$$\sigma(\xi)^{-1} = \Psi_A S_{AA}(\xi) \Psi_A^t + O(|\xi|^{-1}), \quad \text{as } |\xi| \rightarrow 0.$$

from which (2.13) follows. We can extract the dominant term in $S_{AA}(\xi)$ by defining

$$(2.15) \quad \sigma_0(\xi) := \left[\lim_{\varepsilon \rightarrow 0} \varepsilon^2 S_{AA}(\varepsilon\xi) \right]^{-1} = \lim_{\varepsilon \rightarrow 0} \frac{1}{\varepsilon^2} \left[\sigma_{AA}(\varepsilon\xi) - \sigma_{AD}(\varepsilon\xi)\sigma_{DD}(0)^{-1}\sigma_{DA}(\varepsilon\xi) \right],$$

since then $S_{AA}(\xi) = \sigma_0(\xi)^{-1} + O(|\xi|^{-1})$. Note that with M the matrix specified by Corollary 2.10 we have $\sigma_0(\xi) = \xi \cdot ((tM)\xi)$ for some constant t and that tM is easily computed since the only matrix inversion that appears in (2.15) concerns a matrix with constant coefficients. To sum up:

Lemma 2.12: *Consider the conduction problem on a connected lattice. To lowest order, all terms of $\sigma(\xi)^{-1}$ are identical. In particular, with σ_0 defined by (2.15), we have, as $|\xi| \rightarrow 0$,*

$$\sigma(\xi)^{-1} = \Psi_A \sigma_0(\xi)^{-1} \Psi_A^t + O(|\xi|^{-1}).$$

3.3. Mechanical trusses. The analysis of mechanical truss systems follows the analysis of the conduction problem closely. The main difference is that the space of rigid body motions (which forms the null-space \mathcal{N} for mechanical problems) is considerably richer than the set of constants, which makes the use of Lemmas 2.6 and 2.7 somewhat less straight-forward. Another difference is that we need to think of $\sigma(\xi)$ as a matrix consisting of $q \times q$ blocks, each of size $d \times d$. In particular, the result for trusses that corresponds to (2.13) says that all *blocks* of $\sigma(\xi)^{-1}$ are equal to lowest order. To be precise, there exists a matrix $\sigma_0(\xi) \in \mathbb{R}^{d \times d}$, such that

$$(2.16) \quad [\sigma(\xi)^{-1}]_{\kappa\lambda} = \sigma_0(\xi)^{-1} + O(|\xi|^{-1}).$$

All entries of the matrix $\sigma_0(\xi)$ are second order polynomials and σ_0 is the Fourier representation of an elasticity operator (which is a second order elliptic differential operator).

In order to define the projection operators Ψ_A and Ψ_D that are pertinent to the truss problem, we first define I_p as the identity matrix in \mathbb{C}^p , set $\Psi_A := q^{-1/2}[I_d, \dots, I_d]^t$ and define Ψ_D so that $\Psi = [\Psi_A, \Psi_D]$ forms a unitary matrix. Then define splittings $\varphi = \varphi_A \oplus \varphi_D$, and $\mathbf{u} = \mathbf{u}_A \oplus \mathbf{u}_D$ as before. Finally set $L(\xi) = \text{diag}(|\xi|^2 I_d, I_{d(q-1)})$.

Theorem 2.13: *For a locally \mathcal{N} -coercive truss lattice, $\sigma(\xi) \sim \Psi L(\xi) \Psi^t$.*

Proof: The proof follows the proof of Theorem 2.9 closely. We use Lemma 2.6, choosing $\mathbf{v} = \varphi_A$, to prove the upper bound. For the lower bound, define $l_A(\xi)$ and $l_D(\xi)$ according to the formulae (2.14). These functions are still positive for $\xi \neq 0$, by virtue of the fact that $\mathbf{u}(m) = \varphi e^{-i\xi \cdot m} \notin \mathcal{N}$ and we only need to investigate their behavior for small ξ . Since $\mathbf{u}(0)$ is orthogonal (in V_2) to the set of rotations, one proves that $l_D(0) > 0$ in a fashion fully analogous to the conduction problem. However, since the nullspace is larger for the present problem than for the conduction problem, we need to put more effort into proving that $l_A(\xi) \geq c|\xi|^2$.

First note that

$$\langle \varphi, \sigma(\xi), \varphi \rangle = \inf_{\mathbf{v} \in \mathcal{N}} (\|\mathbf{u}_A - \mathbf{v}_A\|_{V_2}^2 + \|\mathbf{u}_D - \mathbf{v}_D\|_{V_2}^2) \geq c \inf_{\mathbf{v} \in \mathcal{N}} \|\mathbf{u}_A - \mathbf{v}_A\|_{V_2}^2.$$

It will be sufficient to keep the linear part of $\mathbf{u}(m)$ so we write

$$\mathbf{u}_A(m) = \varphi_A e^{-i\mathbf{m} \cdot \xi} = \varphi_A - \varphi_A i\mathbf{m} \cdot \xi - \varphi_A (1 - i\mathbf{m} \cdot \xi - e^{-i\mathbf{m} \cdot \xi}),$$

and use the inequality $|a + b|^2 \geq |a|^2 - |b|^2$ to obtain that

$$(2.17) \quad \begin{aligned} \langle \varphi, \sigma(\xi), \varphi \rangle &\geq c \inf_{\mathbf{v} \in \mathcal{N}} \left(\|\varphi_A - \varphi_A i(\mathbf{m} \cdot \xi) - \mathbf{v}_A\|_{V_2}^2 - \|\varphi_A (1 - i\mathbf{m} \cdot \xi - e^{-i\mathbf{m} \cdot \xi})\|_{V_2}^2 \right) \\ &\geq c \inf_{\mathbf{v} \in \mathcal{N}} \|\varphi_A - \varphi_A i(\mathbf{m} \cdot \xi) - \mathbf{v}_A\|_{V_2}^2 - |\varphi_A|^2 |\xi|^4. \end{aligned}$$

Let $\mathbf{v}_A^{(\min)}$ denote the minimizer in the last term. Since $\mathbf{v}^{(\min)}$ is a rigid body motion, $\mathbf{v}_A^{(\min)}$ can be written as a sum of a constant and a rotational component, $\mathbf{v}_A^{(\min)} = \mathbf{v}_{\text{const}}^{(\min)} + \mathbf{v}_{\text{rot}}^{(\min)}$. Clearly $\mathbf{v}_{\text{const}}^{(\min)} = \varphi_A$. In order to determine $\mathbf{v}_{\text{rot}}^{(\min)}$, we introduce a basis for the rotations on \mathbb{R}^d : For $i, j \in \{1, \dots, d\}$ such that $j - i > 0$, define the basis-vectors $\mathbf{w}^{(ij)} \in \mathcal{N}$ by $[\mathbf{w}^{(ij)}(m)]_k = \delta_{ik}m_j - \delta_{jk}m_i$. The minimizing problem can now be written

$$(2.18) \quad \inf_{\mathbf{v} \in \mathcal{N}} \|\varphi_A(m \cdot \xi) - \mathbf{v}_A\|_{V_2}^2 = \inf_{\alpha^{(ij)}} \|\varphi_A(m \cdot \xi) - \sum_{i=1}^{d-1} \sum_{j=i+1}^d \alpha^{(ij)} \mathbf{w}^{(ij)}(m)\|_{V_2}^2.$$

The vectors $\mathbf{w}^{(ij)}$ are orthogonal in V_2 , so the minimizers are given by

$$\alpha^{(ij), \min} = \frac{\langle \varphi_A(m \cdot \xi), \mathbf{w}^{(ij)}(m) \rangle_{V_2}}{\|\mathbf{w}^{(ij)}(m)\|_{V_2}^2} = \dots = \frac{1}{2}(\varphi_{A,i}\xi_j - \varphi_{A,j}\xi_i).$$

We insert these values into (2.18) to obtain

$$\inf_{\alpha^{(ij)}} \|\varphi_A(m \cdot \xi) - \sum_{i=1}^d \sum_{j=i+1}^d \alpha^{(ij)} \mathbf{w}^{(ij)}(m)\|_{V_2}^2 = \dots = 5^d (|\varphi_A|^2 |\xi|^2 + |\varphi_A \cdot \xi|^2) \geq |\varphi_A|^2 |\xi|^2.$$

Combining this expression with (2.17) we find that

$$\langle \varphi, \sigma(\xi), \varphi \rangle \geq c (|\varphi_A|^2 |\xi|^2 - |\varphi_A|^2 |\xi|^4) \geq c |\xi|^2 |\varphi_A|^2,$$

in some neighbourhood of the origin. This completes the proof. \square

Corollary 2.14: *For a locally \mathcal{N} -coercive truss lattice, $\det \sigma(\xi) \geq c |\xi|^{2d}$.*

Corollary 2.15: *For a locally \mathcal{N} -coercive truss lattice, $\sigma(\xi)^{-1} \sim \Psi L(\xi)^{-1} \Psi^t$.*

Defining $\sigma_{\alpha\beta}$ and $S_{\alpha\beta}$ as for the conduction problem, and performing the corresponding analysis, we find that the matrix σ_0 heralded in (2.16) is given by

$$(2.19) \quad \sigma_0(\xi) := \lim_{\varepsilon \rightarrow 0} \frac{1}{\varepsilon^2} [\sigma_{AA}(\varepsilon\xi) - \sigma_{AD}(\varepsilon\xi) \sigma_{DD}(0)^{-1} \sigma_{DA}(\varepsilon\xi)].$$

Lemma 2.16: *Suppose that $\sigma(\xi)$ is the symbol of a locally \mathcal{N} -coercive truss lattice. To lowest order, all blocks of $\sigma(\xi)^{-1}$ are identical. In particular, with σ_0 defined by (2.19), we have, as $|\xi| \rightarrow 0$,*

$$\sigma(\xi)^{-1} = \Psi_A \sigma_0(\xi)^{-1} \Psi_A^t + O(|\xi|^{-1}).$$

3.4. Mechanical frames. For mechanical frames, the links are \mathcal{N} -coercive, so we can again use connectivity as the only regularity requirement on the lattice. The significant additional difficulty about the frame case is that the operator treats the rotational and translational degrees of freedom in distinctly different manners. Splitting the cell-wise average of a function $\varphi \in \mathbb{C}^{p_d}$ into an average of the translational components φ_{at} , an average of the rotational components φ_{ar} and “the rest”, φ_{d} , we will prove that

$$(2.20) \quad c (|\xi|^2 |\varphi_{\text{at}}|^2 + |\varphi_{\text{ar}}|^2 + |\varphi_{\text{d}}|^2) \leq \langle \varphi, \sigma(\xi), \varphi \rangle \leq C (|\xi|^2 |\varphi_{\text{at}}|^2 + |\varphi_{\text{ar}}|^2 + |\varphi_{\text{d}}|^2).$$

The projection operators Ψ_{at} and Ψ_{ar} are defined by

$$\begin{aligned} [\Psi_{\text{at}}\varphi]_i &= \frac{1}{\sqrt{q}} \sum_{j=1}^q \varphi_{i+(j-1)p}, & \text{for } i = 1, \dots, d, \\ [\Psi_{\text{ar}}\varphi]_i &= \frac{1}{\sqrt{q}} \sum_{j=1}^q \varphi_{i+(j-1)p}, & \text{for } i = d+1, \dots, p, \end{aligned}$$

and then Ψ_{d} is defined so that $\Psi = [\Psi_{\text{at}}, \Psi_{\text{ar}}, \Psi_{\text{d}}]$ forms a unitary matrix. The splittings $\varphi = \varphi_{\text{at}} \oplus \varphi_{\text{ar}} \oplus \varphi_{\text{d}}$ and $\mathbf{u} = \mathbf{u}_{\text{at}} \oplus \mathbf{u}_{\text{ar}} \oplus \mathbf{u}_{\text{d}}$ follow. Finally set $L(\xi) = \text{diag}(|\xi|^2 I_d, I_{pq-d})$.

Theorem 2.17: *For a connected frame lattice, $\sigma(\xi) \sim \Psi L(\xi) \Psi^t$.*

Proof: Set $\mathbf{u}(m, \kappa) = \varphi(\kappa) e^{-im \cdot \xi}$, as usual. In order to prove the upper bound in (2.20), simply use Lemma 2.6 with $\mathbf{v}(m, \kappa) = [\varphi_{\text{at}}^t, 0]^t$. For the lower bound, define

$$l_{\text{at}}(\xi) = \inf_{|\varphi|=1} \frac{1}{2} \frac{\langle \varphi, \sigma(\xi), \varphi \rangle}{|\varphi_{\text{at}}|^2}, \quad \text{and} \quad l_{\text{X}}(\xi) = \inf_{|\varphi|=1} \frac{1}{2} \frac{\langle \varphi, \sigma(\xi), \varphi \rangle}{|\varphi_{\text{ar}}|^2 + |\varphi_{\text{d}}|^2}.$$

Since the infimums are taken over compact sets and since $\mathbf{u} \notin \mathcal{N}$ when $\xi \neq 0$, it is clear that both l_{at} and l_{X} are strictly positive for $\xi \neq 0$. Likewise, if $l_{\text{X}}(0) = 0$, then by compactness there must exist a minimizer φ' such that $\langle \varphi', \sigma(0), \varphi' \rangle = 0$. By lemma 2.5, this means that the function \mathbf{u}' generated by φ' must belong to \mathcal{N} . Now, since \mathbf{u}' is constant from cell to cell, it cannot have a rotational component, and must therefore be a pure translation. But this implies that $\varphi'_{\text{ar}} = \varphi'_{\text{d}} = 0$, which shows that such a minimizer cannot exist.

Finally we need to prove that $l_{\text{at}}(\xi) \geq c|\xi|^2$. Starting with the simple inequality

$$\langle \varphi, \sigma(0), \varphi \rangle \geq c \inf_{\mathbf{v} \in \mathcal{N}} \|\mathbf{u} - \mathbf{v}\|_{V_1}^2 \geq c \inf_{\mathbf{v} \in \mathcal{N}} \|\mathbf{u}_{\text{at}} - \mathbf{v}_{\text{at}}\|_{V_1}^2,$$

this part of the proof then proceeds exactly like the corresponding part of the proof for trusses. \square

Corollary 2.18: *For a locally \mathcal{N} -coercive frame lattice, $\det \sigma(\xi) \geq c|\xi|^{2d}$.*

Corollary 2.19: *For a locally \mathcal{N} -coercive frame lattice, $\sigma(\xi)^{-1} \sim \Psi L(\xi)^{-1} \Psi^t$.*

In order to prove a result about the dominant terms of $\sigma(\xi)^{-1}$, we set $\Psi_{\text{A}} := \Psi_{\text{at}}$, $\Psi_{\text{D}} := [\Psi_{\text{ar}}, \Psi_{\text{d}}]$ and define $\sigma_{\alpha\beta}$ for $\alpha, \beta = \text{A}, \text{D}$ accordingly.

Lemma 2.20: *Suppose that $\sigma(\xi)$ is the symbol of a connected frame lattice. Then, with σ_0 defined by (2.19), we have, as $|\xi| \rightarrow 0$,*

$$\sigma(\xi)^{-1} = \Psi_{\text{A}} \sigma_0^{-1}(\xi) \Psi_{\text{A}}^t + O(|\xi|^{-1}).$$

Note in particular that according to the lemma, several entries of the inverse symbol have singularities that are weaker than the $O(|\xi|^{-2})$ -singularity of the dominant terms. The consequences of this imbalance will be discussed further in Section 6 of Ch. 3.

4. Well-posedness of the lattice equations

4.1. Introduction. In this section we will study the well-posedness of the equation

$$(2.21) \quad \begin{cases} \mathfrak{A}\mathbf{u} = \mathbf{f}, \\ \|\mathbf{u}\|_{\mathfrak{A}} < \infty. \end{cases}$$

Guided by the findings in the previous section, we will suppose that there exists a unitary matrix $\Psi = [\Psi_A, \Psi_D] \in \mathbb{R}^{qp \times qp}$ such that

$$(2.22) \quad \sigma(\xi) \sim |\xi|^2 \Psi_A \Psi_A^t + \Psi_D \Psi_D^t.$$

Note that this inequality implies that the point $\{0\}$ forms part of the spectrum of \mathfrak{A} , and thus \mathfrak{A}^{-1} cannot be a bounded operator on V . However, the zero is not an eigenvalue, which means that \mathfrak{A} is injective, and we expect to be able to define \mathfrak{A}^{-1} on a dense subset of V .

In this section, we will first derive an explicit representation for \mathfrak{A}^{-1} in terms of Fourier integrals, and then study a variational formulation of (2.21). The second approach will give somewhat sharper results, but in the remainder of the thesis, we will work extensively with the Fourier inverse, and it is therefore necessary to study this formulation as well.

4.2. A Fourier inverse. A solution \mathbf{u} of equation (2.21) is given by $\tilde{\mathbf{u}} = \sigma^{-1} \tilde{\mathbf{f}}$. Using the Fourier inversion formula, we therefore expect that the solution should be

$$(2.23) \quad \mathbf{u}(m) = [\mathfrak{A}^{-1} \mathbf{f}](m) = \left[\mathcal{F}^{-1}[\sigma^{-1} \tilde{\mathbf{f}}] \right](m) = \frac{1}{(2\pi)^d} \int_{I^d} e^{-im \cdot \xi} \sigma(\xi)^{-1} \tilde{\mathbf{f}}(\xi) d\xi.$$

Note however that the function $\sigma(\xi)^{-1}$ is unbounded which necessitates an investigation of when the integral is well-defined. Setting $S_{\alpha\beta}(\xi) = \Psi_\alpha^t \sigma(\xi)^{-1} \Psi_\beta$, the condition (2.22) implies that

$$(2.24) \quad \begin{aligned} |S_{AA}(\xi)| &= |\Psi_A^t \sigma(\xi)^{-1} \Psi_A| \leq C |\xi|^{-2}, \\ |S_{AD}(\xi)| &= |\Psi_A^t \sigma(\xi)^{-1} \Psi_D| \leq C |\xi|^{-1}, \\ |S_{DA}(\xi)| &= |\Psi_D^t \sigma(\xi)^{-1} \Psi_A| \leq C |\xi|^{-1}, \\ |S_{DD}(\xi)| &= |\Psi_D^t \sigma(\xi)^{-1} \Psi_D| \leq C. \end{aligned}$$

Defining the function spaces

$$\Xi_k^r := \{\mathbf{v} \in \mathcal{V} : \|\mathbf{v}\|_{\Xi_k^r} < \infty\}, \quad \text{where} \quad \|\mathbf{v}\|_{\Xi_k^r} = \left[\int_{I^d} (|\xi|^{-k} |\tilde{\mathbf{v}}(\xi)|)^r d\xi \right]^{1/r},$$

we can then state the following result. (Note that $\Xi_0^2 = l^2$.)

Theorem 2.21: *Suppose that \mathbf{f} is a function such that $\mathbf{f}_A \in \Xi_2^1 \cap \Xi_1^2$ and $\mathbf{f}_D \in \Xi_1^1 \cap \Xi_0^2$. Then equation (2.21) has a solution given by (2.23), such that $\langle \mathbf{u}, \mathfrak{A}, \mathbf{u} \rangle \leq C \left(\|\mathbf{f}_A\|_{\Xi_1^2}^2 + \|\mathbf{f}_D\|_{\Xi_0^2}^2 \right)$.*

Proof: The Fourier integral in (2.23) is well-defined since

$$\begin{aligned} |\sigma(\xi)^{-1} \tilde{\mathbf{f}}(\xi)| &\leq (|S_{AA}(\xi)| + |S_{DA}(\xi)|) |\tilde{\mathbf{f}}_A(\xi)| + (|S_{AD}(\xi)| + |S_{DD}(\xi)|) |\tilde{\mathbf{f}}_D(\xi)| \\ &\leq C \left(|\xi|^{-2} |\tilde{\mathbf{f}}_A(\xi)| + |\xi|^{-1} |\tilde{\mathbf{f}}_D(\xi)| \right) \in L^1(I^d). \end{aligned}$$

In order to demonstrate that \mathbf{u} solves (2.21), simply apply \mathfrak{A} to the integral, use the absolute convergence to move the operator inside the integral, and note that $\mathfrak{A}(\varphi e^{-in \cdot \xi}) = \sigma(\xi) \varphi e^{-in \cdot \xi}$.

When proving the bound for $\|\mathbf{u}\|_A = \sqrt{\langle \mathbf{u}, \mathfrak{A}, \mathbf{u} \rangle}$ we use that $\tilde{\mathbf{u}} = \sigma^{-1} \tilde{\mathbf{f}}$ to obtain

$$\|\mathbf{u}\|_{\mathfrak{A}}^2 = \frac{1}{(2\pi)^d} \int_{I^d} \overline{\tilde{\mathbf{u}}(\xi)} [\sigma(\xi) \tilde{\mathbf{u}}(\xi)] d\xi = \frac{1}{(2\pi)^d} \int_{I^d} \overline{\tilde{\mathbf{f}}(\xi)} [\sigma(\xi)^{-1} \tilde{\mathbf{f}}(\xi)] d\xi \leq \int_{I^d} \left(\frac{|\tilde{\mathbf{f}}_A(\xi)|^2}{|\xi|^2} + |\tilde{\mathbf{f}}_D(\xi)|^2 \right) d\xi.$$

□

In order to illuminate the nature of the spaces Ξ_k^r , we provide the following lemmas.

Lemma 2.22: *If $kr < d$, then $\|\cdot\|_{\Xi_k^r} \leq C\|\cdot\|_{l^1}$ and thus $l^1(\Omega) \subseteq \Xi_k^r$.*

Proof: If $\mathbf{v} \in l^1$, then $|\tilde{\mathbf{v}}(\xi)| \leq C\|\mathbf{v}\|_{l^1}$, and thus

$$\|\mathbf{v}\|_{\Xi_k^r}^r = \int_{I^d} (|\xi|^{-k} |\tilde{\mathbf{v}}(\xi)|)^r d\xi \leq C \int_0^{\sqrt{d}\pi} (\rho^{-k} \|\mathbf{v}\|_{l^1})^r \rho^{d-1} d\rho = C \|\mathbf{v}\|_{l^1}^r \int_0^{\sqrt{d}\pi} \rho^{d-kr-1} d\rho,$$

which is finite if $d - kr > 0$. \square

Lemma 2.23: *A sufficient condition for $\mathbf{v} \in \Xi_k^r$ is that for some integer $l > k - d/r$ the following conditions hold:*

A: $\sum (1 + |m|^l) |\mathbf{v}(m)| < \infty$.

B: $\sum m^\alpha \mathbf{v}(m) = 0$, for every $\alpha \in \mathbb{N}^d$ such that $|\alpha| < l$.

Proof: Condition **A** implies that $\tilde{\mathbf{v}}$ has l continuous derivatives, and then condition **B** implies that $\tilde{\mathbf{v}}$ has l vanishing moments. Thus, $|\tilde{\mathbf{v}}(\xi)| \leq C|\xi|^l$, whence

$$\|\mathbf{v}\|_{\Xi_k^r}^r = \int_{I^d} (|\xi|^{-k} |\tilde{\mathbf{v}}(\xi)|)^r d\xi \leq C \int_{I^d} (|\xi|^{-k} |\xi|^l)^r d\xi \leq C \int_0^{\sqrt{d}\pi} \rho^{r(l-k)} \rho^{d-1} d\rho,$$

which is finite if $r(l - k) + d > 0$. \square

Combining Theorem 2.21 with either Lemma 2.22 or Lemma 2.23, we obtain the next two results, which give more familiar conditions on \mathbf{f} than does Theorem 2.21.

Corollary 2.24: *Suppose that $d = 3$ and that $\mathbf{f} \in l^1(\Omega)$. Then one solution of equation (2.21) is provided by (2.23). This solution satisfies $\|\mathbf{u}\|_{\mathfrak{A}} \leq C\|\mathbf{f}\|_{l^1}$.*

Corollary 2.25: *Suppose that $d = 2$, that $m\mathbf{f}(m) \in l^1(\Omega)$ and that $\sum \mathbf{f} = 0$. Then one solution of equation (2.21) is provided by (2.23). This solution satisfies $\|\mathbf{u}\|_{\mathfrak{A}} \leq C\|m\mathbf{f}(m)\|_{l^1}$.*

Note that for an \mathcal{N} -coercive operator, any two solutions \mathbf{u} and \mathbf{v} of (2.21) satisfy $\mathbf{u} - \mathbf{v} \in \mathcal{N}$.

4.3. Variational analysis. It is unsatisfactory that the existence results in the previous section require conditions on \mathbf{f} that do not appear in the stability bounds. This is a consequence of the unnecessarily stringent requirement that the integral (2.23) be absolutely convergent. We will provide results that require only that $\mathbf{f}_A \in \Xi_1^2$ and $\mathbf{f}_D \in \Xi_0^2 = l^2$ by studying the variational formulation

$$\langle \mathbf{v}, \mathfrak{A}, \mathbf{u} \rangle = \langle \mathbf{v}, \mathbf{f} \rangle$$

easily obtained from equation (2.21). We must find a Hilbert space in which the sesqui-linear form $\langle \cdot, \mathfrak{A}, \cdot \rangle$ is coercive, and the semi-linear form $\Lambda_{\mathbf{f}}(\cdot) = \langle \cdot, \mathbf{f} \rangle$ is bounded.

First we define an inner product that is equivalent to $\langle \cdot, \cdot \rangle_{\mathfrak{A}}$. Introduce the discrete Laplace operator \mathfrak{A}_o and its Fourier transform $\sigma_o(\xi)$ by

$$(2.25) \quad \mathfrak{A}_o := \sum_{j=1}^d (-\tau_{e_j} + 2 - \tau_{-e_j}), \quad \sigma_o(\xi) := \sum_{j=1}^d \left(-e^{-i\xi_j} + 2 - e^{i\xi_j} \right) = \sum_{j=1}^d 4 \sin^2 \frac{\xi_j}{2},$$

and set

$$\langle \mathbf{v}, \mathbf{u} \rangle_W := \langle \mathbf{v}_A, \mathfrak{A}_o, \mathbf{u}_A \rangle + \langle \mathbf{v}_D, \mathbf{u}_D \rangle = \frac{1}{(2\pi)^d} \int_{I^d} \left[\sigma_o(\xi) \left(\overline{\tilde{\mathbf{v}}_A(\xi)} \cdot \tilde{\mathbf{u}}_A(\xi) \right) + \overline{\tilde{\mathbf{v}}_D(\xi)} \cdot \tilde{\mathbf{u}}_D(\xi) \right] d\xi.$$

Then the corresponding semi-norm $\|\cdot\|_W = \sqrt{\langle \cdot, \cdot \rangle_W}$ is equivalent to $\|\cdot\|_{\mathfrak{A}}$, by virtue of (2.22). We next define the space W as the closure of the set of compactly supported functions in \mathcal{V} under the norm $\|\cdot\|_W$ (identifying functions for which $\|\mathbf{u}\|_W = 0$ with zero). We now find that Λ_f is bounded precisely when $f_A \in \Xi_1^2$ and $f_D \in \Xi_0^2$:

$$\begin{aligned} |\Lambda_f(\mathbf{v})| &\leq C \int_{I^d} \left(|\tilde{\mathbf{v}}_A(\xi)| |\tilde{f}_A(\xi)| + |\tilde{\mathbf{v}}_D(\xi)| |\tilde{f}_D(\xi)| \right) d\xi \\ &\leq C \left[\int_{I^d} \frac{|\tilde{f}_A(\xi)|^2}{\sigma_\circ(\xi)} d\xi \right]^{1/2} \left[\int_{I^d} \sigma_\circ(\xi) |\tilde{\mathbf{v}}_A(\xi)|^2 d\xi \right]^{1/2} + \|\mathbf{v}_D\| \|f_D\| \leq C \|\mathbf{v}\|_W \left(\|f_A\|_{\Xi_1^2}^2 + \|f_D\|_{\Xi_0^2}^2 \right). \end{aligned}$$

Thus, a well-posed formulation of (2.21) is:

$$(2.26) \quad \text{Find } \mathbf{u} \in W \text{ such that } \langle \mathbf{v}, \mathfrak{A}, \mathbf{u} \rangle = \Lambda_f(\mathbf{v}) \text{ for every } \mathbf{v} \in W.$$

A straight-forward application of the Riesz' representation theorem now gives:

Theorem 2.26: *Suppose that $f_A \in \Xi_1^2$ and $f_D \in \Xi_0^2$. Then equation (2.26) has a unique solution. This solution satisfies $\|\mathbf{u}\|_W \leq C(\|f_A\|_{\Xi_1^2} + \|f_D\|_{\Xi_0^2})$.*

We close by remarking that the requirement that the solution belong to W gives a stronger uniqueness-result than \mathcal{N} -coercivity by itself. First note that

$$\|\mathbf{u}\|_W^2 = \sum_{m \in \mathbb{Z}^d} \left[\sum_{j=1}^d |\mathbf{u}_A(m - e_j) - \mathbf{u}_A(m)|^2 + |\mathbf{u}_D(m)|^2 \right].$$

Thus, if $\|\mathbf{u}\|_W = 0$, then $\mathbf{u}_D = 0$ and \mathbf{u}_A is constant from cell to cell. Now, suppose that both \mathbf{u} and \mathbf{v} solve (2.21). Then $\|\mathbf{u} - \mathbf{v}\|_W = 0$ which means that $\mathbf{u}_D = \mathbf{v}_D$ and $\mathbf{u}_A = \mathbf{v}_A + \varphi$, for some constant $\varphi \in \Psi_A^t \mathbb{C}^{qp}$. Applying this reasoning to the lattice models discussed in this section we find the following result:

Proposition 2.27: *Suppose that $\mathbf{u}, \mathbf{v} \in W$ solve (2.21). Then for conduction problems, \mathbf{u} and \mathbf{v} differ by a constant only. For mechanical problems (either trusses or frames), they differ by a constant translation only.*

CHAPTER 3

Homogenization

1. Introduction

In this section we will show that when the size of the unit cell in a lattice is much smaller than the length-scale over which the load changes, then oftentimes, an approximate solution to the lattice equation can be found by solving a quasi-differential equation with constant coefficients.

We capture the concept of different lengthscales by supposing that the scale over which the load changes is 1, and the cell size is $\varepsilon \ll 1$. A lattice potential will now be denoted $\mathbf{u}^{(\varepsilon)}$ to mark that it is a potential on a scaled lattice, and the corresponding lattice operator is $\mathfrak{A}^{(\varepsilon)}$. The lattice load $\mathfrak{f}^{(\varepsilon)}$ is assumed to be derived from some fix function f by an operator P_ε that projects a function of a continuous variable to a lattice function, $\mathfrak{f}^{(\varepsilon)} := P_\varepsilon f$. This projection will be done by a local averaging in such a way that for a “nice” function f , we will get $\mathfrak{f}^{(\varepsilon)}(m) \approx f(\varepsilon m)$. The scaled lattice equation now reads

$$\mathfrak{A}^{(\varepsilon)} \mathbf{u}^{(\varepsilon)} = \mathfrak{f}^{(\varepsilon)}.$$

The main purpose of this section is to demonstrate how for any p , one can derive constant coefficient, quasi-differential operators $A^{(\varepsilon,p)}$ such that the solution $u^{(\varepsilon,p)}$ of the *homogenized* equation

$$A^{(\varepsilon,p)} u^{(\varepsilon,p)} = f,$$

satisfies

$$\mathbf{u}^{(\varepsilon)}(m) = u^{(\varepsilon,p)}(\varepsilon m) + O(\varepsilon^{2p+2}),$$

provided that f is regular enough (the regularity requirements will increase quite rapidly with increasing p). Both the derivation of the homogenized equation and the convergence proofs will rely heavily on Fourier methods, *cf.* Babuška and Morgan [5, 46, 47, 48].

We give a detailed description of the homogenization procedue for scalar conduction problems only. However, the corresponding results for more general lattice models can be derived in a very similar fashion, as indicated in section 6.

The plan of the chapter is as follows: In section 2 we formally define the scaled lattices and introduce scaled Fourier transforms and norms. In section 3 we define the projection operator P_ε and prove that the discrete Fourier transform of $P_\varepsilon f$ closely approximates the continuous Fourier transform of f . In section 4 we derive the homogenized equations for the conduction problem on mono-atomic lattices and prove convergence in energy and L^∞ -norms. In section 5 we extend the analysis to multi-atomic conduction problems. In section 6 we indicate how the analysis can be extended to mechanical problems and give some illustrative examples.

2. Scaled lattices and function spaces

Let $\mathbf{u}^{(\varepsilon)}(m, \kappa) \in \mathbb{C}$ denote the potential of the node (m, κ) in the scaled lattice. We measure such potentials using the scaled norms l_ε^p defined by

$$\|\mathbf{u}^{(\varepsilon)}\|_{l_\varepsilon^p} := \left[\varepsilon^d \sum_{m \in \mathbb{Z}^d} |\mathbf{u}^{(\varepsilon)}(m)|^p \right]^{1/p}.$$

We also introduce a scaled Fourier transform

$$\tilde{\mathbf{u}}^{(\varepsilon)}(\xi) = [\mathfrak{F}_\varepsilon \mathbf{u}^{(\varepsilon)}](\xi) := \varepsilon^d \sum_{m \in \mathbb{Z}^d} e^{i\varepsilon m \cdot \xi} \mathbf{u}^{(\varepsilon)}(m), \quad \text{for } \xi \in I_\varepsilon^d := (-\pi/\varepsilon, \pi/\varepsilon)^d.$$

The scaling is chosen so that if $\mathbf{u}^{(\varepsilon)}$ is defined by $\mathbf{u}^{(\varepsilon)}(m) := u(\varepsilon m)$ for some function u of a continuous variable, then $\tilde{\mathbf{u}}^{(\varepsilon)}(\xi)$ is a Riemann sum of the continuous Fourier transform

$$\hat{u}(\xi) = [\mathcal{F}u](\xi) := \int_{\mathbb{R}^d} e^{i x \cdot \xi} u(x) dx,$$

and $\|\mathbf{u}^{(\varepsilon)}\|_{l_\varepsilon^p}^p$ is a Riemann sum of

$$\|u\|_{L^p}^p := \int_{\mathbb{R}^d} |u(x)|^p dx.$$

In particular, if u is “nice” (say smooth and compactly supported), then as $\varepsilon \rightarrow 0$,

$$\tilde{\mathbf{u}}^{(\varepsilon)}(\xi) \rightarrow \hat{u}(\xi), \quad \text{and} \quad \|\mathbf{u}^{(\varepsilon)}\|_{l_\varepsilon^p} \rightarrow \|u\|_{L^p}.$$

For future reference, we note that Plancherel’s lemma takes the form

$$\|\mathbf{u}^{(\varepsilon)}\|_{l_\varepsilon^2}^2 = \frac{1}{(2\pi)^d} \int_{I_\varepsilon^d} |\tilde{\mathbf{u}}^{(\varepsilon)}(\xi)|^2 d\xi = \|\tilde{\mathbf{u}}^{(\varepsilon)}\|_{L^2(I_\varepsilon^d)}^2.$$

We will next determine how the scaled lattice operator $\mathfrak{A}^{(\varepsilon)}$ relates to the unscaled operator \mathfrak{A} . When a link that originally had a conductivity $\alpha^{(\kappa, n, \lambda)}$ is scaled by a factor ε , its new conductivity will be $\varepsilon^{d-2} \alpha^{(\kappa, n, \lambda)}$ (since the cross-section shrinks by a factor ε^{d-1} and the length by a factor ε). The scaled load $\mathfrak{f}^{(\varepsilon)}$ is defined so that the actual source at node (m, κ) is $\varepsilon^d \mathfrak{f}^{(\varepsilon)}(m, \kappa)$. Thus, the factor ε^d cancels and we find that the appropriate scaling is

$$\mathfrak{A}^{(\varepsilon)} := \varepsilon^{-2} \mathfrak{A}.$$

The symbol of the scaled operator, $\sigma^{(\varepsilon)} = \mathfrak{F}_\varepsilon \mathfrak{A}^{(\varepsilon)} \mathfrak{F}_\varepsilon^{-1}$, relates to the unscaled symbol as follows;

$$(3.1) \quad \sigma^{(\varepsilon)}(\xi) = \varepsilon^{-2} \sigma(\varepsilon \xi).$$

whence the inequalities (2.12) take the form

$$(3.2) \quad c (|\xi|^2 |\varphi_A|^2 + \varepsilon^{-2} |\varphi_D|^2) \leq \langle \varphi, \sigma^{(\varepsilon)}(\xi), \varphi \rangle \leq C (|\xi|^2 |\varphi_A|^2 + \varepsilon^{-2} |\varphi_D|^2),$$

and the corresponding inverse inequalities are

$$(3.3) \quad c (|\xi|^{-2} |\varphi_A|^2 + \varepsilon^2 |\varphi_D|^2) \leq \langle \varphi, \sigma^{(\varepsilon)}(\xi)^{-1}, \varphi \rangle \leq C (|\xi|^{-2} |\varphi_A|^2 + \varepsilon^2 |\varphi_D|^2).$$

In the scaled variables, the claim of Lemma 2.12 is that there exists a matrix M such that

$$\sigma^{(\varepsilon)}(\xi)^{-1} = (\xi \cdot (M\xi))^{-1} \Psi_A \Psi_A^t + \varepsilon^2 O(|\varepsilon\xi|^{-1}), \quad \text{as } |\varepsilon\xi| \rightarrow 0.$$

We close this section by giving the scaled lattice equation:

$$(3.4) \quad \begin{cases} \mathfrak{A}^{(\varepsilon)} \mathbf{u}^{(\varepsilon)} = \mathfrak{f}^{(\varepsilon)}, \\ \|\mathbf{u}^{(\varepsilon)}\|_{\mathfrak{A}^{(\varepsilon)}} < \infty. \end{cases}$$

3. Projection operators

In order to derive a projection operator that creates a lattice function out of a function of a continuous variable we fix a compactly supported function μ such that $\int_{\mathbb{R}^d} \mu(x) dx = 1$. Then define the projection operator by taking local averages

$$(3.5) \quad [\mathbb{P}_\varepsilon v](m) = \varepsilon^{-d} \int_{\mathbb{R}^d} v(x) \mu(\varepsilon^{-1}x - m) dx.$$

We use the same function μ to create a function of a continuous variable out of a lattice function. The associated projection operator, \mathbb{P}_ε^* , is defined by

$$[\mathbb{P}_\varepsilon^* \mathbf{v}^{(\varepsilon)}](x) = \sum_{m \in \mathbb{Z}^d} \mathbf{v}^{(\varepsilon)}(m) \mu(\varepsilon^{-1}x - m).$$

Note that \mathbb{P}_ε^* is typically injective but that \mathbb{P}_ε is not. The compact support of μ is important because it implies that the operator $\mathbb{P}_\varepsilon : L^p \rightarrow l_\varepsilon^p$ is bounded.

Lemma 3.1: *If μ is bounded and compactly supported, then for any $p \in [1, \infty]$, there exists a finite C_p such that $\|\mathbb{P}_\varepsilon f\|_{l_\varepsilon^p} \leq C_p \|f\|_{L^p}$.*

Proof: Consider first the case $p < \infty$ and let ω denote the support of μ , then

$$\|\mathbb{P}_\varepsilon f\|_{l_\varepsilon^p}^p = \varepsilon^d \sum_{m \in \mathbb{Z}^d} \left| \frac{1}{\varepsilon^d} \int_{\mathbb{R}^d} \mu\left(\frac{x - \varepsilon m}{\varepsilon}\right) f(x) dx \right|^p = \varepsilon^d \sum_{m \in \mathbb{Z}^d} \left| \int_{\omega+m} \mu(y - m) f(\varepsilon y) dy \right|^p,$$

and using Hölder's inequality, with q the conjugate of p ,

$$\begin{aligned} \|\mathbb{P}_\varepsilon f\|_{l_\varepsilon^p}^p &\leq \varepsilon^d \sum_{m \in \mathbb{Z}^d} \left[\int_{\omega+m} |\mu(y - m)|^q dy \right]^{p/q} \left[\int_{\omega+m} |f(\varepsilon y)|^p dy \right] \\ &\leq \|\mu\|_{L^q}^p \sum_{m \in \mathbb{Z}^d} \int_{\omega+m} |f(x)|^p dx \leq C \|\mu\|_{L^q}^p \|f\|_{L^p}^p, \end{aligned}$$

where in the last step, we used that ω is finite. The case $p = \infty$ is trivial. \square

We can now formulate a scaled incarnation of Theorem 2.26:

Theorem 3.2: *Suppose that $\mathfrak{f}^{(\varepsilon)} = \mathbb{P}_\varepsilon f$ for some function $f \in L^1 \cap L^2$, and that the projection function μ is bounded and compactly supported. Then $\mathbf{u}^{(\varepsilon)} = \mathfrak{F}_\varepsilon^{-1}[(\sigma^{(\varepsilon)})^{-1} \tilde{\mathfrak{f}}^{(\varepsilon)}]$ is well-defined and solves equation 3.4. This solution is unique up to a constant and satisfies*

$$\|\mathbf{u}^{(\varepsilon)}\|_{\mathfrak{A}^{(\varepsilon)}} \leq C(\|f_A\|_{L^1} + \|f_A\|_{L^2} + \varepsilon \|f_D\|_{L^2}),$$

where f_A and f_D are defined pointwise, $f_A(x) := \Psi_A^t f(x)$ and $f_D(x) := \Psi_D^t f(x)$.

Proof: Existence and uniqueness follow from Theorem 2.26, since $\mathbf{f}^{(\varepsilon)} \in l_\varepsilon^1$. For the stability result, use that $\|\mathbf{u}\|_{\mathfrak{X}}^2 = \left\langle \tilde{\mathbf{f}}^{(\varepsilon)}, \sigma^{-1}, \tilde{\mathbf{f}}^{(\varepsilon)} \right\rangle_{L^2(I_\varepsilon^d)}$ and (3.3) to get, with B_1 the unit ball in \mathbb{R}^d ,

$$\|\mathbf{u}\|_{\mathfrak{X}}^2 \leq C \frac{1}{(2\pi)^d} \int_{B_1} \frac{|\tilde{\mathbf{f}}_A^{(\varepsilon)}(\xi)|^2}{|\xi|^2} d\xi + C \frac{1}{(2\pi)^d} \int_{I_\varepsilon^d \setminus B_1} \frac{|\tilde{\mathbf{f}}_A^{(\varepsilon)}(\xi)|^2}{|\xi|^2} d\xi + C \frac{1}{(2\pi)^d} \varepsilon^2 \int_{I_\varepsilon^d} |\tilde{\mathbf{f}}_D^{(\varepsilon)}(\xi)|^2 d\xi.$$

Now use that $|\tilde{\mathbf{f}}_A^{(\varepsilon)}(\xi)| \leq \|\mathbf{f}_A^{(\varepsilon)}\|_{l_\varepsilon^1}$ in the first term, and Plancherel's identity for the other two

$$\begin{aligned} \|\mathbf{u}\|_{\mathfrak{X}}^2 &\leq C \int_{B_1} \frac{\|\mathbf{f}_A^{(\varepsilon)}\|_{l_\varepsilon^1}^2}{|\xi|^2} d\xi + C \int_{I_\varepsilon^d \setminus B_1} |\tilde{\mathbf{f}}_A^{(\varepsilon)}(\xi)|^2 d\xi + C \varepsilon^2 \int_{I_\varepsilon^d} |\tilde{\mathbf{f}}_D^{(\varepsilon)}(\xi)|^2 d\xi \\ &\leq C \left(\|\mathbf{f}_A^{(\varepsilon)}\|_{l_\varepsilon^1}^2 + \|\mathbf{f}_A^{(\varepsilon)}\|_{l_\varepsilon^2}^2 + \varepsilon^2 \|\mathbf{f}_D^{(\varepsilon)}\|_{l_\varepsilon^2}^2 \right), \end{aligned}$$

whence the claim follows from Lemma 3.1. \square

The main results of this chapter concern the asymptotic behavior of the solution $\mathbf{u}^{(\varepsilon)}$ given in Theorem 3.2 as $\varepsilon \rightarrow 0$. This analysis will be carried out primarily on the Fourier side and it is therefore of interest to determine how $\tilde{\mathbf{f}}^{(\varepsilon)}$ relates to $\hat{\mathbf{f}}$ when $\mathbf{f}^{(\varepsilon)} = \mathbf{P}_\varepsilon f$.

Lemma 3.3: *If v and $\mathbf{v}^{(\varepsilon)}$ are functions such that the right hand sides below are well-defined, then*

$$[\mathfrak{F}_\varepsilon \mathbf{P}_\varepsilon v](\xi) = \hat{v}(\xi) \hat{\mu}(\varepsilon \xi) + \sum_{m \in \mathbb{Z}^d, m \neq 0} \hat{v}(\xi + \frac{2\pi}{\varepsilon} m) \hat{\mu}(\varepsilon \xi + 2\pi m), \quad \text{and} \quad [\mathcal{F} \mathbf{P}_\varepsilon^* \mathbf{v}^{(\varepsilon)}](\xi) = \tilde{\mathbf{v}}^{(\varepsilon)}(\xi) \hat{\mu}(\varepsilon \xi).$$

Proof: For the first part set $\mu_{\varepsilon, m}(x) := \mu(\varepsilon^{-1}x - m)$ and apply Plancherel's theorem to (3.5),

$$[\mathbf{P}_\varepsilon v](m) = \frac{1}{\varepsilon^d (2\pi)^d} \int_{\mathbb{R}^d} \hat{v}(\zeta) \hat{\mu}_{\varepsilon, m}(-\zeta) d\zeta = \frac{1}{\varepsilon^d (2\pi)^d} \int_{\mathbb{R}^d} \hat{v}(\zeta) \varepsilon^d e^{-i\varepsilon m \cdot \zeta} \hat{\mu}(\varepsilon \zeta) d\zeta.$$

Inserting this into the definition of \mathfrak{F}_ε gives that

$$(3.6) \quad [\mathfrak{F}_\varepsilon \mathbf{P}_\varepsilon v](\xi) = \int_{\mathbb{R}^d} \hat{v}(\zeta) \hat{\mu}(\varepsilon \zeta) \left(\frac{\varepsilon^d}{(2\pi)^d} \sum_{m \in \mathbb{Z}^d} e^{i\varepsilon(\xi - \zeta) \cdot m} \right) d\zeta.$$

Applying Poisson's summation formula to the function $m \mapsto e^{i\varepsilon(\xi - \zeta) \cdot m}$ we find that

$$\frac{\varepsilon^d}{(2\pi)^d} \sum_{m \in \mathbb{Z}^d} e^{i\varepsilon(\xi - \zeta) \cdot m} = \sum_{m \in \mathbb{Z}^d} \delta(\xi - \zeta + \frac{2\pi}{\varepsilon} m).$$

This identity in combination with (3.6) proves the claim.

The second part is straightforward;

$$[\mathcal{F} \mathbf{P}_\varepsilon^* \mathbf{v}^{(\varepsilon)}](\xi) = \sum_{n \in \mathbb{Z}^d} \mathbf{v}^{(\varepsilon)}(n) \int e^{i\mathbf{x} \cdot \xi} \mu(\varepsilon^{-1}x - n) dx = \sum_{n \in \mathbb{Z}^d} \mathbf{v}^{(\varepsilon)}(n) \int e^{i\varepsilon(y+n) \cdot \xi} \mu(y) \varepsilon^d dy = \tilde{\mathbf{v}}^{(\varepsilon)}(\xi) \hat{\mu}(\varepsilon \xi).$$

\square

For our purposes, it is desirable that $[\mathfrak{F}_\varepsilon \mathbf{P}_\varepsilon f](\xi) = \hat{f}(\xi) + O(\varepsilon^k)$, for some large integer k . In view of the previous lemma, this question appears to be related to whether $\hat{\mu}(\xi) - 1$ has a high

order zero at the origin. In fact, for $O(\varepsilon^{2p+2})$ approximation we need to ask that

$$(3.7) \quad |\hat{\mu}(\xi) - 1| \leq C|\xi|^{2+l}, \quad \text{for } -2 \leq l \leq 2p.$$

We also ask that $\hat{\mu}(\xi)$ decays fast for large ξ (which correspondes to a regularity requirement in physical space) and that $\hat{\mu}(\xi)$ has a high order zero around all points $2\pi n$, for $n \in \mathbb{Z}^d \setminus \{0\}$, *i.e.*

$$(3.8) \quad |\hat{\mu}(\xi - 2\pi n)| \leq C|\xi|^{2+l} \prod_{j=1}^d \frac{1}{1 + n_j^{2(p+1)}}, \quad \text{for } -2 \leq l \leq 2p \quad \text{and } n \in \mathbb{Z}^d \setminus \{0\}.$$

These conditions were formulated by Babuška [4] and Fix and Strang [24, 25]. They correspond to a requirement that μ and its translates should be able to reproduce polynomials of degree $2p + 2$. When they are satisfied, the following result can easily be proved.

Lemma 3.4: *Suppose that μ satisfies (3.7) and (3.8), that P_ε is the corresponding projection and that $\mathfrak{f}^{(\varepsilon)} = P_\varepsilon f$. Then $|\tilde{\mathfrak{f}}^{(\varepsilon)}(\xi) - \hat{f}(\xi)| \leq C|\varepsilon\xi|^{2p+2} \|f\|_{L^1}$.*

We will next demonstrate that it is possible to construct a compactly supported function μ that satisfies (3.7) and (3.8) from basic spline functions. Start by defining the lowest order spline, $\psi^{(1)}$, as the characteristic function for the cube $[-1/2, 1/2]^d$, in other words $\psi^{(1)}(x) = \prod_{j=1}^d \chi_{[-1/2, 1/2]}(x_j)$. Then define the higher splines through successive convolutions $\psi^{(k)} = \psi^{(1)} * \psi^{(k-1)}$ so that

$$\hat{\psi}^{(k)}(\xi) = \prod_{j=1}^d \left(\frac{\sin(\xi_j/2)}{\xi_j/2} \right)^k.$$

Note that $\psi^{(2)}$ satisfies both (3.7) and (3.8) for $p = 0$ and that $\psi^{(2p+2)}$ satisfies (3.8) for any p . However, for $p > 0$, the function $\psi^{(2p+2)}$ does not satisfy (3.7) so we must define μ as a linear combination of high order splines. For example

$$\mu^{(1)}(x) := 3\psi^{(4)}(x) - 2\psi^{(6)}(x)$$

satisfies both conditions for $p = 1$ and

$$\mu^{(2)}(x) := 10\psi^{(6)}(x) - 15\psi^{(8)}(x) + 6\psi^{(10)}(x)$$

works for $p = 2$. We have verified that such constructions exist at least up to $p = 5$.

Henceforth, we will suppose that the projection operators P_ε and P_ε^* are defined using the spline based weight-functions $\mu^{(k)}$, but in principle, any compactly supported and bounded function that satisfies (3.7) and (3.8) could be used.

4. Homogenization of conduction problems on mono-atomic lattices

4.1. Derivation of the homogenized equation. Recall that Theorem 3.2 provides a solution for equation (3.4) that is defined by

$$\tilde{\mathfrak{u}}^{(\varepsilon)}(\xi) := [\sigma^{(\varepsilon)}(\xi)]^{-1} \tilde{\mathfrak{f}}^{(\varepsilon)}(\xi),$$

where $\mathfrak{f}^{(\varepsilon)} = P_\varepsilon f$. According to Lemma 3.4, $\tilde{\mathfrak{f}}^{(\varepsilon)}(\xi) = \hat{f}(\xi) + O(\varepsilon^{2p+2})$. Thus, if we let $S^{(\varepsilon,p)}(\xi)$ denote the first $2p + 2$ terms in the Taylor expansion of the inverse symbol, so that

$$[\sigma^{(\varepsilon)}(\xi)]^{-1} = S^{(\varepsilon,p)}(\xi) + O(\varepsilon^{2p+2}),$$

then

$$\tilde{\mathbf{u}}^{(\varepsilon)}(\xi) = S^{(\varepsilon,p)}(\xi)\hat{f}(\xi) + O(\varepsilon^{2p+2}).$$

We now claim that a function of a continuous variable can be defined by

$$(3.9) \quad u^{(\varepsilon,p)} := \mathcal{F}^{-1} \left[S^{(\varepsilon,p)} \hat{f} \right],$$

and that $\mathbf{u}^{(\varepsilon)}(m) = u^{(\varepsilon,p)}(m) + O(\varepsilon^{2p+2})$. In this section we will (1) prove that the function $u^{(\varepsilon,p)}$ is well-defined, (2) rewrite (3.9) as a (quasi-) differential equation in physical space which is called the *homogenized equation* and (3) prove approximation bounds under certain conditions on f . For now, we restrict attention to conduction problems on mono-atomic lattices, but we will later demonstrate that much of the analysis carries over to multi-atomic lattices (section 5) and more general lattice models (section 6).

4.2. Well-posedness of the homogenized equation. We start by proving that $S^{(\varepsilon,p)}(\xi)$ is a rational function in ξ . To this end, recall that according to Corollary 2.10

$$(3.10) \quad \sigma(\xi) = \xi \cdot M\xi + \sum_{j=2}^{\infty} b_j(\xi), \quad b_j \in \Pi^{2j},$$

where Π^n is the set of homogeneous multinomials of degree n and M is a positive definite matrix.

Lemma 3.5: *Suppose that $\psi(\xi)$ is a function with a convergent series expansion of the form (3.10). Then there exist multinomials $a_{2j} \in \Pi^{4j}$ such that for any $p \in \mathbb{N}$,*

$$\frac{1}{\psi(\xi)} = \frac{1}{\xi \cdot (M\xi)} + \sum_{j=1}^p \frac{a_{2j}(\xi)}{(\xi \cdot M\xi)^{j+1}} + \hat{R}_p(\xi),$$

where the remainder term $\hat{R}_p(\xi)$ satisfies $|\partial^\alpha \hat{R}_p(\xi)| \leq C|\xi|^{2p-|\alpha|}$ in some neighborhood of the origin.

Proof: Using induction, we will prove that

$$(3.11) \quad \hat{R}_p(\xi) = \frac{\sum_{j=2p+2}^{\infty} c_j^p(\xi)}{(\xi \cdot M\xi)^{p+1}\sigma(\xi)}, \quad \text{for } c_j \in \Pi^{2j},$$

and that the multinomials a_{2j} and c_j^p can be determined from the b_j 's through the recursion formula

$$(3.12) \quad \begin{aligned} a_0(\xi) &= 1, & c_j^0(\xi) &= -b_j(\xi), \\ a_{2j}(\xi) &= c_{2j}^{j-1}(\xi), & c_j^{p+1}(\xi) &= -b_{j-2p-2}(\xi)c_{2p+2}^p(\xi) + (\xi \cdot M\xi)c_{j-1}^p(\xi). \end{aligned}$$

Setting $|\xi|_M^2 := \xi \cdot M\xi$, we first verify the statement for $p = 0$,

$$\frac{1}{\sigma(\xi)} = \frac{1}{|\xi|_M^2} + \frac{|\xi|_M^2 - \sigma(\xi)}{|\xi|_M^2 \sigma(\xi)} = \frac{1}{|\xi|_M^2} + \frac{\sum_{j=2}^{\infty} -b_j(\xi)}{|\xi|_M^2 \sigma(\xi)}.$$

Next suppose that it is true up to level $p - 1$, then starting with (3.11) we find

$$\begin{aligned}\hat{R}_{p-1}(\xi) &= \frac{c_{2p}^{p-1}(\xi)}{|\xi|_M^{2p}\sigma(\xi)} + \frac{\sum_{j=2p+1}^{\infty} c_j^{p-1}(\xi)}{|\xi|_M^{2p}\sigma(\xi)} = \\ &= \left[\frac{c_{2p}^{p-1}(\xi)}{|\xi|_M^{2p+2}} + \frac{c_{2p}^{p-1}(\xi)(|\xi|_M^2 - \sigma(\xi))}{|\xi|_M^{2p+2}\sigma(\xi)} \right] + \frac{\sum_{j=2p+1}^{\infty} |\xi|_M^2 c_j^{p-1}(\xi)}{|\xi|_M^{2p+2}\sigma(\xi)} \\ &= \frac{c_{2p}^{p-1}(\xi)}{|\xi|_M^{2p+2}} + \frac{\sum_{j=2p+2}^{\infty} [-c_{2p}^{p-1}(\xi)b_{j-2p}(\xi) + |\xi|_M^2 c_{j-1}^{p-1}(\xi)]}{|\xi|_M^{2p+2}\sigma(\xi)}\end{aligned}$$

which gives the p -level terms of the correct form. \square

Note that the proof provides a simple algorithm for deriving the multinomials a_{2j} from the b_j 's.

Applying the lemma to the scaled symbol $\sigma^{(\varepsilon)}(\xi) = \varepsilon^{-2}\sigma(\varepsilon\xi)$, we find that

$$(3.13) \quad [\sigma^{(\varepsilon)}(\xi)]^{-1} = \frac{1}{\xi \cdot M\xi} + \sum_{j=1}^p \varepsilon^{2j} \frac{a_{2j}(\xi)}{(\xi \cdot M\xi)^{j+1}} + \hat{R}_p^{(\varepsilon)}(\xi), \quad \text{where } |\partial^\alpha \hat{R}_p^{(\varepsilon)}(\xi)| \leq C\varepsilon^{2p+2}|\xi|^{2p-|\alpha|}.$$

This proves our initial claim that $S^{(\varepsilon,p)}$ is a rational function since

$$(3.14) \quad S^{(\varepsilon,p)}(\xi) = \frac{1}{\xi \cdot M\xi} + \sum_{j=1}^p \varepsilon^{2j} \frac{a_{2j}(\xi)}{(\xi \cdot M\xi)^{j+1}}.$$

In dimensions three and higher, $S^{(\varepsilon,p)}$ is a locally integrable rational function, which means that $S^{(\varepsilon,p)}(\xi)\hat{f}(\xi)$ is well-defined as a tempered distribution under very weak conditions on f , say $f \in L^1$. Consequently, the definition (3.9) is well-posed and produces a unique tempered distribution $u^{(\varepsilon,p)}$. Combining (3.9) and (3.14), we find that in a distributional sense

$$(3.15) \quad (-\nabla \cdot M\nabla)^{p+1} u^{(\varepsilon,p)} = (-\nabla \cdot M\nabla)^p f + \sum_{j=1}^p \varepsilon^{2j} (-\nabla M \cdot \nabla)^{p-j} a_{2j}(\partial) f.$$

Note that the right hand side involves derivatives of order $4p$, while the right hand side involves an elliptic operator of order $2p + 2$. This indicates that while the $p = 0$ homogenized equation is regularizing, the equation for $p = 1$ is not, and as p increases the solution $u^{(\varepsilon,p)}$ will be *less* regular than the data. As a consequence, the load must be very smooth indeed for high order homogenizations to be considered.

By combining equation (3.15) with some bounded energy condition, traditional (*i.e.* non-distributional) homogenized equations can be obtained. For instance, the lowest order equation reads

$$(3.16) \quad \begin{cases} -\nabla \cdot M\nabla u^{(0)} = f, \\ |u|_{H^1} < \infty. \end{cases}$$

Note that $u^{(0)} = u^{(\varepsilon,0)}$ does not depend on ε . We give the following existence, uniqueness and stability result for the equation (3.16) since it is instructive to compare this result to Theorem 3.2.

Proposition 3.6: *Suppose that $f \in L^1 \cap L^2$, then (3.9) provides a weak solution $u^{(0)} \in H^1$ for equation (3.16) that is unique up to a constant. This solution satisfies*

$$|u^{(0)}|_{H^1}^2 \leq C (\|f\|_{L^1} + \|f\|_{L^2}).$$

Proof: Let B denote the unit ball and use that $|\hat{u}(\xi)| \leq C|\xi|^{-2}|\hat{f}(\xi)|$ to obtain

$$|u^{(0)}|_{H^1}^2 = \frac{1}{(2\pi)^d} \int_{\mathbb{R}^d} |\xi|^2 |\hat{u}(\xi)|^2 d\xi = \frac{1}{(2\pi)^d} \int_{\mathbb{R}^d} \frac{|\hat{f}(\xi)|^2}{|\xi|^2} d\xi \leq C \int_B \frac{\|f\|_{L^1}^2}{|\xi|^2} d\xi + C \int_{B^c} |\hat{f}(\xi)|^2 d\xi,$$

which is clearly bounded as required. \square

4.3. Convergence proofs. It is time to formally prove that $\mathbf{u}^{(\varepsilon)} = u^{(\varepsilon,p)} + O(\varepsilon^{2p+2})$.

Theorem 3.7: *Suppose that $d \geq 3$, let $\mathbf{u}^{(\varepsilon)}$ be the solution of the lattice equation (3.4), where $\mathfrak{f}^{(\varepsilon)} = \mathbb{P}_\varepsilon f$, and let $u^{(\varepsilon,p)}$ be the approximation defined by (3.9). For ε small and k and l positive integers such that $2p - 2 \leq l \leq 2p$ and $k \leq 2 + l - 2p$ we have*

$$|\mathbb{P}_\varepsilon^* \mathbf{u}^{(\varepsilon)} - u^{(\varepsilon,p)}|_{H^k} \leq C \varepsilon^{2+l-k} \|f\|_{H^l}.$$

Proof: For notational convenience, we set $\sigma^{(\varepsilon,p)}(\xi) := S^{(\varepsilon,p)}(\xi)^{-1}$. Then, since $|\varepsilon\xi|$ is bounded when $\xi \in I_\varepsilon^d$, equation 3.13 implies the following bound:

$$(3.17) \quad \left| \frac{1}{\sigma^{(\varepsilon)}(\xi)} - \frac{1}{\sigma^{(\varepsilon,p)}(\xi)} \right| \leq C \varepsilon^2 |\varepsilon\xi|^l, \quad \text{for } \xi \in I_\varepsilon^d \quad \text{and } 0 \leq l \leq 2p.$$

By invoking Plancherel's equality, the bound can be proved on the Fourier side;

$$\begin{aligned} |\mathbb{P}_\varepsilon^* \mathbf{u}^{(\varepsilon)} - u^{(\varepsilon,p)}|_{H^k}^2 &= \frac{1}{(2\pi)^d} \int_{\mathbb{R}^d} |\xi|^{2k} \left| \tilde{\mathbf{u}}^{(\varepsilon)}(\xi) \hat{\mu}(\varepsilon\xi) - \hat{u}^{(\varepsilon,p)}(\xi) \right|^2 d\xi \\ &= \frac{1}{(2\pi)^d} \int_{I_\varepsilon^d} |\xi|^{2k} |\tilde{\mathbf{u}}^{(\varepsilon)}(\xi) \hat{\mu}(\varepsilon\xi) - \hat{u}^{(\varepsilon,p)}(\xi)|^2 d\xi + \frac{1}{(2\pi)^d} \int_{\mathbb{R}^d \setminus I_\varepsilon^d} |\xi|^{2k} |\tilde{\mathbf{u}}^{(\varepsilon)}(\xi) \hat{\mu}(\varepsilon\xi)|^2 d\xi \\ &\quad + \frac{1}{(2\pi)^d} \int_{\mathbb{R}^d \setminus I_\varepsilon^d} |\xi|^{2k} |\hat{u}^{(\varepsilon,p)}(\xi)|^2 d\xi =: K_1 + K_2 + K_3. \end{aligned}$$

Applying Lemma 3.3 gives that

$$\begin{aligned} K_1 &= \frac{1}{(2\pi)^d} \int_{I_\varepsilon^d} |\xi|^{2k} \left| \frac{\tilde{\mathfrak{f}}^{(\varepsilon)}(\xi) \hat{\mu}(\varepsilon\xi)}{\sigma^{(\varepsilon)}(\xi)} - \frac{\hat{f}(\xi)}{\sigma^{(\varepsilon,p)}(\xi)} \right|^2 d\xi \\ &\leq \underbrace{C \varepsilon^{-2k} \int_{I_\varepsilon^d} \left| \frac{\hat{f}(\xi) \hat{\mu}(\varepsilon\xi)^2}{\sigma^{(\varepsilon)}(\xi)} - \frac{\hat{f}(\xi)}{\sigma^{(\varepsilon,p)}(\xi)} \right|^2 d\xi}_{=: K_{11}} + \underbrace{C \varepsilon^{-2k} \int_{I_\varepsilon^d} \left| \frac{\hat{\mu}(\varepsilon\xi)}{\sigma^{(\varepsilon)}(\xi)} \sum_{n \neq 0} \hat{f}(\xi + \frac{2\pi}{\varepsilon} n) \hat{\mu}(\varepsilon\xi + 2\pi n) \right|^2 d\xi}_{=: K_{12}}. \end{aligned}$$

When bounding K_{11} we use that, by (3.17) and (3.7)

$$\left| \frac{\hat{\mu}^2(\varepsilon\xi)}{\sigma^{(\varepsilon)}(\xi)} - \frac{1}{\sigma^{(\varepsilon,p)}(\xi)} \right|^2 \leq \left| \frac{\hat{\mu}^2(\varepsilon\xi) - 1}{\sigma^{(\varepsilon)}(\xi)} \right|^2 + \left| \frac{1}{\sigma^{(\varepsilon)}(\xi)} - \frac{1}{\sigma^{(\varepsilon,p)}(\xi)} \right|^2 \leq C \varepsilon^4 |\varepsilon\xi|^{2l}.$$

Then, since $|\xi| \leq C \varepsilon^{-1}$ for $\xi \in I_\varepsilon^d$,

$$K_{11} \leq C \varepsilon^{-2k} \int_{I_\varepsilon^d} \left| \frac{\hat{\mu}^2(\varepsilon\xi)}{\sigma^{(\varepsilon)}(\xi)} - \frac{1}{\sigma^{(\varepsilon,p)}(\xi)} \right|^2 |\hat{f}(\xi)|^2 d\xi \leq C \varepsilon^{4+2l-2k} \int_{I_\varepsilon^d} |\xi|^{2l} |\hat{f}(\xi)|^2 d\xi \leq C \varepsilon^{4+2l-2k} \|f\|_{H^l}^2.$$

When bounding K_{12} use first that $|\hat{\mu}(\varepsilon\xi)|$ is bounded,

$$\begin{aligned} K_{12} &\leq \sum_{n \neq 0} \sum_{m \neq 0} C\varepsilon^{-2k} \int_{I_\varepsilon^d} \frac{1}{\sigma^{(\varepsilon)}(\xi)^2} \hat{f}\left(\xi + \frac{2\pi}{\varepsilon}n\right) \hat{\mu}(\varepsilon\xi + 2\pi n) \overline{\hat{f}\left(\xi + \frac{2\pi}{\varepsilon}m\right) \hat{\mu}(\varepsilon\xi + 2\pi m)} d\xi \\ &\leq \sum_{n \neq 0} \sum_{m \neq 0} C\varepsilon^{-2k} \int_{I_\varepsilon^d} \left(\left| \hat{f}\left(\xi + \frac{2\pi}{\varepsilon}n\right) \right|^2 + \left| \hat{f}\left(\xi + \frac{2\pi}{\varepsilon}m\right) \right|^2 \right) \frac{\hat{\mu}(\varepsilon\xi + 2\pi n)}{\sigma^{(\varepsilon)}(\xi)} \frac{\hat{\mu}(\varepsilon\xi + 2\pi m)}{\sigma^{(\varepsilon)}(\xi)} d\xi \end{aligned}$$

Noting that the two terms have the same sum we find that

$$K_{12} \leq \sum_{n \neq 0} \sum_{m \neq 0} C\varepsilon^{-2k} \int_{I_\varepsilon^d} \left| \hat{f}\left(\xi + \frac{2\pi}{\varepsilon}n\right) \right|^2 \frac{\hat{\mu}(\varepsilon\xi + 2\pi n)}{\sigma^{(\varepsilon)}(\xi)} \frac{\hat{\mu}(\varepsilon\xi + 2\pi m)}{\sigma^{(\varepsilon)}(\xi)} d\xi.$$

Then we use (3.8),

$$\begin{aligned} K_{12} &\leq \sum_{n \neq 0} \sum_{m \neq 0} C\varepsilon^{-2k} \int_{I_\varepsilon^d} \left| \hat{f}\left(\xi + \frac{2\pi}{\varepsilon}n\right) \right|^2 \frac{|\varepsilon\xi|^{2+l}}{|\xi|^2} \frac{|\varepsilon\xi|^{2+l}}{|\xi|^2 \prod_{j=1}^d (1 + m_j^{2(p+1)})} d\xi \\ &\leq \sum_{n \neq 0} C\varepsilon^{4+2l-2k} \int_{I_\varepsilon^d} |\xi|^{2l} \left| \hat{f}\left(\xi + \frac{2\pi}{\varepsilon}n\right) \right|^2 d\xi \leq C\varepsilon^{4+2l-2k} \|f\|_{H^l}^2. \end{aligned}$$

We next turn to bounding K_2 . By definition

$$K_2 = \frac{1}{(2\pi)^d} \int_{\mathbb{R}^d \setminus I_\varepsilon^d} |\xi|^{2k} \left| \frac{\tilde{f}^{(\varepsilon)}(\xi) \hat{\mu}(\varepsilon\xi)}{\sigma^{(\varepsilon)}(\xi)} \right|^2 d\xi = \frac{1}{(2\pi)^d} \sum_{n \neq 0} \int_{I_\varepsilon^d} \left| \xi + \frac{2\pi}{\varepsilon}n \right|^{2k} \left| \frac{\tilde{f}^{(\varepsilon)}(\xi) \hat{\mu}(\varepsilon\xi + 2\pi n)}{\sigma^{(\varepsilon)}(\xi)} \right|^2 d\xi$$

Now we invoke the inequality (3.8),

$$K_2 \leq \sum_{n \neq 0} \int_{I_\varepsilon^d} \left| \frac{n}{\varepsilon} \right|^{2k} |\tilde{f}^{(\varepsilon)}(\xi)|^2 \frac{|\varepsilon\xi|^{4+2l}}{|\xi|^4 \prod_{j=1}^d (1 + n_j^{2(p+1)})} d\xi \leq C\varepsilon^{4+2l-2k} \int_{I_\varepsilon^d} |\xi|^{2l} |\tilde{f}^{(\varepsilon)}(\xi)|^2 d\xi.$$

We need to prove that the integral in the last expression is bounded by $\|f\|_{H^l}^2$; by Lemma 3.3,

$$\int_{I_\varepsilon^d} |\xi|^{2l} |\tilde{f}^{(\varepsilon)}(\xi)|^2 d\xi \leq \int_{I_\varepsilon^d} |\xi|^{2l} |\hat{f}(\xi) \hat{\mu}(\varepsilon\xi)|^2 d\xi + \int_{I_\varepsilon^d} |\xi|^{2l} \left| \sum_{n \neq 0} \hat{f}\left(\xi + \frac{2\pi}{\varepsilon}n\right) \hat{\mu}(\varepsilon\xi + 2\pi n) \right|^2 d\xi$$

Expanding the sum as in the bound for K_{12} we find that

$$\int_{I_\varepsilon^d} |\xi|^{2l} |\tilde{f}^{(\varepsilon)}(\xi)|^2 d\xi \leq C\|f\|_{H^l}^2 + C \sum_{n \neq 0} \sum_{m \neq 0} \int_{I_\varepsilon^d} |\xi|^{2l} \left| \hat{f}\left(\xi + \frac{2\pi}{\varepsilon}n\right) \hat{\mu}(\varepsilon\xi + 2\pi n) \hat{\mu}(\varepsilon\xi + 2\pi m) \right|^2 d\xi.$$

By (3.8) the sum over m produces nothing more than a constant. Then use that $\hat{\mu}(\varepsilon\xi + 2\pi n)$ is bounded to obtain

$$\begin{aligned} \int_{I_\varepsilon^d} |\xi|^{2l} |\tilde{f}^{(\varepsilon)}(\xi)|^2 d\xi &\leq C\|f\|_{H^l}^2 + C \sum_{n \neq 0} \int_{I_\varepsilon^d} |\xi|^{2l} \left| \hat{f}\left(\xi + \frac{2\pi}{\varepsilon}n\right) \right|^2 d\xi \\ &\leq C\|f\|_{H^l}^2 + C \sum_{n \neq 0} \int_{I_\varepsilon^d} \left| \xi + \frac{2\pi}{\varepsilon}n \right|^{2l} \left| \hat{f}\left(\xi + \frac{2\pi}{\varepsilon}n\right) \right|^2 d\xi \leq C\|f\|_{H^l}^2, \end{aligned}$$

which shows that K_2 is bounded as required.

Finally we bound K_3 . By definition

$$K_3 = \frac{1}{(2\pi)^d} \int_{\mathbb{R}^d \setminus I_\varepsilon^d} |\xi|^{2k} \left| \frac{\hat{f}(\xi)}{\sigma^{(\varepsilon,p)}(\xi)} \right|^2 d\xi \leq C \int_{\mathbb{R}^d \setminus I_\varepsilon^d} \left(\frac{|\xi|^k}{\sigma^{(\varepsilon,p)}(\xi)} \right)^2 |\hat{f}(\xi)|^2 d\xi.$$

Now use that for $\xi \in \mathbb{R}^d \setminus I_\varepsilon^d$,

$$\frac{|\xi|^k}{\sigma^{(\varepsilon,p)}(\xi)} \leq |\xi|^k C \varepsilon^{2p} |\xi|^{2p-2} = C \varepsilon^{2p} \frac{|\xi|^l}{|\xi|^{2+l-k-2p}} \leq C \varepsilon^{2+l-k} |\xi|^l,$$

since $2+l-k-2p \geq 0$. This immediately yields $K_3 \leq C \varepsilon^{4+2l-2k} \|f\|_{H^l}^2$ and completes the proof. \square

In many cases, $u^{(\varepsilon)} \rightarrow u^{(\varepsilon,p)}$ pointwise, and moreover, this convergence is uniform. Before proving this claim we give a proposition that specifies when $u^{(\varepsilon,p)}$ is continuous.

Proposition 3.8: *Suppose that $f \in L^1 \cap H^{2p+k}$ for some $k > d/2 - 2$. Then the function $u^{(\varepsilon,p)}$ defined by (3.9) is continuous.*

Proof: We prove the claim by proving that $\hat{u}^{(\varepsilon,p)} \in L^1$. First note that, with B the unit ball,

$$\begin{aligned} \|\hat{u}^{(\varepsilon,p)}\|_{L^1} &= \int_{\mathbb{R}^d} |S^{(\varepsilon,p)}(\xi) \hat{f}(\xi)| d\xi \leq C \int_B \frac{|\hat{f}(\xi)|}{|\xi|^2} d\xi + C \int_{B^c} |\xi|^{2p-2} |\hat{f}(\xi)| d\xi \\ &\leq C \int_B \frac{\|f\|_{L^1}^2}{|\xi|^2} d\xi + C \left[\int_{B^c} |\xi|^{-2k-4} d\xi \int_{B^c} |\xi|^{4p+2k} |\hat{f}(\xi)|^2 d\xi \right]^{1/2}, \end{aligned}$$

which is finite precisely when $f \in L^1 \cap H^{2p+k}$ and $2k+4 > d$. \square

Theorem 3.9: *With the same assumptions as in Theorem 3.7 we have, for small ε , and $k > d/2 - 2$,*

$$\sup_{n \in \mathbb{Z}^d} |u^{(\varepsilon)}(n) - u^{(\varepsilon,p)}(\varepsilon n)| \leq C \|f\|_{H^{2p+k}} \begin{cases} \varepsilon^{2(p+1)} & \text{if } k > d/2, \\ \varepsilon^{2(p+1)} |\log \varepsilon| & \text{if } k = d/2, \\ \varepsilon^{2(p+1)+k-d/2} & \text{if } k < d/2. \end{cases}$$

Proof: Due to translation invariance it is enough to bound $|u^{(\varepsilon)}(0) - u^{(\varepsilon,p)}(0)|$. Defining $\sigma^{(\varepsilon,p)}$ as in the proof of Theorem 3.7, we have

$$\begin{aligned} u^{(\varepsilon)}(0) - u^{(\varepsilon,p)}(0) &= \frac{1}{(2\pi)^d} \int_{I_\varepsilon^d} \frac{\tilde{f}^{(\varepsilon)}(\xi)}{\sigma^{(\varepsilon)}(\xi)} d\xi - \frac{1}{(2\pi)^d} \int_{\mathbb{R}^d} \frac{\hat{f}(\xi)}{\sigma^{(\varepsilon,p)}(\xi)} d\xi \\ &= \frac{1}{(2\pi)^d} \int_{I_\varepsilon^d} \left(\frac{\tilde{f}^{(\varepsilon)}(\xi)}{\sigma^{(\varepsilon)}(\xi)} - \frac{\hat{f}(\xi)}{\sigma^{(\varepsilon,p)}(\xi)} \right) d\xi + \frac{1}{(2\pi)^d} \int_{\mathbb{R}^d \setminus I_\varepsilon^d} \frac{\hat{f}(\xi)}{\sigma^{(\varepsilon,p)}(\xi)} d\xi =: J_1 + J_2. \end{aligned}$$

By Lemma 3.3 we find that

$$J_1 = \frac{1}{(2\pi)^d} \int_{I_\varepsilon^d} \left(\frac{\hat{f}(\xi) \hat{\mu}(\varepsilon \xi)}{\sigma^{(\varepsilon)}(\xi)} - \frac{\hat{f}(\xi)}{\sigma^{(\varepsilon,p)}(\xi)} \right) d\xi + \sum_{n \neq 0} \frac{1}{(2\pi)^d} \int_{I_\varepsilon^d} \frac{\hat{f}(\xi + \frac{2\pi}{\varepsilon} n) \hat{\mu}(\varepsilon \xi + 2\pi n)}{\sigma^{(\varepsilon)}(\xi)} d\xi =: J_{11} + J_{12}.$$

When bounding J_{11} use that (3.17) and (3.7) combined provide the inequality

$$\left| \frac{\hat{\mu}(\varepsilon \xi)}{\sigma^{(\varepsilon)}(\xi)} - \frac{1}{\sigma^{(\varepsilon,p)}(\xi)} \right| \leq C \varepsilon^2 |\varepsilon \xi|^{2p},$$

and hence

$$|J_{11}| \leq C\varepsilon^{2+2p} \int_{I_\varepsilon^d} |\xi|^{2p} |\hat{f}(\xi)| d\xi.$$

Now by Cauchy's inequality we find that

$$|J_{11}| \leq C\varepsilon^{2+2p} \left[\int_{I_\varepsilon^d} \frac{1}{(1+|\xi|^2)^k} d\xi \int_{I_\varepsilon^d} (1+|\xi|^2)^k |\xi|^{4p} |\hat{f}(\xi)|^2 d\xi \right]^{1/2} \leq C(\varepsilon, k, d) \varepsilon^{2+2p} \|f\|_{H^{2p+k}},$$

where

$$C(\varepsilon, k, d) = \begin{cases} C & \text{for } k > d/2, \\ C|\log \varepsilon| & \text{for } k = d/2, \\ C\varepsilon^{k-d/2} & \text{for } k < d/2. \end{cases}$$

When bounding J_{12} we need that

$$(3.18) \quad \frac{\hat{\mu}(\varepsilon\xi + 2\pi n)}{\sigma^{(\varepsilon)}(\xi)} \leq C\varepsilon^{2p} |\xi + \frac{2\pi}{\varepsilon}n|^{2p-2}, \quad \text{for } \xi \in I_\varepsilon^d.$$

When $p \geq 1$ the bound (3.18) is proved from (3.7) as follows

$$\frac{\hat{\mu}(\varepsilon\xi + 2\pi n)}{\sigma^{(\varepsilon)}(\xi)} \leq C \frac{|\varepsilon\xi|^{2p}}{|\xi|^2} \leq C\varepsilon^{2p} |\xi|^{2p-2} \leq C\varepsilon^{2p} |\xi + \frac{2\pi}{\varepsilon}n|^{2p-2},$$

since $2p - 2 \geq 0$ and $|\xi| \leq |\xi + \frac{2\pi}{\varepsilon}n|$. When $p = 0$ we use instead

$$\frac{\hat{\mu}(\varepsilon\xi + 2\pi n)}{\sigma^{(\varepsilon)}(\xi)} \leq C \frac{|\varepsilon\xi|^2}{|\xi|^2 \prod_{j=1}^d (1+n_j^2)} \leq C \frac{1}{\prod_{j=1}^d (1+(n_j/\varepsilon)^2)} \leq C |\xi + \frac{2\pi}{\varepsilon}n|^{-2}.$$

Now that it is proved we can use (3.18) when bounding J_{12} as follows

$$\begin{aligned} |J_{12}| &\leq C \sum_{n \neq 0} \int_{I_\varepsilon^d} |\hat{f}(\xi + \frac{2\pi}{\varepsilon}n)| \varepsilon^{2p} |\xi + \frac{2\pi}{\varepsilon}n|^{2p-2} d\xi = C\varepsilon^{2p} \int_{\mathbb{R}^d \setminus I_\varepsilon^d} |\xi|^{2p-2} |\hat{f}(\xi)| d\xi \\ &\leq C\varepsilon^{2p} \left[\int_{\mathbb{R}^d \setminus I_\varepsilon^d} \frac{1}{|\xi|^{4(1+|\xi|^2)^k}} d\xi \right]^{1/2} \left[\int_{\mathbb{R}^d \setminus I_\varepsilon^d} |\xi|^{4p} (1+|\xi|^2)^k |\hat{f}(\xi)|^2 d\xi \right]^{1/2}. \end{aligned}$$

Since $2k > d - 4$ the first factor is bounded by $\varepsilon^{2+k-d/2}$, thus

$$J_{12} \leq C\varepsilon^{2p+2+k-d/2} \|f\|_{H^{2p+k}}.$$

Finally we note that J_2 satisfies

$$|J_2| \leq C \int_{\mathbb{R} \setminus I_\varepsilon^d} |\hat{f}(\xi)| \varepsilon^2 |\varepsilon\xi|^{2p-2} d\xi \leq C\varepsilon^{2p} \int_{\mathbb{R} \setminus I_\varepsilon^d} |\xi|^{2p-2} |\hat{f}(\xi)| d\xi,$$

and thus can be bounded like J_{12} . □

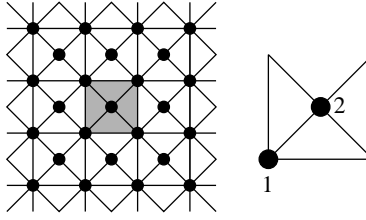


FIGURE 3.1. A bi-atomic lattice. The unit cell is exhibited to the left.

5. Homogenization of conduction problems on multi-atomic lattices

Before giving the general homogenization results for multi-atomic lattices we will consider a simple example that will illustrate the main points.

Example: Consider the two-dimensional lattice illustrated in Figure 3.1. Suppose that all connections have conductivity 1. Then the scaled symbol takes the form

$$\sigma^{(\varepsilon)}(\xi) = \frac{1}{\varepsilon^2} \begin{bmatrix} 4 \sin^2 \frac{\varepsilon \xi_1}{2} + 4 \sin^2 \frac{\varepsilon \xi_2}{2} + 4 & -1 - e^{i\varepsilon \xi_1} - e^{i\varepsilon \xi_2} - e^{i\varepsilon(\xi_1 + \xi_2)} \\ -1 - e^{-i\varepsilon \xi_1} - e^{-i\varepsilon \xi_2} - e^{-i\varepsilon(\xi_1 + \xi_2)} & 4 \end{bmatrix}.$$

The determinant can easily be computed,

$$\det \sigma^{(\varepsilon)}(\xi) = \frac{1}{\varepsilon^4} \left[24 \sin^2 \frac{\varepsilon \xi_1}{2} + 24 \sin^2 \frac{\varepsilon \xi_2}{2} + 4 \sin^2 \frac{\varepsilon(\xi_1 + \xi_2)}{2} + 4 \sin^2 \frac{\varepsilon(\xi_1 - \xi_2)}{2} \right].$$

and thence the inverse symbol

$$(3.19) \quad [\sigma^{(\varepsilon)}(\xi)]^{-1} = \frac{1}{\varepsilon^2 \det \sigma^{(\varepsilon)}(\xi)} \begin{bmatrix} 4 & 1 + e^{i\varepsilon \xi_1} + e^{i\varepsilon \xi_2} + e^{i\varepsilon(\xi_1 + \xi_2)} \\ 1 + e^{-i\varepsilon \xi_1} + e^{-i\varepsilon \xi_2} + e^{-i\varepsilon(\xi_1 + \xi_2)} & 4 \sin^2 \frac{\varepsilon \xi_1}{2} + 4 \sin^2 \frac{\varepsilon \xi_2}{2} + 4 \end{bmatrix}.$$

Now note that $\varepsilon^2 \det \sigma^{(\varepsilon)}(\xi) = 8|\xi|^2 + O(\varepsilon^2|\xi|^4)$, which means that $[\varepsilon^2 \det \sigma^{(\varepsilon)}(\xi)]^{-1}$ has a power series expansion of the form (3.13) and we find that

$$S^{(\varepsilon,0)}(\xi) = \frac{1}{8|\xi|^2} \begin{bmatrix} 4 & 4 + 2\varepsilon i(\xi_1 + \xi_2) \\ 4 - 2\varepsilon i(\xi_1 + \xi_2) & 4 \end{bmatrix}.$$

From the definition (3.9), it is clear that $u^{(\varepsilon,0)}$ satisfies the equation

$$(3.20) \quad \begin{cases} -8\Delta u_1^{(\varepsilon,0)} = 4(f_1 + f_2) + 2\varepsilon(\partial_1 + \partial_2)f_2, \\ -8\Delta u_2^{(\varepsilon,0)} = 4(f_1 + f_2) - 2\varepsilon(\partial_1 + \partial_2)f_1. \end{cases}$$

We make two observations. First that the differential operator on the left hand side is the elliptic operator associated with the matrix M that Corollary 2.10, specifies as the leading term in the series expansion of $\det \sigma(\xi)$. This fact turns out to hold for any multi-atomic lattice and we will capitalize heavily on it in what follows. The second observation is that to first order, the equations for u_1 and u_2 are identical, with a right hand side given by $\sum_{\kappa} f_{\kappa}$. This fact holds for general lattices as well, as we shall demonstrate. \square

For the general case, we first recall that according to Corollary 2.10, there exists a positive definite matrix $M \in \mathbb{R}^{d \times d}$ such that

$$(3.21) \quad \det \sigma(\xi) = \xi \cdot M\xi + O(|\xi|^4).$$

Among other things, this means that $\det \sigma(\xi)$ is the symbol for some fictitious mono-atomic lattice. This lattice will feature frequently in this section, and even more prominently in Chapter 4 on lattice Green's functions and we name it as follows:

Definition: Given a multi-atomic lattice with symbol $\sigma(\xi)$, call the mono-atomic lattice that has the symbol $\det \sigma(\xi)$ the *associated mono-atomic lattice*.

We can also use (3.21) to derive the series expansion for $\sigma(\xi)^{-1}$. First note that all codeterminants of $\sigma(\xi)$ are trigonometric polynomials, which is to say there exist multinomials $p_{\kappa\lambda}$ such that the $\kappa\lambda$ -codeterminant is given by $p_{\kappa\lambda}(e^{i\xi})$. Then by Cramer's rule,

$$[\sigma(\xi)^{-1}]_{\kappa\lambda} = \frac{p_{\kappa\lambda}(e^{i\xi})}{\det \sigma(\xi)}.$$

Lemma 3.5 now provides the series expansion of $(\det \sigma(\xi))^{-1}$. This gives, taking the scaling $\sigma^{(\varepsilon)}(\xi) = \varepsilon^{-2}\sigma(\varepsilon\xi)$ into account,

$$(3.22) \quad \left[[\sigma^{(\varepsilon)}(\xi)]^{-1} \right]_{\kappa\lambda} = \frac{p_{\kappa\lambda}(e^{i\varepsilon\xi})}{\xi \cdot M\xi} + \sum_{j=1}^p \varepsilon^{2j} \frac{p_{\kappa\lambda}(e^{i\varepsilon\xi}) a_{2j}(\xi)}{(\xi \cdot M\xi)^{j+1}} + \varepsilon^2 O(|\varepsilon\xi|^{2p}).$$

Since every $p_{\kappa\lambda}$ is a multi-nomial, the Taylor expansion of $S^{(\varepsilon,p)}(\xi)$ can now easily be derived.

While equation (3.22) can be used to derive homogenizations of arbitrary order, we will for the rest of this section study the lowest order equation only. First we recall that according to Lemma 2.12, Ch. 2, the series expansion of the co-determinants must take the form $p_{\kappa\lambda}(e^{i\xi}) = c_0 + v^{(\kappa\lambda)} \cdot (i\xi) + O(|\xi|^2)$, for some $c_0 > 0$ that does not depend on $\kappa\lambda$. Thus

$$\left[[\sigma^{(\varepsilon)}(\xi)]^{-1} \right]_{\kappa\lambda} = \underbrace{\frac{c_0 + \varepsilon v^{(\kappa\lambda)} \cdot (i\xi)}{\xi \cdot M\xi}}_{=: [S^{(\varepsilon,0)}(\xi)]_{\kappa\lambda}} + \varepsilon^2 O(|\varepsilon\xi|^0), \quad \text{as } \varepsilon\xi \rightarrow 0.$$

The homogenized equation then reads

$$(3.23) \quad \begin{cases} -\nabla \cdot (M\nabla u_{\kappa}^{(\varepsilon,0)}) &= c_0 f_{\kappa} + \varepsilon \sum_{\lambda=1}^q v^{(\kappa\lambda)} \cdot \nabla f_{\lambda}, & \kappa = 1, \dots, q. \\ \sum_{\kappa=1}^q \int |\nabla u_{\kappa}^{(\varepsilon,0)}|^2 &< \infty. \end{cases}$$

Note that $-\nabla \cdot (M\nabla)$ is the homogenized operator of the associated mono-atomic lattice.

Error bounds can be derived in a fashion very similar to the mono-atomic case. The only adjustments needed arise because of the slightly weaker regularizing effect of the new homogenized equations. As an illustration we formulate and prove the pointwise bound. Note that for the solution to be continuous we now need that $f \in H^k \cap L^1$ for some $k > d/2 - 1$, cf. Prop. 3.8.

Theorem 3.10: *Suppose that $d \geq 3$, let $u^{(\varepsilon)}$ be the solution of (3.4) with $f^{(\varepsilon)} = \mathbb{P}_\varepsilon f$, and let $u^{(\varepsilon,p)}$ be the solution of (3.23). Then if ε is small and $k > d/2 - 1$,*

$$\sup_{n \in \mathbb{Z}^d} |u^{(\varepsilon)}(n) - u^{(\varepsilon,p)}(\varepsilon n)| \leq C \|f\|_{H^{2p+k}} \begin{cases} \varepsilon^{2(p+1)} & \text{if } k > d/2, \\ \varepsilon^{2(p+1)} |\log \varepsilon| & \text{if } k = d/2, \\ \varepsilon^{2(p+1)+k-d/2} & \text{if } k < d/2. \end{cases}$$

Proof: The proof follows the proof of Theorem 3.9 closely. Simply replace $[\sigma^{(\varepsilon,p)}(\xi)]^{-1}$ by the matrix $S^{(\varepsilon,p)}(\xi)$ and then split the error into J_{11} , J_{12} and J_2 as before. Bound J_{11} using that

$$|\hat{\mu}(\varepsilon \xi) [\sigma^{(\varepsilon)}(\xi)]^{-1}_{\kappa\lambda} - [S^{(\varepsilon,0)}(\xi)]_{\kappa\lambda}| \leq C \varepsilon^2, \quad \forall \xi \in I_\varepsilon^d.$$

The bound for J_{12} is also entirely analogous since $|[\sigma^{(\varepsilon)}(\xi)]^{-1}_{\kappa\lambda}| \leq C |\xi|^{-2}$ in I_ε^d .

The only real difference lies in the bound for J_2 . Since $[S^{(\varepsilon,0)}(\xi)]_{\kappa\lambda}$ decays somewhat more slowly than $|\xi|^{-2}$ we get

$$\begin{aligned} |J_2| &\leq \max_{\kappa} \sum_{\lambda=1}^q \frac{1}{(2\pi)^d} \int_{\mathbb{R}^d \setminus I_\varepsilon^d} |[S^{(\varepsilon,0)}(\xi)]_{\kappa\lambda}| |\hat{f}_\lambda(\xi)| d\xi \leq C \sum_{\lambda=1}^q \int_{\mathbb{R}^d \setminus I_\varepsilon^d} \left(\frac{1}{|\xi|^2} + \frac{\varepsilon}{|\xi|} \right) |\hat{f}_\lambda(\xi)| d\xi \\ &\leq C \varepsilon \sum_{\lambda=1}^q \int_{\mathbb{R}^d \setminus I_\varepsilon^d} \frac{1}{|\xi|} |\hat{f}_\lambda(\xi)| d\xi \leq C \varepsilon \sum_{\lambda=1}^q \left[\int_{\mathbb{R}^d \setminus I_\varepsilon^d} \frac{1}{|\xi|^2 (1 + |\xi|^2)^k} d\xi \int_{\mathbb{R}^d \setminus I_\varepsilon^d} (1 + |\xi|^2)^k |\hat{f}(\xi)|^2 d\xi \right]^{1/2}. \end{aligned}$$

We see that the bound evaluates to the same quantity, $C \varepsilon^{2+k-d/2} \|f\|_{H^k}$, as in the mono-atomic case, but that a necessary condition for convergence of the first integral is now that $k > d/2 - 1$. \square

Before closing this section we will show that by re-structuring the equations the nature of the homogenization can be rendered more transparent. Note that by setting $f_A := (f_1 + f_2)/2$, $f_D := (f_1 - f_2)/2$, and likewise $u_A^{(\varepsilon,0)} := (u_1^{(\varepsilon,p)} + u_2^{(\varepsilon,p)})/2$, $u_D^{(\varepsilon,0)} := (u_1^{(\varepsilon,p)} - u_2^{(\varepsilon,p)})/2$, the homogenized equations for the model problem (3.20), can be rearranged as

$$\begin{cases} -4\Delta u_A^{(\varepsilon,0)} = 4f_A - \varepsilon(\partial_1 + \partial_2)f_D, \\ -4\Delta u_D^{(\varepsilon,0)} = \varepsilon(\partial_1 + \partial_2)f_A. \end{cases}$$

What is significant here is that to lowest order, $u_A^{(\varepsilon,0)}$ satisfies Poisson's equation with right hand side f_A , and that $u_D = O(\varepsilon)$. In order to generalize this observation we split the functions $u^{(\varepsilon,0)}$ and f into averages and differences by applying the operators Ψ_A and Ψ_D from section 4 to $u^{(\varepsilon,0)}$ and f pointwise,

$$u_\alpha^{(\varepsilon,0)}(x) = \Psi_\alpha^t u^{(\varepsilon,0)}(x), \quad f_\alpha(x) = \Psi_\alpha^t f(x), \quad \alpha = A, D,$$

and define the elliptic operator \mathbf{A}_{dom} as the differential operator corresponding to the matrix M in the series expansion (3.21), $\mathbf{A}_{\text{dom}} := -\nabla(M\nabla)$. Now, invoking Lemma 2.12, we can write the lowest order homogenized equations as

$$\begin{aligned} \mathbf{A}_{\text{dom}} u_A^{(\varepsilon,p)} &= c_0 f_A + \varepsilon \mathcal{B} f_D, \\ \mathbf{A}_{\text{dom}} u_D^{(\varepsilon,p)} &= \varepsilon \mathcal{B}^* f_A, \end{aligned}$$

where \mathcal{B} is a vector of first order difference operators.

6. Homogenization of mechanical lattices

6.1. Preliminaries. In this section we will show how the analysis of conduction problems in sections 4 and 5 can be extended to cover mechanical lattice models. It will become apparent that while the analysis of truss lattices is a very straight-forward generalization of the material covered, the case of frame lattices is more involved. For simplicity, we treat only the first order homogenization, although higher order models can easily be derived. Throughout, we will assume that the truss lattices are locally \mathcal{N} -coercive and that the frame lattices are connected.

In a mechanical lattice model, the scaled symbol $\sigma^{(\varepsilon)}$ is a matrix consisting of $q \times q$ blocks, each of size $k \times k$ (where $k = d$ for trusses and $k = d(d+1)/2$ for frames). Set

$$\tau^{(\kappa\lambda)}(\xi) := \left[\lim_{\varepsilon \rightarrow 0} \sigma^{(\varepsilon)}(\xi)^{-1} \right]_{\text{Block}(\kappa\lambda)},$$

where the subscript “Block($\kappa\lambda$)” indicates that the submatrix corresponding to the $\kappa\lambda$ -block should be extracted. We also define

$$\sigma_{\text{H}}^{(\kappa\lambda)}(\xi) := \tau^{(\kappa\lambda)}(\xi)^{-1}.$$

It can be demonstrated that for the models under consideration, the matrix $\tau^{(\kappa\lambda)}(\xi)$ has entries that are rational functions in ξ , and $\sigma_{\text{H}}^{(\kappa\lambda)}(\xi)$ has entries that are polynomials in ξ .

6.2. Truss lattices. We will first determine how $\sigma^{(\varepsilon)}$ scales with ε . As an axial spring is scaled, its cross-section scales as ε^{d-1} and its length scales as ε so every element of the local stiffness matrix scales as ε^{d-2} . Since the load scales as ε^d , this implies that the relation (3.1) derived for the conduction problem remains valid, *i.e.* $\sigma^{(\varepsilon)}(\xi) = \varepsilon^{-2}\sigma(\varepsilon\xi)$. Combining this scaling relation with Lemma 2.16 we find that, with σ_0 defined by (2.19),

$$\lim_{\varepsilon \rightarrow 0} \sigma^{(\varepsilon)}(\xi)^{-1} = \lim_{\varepsilon \rightarrow 0} (\varepsilon^2 \Psi_{\text{A}} \sigma_0(\varepsilon\xi)^{-1} \Psi_{\text{A}}^{\text{t}} + \varepsilon^2 O(|\varepsilon\xi|^{-1})) = \Psi_{\text{A}} \sigma_0(\xi)^{-1} \Psi_{\text{A}}^{\text{t}}.$$

We used that $\varepsilon^2 \sigma_0(\varepsilon\xi)^{-1} = \sigma_0(\xi)^{-1}$ (since every entry of $\sigma_0(\xi)$ is a second order polynomial). This means that $\tau^{(\kappa\lambda)} = \sigma_0^{-1}$, and thus $\sigma_{\text{H}}^{(\kappa\lambda)} = \sigma_0$. Thus, to lowest order, the homogenized equations for the $qd \times qd$ system of equations $\mathfrak{A}\mathbf{u} = \mathfrak{f}$, consists of the $d \times d$ system, $A\mathbf{u} = \mathbf{f}$, where A is the matrix of second order differential operators that has the symbol σ_0 . It is our belief (although this is not yet proved) that A will always be an elasticity operator. Some examples are given in Appendix B.

The convergence will be $O(\varepsilon^2)$ for mono-atomic lattices and $O(\varepsilon)$ for multi-atomic ones. This can be proved using the same techniques used for the conduction problem, the only difference being that for the present case, all entries of $\sigma^{(\varepsilon)}(\xi)^{-1}$ will have as their dominant term a rational function consisting of a polynomial of degree $2(d-1)$ that is divided by a polynomial of degree $2d$. For the conduction problem, the corresponding dominant term was a constant divided by a polynomial of degree 2. However, the relevant bounds on derivatives and decay rates are the same for both cases.

6.3. Frame lattices. The homogenization of frame lattices is more subtle than the previous cases considered because different terms of $\sigma^{(\varepsilon)}$ scale differently with ε . Let ‘t’ and ‘r’ denote translational and rotational degrees of freedom, as in the discussion near equation (2.8), and write the equilibrium equations in the form

$$\left(\left[\begin{array}{cc} \sigma_{\text{tt}}^{\text{axial}}(\xi) & 0 \\ 0 & 0 \end{array} \right] + \left[\begin{array}{cc} \sigma_{\text{tt}}^{\text{bending}}(\xi) & \sigma_{\text{tr}}^{\text{bending}}(\xi) \\ \sigma_{\text{rt}}^{\text{bending}}(\xi) & \sigma_{\text{rr}}^{\text{bending}}(\xi) \end{array} \right] \right) \left[\begin{array}{c} \tilde{\mathbf{u}}_{\text{t}}(\xi) \\ \tilde{\mathbf{u}}_{\text{r}}(\xi) \end{array} \right] = \left[\begin{array}{c} \tilde{\mathbf{f}}_{\text{t}}(\xi) \\ \tilde{\mathbf{f}}_{\text{r}}(\xi) \end{array} \right].$$

The first matrix, $\sigma_{\text{tt}}^{\text{axial}}$, is the same symbol as in the truss model, so it scales as ε^{-2} . When determining the scaling of the bending components, we note that, *cf.* (A.1),

$$\sigma_{\text{tt}}^{\text{bending}}(\xi) \sim \frac{I}{L^3}, \quad \sigma_{\text{tr}}^{\text{bending}}(\xi) = [\sigma_{\text{rt}}^{\text{bending}}(\xi)]^t \sim \frac{I}{L^2}, \quad \sigma_{\text{rr}}^{\text{bending}}(\xi) \sim \frac{I}{L},$$

where I is the moment of inertia of a beam and L is its length. As the beam is scaled, $I_\varepsilon = I_0\varepsilon^{d+1}$, and $L_\varepsilon = L_0\varepsilon$. Taking into account that the load scales as ε^d , this gives the aggregate scaling

$$\begin{bmatrix} \sigma_{\text{tt}}^{(\varepsilon)}(\xi) & \sigma_{\text{tr}}^{(\varepsilon)}(\xi) \\ \sigma_{\text{rt}}^{(\varepsilon)}(\xi) & \sigma_{\text{rr}}^{(\varepsilon)}(\xi) \end{bmatrix} = \begin{bmatrix} \varepsilon^{-2}\sigma_{\text{tt}}(\varepsilon\xi) & \varepsilon^{-1}\sigma_{\text{tr}}(\varepsilon\xi) \\ \varepsilon^{-1}\sigma_{\text{rt}}(\varepsilon\xi) & \sigma_{\text{rr}}(\varepsilon\xi) \end{bmatrix}.$$

This means that when the limit is computed and $\sigma_{\text{H}}^{(\kappa\lambda)}$ is split up,

$$\sigma_{\text{H}}^{(\kappa\lambda)}(\xi) = \begin{bmatrix} \sigma_{\text{H,tt}}^{(\kappa\lambda)}(\xi) & \sigma_{\text{H,tr}}^{(\kappa\lambda)}(\xi) \\ \sigma_{\text{H,rt}}^{(\kappa\lambda)}(\xi) & \sigma_{\text{H,rr}}^{(\kappa\lambda)}(\xi) \end{bmatrix},$$

one will find that $\sigma_{\text{H,tt}}^{(\kappa\lambda)}$ consists of second order polynomials, $\sigma_{\text{H,rt}}^{(\kappa\lambda)}$ and $\sigma_{\text{H,tr}}^{(\kappa\lambda)}$ consist of first order polynomials and $\sigma_{\text{H,rr}}^{(\kappa\lambda)}$ has constant entries. Unlike the previous cases studied, it is *not* the case that all $\sigma_{\text{H}}^{(\kappa\lambda)}$ are identical. Consequently, the $O(\varepsilon)$ homogenized equations, $Au = f$, is a large system governing $qd(d+1)/2$ variables. The displacement variable u represents both translational and rotational degrees of freedom and f both force and torque loading.

The reason that the blocks $\sigma_{\text{H}}^{(\kappa\lambda)}$ are all different is that a torque load produces distinctly different responses depending on the point of application. In a case where $\mathbf{f}_{\text{r}} = 0$, the rotational degrees of freedom can be eliminated by forming the Schur complement of the matrices $\sigma_{\text{H}}^{(\kappa\lambda)}$,

$$\sigma_{\text{H,reduced}}^{(\kappa\lambda)} = \sigma_{\text{H,tt}}^{(\kappa\lambda)} - \sigma_{\text{H,tr}}^{(\kappa\lambda)}[\sigma_{\text{H,rr}}^{(\kappa\lambda)}]^{-1}\sigma_{\text{H,rt}}^{(\kappa\lambda)}.$$

These matrices are the same for every $\kappa\lambda$. In fact, $\sigma_{\text{H,reduced}}^{(\kappa\lambda)} = \sigma_0$, where σ_0 is defined as in section 3.4, Ch. 2. The matrix $\sigma_0(\xi)$ is a $d \times d$ matrix whose entries are second order polynomials. In every case that we have studied, it is the symbol of a classical elasticity operator.

In Appendix B we give examples that illustrate the main concepts discussed here. For lattice A we explicitly derive the homogenized equations. Lattices D and E illustrate how the different matrices $\sigma_{\text{H}}^{(\kappa\lambda)}$ may be different but still have the same Schur complement.

CHAPTER 4

The lattice Green's function

1. Introduction

Consider the basic lattice equation

$$(4.1) \quad \begin{cases} \mathfrak{A}u = f, \\ \|u\|_{\mathfrak{A}} < \infty, \end{cases}$$

in dimension $d \geq 3$. We suppose that $f \in l^1$, so that the solution is given by $u = \mathfrak{F}^{-1}[\sigma^{-1}\tilde{f}]$ (cf. Theorem 2.21). Since multiplication in Fourier space corresponds to a convolution in physical space we can write $u = [\mathfrak{F}^{-1}\sigma^{-1}] * f$. Thus, setting

$$(4.2) \quad \mathfrak{G}(m) := [\mathfrak{F}^{-1}\sigma^{-1}](m) = \frac{1}{(2\pi)^d} \int_{I^d} e^{-im \cdot \xi} \sigma^{-1}(\xi) d\xi,$$

we can write the solution of (4.1) as

$$(4.3) \quad u(m) = [\mathfrak{G} * f](m) = \sum_{n \in \mathbb{Z}^d} \mathfrak{G}(m - n) f(n).$$

In this section we will investigate the asymptotic behavior of $\mathfrak{G}(m)$ for large m . We will first show that for conduction problems on mono-atomic lattices we can, for any natural integer P , find a rational function G_P such that

$$\mathfrak{G}(m) = G_P(m) + O(|m|^{-2P-d}).$$

We will also show that each function G_P satisfies the poly-harmonic condition

$$(-\nabla \cdot (M\nabla))^{P+1} G_P(x) = 0, \quad \text{for } x \neq 0,$$

where M is the matrix given by Corollary 2.10. In fact, the function G_P is the fundamental solution of the homogenized operator $A^{(\varepsilon, p)}$ derived in Chapter 3, evaluated at $\varepsilon = 1$. Considering next multi-atomic lattices (for which $\mathfrak{G}(m)$ is a matrix), we will construct a scalar Green's function \mathfrak{G}_H such that any entry of $\mathfrak{G}(m)$ can be obtained by adding a finite number of shifts of \mathfrak{G}_H . The asymptotic expansion then follows directly from the expansion of \mathfrak{G}_H . The function \mathfrak{G}_H turns out to be the Green's function connected with the associated mono-atomic lattice from section 5 in Ch. 3

We restricted attention to dimensions three and higher because in two dimensions, the integral in the definition (4.2) is divergent. However, for loads f such that $\sum_n f(n) = 0$, a renormalized Green's function \mathfrak{G} can be defined in such a way that equation (4.3) is still valid and asymptotic expansions of the kind described can be derived (see section 3).

The structure of the chapter is as follows: In section 2 we consider the conduction problem and derive the asymptotic expansion for a mono-atomic lattice in three dimensions. In section 3 we

extend the analysis to mono-atomic lattices in arbitrary dimension. In section 4 we consider multi-atomic lattices. In section 5 we give some numerical examples that indicate that the constants in the error estimates of the previous sections are small.

For some classical lattices, we give the functions G_P in Appendix B.

2. Mono-atomic lattices in three dimensions

Consider the conduction problem on a connected mono-atomic lattice in three dimensions. For this case, the function $\sigma(\xi)^{-1}$ is analytic for $\xi \neq 0$. This means that the contribution to the integral in (4.2) from any domain bounded away from the origin decays faster than any rational function as $|m| \rightarrow \infty$ and the asymptotic behavior of $\mathfrak{G}(m)$ is determined entirely by the $|\xi|^{-2}$ -singularity at the origin. We will capture this behavior using the series expansion of $\sigma(\xi)^{-1}$ provided by Lemma 3.5.

For notational convenience we assume for the moment that the matrix M in the expansion (3.10) equals unity, so that

$$(4.4) \quad \sigma(\xi) = |\xi|^2 + \sum_{j=2}^{\infty} b_j(\xi), \quad \text{for } b_j \in \Pi^{2j}.$$

Then for any P , Lemma 3.5 furnishes an expansion

$$\frac{1}{\sigma(\xi)} = \sum_{p=0}^P \frac{a_{2p}(\xi)}{|\xi|^{2p+2}} + \hat{R}_P(\xi),$$

where $a_0(\xi) = 1$, $a_{2q} \in \Pi^{4q}$, and $|\partial^\alpha \hat{R}_P(\xi)| \leq C|\xi|^{2P-|\alpha|}$, for $\xi \in I^3$. Recall that the multi-nomials a_{2p} can be obtained from the multi-nomials b_j 's through the recursive relation (3.12). Now we define

$$(4.5) \quad G_P := \mathcal{F}^{-1} \left[\sum_{p=0}^P \frac{a_{2p}(\xi)}{|\xi|^{2p+2}} \right].$$

Note that the integral is strongly divergent since the integrand actually grows as $|\xi| \rightarrow \infty$. We therefore interpret \mathcal{F} as an operator on the tempered distributions. Following Gel'fand & Shilov (1964), we let \mathcal{S} denote the set of Schwartz functions and set, for $\varphi \in \mathcal{S}$,

$$\hat{\varphi}(x) := [\mathcal{F}\varphi](x) = \int_{\mathbb{R}^3} e^{ix \cdot \xi} \varphi(\xi) dx, \quad \text{and} \quad \check{\varphi}(x) := [\mathcal{F}^{-1}\varphi](x) = \frac{1}{(2\pi)^d} \int_{\mathbb{R}^3} e^{-ix \cdot \xi} \varphi(\xi) dx, .$$

Then $G_P \in \mathcal{S}'$ is defined as the function for which

$$\langle G_P, \varphi \rangle = \int_{\mathbb{R}^d} \left(\sum_{p=0}^P \frac{a_{2p}(\xi)}{|\xi|^{2p+2}} \right) \check{\varphi}(\xi) d\xi, \quad \forall \varphi \in \mathcal{S},$$

where $\langle \cdot, \cdot \rangle$ is the usual pairing between \mathcal{S}' and \mathcal{S} .

Even though the definition of G_P is somewhat involved, it is actually a simple matter to evaluate the inverse Fourier transform in (4.5):

Proposition 4.1: *Given a function $a_{2p} \in \Pi^{4p}$ we have, for $p \geq 1$,*

$$g_p(x) := \mathcal{F}^{-1} \left[\frac{a_{2p}(\xi)}{|\xi|^{2p+2}} \right] (x) = \frac{(-1)^p}{\pi 2^{p+2} p! (2p-1)!!} a_{2p}(\partial) |x|^{2p-1},$$

where $\partial = (\partial_1, \partial_2, \partial_3)$ is the vector of first order partial differential operators.

Proof: We first use induction to show that the function $f_p(x) := \alpha_p |x|^{2p-1}$, where $\alpha_0 = (4\pi)^{-1}$ and $\alpha_p = (-1)^p (\pi 2^{p+2} p! (2p-1)!!)^{-1}$ for $p \geq 1$, solves the distributional equation

$$(4.6) \quad (-\Delta)^{p+1} f_p(x) = \delta(x).$$

It is well known that this is true for $p = 0$. Next suppose that it is true for all integers up to $(p-1)$. Then, recalling that the product rule for differentiation holds for distributions of the type ψF , where ψ is a multi-nomial and F is any distribution, we find that

$$\begin{aligned} (-\Delta)^{p+1} f_p(x) &= -(-\Delta)^p \alpha_p [(\Delta |x|^{2p}) |x|^{-1} + 2(\nabla |x|^{2p}) \cdot (\nabla |x|^{-1}) + |x|^{2p} (\Delta |x|^{-1})] \\ &= -(-\Delta)^p \alpha_p [2p(2p+1) |x|^{2p-3} - 4p |x|^{2p-3} - 4\pi |x|^{2p} \delta(x)] \\ &= -(-\Delta)^p \alpha_p (4p^2 - 2p) |x|^{2p-3}. \end{aligned}$$

At this point we apply the induction assumption which completes the proof of (4.6).

Applying the Fourier transform to equation (4.6) we find that $|\xi|^{2p+2} \hat{f}_p(\xi) = 1$ and so

$$(4.7) \quad |\xi|^{-(2p+2)} = \hat{f}_p(\xi) + \hat{\varphi}(\xi)$$

where $\varphi(x)$ is a distribution such that $|\xi|^{2p+2} \hat{\varphi}(\xi) = 0$. Consequently, $\text{support}(\hat{\varphi}) = \{0\}$ and since $\hat{\varphi}$ is a tempered distribution we then know that $\hat{\varphi}(\xi)$ is a finite sum of delta-functions and derivatives of delta-functions, all supported at the origin. This in turn means that φ is a finite multi-nomial. Multiplying equation (4.7) by $a_{2p}(\xi)$ and taking inverse Fourier transforms we find that

$$g_p(x) = a_{2p}(\partial) f_p(x) + a_{2p}(\partial) \varphi(x).$$

It remains to prove that the last term on the right hand side vanishes. Since it is a multi-nomial it is sufficient to prove that it tends to zero as $|x| \rightarrow \infty$. The term $a_{2p}(\partial) f_p$ clearly decays in this fashion so we only need to prove that g_p decays. To this end fix a compactly supported, infinitely differentiable function ψ such that $\psi(x) \equiv 1$ in some neighbourhood of the origin and set $g'_p := \mathcal{F}^{-1}[\psi \hat{g}_p]$ and $g''_p := \mathcal{F}^{-1}[(1-\psi) \hat{g}_p]$ so that $g_p = g'_p + g''_p$. Then

$$|x|^{2p} g'_p(x) = |x|^{2p} \mathcal{F}^{-1}[\psi \hat{g}_p](x) = \mathcal{F}^{-1}[(-\Delta)^p (\psi \hat{g}_p)](x),$$

which is uniformly bounded since $(-\Delta)^p (\psi \hat{g}_p) \in L^1$. The proof for g''_p is analogous. \square

We are now prepared to state and prove a bound on the truncation error.

Theorem 4.2: *Let \mathfrak{G} be defined by (4.2) and G_P by (4.5). Then*

$$|\mathfrak{G}(n) - G_P(n)| \leq \frac{C}{|n|^{2P+3}}, \quad \forall n \in \mathbb{Z}^3,$$

where C depends on P but not on n .

Proof: First note that, with g_p defined in Proposition 4.1,

$$\mathfrak{G} - G_P = \mathfrak{G} - G_{P+1} + g_{P+1}.$$

By Proposition 4.1, $g_{P+1}(n) = O(|n|^{-2P-3})$. Therefore we only need to prove that $|\mathfrak{G}(n) - G_{P+1}(n)| \leq C|n|^{-2P-3}$. This reformulation is necessary because our technique for bounding the remainder term does not give a sharp bound.

Fix an infinitely differentiable function ψ such that $\psi(\xi) \equiv 1$ for $|\xi| \leq 1$ and $\psi(\xi) \equiv 0$ for $|\xi| \geq 2$. Using that $\mathfrak{F}^{-1}[\psi\varphi] = \mathcal{F}^{-1}[\psi\varphi]$ for any φ , we obtain the representation

$$\begin{aligned} \mathfrak{G} - G_{P+1} &= \mathfrak{F}^{-1}[\sigma^{-1}] - \mathcal{F}^{-1}[\hat{G}_{P+1}] \\ &= \mathfrak{F}^{-1}[\sigma^{-1}] - \mathfrak{F}^{-1}[\psi \hat{G}_{P+1}] + \mathcal{F}^{-1}[\psi \hat{G}_{P+1}] - \mathcal{F}^{-1}[\hat{G}_{P+1}] \\ &= \mathfrak{F}^{-1}[\sigma^{-1} - \psi \hat{G}_{P+1}] + \mathcal{F}^{-1}[(\psi - 1)\hat{G}_{P+1}] =: E_1 + E_2. \end{aligned}$$

We start by bounding E_1 . Set $R = \sigma^{-1} - \psi \hat{G}_{P+1}$ so that $E_1 = \mathfrak{F}^{-1}[R]$. Note that R is I^3 -periodic, has partial derivatives of all orders away from the origin, and that $|\partial^\alpha R(\xi)| \leq C|\xi|^{2P+2-|\alpha|}$. Then

$$\begin{aligned} |n|^{2P+4}E_1(n) &= \frac{1}{(2\pi)^3} \int_{I^3} [(-\Delta)^{P+2}e^{-in \cdot \xi}] R(\xi) d\xi \\ &= \lim_{\varepsilon \rightarrow 0} \frac{1}{(2\pi)^3} \int_{I^3 \setminus B_\varepsilon} [(-\Delta)^{P+2}e^{-in \cdot \xi}] R(\xi) d\xi. \end{aligned}$$

where B_ε is the ball of radius ε around the origin. We use Green's theorem to move all the derivatives onto R . The volume integrals will then contain a $|\xi|^{-2}$ singularity at the origin and the surface integrals a $|\xi|^{-1}$ singularity. Consequently the integral is bounded as $\varepsilon \rightarrow 0$, which means that $|n|^{2P+4}|E_1(n)|$ is uniformly bounded in n .

To bound E_2 , we use that for any positive integer p

$$|n|^{2p}E_2(n) = |n|^{2p}\mathcal{F}^{-1}[(\psi - 1)\hat{G}_{P+1}](n) = \mathcal{F}^{-1}[(-\Delta)^p(\psi - 1)\hat{G}_{P+1}](n).$$

Note that the function $(\psi - 1)\hat{G}_{P+1}$ is infinitely differentiable and that it equals a rational function outside the sphere $|\xi| = 2$. This means that for sufficiently large p , the function $(-\Delta)^p(\psi - 1)\hat{G}_{P+1}$ is integrable and thus $E_2(n)$ decays faster than any inverse polynomial. \square

Remark I: If the series expansion of the symbol has the general form $\sigma(\xi) = \xi \cdot (M\xi) + O(|\xi|^4)$ so that (4.4) does not hold, then set $\xi' := M^{1/2}\xi$ and change variables in (4.2) so that

$$\mathfrak{G}(n) = \frac{1}{(2\pi)^3 \sqrt{\det M}} \int_{M^{-1/2}I^3} e^{-i(M^{-1/2}n) \cdot \xi'} \frac{1}{\sigma(M^{-1/2}\xi')} d\xi'.$$

Since the function $\xi' \mapsto \sigma(M^{-1/2}\xi')$ does have the series expansion (4.4), the asymptotic expansion results provided can be applied to approximate this integral. \square

Remark II: When considering the definition (4.2) we note that $\sum_{p=0}^P a_{2p}(\xi)/|\xi|^{2p+2} = S^{(1,P)}(\xi)$, where $S^{(\varepsilon,P)}$ is defined as in Chapter 3. Thus $G_P = \mathcal{F}^{-1}[S^{(1,P)}]$ which means that G_P is the fundamental solution of the quasi-differential equation (3.15). \square

3. Mono-atomic lattices in dimensions other than three

First note that the analysis in section 2 can trivially be extended to dimensions $d > 3$. The case $d = 2$ requires more care since for this case, the $O(|\xi|^{-2})$ singularity at the origin is not integrable.

We recall from the existence results of section 4 in Ch. 2 that for the two-dimensional counterpart of the basic lattice equation (4.1), to be well-posed, we need to ask that $\sum_m |mf(m)| < \infty$ and that

$$\sum_{m \in \mathbb{Z}^2} f(m) = 0.$$

Under these conditions equation (4.1) is guaranteed to have a solution that is unique up to a constant. Furthermore, under these conditions one can easily verify that a solution is given by

$$u(m) = [\mathfrak{G} * f](m) = \sum_{n \in \mathbb{Z}^2} \mathfrak{G}(m - n)f(n),$$

where the lattice Green's function is now defined by

$$(4.8) \quad \mathfrak{G}(m) := \frac{1}{(2\pi)^2} \int_{I^2} \left[e^{-im \cdot \xi} \frac{1}{\sigma(\xi)} - \frac{1}{\sigma(\xi)} \right] d\xi.$$

Note that we needed to insert a regularising term since the $O(|\xi|^{-2})$ singularity at the origin is not integrable in two dimensions. This singularity is fundamental and cannot be overcome by defining the integral in a distributional sense.

Let b_j and a_j be defined as in section 2 and assume (without loss of generality) that $\sigma(\xi) = |\xi|^2 + O(|\xi|^4)$. Then define the first term in the approximation of \mathfrak{G} by

$$(4.9) \quad g_0(x) := \frac{1}{(2\pi)^2} \int_{\mathbb{R}^2} \left[\frac{e^{-ix \cdot \xi}}{|\xi|^2} - \frac{\chi(\xi)}{\sigma(\xi)} \right] d\xi,$$

where χ is the characteristic function for the square I^2 . Strictly speaking this definition is made in a distributional sense;

$$\langle g_0, \varphi \rangle := \frac{1}{(2\pi)^2} \int_{\mathbb{R}^2} \left(\frac{\check{\varphi}(\xi)}{|\xi|^2} - \frac{\chi(\xi)\check{\varphi}(0)}{\sigma(\xi)} \right) d\xi, \quad \forall \varphi \in \mathcal{S}.$$

For $p \geq 1$ the terms are straight-forwardly defined by $g_p := \mathcal{F}^{-1}[a_{2p}(\xi)/|\xi|^{2p+2}]$ and then

$$(4.10) \quad G_P := \sum_{p=0}^P g_p.$$

The next two results provide elementary methods for calculating G_P given the symbol.

Proposition 4.3: *The function g_0 defined by (4.9) evaluates to*

$$g_0(x) = -\frac{1}{2\pi} \log |x| + C_{\text{fund}} + \frac{1}{(2\pi)^2} \int_{I^2} \left[\frac{1}{|\xi|^2} - \frac{1}{\sigma(\xi)} \right] d\xi,$$

where C_{fund} does not depend on σ . Numerically, $C_{\text{fund}} = -0.18124942796 \dots$

Proof: We rewrite the definition of g_0 as follows

$$g_0(x) = G_{\text{fund}}(x) + \frac{1}{(2\pi)^2} \int_{\mathbb{R}^2} \left[\frac{\chi(\xi)}{|\xi|^2} - \frac{\chi(\xi)}{\sigma(\xi)} \right] d\xi,$$

where

$$G_{\text{fund}}(x) := \frac{1}{(2\pi)^2} \int_{\mathbb{R}^2} \frac{e^{-ix \cdot \xi} - \chi(\xi)}{|\xi|^2} d\xi,$$

which as usual is short-hand for the strict definition: For any $\varphi \in \mathcal{S}$,

$$(4.11) \quad \langle G_{\text{fund}}, \varphi \rangle = \frac{1}{(2\pi)^2} \int_{\mathbb{R}^2 \times \mathbb{R}^2} \varphi(x) \frac{e^{-ix \cdot \xi} - \chi(\xi)}{|\xi|^2} dx d\xi = \frac{1}{(2\pi)^2} \int_{\mathbb{R}^2} \frac{\hat{\varphi}(\xi) - \hat{\varphi}(0)\chi(\xi)}{|\xi|^2} d\xi.$$

First we demonstrate that $-\Delta G_{\text{fund}} = \delta$,

$$\begin{aligned} \langle -\Delta G_{\text{fund}}, \varphi \rangle &= \langle G_{\text{fund}}, -\Delta \varphi \rangle = \frac{1}{(2\pi)^2} \int_{\mathbb{R}^2} \frac{|\xi|^2 \hat{\varphi}(\xi) - 0 \cdot \hat{\varphi}(0)\chi(\xi)}{|\xi|^2} d\xi \\ &= \frac{1}{(2\pi)^2} \int_{\mathbb{R}^2} \hat{\varphi}(\xi) d\xi = \varphi(0). \end{aligned}$$

Define $h \in \mathcal{S}'$ by $h(x) = G_{\text{fund}}(x) + (2\pi)^{-1} \log|x|$ so that $\Delta h = 0$. Then h is a harmonic multi-nomial. Since G_{fund} is a radial function, so is h . Finally note that all radial harmonic multi-nomials are constant and thus there exists a constant C_{fund} such that $G_{\text{fund}}(x) = -(2\pi)^{-1} \log|x| + C_{\text{fund}}$. \square

We remark, in passing, that the function $G_{\text{fund}} \in \mathcal{S}'$ that was defined in equation (4.11), is a viable candidate for a distributional fundamental solution to the Laplace operator on \mathbb{R}^2 .

Proposition 4.4: *For any $a_{2p} \in \Pi^{4p}$*

$$\mathcal{F}^{-1} \left[\frac{a_{2p}(\xi)}{|\xi|^{2p+2}} \right] = -\frac{1}{2\pi(p!)^2(-4)^p} a_{2p}(\partial) |x|^{2p} \log|x|.$$

The proof of this result is completely analogous to the proof of Proposition 4.1. The final result of this section also mimics its three-dimensional counterpart and we omit the proof.

Theorem 4.5: *Let \mathfrak{G} be defined by (4.8) and G_P by (4.10). Then*

$$|\mathfrak{G}(n) - G_P(n)| \leq \frac{C}{|n|^{2P+2}}, \quad \forall n \in \mathbb{Z}^2,$$

where C depends on P but not on n .

4. Multi-atomic lattices

For multi-atomic lattices, $\mathfrak{G}(m)$ is a $q \times q$ -matrix. We will demonstrate that each entry of this matrix can be obtained by adding a finite number of shifts of the (scalar) Green's function for the associated mono-atomic lattice introduced in section 5 in Ch. 3. The asymptotic expansion is then easily obtained through the asymptotic expansion of the Green's function for the associated mono-atomic lattice. Before giving a general result, we illustrate how these ideas apply to the bi-atomic lattice introduced in section 5 in Ch. 3.

Example: Consider heat conduction through the lattice illustrated in Figure 3.1, with the nodes labeled as illustrated. The equilibrium equations read

$$\begin{aligned} f(n, 1) &= 8u(n, 1) - u(n - e_1, 1) - u(n + e_1, 1) - u(n - e_2, 1) - u(n + e_2, 1) \\ &\quad - u(n, 2) - u(n - e_1, 2) - u(n - e_1 - e_2, 2) - u(n - e_2, 2), \\ f(n, 2) &= 4u(n, 2) - u(n, 1) - u(n + e_1, 1) - u(n + e_1 + e_2, 1) - u(n + e_2, 1). \end{aligned}$$

The symbol then takes the form

$$\sigma(\xi) = \begin{bmatrix} 8 - e^{i\xi_1} - e^{-i\xi_1} - e^{i\xi_2} - e^{-i\xi_2} & -1 - e^{i\xi_1} - e^{i\xi_2} - e^{i(\xi_1+\xi_2)} \\ -1 - e^{-i\xi_1} - e^{-i\xi_2} - e^{-i(\xi_1+\xi_2)} & 4 \end{bmatrix}.$$

The determinant of the symbol is given by

$$\det \sigma(\xi) = \left[24 \sin^2 \frac{\xi_1}{2} + 24 \sin^2 \frac{\xi_2}{2} + 4 \sin^2 \frac{(\xi_1 + \xi_2)}{2} + 4 \sin^2 \frac{(\xi_1 - \xi_2)}{2} \right],$$

and the inverse is given by

$$(4.12) \quad \sigma(\xi)^{-1} = \frac{1}{\det \sigma(\xi)} \begin{bmatrix} 4 & 1 + e^{i\xi_1} + e^{i\xi_2} + e^{i(\xi_1 + \xi_2)} \\ 1 + e^{-i\xi_1} + e^{-i\xi_2} + e^{-i(\xi_1 + \xi_2)} & 8 - e^{i\xi_1} - e^{-i\xi_1} - e^{i\xi_2} - e^{-i\xi_2} \end{bmatrix}$$

Defining \mathfrak{G}_H as the Green's function for the associated mono-atomic lattice,

$$\mathfrak{G}_H(n) := \int_{I^2} \left(e^{-in \cdot \xi} \frac{1}{\det \sigma(\xi)} - 1 \right) d\xi,$$

we then use that $\mathfrak{F}^{-1}[e^{i\xi_1} \hat{\varphi}](n_1, n_2) = \varphi(n_1 - 1, n_2)$ to obtain that,

$$\begin{aligned} [\mathfrak{G}(n)]_{11} &= 4\mathfrak{G}_H(n), \\ [\mathfrak{G}(n)]_{12} &= \mathfrak{G}_H(n) + \mathfrak{G}_H(n_1 - 1, n_2) + \mathfrak{G}_H(n_1, n_2 - 1) + \mathfrak{G}_H(n_1 - 1, n_2 - 1), \\ [\mathfrak{G}(n)]_{21} &= \mathfrak{G}_H(n) + \mathfrak{G}_H(n_1 + 1, n_2) + \mathfrak{G}_H(n_1, n_2 + 1) + \mathfrak{G}_H(n_1 + 1, n_2 + 1), \\ [\mathfrak{G}(n)]_{22} &= 8\mathfrak{G}_H(n) - \mathfrak{G}_H(n_1 - 1, n_2) - \mathfrak{G}_H(n_1 + 1, n_2) - \mathfrak{G}_H(n_1, n_2 - 1) - \mathfrak{G}_H(n_1, n_2 + 1). \end{aligned}$$

□

For the general case, we define \mathfrak{G}_H as the Green's function of the associated mono-atomic lattice defined in section 5 in Ch. 3, so that (for dimensions three and higher)

$$(4.13) \quad \mathfrak{G}_H(n) := \mathfrak{F}^{-1} \left[\frac{1}{\det \sigma(\xi)} \right].$$

The asymptotic expansions we derived in sections 2 and 3 all apply to \mathfrak{G}_H . The main result of this section states that the full Green's function of the multi-atomic lattice is given by adding up a finite number of shifts of \mathfrak{G}_H .

Theorem 4.6: *Given a general lattice Green's function \mathfrak{G} , let \mathfrak{G}_H be the associated Green's function defined by (4.13). Then there exists a local convolution operator \mathfrak{D} such that $\mathfrak{G} = \mathfrak{G}_H * \mathfrak{D}$.*

Proof: Start with Cramer's rule,

$$[\sigma(\xi)^{-1}]_{\kappa\lambda} = \frac{p_{\kappa\lambda}(e^{i\xi})}{\det \sigma(\xi)},$$

where $p_{\kappa\lambda}$ is a multinomial of the form (cf. the derivation of the homogenized equations for a multi-atomic lattice in section 5 in Ch. 3)

$$p_{\kappa\lambda}(e^{i\xi}) = \sum_{m \in \mathbb{D}_{\kappa\lambda}} c_{\kappa\lambda, m} e^{im \cdot \xi}.$$

for some finite sets $\mathbb{D}_{\kappa\lambda} \subset \mathbb{Z}^d$ and constants $\{c_{\kappa\lambda, m}\}_{m \in \mathbb{D}_{\kappa\lambda}}$. Then for any lattice function \mathfrak{v} ,

$$\mathfrak{F}^{-1}[p_{\kappa\lambda}(e^{i\xi}) \tilde{\mathfrak{v}}(\xi)](n) = \sum_{m \in \mathbb{D}_{\kappa\lambda}} c_{\kappa\lambda, m} \mathfrak{v}(n - m) =: [\mathfrak{D}_{\kappa\lambda} * \mathfrak{v}](n),$$

which defines the $\kappa\lambda$ component of the convolution operator \mathfrak{D} . Evaluating $\mathfrak{G}_{\kappa\lambda}$, we find that

$$\mathfrak{G}_{\kappa\lambda} = \mathfrak{F}^{-1} \left[\frac{p_{\kappa\lambda}(e^{i\xi})}{\det \sigma(\xi)} \right] = \mathfrak{D}_{\kappa\lambda} * \mathfrak{F}^{-1} \left[\frac{1}{\det \sigma(\xi)} \right] = \mathfrak{D}_{\kappa\lambda} * \mathfrak{G}_H = \mathfrak{G}_H * \mathfrak{D}_{\kappa\lambda},$$

which proves the claim. \square

Remark: By Lemma 2.12, we know that there exists a positive c_0 such that $\sum_{\kappa\lambda} c_{\kappa\lambda,m} = c_0$. To lowest order, all components of \mathfrak{G} are thus identical. \square

5. A numerical example

In this section, we compute the first terms in the asymptotic expansion for the simple square lattice in two dimensions. These are compared to highly accurate estimates of $\mathfrak{G}(n)$ obtained by numerical quadrature, to indicate that the numbers $C = C(P)$ in Theorem 4.5 are small.

Consider the two-dimensional square lattice \mathbb{Z}^2 where each node is connected to its four nearest neighbours so that the lattice operator equals the five-point discrete Laplace operator. Then

$$\sigma(\xi) = 4 \sin^2 \frac{\xi_1}{2} + 4 \sin^2 \frac{\xi_2}{2}.$$

Using Lemma 3.5 we compute the series expansion of the inverse symbol and find that

$$\begin{aligned} \frac{1}{\sigma(\xi)} &= \frac{1}{|\xi|^2} + \frac{1}{|\xi|^4} \left(\frac{\xi_1^4}{12} + \frac{\xi_2^4}{12} \right) + \frac{1}{|\xi|^6} \left(\frac{\xi_1^8}{240} - \frac{\xi_1^6 \xi_2^2}{360} + \frac{\xi_1^4 \xi_2^4}{72} - \frac{\xi_1^2 \xi_2^6}{360} + \frac{\xi_2^8}{240} \right) + \\ &\quad \frac{1}{|\xi|^8} \left(\frac{\xi_1^{12}}{6048} - \frac{11 \xi_1^{10} \xi_2^2}{30240} + \frac{\xi_1^8 \xi_2^4}{756} - \frac{\xi_1^6 \xi_2^6}{1080} + \frac{\xi_1^4 \xi_2^8}{756} - \frac{11 \xi_1^2 \xi_2^{10}}{30240} + \frac{\xi_2^{12}}{6048} \right) + O(|\xi|^6). \end{aligned}$$

By virtue of Propositions 4.3 and 4.4 we can now compute the $g_p(x)$'s, which are most easily given in polar coordinates, $(x_1, x_2) = r(\cos \theta, \sin \theta)$,

$$\begin{aligned} g_0(x) &= -\frac{1}{2\pi} \log r + C, \quad \text{where } C = -0.2573434264137 \dots \\ g_1(x) &= \left(\frac{\partial_1^4}{12} + \frac{\partial_2^4}{12} \right) \frac{1}{8\pi} |x|^2 \log |x| = \frac{1}{24\pi} \frac{x_1^4 - 6x_1^2 x_2^2 + x_2^4}{|x|^6} = \frac{1}{24\pi} \frac{\cos(4\theta)}{r^2}, \\ g_2(x) &= \dots = \frac{1}{480\pi} \frac{25 \cos(8\theta) + 18 \cos(4\theta)}{r^4} \\ g_3(x) &= \dots = \frac{1}{2016\pi} \frac{490 \cos(12\theta) + 459 \cos(8\theta)}{r^6}. \end{aligned} \tag{4.14}$$

and set $G_P = \sum_{p=0}^P g_p$.

In order to estimate the approximation error

$$E_P(n) := \mathfrak{G}(n) - G_P(n)$$

we randomly distributed 500 points $n \in \mathbb{Z}^2$ in the annulus $5 \leq |n| \leq 100$. For each point we computed the error and plotted $|E_P(n)|$ versus $|n|$ in a log-log diagram, see Figure 4.1. Note that the remainder terms are very small, and that they seem to decay as Theorem 4.5 claimed; $|E_P(n)| \leq C(P)|n|^{-(2P+2)}$. In order to estimate $C(P)$ numerically we plotted $|n|^{2P+2}|E_P(n)|$ versus $|n|$, see Figure 4.2. We estimate that for $|n| \geq 20$, the bound in the theorem is valid with the constants

$$C(0) \approx 0.015, \quad C(1) \approx 0.03, \quad C(2) \approx 0.15.$$

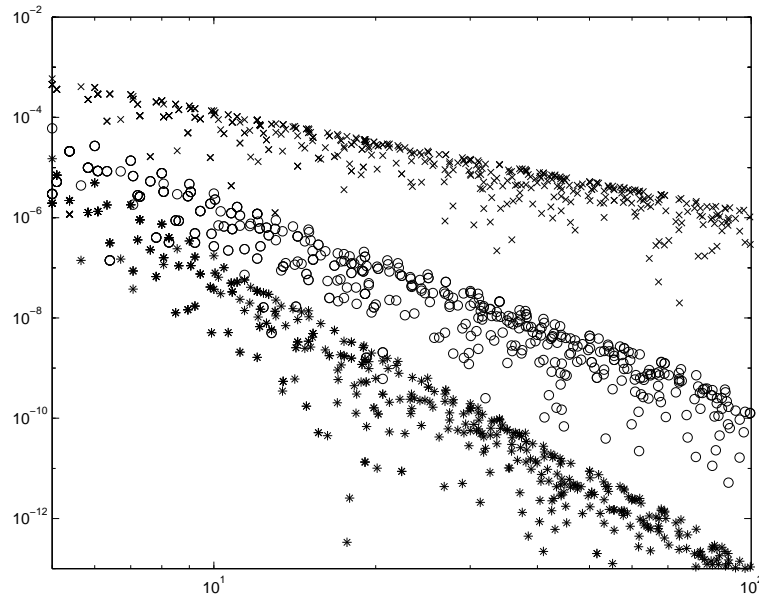


FIGURE 4.1. The absolute error $|E_P(n)|$ plotted versus $|n|$. $|E_0|$ is marked with \times , $|E_1|$ with \circ and $|E_2|$ with $*$.

These numbers indicate that for large n , the remainder term $E_P(n)$ is entirely dominated by the next term in the asymptotic expansion g_{P+1} since

$$\sup_x |x|^2 |g_1(x)| \approx 0.013, \quad \sup_x |x|^4 |g_2(x)| \approx 0.029, \quad \sup_x |x|^6 |g_3(x)| \approx 0.15.$$

Remark: Duffin and Shelly [20] and Cserti [15] give the analytic expression $g_0(x) = -(\log |x| + \gamma + (\log 8)/2)/(2\pi)$, where $\gamma = 0.5772\dots$ is the Euler constant. \square

4. THE LATTICE GREEN'S FUNCTION

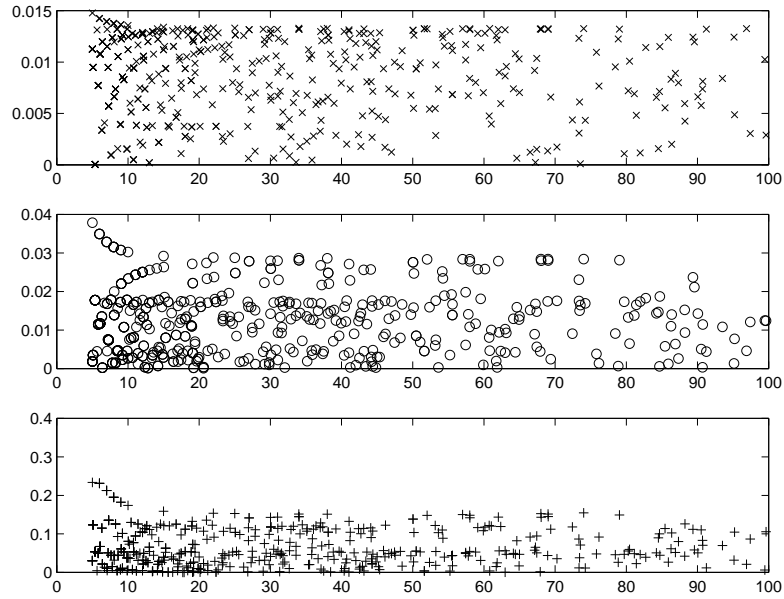


FIGURE 4.2. Plots of $|n|^{2P+2}|E_P(n)|$ versus $|n|$ for $P = 0, 1, 2$, respectively.

CHAPTER 5

Fast summation methods for poly-harmonic kernels

1. Introduction

In this chapter we will derive a fast algorithm for computing convolutions of the form

$$(5.1) \quad \mathbf{u}(m) = [\mathfrak{G} * \mathfrak{f}](m) = \sum_{n \in \Omega_1} \mathfrak{G}(m - n) \mathfrak{f}(n) \quad \forall m \in \Omega_2,$$

where \mathfrak{G} is the lattice Green's function and Ω_1 and Ω_2 are two sets in \mathbb{Z}^d . Letting k_j denote the number of elements in the set Ω_j , we see that a naive evaluation of the sum (5.1) would require evaluating and adding $k_1 k_2$ terms, for each of which, we need to somehow determine $\mathfrak{G}(m - n)$. We will present a method that computes the sum (5.1) to any level of accuracy, using no quadrature, in $O(k_1 + k_2)$ operations. The first step is to approximate $\mathfrak{G}(m - n)$ by the asymptotic expansion $G_P(m - n)$ (defined by (4.5)) when $|m - n|$ is larger than some cut-off range R ,

$$(5.2) \quad \mathbf{u}(m) = \sum_{n \in \Omega_1 \cap B_R(m)} \mathfrak{G}(m - n) \mathfrak{f}(n) + \sum_{n \in \Omega_1 \setminus B_R(m)} G_P(m - n) \mathfrak{f}(n) + \sum_{n \in \Omega_1 \setminus B_R(m)} (\mathfrak{G}(m - n) - G_P(m - n)) \mathfrak{f}(n),$$

where $B_R(m) = \{x : |x - m| \leq R\}$. The last term is an error term that is bounded by $C \|\mathfrak{f}\|_{l^1(\Omega_1)} / R^{2P+d}$. Thus, by making R sufficiently large, this term can be made as small as desired. The first term can be evaluated in $O(k_2)$ operations since for any m , the number of nodes in $\Omega_1 \cap B_R(m)$ is bounded by a constant (for a fixed R). Furthermore, $B_R(m) \cap \mathbb{Z}^d$ is typically a set of very modest¹ size, which makes it possible to precompute the values of $\mathfrak{G}(m - n)$ that enter the first term.

For the middle term in (5.2) we will use a variation of the Fast Multipole Method by Greengard and Rokhlin [31, 32]. This algorithm was originally presented as a tool for evaluating convolutions between a charge distribution f and the fundamental solution of the Laplace equation,

$$(5.3) \quad \Phi(x) = \begin{cases} -(4\pi|x|)^{-1}, & d = 3, \\ -(2\pi)^{-1} \log|x|, & d = 2, \end{cases}$$

and reduces the work required to evaluate the potential from N point charges at N sites from $O(N^2)$ to $O(N)$. This is accomplished through the use of hierarchical data-structures and a representation of harmonic potential fields through multipole expansions. The main goal of this chapter is to demonstrate how to extend the FMM to cover poly-harmonic kernel functions such as G_P .

¹For a typical lattice such as the square, triangular or honeycomb lattices described in Appendix B, choosing $P = 2$ and $R = 30$ gives a relative accuracy of 10^{-10} , which is sufficient for most purposes. Then $\#[B_{30} \cap \mathbb{Z}^2] \approx 3000$, but due to symmetry, only an eighth of those values actually need to be computed.

We will not in this context give a full presentation of the FMM since this can be found in the references mentioned. Our goal is exclusively to provide the mathematical results that are required to extend the FMM to cover poly-harmonic kernels. For this purpose, it is sufficient to consider the following toy problem: Suppose that we want to evaluate

$$(5.4) \quad u(x_i) = \sum_{j=1}^{k_1} f_j G(x_i - y_j) \quad \text{for } i = 1, \dots, k_2,$$

where $x_i \in \Omega_1$ and $y_j \in \Omega_2$ for two well-separated sets Ω_1 and Ω_2 . It is then advantageous to introduce a separation of variables

$$(5.5) \quad G(x - y) = \sum_{q=0}^{\infty} \sum_{\alpha \in I_q} h_\alpha(y) H_\alpha(x),$$

where the I_q 's are index sets, the h_α 's are polynomials of degree q and H_α are some basis functions. When such a separation of variables is available, the sum (5.4) can be reorganized as follows;

$$u(x_i) = \sum_{j=1}^{k_1} f_j \sum_{q=0}^{\infty} \sum_{\alpha \in I_q} h_\alpha(y_j) H_\alpha(x_i) = \sum_{q=0}^{\infty} \sum_{\alpha \in I_q} \left[\sum_{j=1}^{k_1} f_j h_\alpha(y_j) \right] H_\alpha(x_i).$$

If the sum converges fast, it can be truncated after Q terms, so that

$$u(x_i) \approx \sum_{q=0}^Q \sum_{\alpha \in I_q} c_\alpha H_\alpha(x_i), \quad \text{where} \quad c_\alpha = \sum_{j=1}^{k_1} f_j h_\alpha(y_j).$$

The coefficients c_α can be precomputed using $O(k_1)$ operations, so that then $u(x_i)$ can be computed using $O(k_2)$ operations, which gives a total operation count of $O(k_1 + k_2)$. For this algorithm to be efficient, the separation (5.5) must be economical, in the sense that the index sets I_q are small, and it must converge fast, so that a small Q gives high accuracy. The classical FMM deals with the kernel $G = \Phi$, and achieves both of these goals using a classical multipole expansion in (5.5).

In this chapter we will present a generalized multipole expansion of the form (5.5) that is valid for a poly-harmonic kernel G . In section 2 we derive the expansion and show that the poly-harmonicity can be used to attain sparsity. In section 3 we will show that when G is a rational function (which it is in our case), the expansion converges almost as fast as for the harmonic case. For simplicity, we restrict attention to two-dimensional problems in this section. In section 4 we give some numerical examples that indicate that the constants in the asymptotic error bounds provided in section 3 are small. Without loss of generality, we will throughout this chapter assume that the matrix M in (3.10) equals unity.

2. Multipole expansions of poly-harmonic functions

When deriving the multipole expansion for a poly-harmonic function we will start from a plain MacLaurin expansion,

$$(5.6) \quad f(x) = \sum_{q=0}^{\infty} \sum_{\alpha \in \mathbb{I}_q} \frac{1}{\alpha!} c_\alpha x^\alpha, \quad \text{where } c_\alpha = \partial^\alpha f(0), \quad \mathbb{I}_q = \{\alpha \in \mathbb{N}^d : |\alpha| = q\}.$$

We suppose that this series is absolutely convergent in some neighborhood Ω containing the origin and that f satisfies $(-\Delta)^{P+1}f = 0$ in Ω (the variable P is set to conform with the P defined in Chapter 4). This imposes the following condition on the coefficients c_α : For any positive integer q

$$(5.7) \quad (-\Delta)^{P+1} \sum_{\alpha \in \mathbb{I}_q} \frac{1}{\alpha!} c_\alpha x^\alpha = 0, \quad \forall x \in \Omega.$$

Let the constants b_β^α be such that $(-\Delta)^{P+1}x^\alpha = \sum_{\beta \in \mathbb{I}_{|\alpha|-2(P+1)}} b_\beta^\alpha x^\beta$. Then we can write (5.7) as

$$\sum_{\beta \in \mathbb{I}_{q-2(P+1)}} \left[\sum_{\alpha \in \mathbb{I}_q} b_\beta^\alpha c_\alpha \right] x^\beta = 0,$$

which forms a system of $\#\mathbb{I}_{q-2(P+1)}$ equations for $\#\mathbb{I}_q$ unknowns. This system is of full rank (since the equation $(-\Delta)^{P+1}\phi = x^\beta$ has a solution $\phi \in \Pi^q$ for any $\beta \in \mathbb{I}_{q-2(P+1)}$). As a consequence we can find a subset $I_q \subset \mathbb{I}_q$ (of cardinality $\#\mathbb{I}_q - \#\mathbb{I}_{q-2(P+1)}$) such that any c_α is entirely determined by the values $\{c_\beta\}_{\beta \in I_q}$. In other words, there exist numbers d_α^β such that for any α

$$(5.8) \quad c_\alpha = \sum_{\beta \in I_q} d_\alpha^\beta c_\beta.$$

Recalling that $c_\alpha = [\partial^\alpha f](0)$, we see that (5.8) is simply a relationship between the partial derivatives of a poly-harmonic function.

Lemma 5.1: *If f satisfies $(-\Delta)^{P+1}f = 0$, then $\partial^\alpha f = \sum_{\beta \in I_q} d_\alpha^\beta \partial^\beta f$.*

Next, we insert (5.8) into the expansion (5.6) and obtain

$$(5.9) \quad f(x) = \sum_{q=0}^{\infty} \sum_{\alpha \in \mathbb{I}_q} \frac{1}{\alpha!} \sum_{\beta \in I_q} d_\alpha^\beta c_\beta x^\alpha = \sum_{q=0}^{\infty} \sum_{\beta \in I_q} c_\beta \left[\sum_{\alpha \in \mathbb{I}_q} \frac{1}{\alpha!} d_\alpha^\beta x^\alpha \right].$$

Defining poly-harmonic ‘‘basis’’-functions

$$(5.10) \quad h_\beta(x) = \sum_{\alpha \in \mathbb{I}_{|\beta|}} \frac{1}{\alpha!} d_\alpha^\beta x^\alpha,$$

we get the following result (which uses that poly-harmonicity implies analyticity):

Lemma 5.2: *Suppose that $(-\Delta)^{P+1}f = 0$ on $\Omega \ni 0$. Then*

$$f(x) = \sum_{q=0}^{\infty} \sum_{\alpha \in I_q} c_\alpha h_\alpha(x), \quad \text{where } c_\alpha = \partial^\alpha f(0).$$

This lemma directly gives the multipole expansion for poly-harmonic kernels.

Theorem 5.3: Multipole expansion. *If $(-\Delta)^{P+1}G = 0$ in $\mathbb{R}^d \setminus \{0\}$, then for $|y| < |x|$,*

$$(5.11) \quad G(x-y) = \sum_{q=0}^{\infty} \sum_{\alpha \in I_q} h_\alpha(-y) H_\alpha(x), \quad \text{where } H_\alpha(x) = [\partial^\alpha G](x).$$

Proof: The function $y \mapsto G(x - y)$ is poly-harmonic in the open ball $\{y : |y| < |x|\}$ and is thus analytic in this region. An application of Lemma 5.2 then yields the desired result. \square

Note the sparsity of the representation (5.11). Using the poly-harmonicity of the kernel function, we reduced the number of terms at level q from $\#\mathbb{I}_q$ to $\#I_q = \#\mathbb{I}_q - \#\mathbb{I}_{q-2(P+1)}$. In two dimensions, $\#\mathbb{I}_q = q + 1$ and thus the representation (5.11) has at most $2(P + 1)$ terms at each level. In three dimensions, $\#\mathbb{I}_q = (q + 2)(q + 1)/2$ and thus $\#I_q = (P + 1)(2q + 1 - 2P)$. Happily, these results conform with the familiar results for harmonic functions (the case $P = 0$).

Examples: Consider the kernel $\Phi(x) = -(2\pi)^{-1} \log|x|$. Setting $I_q := \{(q, 0), (q - 1, 1)\}$ in the new formalism, we retrieve the classical expansion in multipoles. In polar coordinates $(x_1, x_2) = r(\cos \theta, \sin \theta)$ these take the form

$$h_{(q,0)}(x) = r^q \cos(q\theta), \quad h_{(q-1,1)}(x) = r^q \sin(q\theta),$$

$$H_{(q,0)}(x) = \frac{(-1)^q \cos(q\theta)}{2\pi q} \frac{1}{r^q}, \quad H_{(q-1,1)}(x) = \frac{(-1)^q \sin(q\theta)}{2\pi q} \frac{1}{r^q}.$$

Consider next the bi-harmonic kernel $G_1(x) = \Phi(x) + (x_1^4 - 6x_1^2x_2^2 + x_2^4)/(24\pi|x|^6)$, cf. (4.14). We then set $I_q := \{(q, 0), (q - 1, 1), (q - 2, 2), (q - 3, 3)\}$ and obtain, e.g.

$$h_{(4,3)}(x) = r^7 \left(-\frac{5}{4} \sin(7\theta) + \frac{7}{4} \sin(5\theta) \right), \quad H_{(4,3)}(x) = \frac{1}{14\pi} \frac{\sin(7\theta)}{r^7} + \frac{9 \sin(11\theta) - \sin(9\theta)}{6\pi r^9}.$$

\square

The FMM relies on three ‘‘shift theorems’’ that specify (1) how to change the origin of a multipole expansion, (2) how to convert a multipole to a local expansion and (3) how to shift the origin of a local expansion. We next give analogues of these results valid for poly-harmonic functions.

Proposition 5.4: [*Translation of a multipole expansion.*] Suppose that for a fixed $y \in \mathbb{R}^d$ a potential $\varphi(x)$ is defined for $|x| > |y|$ by

$$(5.12) \quad \varphi(x) = \sum_{q=0}^{\infty} \sum_{\alpha \in I_q} c_\alpha H_\alpha(x - y),$$

with H_α defined in Theorem 5.3. Then

$$\varphi(x) = \sum_{r=0}^{\infty} \sum_{\gamma \in I_r} c'_\gamma H_\gamma(x),$$

where

$$c'_\gamma = \sum_{q=0}^{|\gamma|} \sum_{\alpha \in I_q} c_\alpha \sum_{\beta \in I_{|\gamma|-q}} d_{\alpha+\beta}^\gamma h_\beta(-y).$$

Proof: First we apply Lemma 5.2 to the function $y \mapsto H_\alpha(x - y)$,

$$H_\alpha(x - y) = \sum_{p=0}^{\infty} \sum_{\beta \in I_p} h_\beta(-y) \partial^\beta H_\alpha(x).$$

Then apply Lemma 5.1

$$\partial^\beta H_\alpha(x) = \partial^{\alpha+\beta} G(x) = \sum_{\gamma \in I_{|\alpha+\beta|}} d'_{\alpha+\beta} \partial^\gamma G(x) = \sum_{\gamma \in I_{|\alpha+\beta|}} d'_{\alpha+\beta} H_\gamma(x).$$

Combining these expressions with (5.12) we get

$$\varphi(x) = \sum_{q=0}^{\infty} \sum_{\alpha \in I_q} c_\alpha \sum_{p=0}^{\infty} \sum_{\beta \in I_p} h_\beta(-y) \sum_{\gamma \in I_{p+q}} d'_{\alpha+\beta} H_\gamma(x),$$

and changing summation variables, $r = p + q$,

$$\varphi(x) = \sum_{r=0}^{\infty} \sum_{\gamma \in I_r} \left[\sum_{q=0}^r \sum_{\alpha \in I_q} c_\alpha \sum_{\beta \in I_{r-q}} d'_{\alpha+\beta} h_\beta(-y) \right] H_\gamma(x).$$

□

Proposition 5.5: [*Conversion of a multipole expansion into a local expansion.*] Suppose that $\varphi(x)$ is defined by equation (5.12), then for $|x| < |y|$,

$$\varphi(x) = \sum_{p=0}^{\infty} \sum_{\beta \in I_p} c'_\beta h_\beta(x),$$

where

$$c'_\beta = \sum_{q=0}^{\infty} \sum_{\alpha \in I_q} c_\alpha \sum_{\gamma \in I_{|\alpha+\beta|}} d'_{\alpha+\beta} H_\gamma(-y).$$

Proof: This is very similar to the previous proof, but with the variables reversed,

$$H_\alpha(x-y) = \sum_{p=0}^{\infty} \sum_{\beta \in I_p} h_\beta(x) H_{\alpha+\beta}(-y) = \sum_{p=0}^{\infty} \sum_{\beta \in I_p} h_\beta(x) \sum_{\gamma \in I_{|\alpha+\beta|}} d'_{\alpha+\beta} H_\gamma(-y),$$

and so

$$\varphi(x) = \sum_{q=0}^{\infty} \sum_{\alpha \in I_q} c_\alpha \sum_{p=0}^{\infty} \sum_{\beta \in I_p} h_\beta(x) \sum_{\gamma \in I_{|\alpha+\beta|}} d'_{\alpha+\beta} H_\gamma(-y),$$

whence the claims follows upon a simple interchange of summation order. □

Proposition 5.6: [*Translation of a local expansion.*] For any x and y we have

$$(5.13) \quad \sum_{q=0}^Q \sum_{\alpha \in I_q} c_\alpha h_\alpha(x-y) = \sum_{p=0}^Q \sum_{\beta \in I_p} c'_\beta h_\beta(x),$$

where

$$c'_\beta = \sum_{q=|\beta|}^Q \sum_{\alpha \in I_q} c_\alpha [\partial^\beta h_\alpha](-y).$$

Proof: Applying Lemma 5.2 to the function $x \mapsto h_\alpha(x - y)$ we get

$$h_\alpha(x - y) = \sum_{p=0}^{\infty} \sum_{\beta \in I_p} h_\beta(x) [\partial^\beta h_\alpha](-y) = \sum_{p=0}^{|\alpha|} \sum_{\beta \in I_p} h_\beta(x) [\partial^\beta h_\alpha](-y),$$

whence the claim follows immediately. \square

Remark 1: According to the Almansi representation formula (see [41]) a polyharmonic function ψ of degree k can be written $\psi(x) = \sum_{j=0}^{k-1} |x|^{2j} \phi_j(x)$, for some harmonic functions ϕ_j . A series expansion analogous to (5.11) can be obtained by combining this representation with the well-known expansions of harmonic functions ([41] section 10.14). This derivation requires more work than the one presented here but is very relevant in that it directly shows that the new basis functions h_α and H_α can be constructed from the well-known spherical harmonics.

Remark 2: In two dimensions, the multipole expansion can be derived using complex variables (Vekua [64, 65]). This is faster and yields explicit expressions for h_α and H_α but since this derivation obscures the key point we want to make that the multipole expansion is a “culled” Taylor expansion and since it does not generalize to higher dimensions we have relegated this derivation to Appendix C.

Remark 3: The formula given in Proposition 5.5 for shifting a multipole to a local expansion is a direct analogue of the formula for harmonic functions given in the original version of the FMM. In three dimensions, this formula requires $O(Q^4)$ operations to shift a multipole expansion that is truncated after Q terms to a local expansion. This is oftentimes prohibitively expensive but it has been discovered that a quite simple trick can be used to reduce the cost to $O(Q^3)$, while a more elaborate method brings it down to $O(Q^2)$, see Greengard and Rokhlin [32]. The first of these enhancements certainly generalizes to the present case (since it builds on a simple property of the spherical harmonics) and it is our belief that the second does as well.

3. Convergence of the new multipole expansions

In section 1 we stated that the two key properties that a separation of variables (5.5) must satisfy are sparsity and fast convergence. In section 2, we showed that poly-harmonicity implies sparsity. In this section we show that when the kernel is a rational function

$$(5.14) \quad G(x - y) = \frac{\varphi(x - y)}{|x - y|^{2k}},$$

for some polynomial φ of degree $l < 2k$, then

$$(5.15) \quad \left| G(x - y) - \sum_{q=0}^Q \sum_{\alpha \in I_q} h_\alpha(y) H_\alpha(x) \right| \leq (C + cQ^{2k-1}) \frac{1}{(1 - |y|/|x|)^{2k}} \frac{1}{|x|^{2k}} \left(\frac{|y|}{|x|} \right)^{Q+1}$$

for some C and c that do not depend on Q , x or y . Since the Taylor and the multipole expansions are identical, it will be sufficient to prove (5.15) for the Taylor expansion. This observation significantly simplifies the analysis. All results in this section are proved for the case $d = 2$ only.

Since the asymptotic expansion G_P of a lattice Green’s function is a sum of rational functions of the form (5.14), the bound (5.15) will apply to the situation discussed in section 1.

Definition: Given a function $f(y)$ we let $[T_Q f](y)$ denote its Q 'th order MacLaurin expansion and $[R_Q f](y)$ the remainder part so that $f(y) = [T_Q f](y) + [R_Q f](y)$.

Lemma 5.7: Let k be an integer and fix an $x \in \mathbb{R}^2$ such that $x \neq 0$. Then the function $f_x(y) = |x - y|^{-2k}$ has the MacLaurin series

$$(5.16) \quad \frac{1}{|x - y|^{2k}} = \frac{1}{|x|^{2k}} \sum_{q=0}^{\infty} \sum_{n=0}^q \binom{n+k-1}{k-1} \binom{q-n+k-1}{k-1} \left(\frac{y_1 + \mathbf{i}y_2}{x_1 + \mathbf{i}x_2} \right)^n \left(\frac{y_1 - \mathbf{i}y_2}{x_1 - \mathbf{i}x_2} \right)^{q-n},$$

which converges absolutely for $|y| < |x|$. The truncation error is bounded by

$$|[R_Q f_x](y)| \leq C \frac{Q^{2k-1}}{(1 - |y|/|x|)^{2k}} \frac{1}{|x|^{2k}} \left(\frac{|y|}{|x|} \right)^{Q+1}$$

where C depends on k but not on x , y or Q .

Proof: Identifying the points x and y with their complex representations we have

$$(5.17) \quad \frac{1}{|x - y|^{2k}} = \frac{1}{|x|^{2k}} \frac{1}{(1 - y/x)^k} \frac{1}{(1 - \bar{y}/\bar{x})^k}.$$

Then use that $w \mapsto (1 - w)^{-k}$ has the MacLaurin expansion

$$(5.18) \quad \frac{1}{(1 - w)^k} = \sum_{n=0}^{\infty} \binom{n+k-1}{k-1} w^n,$$

absolutely convergent for $|w| < 1$. The expression (5.16) then follows by inserting (5.18) into (5.17) and interchanging the summation order.

We will prove below that there exists a $C = C(k)$ such that

$$(5.19) \quad \sum_{n=0}^q \binom{n+k-1}{k-1} \binom{q-n+k-1}{k-1} \leq C q^{2k-1}.$$

We use this to bound the truncation error,

$$\begin{aligned} |[R_Q f_x](y)| &\leq \frac{1}{|x|^{2k}} \sum_{q=Q+1}^{\infty} C q^{2k-1} \frac{|y|^q}{|x|^q} = C \frac{1}{|x|^{2k}} \left(\frac{|y|}{|x|} \right)^{Q+1} \sum_{q=0}^{\infty} (q+Q+1)^{2k-1} \left(\frac{|y|}{|x|} \right)^q \\ &\leq C \frac{1}{|x|^{2k}} \left(\frac{|y|}{|x|} \right)^{Q+1} \sum_{q=0}^{\infty} \left(Q^{2k-1} + (q+1)^{2k-1} \right) \left(\frac{|y|}{|x|} \right)^q \\ &\leq C \frac{1}{|x|^{2k}} \left(\frac{|y|}{|x|} \right)^{Q+1} \left[\frac{Q^{2k-1}}{1 - |y|/|x|} + \frac{1}{(1 - |y|/|x|)^{2k}} \right]. \end{aligned}$$

It remains only to demonstrate (5.19),

$$\begin{aligned} \sum_{n=0}^q \binom{n+k-1}{k-1} \binom{q-n+k-1}{k-1} &= \sum_{n=0}^q \frac{(n+k-1) \cdots (n+1)}{(k-1)!} \frac{(q-n+k-1) \cdots (q-n+1)}{(k-1)!} \\ &\leq \sum_{n=0}^q \frac{(q+k-1)^{k-1}}{(k-1)!} \frac{(q+k-1)^{k-1}}{(k-1)!} = (q+1) \frac{(q+k-1)^{2(k-1)}}{((k-1)!)^2} \leq C(k) q^{2k-1}. \end{aligned}$$

□

Lemma 5.8: *Let φ be a multinomial of degree l , where $l < 2k$. Then the function*

$$g_x(y) = \frac{\varphi(x-y)}{|x-y|^{2k}}$$

has a MacLaurin series, convergent for $|y| < |x|$, such that

$$|[R_Q g_x](y)| \leq C \frac{Q^{2k-1}}{(1-|y|/|x|)^{2k}} \frac{1}{|x|^{2k-l}} \left(\frac{|y|}{|x|}\right)^{Q+1}.$$

Proof: There exist coefficients $c_{\beta\gamma}$ such that

$$\varphi(x-y) = \sum_{|\beta|+|\gamma|=l} c_{\beta\gamma} (-y)^\beta x^\gamma.$$

Let $f_x(y)$ be defined as in Lemma 5.7. Then, since $g_x(y) = \varphi(x-y)f_x(y)$,

$$g_x(y) = \underbrace{\sum_{|\beta|+|\gamma|=l} c_{\beta\gamma} (-y)^\beta x^\gamma [T_{Q-|\beta|} f_x](y)}_{=: [T_Q g_x](y)} + \underbrace{\sum_{|\beta|+|\gamma|=l} c_{\beta\gamma} (-y)^\beta x^\gamma [R_{Q-|\beta|} f_x](y)}_{=: [R_Q g_x](y)}.$$

Using the bound in Lemma 5.7 for $[R_Q f_x](y)$ we now get

$$\begin{aligned} |[R_Q g_x](y)| &\leq \sum_{|\beta|+|\gamma|=l} |c_{\beta\gamma}| |y|^{|\beta|} |x|^{|\gamma|} C \frac{(Q-|\beta|)^{2k-1}}{(1-|y|/|x|)^{2k}} \frac{1}{|x|^{2k}} \left(\frac{|y|}{|x|}\right)^{Q+1-|\beta|} \\ &\leq \sum_{|\beta|+|\gamma|=l} |c_{\beta\gamma}| C \frac{Q^{2k-1}}{(1-|y|/|x|)^{2k}} \frac{1}{|x|^{2k-|\beta|-|\gamma|}} \left(\frac{|y|}{|x|}\right)^{Q+1}, \end{aligned}$$

which simplifies to the required bound. □

In the last result of this chapter, we sum up the various findings of this section and section 2 and demonstrate how they apply to the asymptotic approximation of the lattice Green's function.

Theorem 5.9: *Let $G = G_P$ be the asymptotic expansion of a lattice Green's function defined by (4.5). Its multipole expansion is given by Theorem 5.3. The translation formulas are given in Propositions 5.4, 5.5 and 5.6. If any of these expansions is truncated after Q terms, then for any $\rho < |y|/|x|$, there is a constant C such that the truncation error is bounded by $C\rho^Q$.*

Remark: The term Q^{2k-1} in the bound in Lemma 5.8 indicates that the expansion of a polyharmonic function may converge significantly slower than a that of a harmonic function. When the results are applied to the function G_P defined by (4.5), this is not observed. A careful investigation of the error bounds indicate why. First, we note that the bound (5.19) is very coarse, a more careful analysis shows that as $p \rightarrow \infty$

$$\sum_{n=0}^q \binom{n+k-1}{k-1} \binom{q-n+k-1}{k-1} = \frac{1}{2^{k-1} (k-1)! (2k-1)!!} q^{2k-1} + O(q^{2k-2}),$$

which shows that even though the sum does indeed grow like q^{2k-1} , the coefficient in front of the leading factor is very small. Second, for the present application, the terms with $k = 2, 3, 4$ have very small coefficients in front of them, and furthermore, the negative effect that the Q^{2k-1} term may

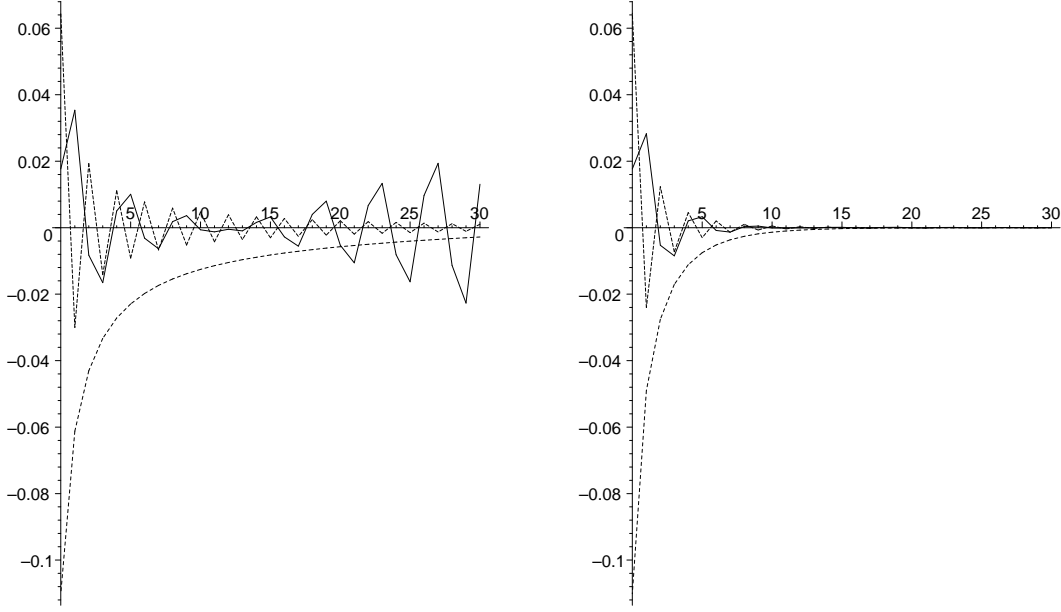


FIGURE 5.1. **Left:** Plot of $Q \mapsto (|x|/|y|)^Q |G_P - G_{PQ}|$ for $Q = 1$, $x = (10, 10)$ and $y = (5, 5)$ (dotted line), $y = (5, -5)$ (solid line) and $y = (-5, -5)$ (dashed line). **Right:** Plot of $Q \mapsto (4|x|/5|y|)^Q |G_P - G_{PQ}|$ for the same parameter values.

induce is ameliorated by the decay factor $|x|^{-2k}$. Thus, in practical applications, the truncation error is dominated by the error incurred by the leading term in the expansion, which is precisely the harmonic kernel Φ that the classical FMM deals with. \square

4. Numerical experiments

Our goal in this section is to estimate the constants that occur in the error bound (5.15) by applying the results derived in this section to a concrete example.

Let G_P denote the P term asymptotic expansion of the Green's function for a square lattice, as specified by (4.14), and let G_{PQ} denote a multipole expansion of the form (5.11) that has been truncated after Q levels. We expect that, if $|y|/|x| \leq c < 1$, then

$$(5.20) \quad |G_P(x - y) - G_{PQ}(x, y)| \leq C(Q) \left(\frac{|y|}{|x|} \right)^Q,$$

where C does not depend on Q for $P = 0$ but may grow at most polynomially with Q for $Q \geq 1$. Inspired by the form (5.20) we plot the function $Q \mapsto (|x|/|y|)^Q |G_P(x - y) - G_{PQ}(x, y)|$ for different P , x and y . In the left graph of Figure 5.1 we chose $Q = 1$, $x = (10, 10)$ and $y = (5, 5)$, $(5, -5)$, $(-5, -5)$. We note first that in this situation the bound (5.20) holds with $C = 0.1$. Similar experiments carried out for many different values of x and y confirmed the estimate $C \approx 0.1$ when $P \leq 30$. What is less satisfying is that it appears that $C(P)$ does start to grow for large P in certain situations. Fortunately, this is significant only for values of P that would not normally be used (note that $P = 30$ corresponds to a relative accuracy of 10^{-9}). We also note that since the

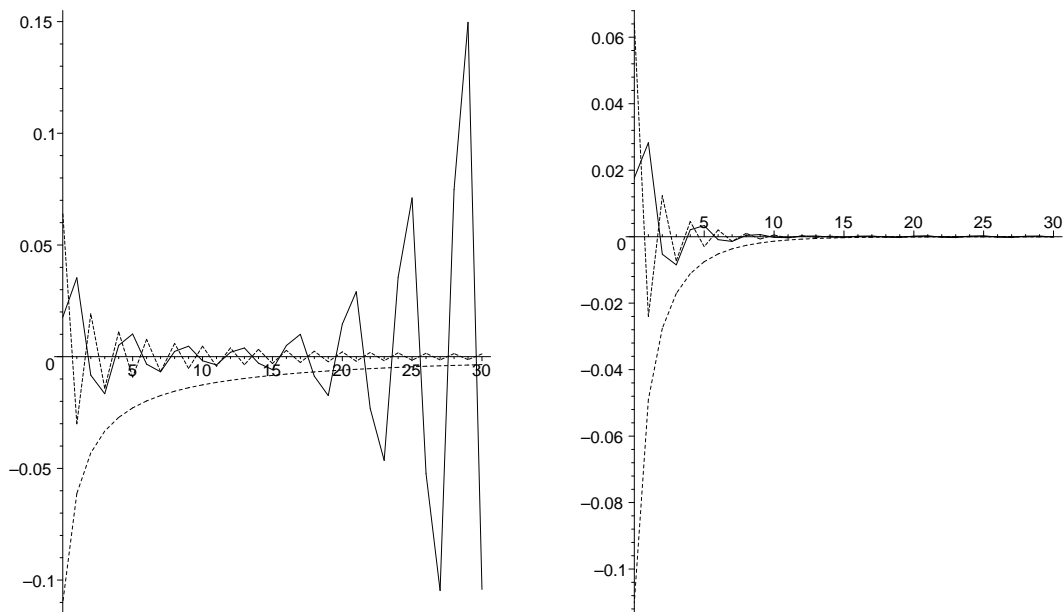


FIGURE 5.2. **Left:** Plot of $Q \mapsto (|x|/|y|)^Q |G_P - G_{PQ}|$ for $Q = 2$, $x = (10, 10)$ and $y = (5, 5)$ (dotted line), $y = (5, -5)$ (solid line) and $y = (-5, -5)$ (dashed line). **Right:** Plot of $Q \mapsto (4|x|/5|y|)^Q |G_P - G_{PQ}|$ for the same parameter values.

growth is polynomial the entity $\rho^{-Q} |G_P - G_{PQ}|$ should be uniformly bounded for any $\rho < |y|/|x|$. The plot of $Q \mapsto ((4/5)(|x|/|y|))^Q |G_P - G_{PQ}|$ to the right in Figure 5.1 seems to confirm this prediction.

In Figure 5.2 give show the results of the same experiment carried out for $Q = 2$. We see that the situation remains qualitatively the same.

CHAPTER 6

Boundary equation methods for problems on finite domains

1. Introduction

In this chapter we present methods for solving lattice problems on finite domains. Given a homogeneous Dirichlet or Neumann problem, we reformulate it as a boundary equation very similar in spirit to the boundary integral equations of classical potential theory, but with the lattice Green function as the kernel, rather than the fundamental solution of the Laplace operator. These boundary equations have low condition numbers and can be solved very efficiently using iterative solvers. The most time-consuming step of such a solver is the application of a dense matrix to a vector, but this matrix-vector multiplication is of a form very close to the convolution (5.1) for which we derived fast methods in the previous chapter.

An inhomogeneous discrete boundary value problem (*i.e.* one including a body load) can be split into one inhomogeneous problem on \mathbb{Z}^d and one homogeneous boundary value problem using the “fictitious domain method”, as done in Beylkin *et al* [3] for the continuous case, and can thus be treated by combining the techniques presented in Chapter 5 and the present chapter.

Since we have not heretofore discussed problems on finite domains, we need to introduce some new notation. Let $\Omega \subset \mathbb{Z}^2$ denote a domain, let $\Gamma \subset \Omega$ denote those nodes in Ω that connect to Ω^c and set $\Omega_- := \Omega \setminus \Gamma$. Similarly, let Γ_+ be those nodes of Ω^c that connect to Ω . For $n \in \Gamma$, let $\mathbb{D}_n \subset \Gamma_+$ denote the nodes in Ω^c that connect to n and set $[\delta_\nu \mathbf{u}](n) = \sum_{k \in \mathbb{D}_n} (\mathbf{u}(k) - \mathbf{u}(n))$.

The Dirichlet problem reads

$$(D) \quad \begin{cases} [\mathfrak{A}\mathbf{u}](m) = 0, & m \in \Omega_-, \\ \mathbf{u}(m) = \mathbf{g}(m), & m \in \Gamma. \end{cases}$$

Note in particular that the condition $\mathfrak{A}\mathbf{u} = 0$ is enforced only at the *internal* nodes. The Neumann problem reads

$$(N) \quad \begin{cases} [\mathfrak{A}\mathbf{u}](m) = 0, & m \in \Omega, \\ [\delta_\nu \mathbf{u}](m) = \mathbf{g}(m), & m \in \Gamma. \end{cases}$$

For $m \in \Gamma$, the operator $[\mathfrak{A}\mathbf{u}](m)$ formally involves values of \mathbf{u} on Γ_+ which are as yet undefined. However, their contribution to the equation at $m \in \Gamma$ is fully specified by the value of $[\delta_\nu \mathbf{u}](m)$.

2. Indirect formulations of the Dirichlet problem

2.1. A single layer formulation: The single layer potential S maps a function defined on Γ to a function on \mathbb{Z}^d . Given $\phi : \Gamma \rightarrow \mathbb{R}$ we set

$$S\phi : \mathbb{Z}^d \rightarrow \mathbb{R} : m \mapsto \sum_{n \in \Gamma} \mathfrak{G}(m - n)\phi(n).$$

Note that $[\mathfrak{A}(\mathbf{S}\phi)](m) = 0$ for any $m \notin \Gamma$. Thus, if we can find a ϕ such that

$$(2.3) \quad [\mathbf{S}\phi](m) = \mathbf{g}(m), \quad \forall m \in \Gamma,$$

then $\mathbf{S}\phi$ satisfies (D). We refer to (2.3) as a *(discrete) single layer boundary equation*. In this context it is a linear system with a square matrix K_S .

Proposition 6.1: *The matrix K_S associated with (2.3) is non-singular.*

Proof: We consider first the case $d \geq 3$. Suppose that $\mathbf{u} = \mathbf{S}\phi$ and that $\mathbf{u}|_\Gamma = 0$. Then \mathbf{u} satisfies

$$(2.4) \quad \begin{cases} [\mathfrak{A}\mathbf{u}](m) = 0, & m \in \mathbb{Z}^d \setminus \Gamma, \\ \mathbf{u}(m) = 0, & m \in \Gamma, \\ \|\mathbf{u}\|_{\mathfrak{A}} < \infty. \end{cases}$$

In other words, \mathbf{u} satisfies homogeneous Dirichlet problems with zero boundary data on both the interior and exterior domains. This implies that $\mathbf{u} \equiv 0$, and thus $\phi = 0$.

What complicates the two dimensional case is that unless $\sum \phi = 0$, the function \mathbf{u} does not have finite energy. We must therefore fall back on a limit argument to prove the statement. Let $\mathfrak{G}^{(J)}$ be the Green's function for a homogeneous Dirichlet problem with zero boundary data on $\partial\Omega_J$, where J is large enough that $\Omega \subset \Omega_J$. Let $K_S^{(J)}$ be the matrix with entries $\mathfrak{G}^{(J)}(m, n)$. Then the argument made for the three dimensional case can be used to prove that $K_S^{(J)}$ is non-singular (the exterior problem in (2.4) is replaced by a problem on $\Omega_J \setminus \Omega$). The last point of the argument is to note that as $J \rightarrow \infty$, $\mathfrak{G}^{(J)}(m, n) \rightarrow \mathfrak{G}(m - n) + (2\pi)^{-1} \log R$ and so $K_S^{(J)} - (2\pi)^{-1} \log R \rightarrow K_S$. \square

2.2. A double layer formulation: The double layer potential \mathbf{D} maps a boundary function to a global function as follows,

$$\mathbf{D}\phi : \mathbb{Z}^d \rightarrow \mathbb{R} : m \mapsto \sum_{n \in \Gamma} \mathfrak{G}_\nu(m, n) \phi(n),$$

where the kernel \mathfrak{G}_ν is a discrete analogue of the double layer kernel, $\partial_{\nu_y} G(x - y)$,

$$\mathfrak{G}_\nu(m, n) := \sum_{k \in \mathbb{D}_n} (\mathfrak{G}(m - k) - \mathfrak{G}(m - n)) = \delta_{\nu_n} \mathfrak{G}(m - n).$$

Physically, the function $\mathbf{D}\phi$ is the potential produced by a double layer source field on $\Gamma \cup \Gamma_+$. For $n \in \Gamma$, node n is given a charge $-|\mathbb{D}_n| \phi(n)$ and each node in $\mathbb{D}_n \subset \Gamma_+$ is given a charge $\phi(n)$, see Figure 6.1. Consequently, $[\mathfrak{A}(\mathbf{D}\phi)](m) = 0$ if $m \notin \Gamma \cup \Gamma_+$. Now, $\mathbf{D}\phi$ is a solution of (D) if ϕ satisfies

$$(2.5) \quad [\mathbf{D}\phi](m) = \mathbf{g}(m), \quad \forall m \in \Gamma,$$

which is our *(discrete) double layer boundary equation*.

The form of the equation (2.5) makes it look like a discrete analogue of an integral equation of the first kind. This is disconcerting since we know that in the continuous case, the double layer equation is a second kind Fredholm equation, *cf.* (1.14). In order to demonstrate the connection between the discrete and the continuous equations, we introduce \mathfrak{B} as a local averaging operator (τ_m is the shift operator defined by (2.4)),

$$\mathfrak{B}\mathbf{u} := \frac{1}{2d} \sum_{j=1}^d (\tau_{e_j} \mathbf{u} + \tau_{-e_j} \mathbf{u}),$$

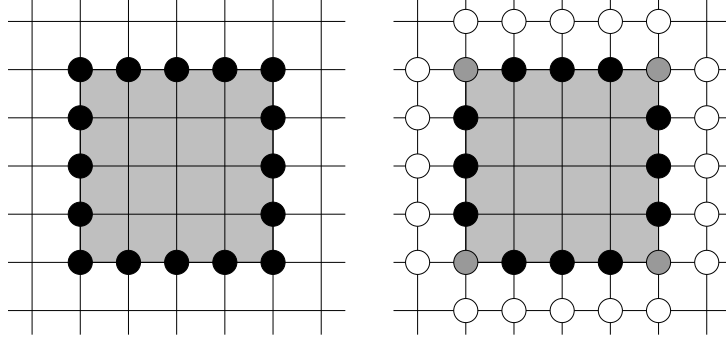


FIGURE 6.1. The double layer potential. Given a function ϕ defined on the black circles, place charges at all nodes marked with circles in the right picture in such a way that node k gets the charge $-|\mathbb{D}_k|\phi(k)$ and its nearest neighbors (white circles) get the charge $\phi(k)$. Note that the corner nodes (gray) get the charge $-2\phi(k)$.

so that $\mathfrak{A} = 2d(I - \mathfrak{B})$. Let $\bar{u} = D\phi$ be the global potential induced by ϕ so that, for $m \in \Gamma$,

$$-|\mathbb{D}_m|\phi(m) = [\mathfrak{A}\bar{u}](m) = 2d\bar{u}(m) - 2d[\mathfrak{B}\bar{u}](m) = 2d\mathfrak{g}(m) - 2d[\mathfrak{B}D\phi](m).$$

We can then write (2.5) in the equivalent form

$$-\frac{|\mathbb{D}_m|}{2d}\phi + \mathfrak{B}D\phi = \mathfrak{g},$$

which looks more like the second kind equation (1.14).

Proposition 6.2: *The matrix K_D associated with (2.5) is non-singular.*

Proof: The proof goes along the same lines as the proof of Proposition 6.1, we set $\mathbf{u} = D\phi$, suppose that $\mathbf{u}|_\Gamma = 0$ and will prove that then ϕ must be zero. Since in this case \mathbf{u} has finite energy even in two dimensions, we do not need to resort to the limiting argument in the previous proof.

When $\mathfrak{A}\mathbf{u} = \phi$ and $\mathbf{u}|_\Omega = 0$, the function \mathbf{u} satisfies a homogeneous Neumann problem on Ω^c with zero boundary data. To see this, loop over all nodes $n \in \Gamma$. For each node, lift out all the links that connect the node to nodes in Γ_+ . If we simultaneously remove the loads on Γ and Γ_+ that are due to $\phi(n)$, then \mathbf{u} will still be in equilibrium on the reduced lattice (since there are no flows going inside Ω). After having removed all links that connect Ω to Ω^c , we will see that indeed, \mathbf{u} will be in equilibrium on Ω^c and there will be no flows going into Ω^c . Thus \mathbf{u} is constant on Ω^c , and since $\mathbf{u}(m)$ is the potential due to a number of dipole charges, it tends to zero as $|m| \rightarrow \infty$. This shows that $\mathbf{u} \equiv 0$ on Ω^c , thus $\mathbf{u} \equiv 0$, and $\phi = 0$. \square

3. Inclusions

The boundary equation method can be used to treat equations modeling lattices with inclusions that destroy the periodicity of the equilibrium operator. Consider the perturbed Dirichlet problem

$$(3.6) \quad \begin{cases} [(\mathfrak{A} - \mathfrak{A}_r)\mathbf{u}](m) = 0, & m \in \Omega_-, \\ \mathbf{u}(m) = \mathfrak{g}(m), & m \in \Gamma, \end{cases}$$

where \mathfrak{A}_r represents a (typically local) perturbation. We reformulate (3.6) as an unperturbed problem with a ‘‘fictitious’’ load

$$(3.7) \quad \begin{cases} [\mathfrak{A}\mathbf{u}](m) = \mathfrak{f}_r, & m \in \Omega_-, \\ \mathbf{u}(m) = \mathfrak{g}(m), & m \in \Gamma, \end{cases}$$

where $\mathfrak{f}_r = \mathfrak{A}\mathbf{u}_r$. This term can be determined using the boundary equation framework derived earlier. As an illustration, suppose that \mathfrak{A}_r corresponds to removing the bars connecting the nodes $k_-^{(j)}$ to $k_+^{(j)}$ for $j = 1, \dots, J$. Since $\mathfrak{f}_r \in \text{Ran}(\mathfrak{A}_r)$, there exist loads $\psi(j)$ such that

$$\mathfrak{f}_r(m) = \sum_{j=1}^J \psi(j) \left[\delta(m - k_+^{(j)}) - \delta(m - k_-^{(j)}) \right].$$

We make the Ansatz

$$\mathbf{u}(m) = \sum_{n \in \Gamma} \mathfrak{G}(m - n) \phi(n) + \sum_{j=1}^J [\mathfrak{G}(m - k_+^{(j)}) - \mathfrak{G}(m - k_-^{(j)})] \psi(j).$$

Inserting the Ansatz directly into the boundary condition we get the equations

$$(3.8) \quad \mathfrak{g}(m) = \sum_{n \in \Gamma} \mathfrak{G}(m - n) \phi(n) + \sum_{j=1}^J [\mathfrak{G}(m - k_+^{(j)}) - \mathfrak{G}(m - k_-^{(j)})] \psi(j), \quad m \in \Gamma.$$

The condition at the removed bars is that $\mathbf{u}(k_+^{(i)}) - \mathbf{u}(k_-^{(i)}) = \psi(i)$, or that for $i = 1, \dots, J$,

$$(3.9) \quad \psi(i) = \sum_{n \in \Gamma} [\mathfrak{G}(k_+^{(i)} - n) - \mathfrak{G}(k_-^{(i)} - n)] \phi(n) + \sum_{j=1}^J [\mathfrak{G}(k_+^{(i)} - k_+^{(j)}) - \mathfrak{G}(k_+^{(i)} - k_-^{(j)}) - \mathfrak{G}(k_-^{(i)} - k_+^{(j)}) + \mathfrak{G}(k_-^{(i)} - k_-^{(j)})] \psi(j).$$

Combined, the equations (3.8) and (3.9) determine the fictitious loads ϕ and ψ .

A double layer formulation can be derived in an entirely analogous fashion from the Ansatz

$$\mathbf{u}(m) = \sum_{n \in \Gamma} \mathfrak{G}_\nu(m, n) \phi(n) + \sum_{j=1}^J [\mathfrak{G}(m - k_+^{(j)}) - \mathfrak{G}(m - k_-^{(j)})] \psi(j).$$

Finally, we note that the case of a lattice where the the pairs $\{k_+^{(j)}, k_-^{(j)}\}_{j=1}^J$ have been shortcut can be solved using the same technique by adjusting the condition at the inclusion to read $\mathbf{u}(k_+^{(i)}) - \mathbf{u}(k_-^{(i)}) = 0$.

4. Partial summation and direct formulations

In sections 2 and 3 the boundary equations were derived from the Ansatz $\mathbf{u} = \mathbf{S}\phi$ or $\mathbf{u} = \mathbf{D}\phi$, respectively. This method is a straight-forward analogue of the ‘‘direct’’ derivation of boundary

integral equations in classical potential theory, see [45] or [2]. The other common technique for deriving integral equations is to start with the Green's identity

$$(4.10) \quad \int_{\Omega} ((\Delta u)v - u(\Delta v)) = \int_{\partial\Omega} \left(\frac{\partial u}{\partial n} v - u \frac{\partial v}{\partial n} \right).$$

Then by letting v denote the fundamental solution, and u the solution of the boundary value problem it is possible to relate $u|_{\Gamma}$ and $\partial_{\nu} u|_{\Gamma}$. For, say, a Dirichlet problem, $u|_{\Gamma}$ is known and using the derived relation, $\partial_{\nu} u|_{\Gamma}$ can be determined. It is then a simple matter to reconstruct u in the entire domain. In this section we will illustrate how the discrete boundary equations can similarly be derived from a discrete analogue of (4.10) and then use it to derive the boundary equations. We will restrict attention to the square lattice with the standard five-point stencil on a square domain $\Omega = \{-N, \dots, N\}^2$. The results can easily be generalized to other domains but due to the plethora of lattice geometries and different domains, this has to be done on a case by case basis.

First we need to derive some ‘‘partial summation’’ results. For a function $\mathbf{u} : \mathbb{Z} \rightarrow \mathbb{R}$ set

$$[\delta \mathbf{u}](n) := \mathbf{u}(n+1) - \mathbf{u}(n), \quad \text{and} \quad [\bar{\delta} \mathbf{u}](n) := \mathbf{u}(n) - \mathbf{u}(n-1).$$

For such operators we have

$$\begin{aligned} \sum_{n=-N}^N [\delta \mathbf{u}](n) \mathbf{v}(n) &= - \sum_{n=-N}^N \mathbf{u}(n) [\bar{\delta} \mathbf{v}](n) + \mathbf{u}(N+1) \mathbf{v}(N) - \mathbf{u}(-N) \mathbf{v}(-N-1), \\ \sum_{n=-N}^N [\bar{\delta} \mathbf{u}](n) \mathbf{v}(n) &= - \sum_{n=-N}^N \mathbf{u}(n) [\delta \mathbf{v}](n) + \mathbf{u}(N) \mathbf{v}(N+1) - \mathbf{u}(-N-1) \mathbf{v}(-N). \end{aligned}$$

Applying these results to the operator $[\delta \bar{\delta} \mathbf{u}](n) = \mathbf{u}(n+1) - 2\mathbf{u}(n) + \mathbf{u}(n-1)$ we find that

$$(4.11) \quad \sum_{-N}^N [\delta \bar{\delta} \mathbf{u}](n) \mathbf{v}(n) = \sum_{-N}^N \mathbf{u}(n) [\delta \bar{\delta} \mathbf{v}](n) + ([\delta \mathbf{u}](N) \mathbf{v}(N) - \mathbf{u}(N) [\delta \mathbf{v}](N)) + (-[\bar{\delta} \mathbf{u}](-N) \mathbf{v}(-N) + \mathbf{u}(-N) [\bar{\delta} \mathbf{v}](-N)).$$

For a multi-variate function $\mathbf{u} : \mathbb{Z}^d \rightarrow \mathbb{R}$, let δ_j and $\bar{\delta}_j$ denote the ‘‘partial’’ difference operators, so that for instance $[\delta_1 \mathbf{u}](n) = \mathbf{u}(n_1+1, n_2, \dots, n_d) - \mathbf{u}(n_1, n_2, \dots, n_d)$. Setting $\Omega = \{-N, \dots, N\}^2$, $\Gamma = \partial\Omega$ and $\Delta = \delta_1 \bar{\delta}_1 + \delta_2 \bar{\delta}_2$ we then get

$$\begin{aligned} \sum_{\Omega} ([\Delta \mathbf{u}] \mathbf{v} - \mathbf{u} [\Delta \mathbf{v}]) &= \sum_{n_2=-N}^N ([\delta_1 \mathbf{u}](N, n_2) \mathbf{v}(N, n_2) - \mathbf{u}(N, n_2) [\delta_1 \mathbf{v}](N, n_2)) + \\ &\quad \sum_{n_2=-N}^N (-[\bar{\delta}_1 \mathbf{u}](-N, n_2) \mathbf{v}(-N, n_2) + \mathbf{u}(-N, n_2) [\bar{\delta}_1 \mathbf{v}](-N, n_2)) + \\ &\quad \sum_{n_1=-N}^N ([\delta_2 \mathbf{u}](n_1, N) \mathbf{v}(n_1, N) - \mathbf{u}(n_1, N) [\delta_2 \mathbf{v}](n_1, N)) + \\ &\quad \sum_{n_1=-N}^N (-[\bar{\delta}_2 \mathbf{u}](n_1, -N) \mathbf{v}(n_1, -N) + \mathbf{u}(n_1, -N) [\bar{\delta}_2 \mathbf{v}](n_1, -N)). \end{aligned}$$

This can be written compactly using the external difference operator δ_ν defined in section 1,

$$(4.12) \quad \sum_{\Omega} ([\Delta \mathbf{u}] \mathbf{v} - \mathbf{u} [\Delta \mathbf{v}]) = \sum_{\Gamma} ((\delta_\nu \mathbf{u}) \mathbf{v} - \mathbf{u} (\delta_\nu \mathbf{v})).$$

Note that at the corners we have

$$\delta_\nu|_{(N,N)} = \delta_1 + \delta_2, \quad \delta_\nu|_{(-N,N)} = -\bar{\delta}_1 + \delta_2, \quad \delta_\nu|_{(-N,-N)} = -\bar{\delta}_1 - \bar{\delta}_2, \quad \delta_\nu|_{(N,-N)} = \delta_1 - \bar{\delta}_2.$$

Next, let \mathbf{u} denote the solution of (D) and let $\bar{\mathbf{u}}$ denote an extension of \mathbf{u} that is harmonic in Ω . (To construct $\bar{\mathbf{u}}$, let $\phi(n)$ denote the flow out of node $n \in \Gamma$ in the solution of (D). Then note that for any $k \in \Gamma_+$ there is a unique $n \in \Gamma$ such that $k \in \mathbb{D}_n$ and set $\bar{\mathbf{u}}(k) = \mathbf{u}(n) + \frac{1}{|\mathbb{D}_n|} \varphi(n)$ and $\bar{\mathbf{u}}(m) = 0$ for $m \notin \Omega \cup \Gamma_+$.) Then fix $m \in \Gamma$ and apply the representation (4.12) to the functions $\bar{\mathbf{u}}$ and $n \mapsto \mathfrak{G}(m-n)$, this gives that

$$(4.13) \quad \bar{\mathbf{u}}(m) = \sum_{n \in \Gamma} ([\delta_\nu \bar{\mathbf{u}}](n) \mathfrak{G}(m-n) - \bar{\mathbf{u}}(n) \mathfrak{G}_\nu(m,n)),$$

which we rewrite as

$$(4.14) \quad \mathbf{S}[\delta_\nu \bar{\mathbf{u}}] = (\mathbf{I} + \mathbf{D})[\bar{\mathbf{u}}].$$

When either $\mathbf{u}|_\Gamma$ or $\delta_\nu \mathbf{u}|_\Gamma$ is given, the other quantity can be determined using (4.14) and then (4.13) is used to construct the solution. We point out that for the continuous case, a delicate limit process is required before the double layer potential can be ascribed a value on the boundary. This complication is absent in the discrete case.

Finally, we note that starting with the basic partial summation result (4.11) equations similar to (4.12) can be derived for general lattices and general domains. For domains that are more complicated than the example above, especially ones that have re-entrant corners, it is sometimes necessary to enrich the space of boundary functions by adding a few ‘‘fictitious’’ loads near the trouble region in a fashion similar to how we handled inclusions in section 3.

5. Conditioning of the boundary equations

As mentioned in section 1, a main reason for working with boundary formulations of boundary value problems is that we expect these to be well conditioned. An indication that this is the case is that as the lattice cell size tends to zero, the discrete boundary equations appear to converge to continuous boundary equations that are very similar to those of classical potential theory. These equations, especially those associated with second kind equations with a compact integral operator, are known to produce well-conditioned systems upon discretization.

In this section we will present numerical results that indicate that (2.3) and (2.5) are well-conditioned. We assembled K_S and K_D for some different problems and computed the condition-numbers numerically. The experiments were carried out for the Dirichlet problem with a square lattice on the four geometries illustrated in Figure 6.2. The **square** is a simple square with $(2N+1) \times (2N+1)$ nodes. The **L-shape** is the square with one quadrant removed. For the **slit** we removed the vertical connections in the middle third of the middle row. In the **shortcut** we connected the nodes in the middle third of the middle row by an infinitely conductive strip. For each case, we assembled the matrices K_S and K_D associated with the single and double layer formulations and computed their condition numbers. For the problems with inclusions, the technique given in section 3 was used. For comparison, we also assembled the matrix K associated with the five-point

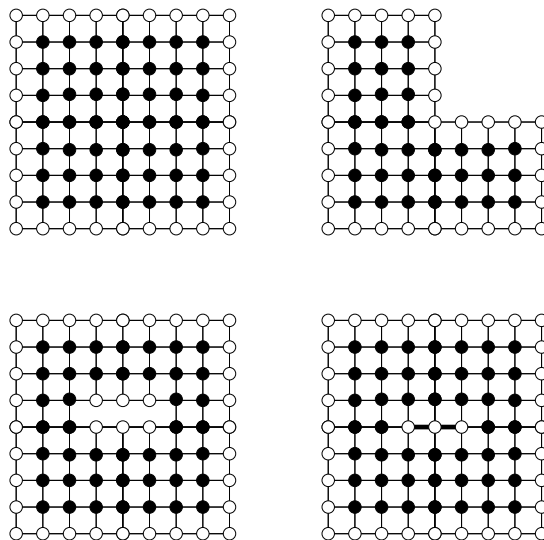


FIGURE 6.2. The geometries we used to estimate the condition numbers. Reading from left to right, first row first, we label them: “the square”, “the L-shape”, “the slit” and “the shortcut”. The long side of the square has $2N + 1$ nodes.

	Square	L-shape	Slit	Shortcut
$\text{cond}(K)$	$1.6N^2$	$0.83N^2$	$1.6N^2$	$0.28N^3$
$\text{cond}(K_S)$	$40N$	$40N$	$4N^2$	$4.2N^2$
$\text{cond}(K_D)$	7.0	7.3	0.63N	0.68N

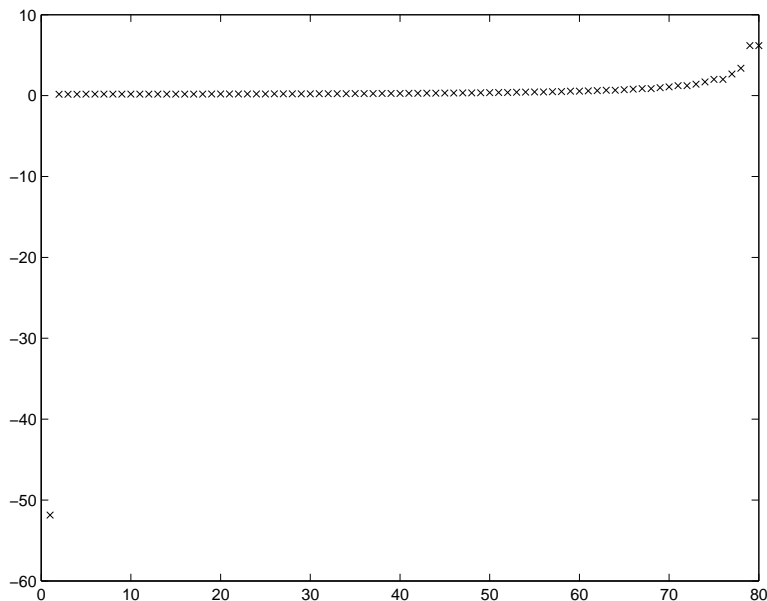
TABLE 6.1. Asymptotic estimates of the condition numbers for different boundary equations and different geometries.

difference operator on the domain itself. The exact values obtained are given in tables at the end of this chapter. A summary of the results is given in table 6.1.

The numbers in the table strongly support our belief that the condition numbers should improve upon reformulating a problem as a boundary equation. This is especially true for the double layer formulation, for which the condition number for the two physically reasonable geometries are not only uniformly bounded as N grows, but are also very low in absolute numbers. We note that although the condition numbers for the single layer potential perform somewhat poorer, the estimates in the tables can be improved considerably by a simple trick, see the remark 2 below.

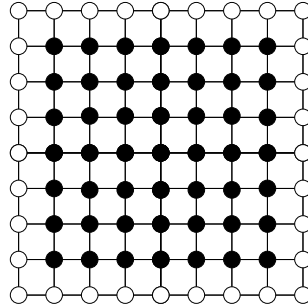
Remark 1: In order to compute the entries of K_S and K_D one needs to numerically evaluate $\mathfrak{G}(k)$ for a large numbers of k 's. For $|k| \leq 30$, we precomputed $\mathfrak{G}(k)$ by integrating analytically in one dimension and then used numerical quadrature to evaluate the resulting one dimensional integral, see Appendix D. For larger values the asymptotic expansion G_3 was used. This yielded an absolute accuracy of about 10^{-14} .

Remark 2: The eigenstructure of K_S is interesting. In Figure 6.3 we plot the eigenvalues for the square with $N = 10$. The lone negative eigenvalue $\lambda_0 \approx -52$ corresponds to an almost constant

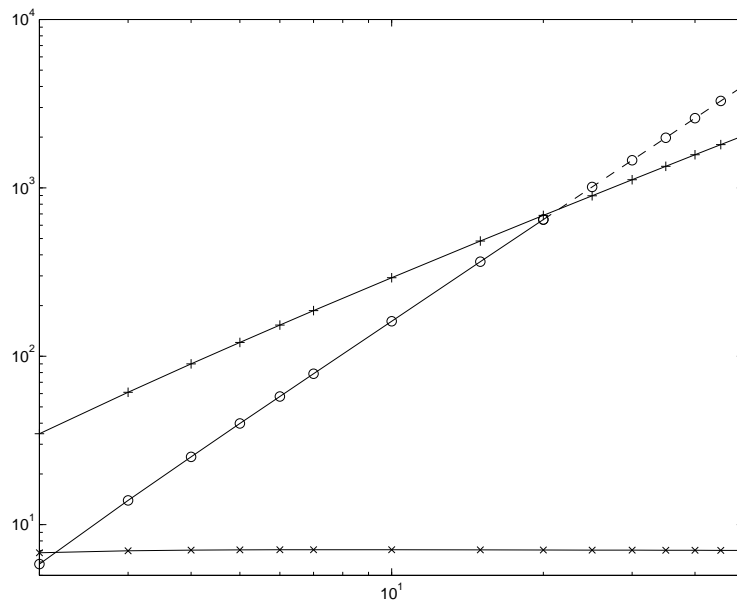
FIGURE 6.3. Eigenvalues for K_S when $N = 10$

eigenvector. We found that by restricting K_S to the orthogonal complement of the constants the condition number can be reduced by over 90% and we found that asymptotically $K_S \sim 3.5N$.

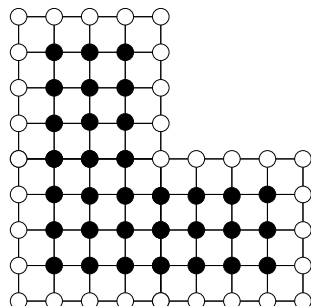
Legend for the numerical data: In the last pages of this chapter we provide the raw data for the experiments on the condition numbers. For each of the four geometries, we present the condition numbers of K , K_S and K_D for values of N between 2 and 50. These numbers are also presented as log-log plots in which ‘o’ represents $\text{cond}(K)$, ‘+’ represents $\text{cond}(K_S)$ and ‘x’ represents $\text{cond}(K_D)$.

1: A square domain

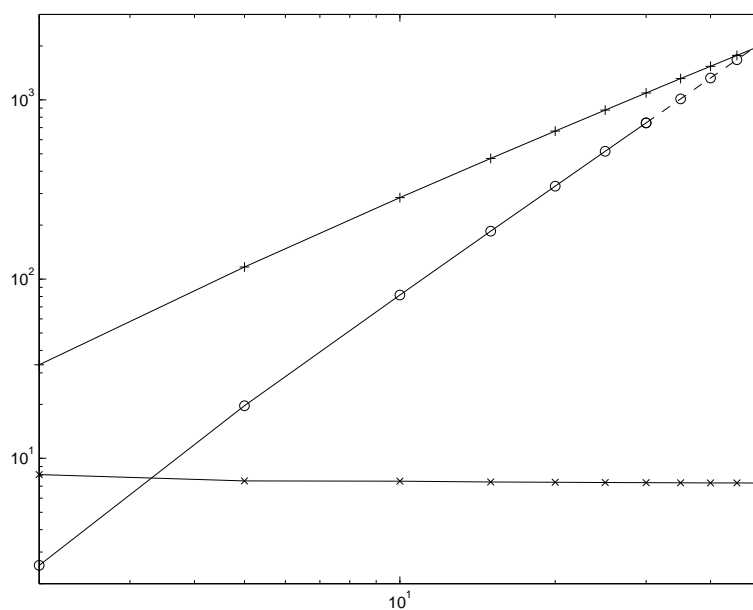
N	$\text{cond}(K)$	$\text{cond}(K)/N^2$	$\text{cond}(K_S)$	$\text{cond}(K_S)/N$	$\text{cond}(K_D)$
2	5.83	1.48	34.6	17.3	6.81
5	39.9	1.59	121	24.2	7.08
10	161	1.61	292	29.3	7.09
15	364	1.62	483	32.3	7.08
20	648	1.62	686	34.3	7.07
25	1010	1.62	898	35.9	7.06
30	1460	1.62	1120	37.2	7.05
35	—	—	1340	38.3	7.04
40	—	—	1570	39.3	7.04
45	—	—	1810	40.1	7.04
50	—	—	2050	40.9	7.03

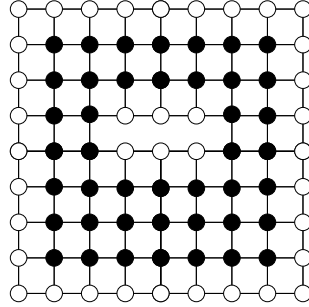


2: An L-shaped domain

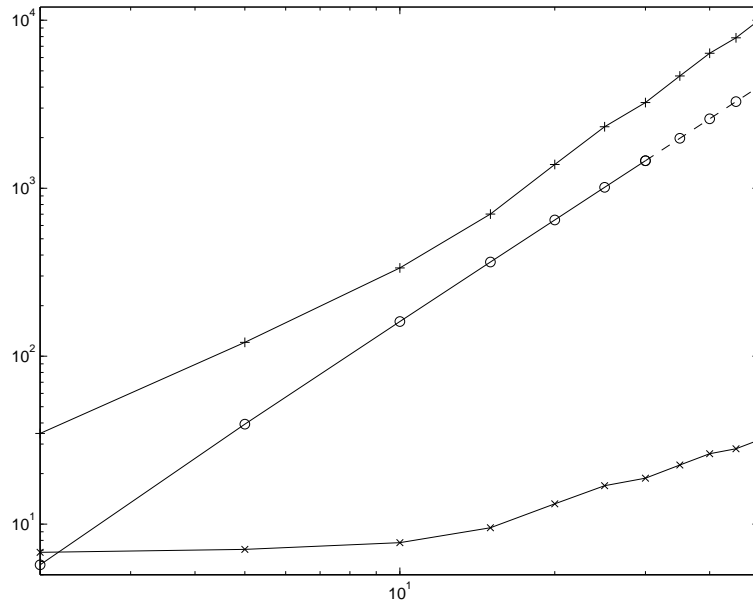


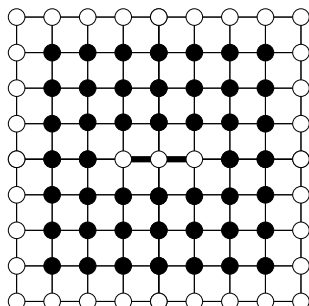
N	$\text{cond}(K)$	$\text{cond}(K)/N^2$	$\text{cond}(K_S)$	$\text{cond}(K_S)/N$	$\text{cond}(K_D)$
2	2.53	0.63	33.3	16.6	8.12
5	19.7	0.79	117	23.4	7.48
10	82.6	0.82	285	28.5	7.45
15	185	0.82	471	31.4	7.38
20	330	0.83	670	33.5	7.36
25	517	0.83	878	35.1	7.33
30	745	0.83	1090	36.4	7.32
35	—	—	1310	37.6	7.31
40	—	—	1540	38.5	7.30
45	—	—	1770	39.4	7.29
50	—	—	2010	40.1	7.28



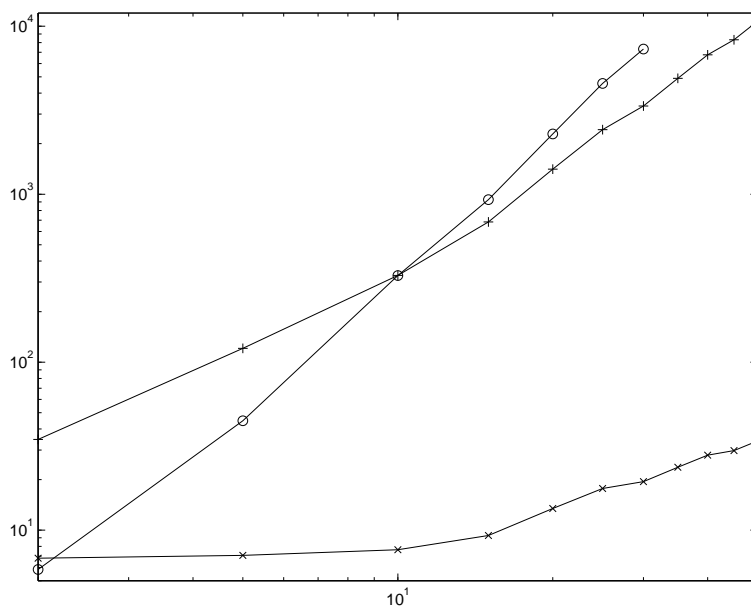
3: A domain with a slit

N	$\text{cond}(K)$	$\text{cond}(K)/N^2$	$\text{cond}(K_S)$	$\text{cond}(K_S)/N^2$	$\text{cond}(K_D)$	$\text{cond}(K_D)/N$
2	5.72	1.43	34.6	8.66	6.80	3.40
5	39.3	1.57	121	4.83	7.08	1.42
10	161	1.61	336	3.36	7.76	0.776
15	363	1.61	702	3.12	9.52	0.635
20	647	1.62	1380	3.46	13.2	0.661
25	1010	1.62	2320	3.72	16.9	0.677
30	1460	1.62	3240	3.60	18.8	0.626
35	—	—	4660	3.80	22.5	0.643
40	—	—	6360	3.97	26.2	0.656
45	—	—	7860	3.88	28.1	0.624
50	—	—	10100	4.03	31.8	0.637



4: A domain with a shortcut

N	$\text{cond}(K)$	$\text{cond}(K)/N^3$	$\text{cond}(K_S)$	$\text{cond}(K_S)/N^2$	$\text{cond}(K_D)$	$\text{cond}(K_D)/N$
2	5.83	0.729	34.6	8.66	6.81	3.40
5	44.8	0.358	121	4.83	7.08	1.42
10	328	0.328	329	3.28	7.64	0.764
15	929	0.275	684	3.04	9.29	0.619
20	2280	0.285	1410	3.53	13.5	0.673
25	4560	0.292	2430	3.88	17.7	0.708
30	7322	0.270	3350	3.72	19.5	0.649
35	—	—	4890	4.00	23.7	0.677
40	—	—	6760	4.22	28.0	0.699
45	—	—	8300	4.10	29.7	0.661
50	—	—	10700	4.29	34.0	0.680



Vibrations of lattices and acoustic bandgaps

Synopsis: This chapter concerns analysis of elastic waves in lattice structures. We analyse the propagating modes as well as filtering properties of lattices. Special attention is paid to the connection between micro-structural geometry and the presence of so-called “phononic bandgaps”, intervals of frequencies for which there exist no propagating wave-modes.

Note: *This chapter does not directly inter-connect with the preceding chapters. We therefore present the material here in a self-contained fashion and avoid making references to results that are presented earlier.*

1. Introduction.

1.1. Background. In this chapter we will demonstrate that for many mechanical lattice structures there are intervals of frequencies for which no propagating elastic waves exist. This raises the possibility of designing materials, or structures, that can completely block mechanical waves of certain frequencies. We will present a method of analysis that can be used to determine such bandgaps and then show how lattices can be constructed that have bandgaps around prescribed frequencies.

There are many observations of bandgap phenomena in nature; in the classical literature (see for example Kittel [40] and Brillouin [11]), examples are given of real life molecular structures that exhibit bandgaps in both the acoustic and electro-magnetic spectra (referred to as phononic and photonic bandgaps, respectively). A comprehensive bibliography including more than one thousand articles on photonic band structures was compiled by Dowling, Everitt and Yablonovitch [18]. Theoretical and numerical studies based on the plane wave expansion method were published by Sigalas and Economou [58, 59, 60], who considered scalar problems for acoustic wave band structures as well as vector problems for elastic waves in plates containing periodic sets of inclusions. For continuum elastic structures the phononic bandgap phenomena were studied in the paper by Poulton *et al.* [54], where a generalisation of the Rayleigh method was developed to analyse the elastic wave propagation through a two-dimensional array of circular voids.

It is evident that one can establish a correspondence between continuum structures and discrete lattices. For example, for the case of a normal incidence of an anti-plane wave on a stack of two types of elastic layers (see Figure 7.1a) we can assume that the layers of one of the groups are thin and soft. In this case, it can be shown (Movchan and Zalipaev [49]) that asymptotically the dispersion equation for this structure would be equivalent to the one corresponding to a bi-atomic one-dimensional chain of particles of different mass connected by weightless elastic springs (see Figure 7.1b). The dispersion diagram given in Figure 7.2 shows the normalized frequency versus the magnitude of the Bloch vector and exhibits the bandgap between the acoustic and optical modes for this one-dimensional problem. The comparison of certain anti-plane problems for

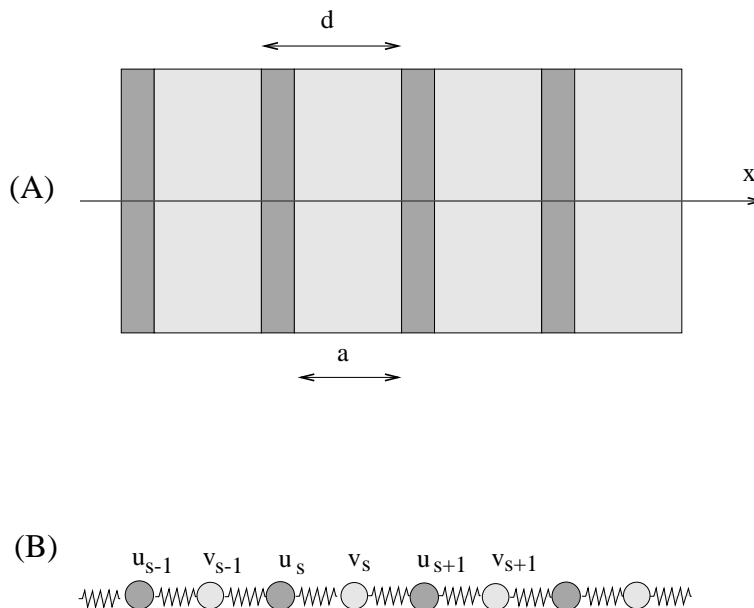


FIGURE 7.1. One-dimensional array, of period d , involving two types of layers, of thickness a and $(d - a)$ (A), and a two-particle system with springs (B).

continuous systems in two dimensions and two-dimensional lattice structures was also included in Movchan and Zalpaev [49]. It is noted that the analysis of lattice structures is easy compared to numerical computations for continuum systems of complicated geometries; on the other hand the lattice structure may exhibit the physical phenomena similar to continuum structures, and hence it is highly important to be able to evaluate the transmission and reflection characteristics of the lattice structures.

In this chapter, we emphasise analysis of vector problems of elasticity for lattice structures and pay particular attention to the emergence of phononic bandgaps. Our analysis is restricted to two dimensions but the methodology easily generalizes to three-dimensional structures. The plan of the chapter is as follows:

- In the following subsection of the introduction we consider elementary examples of membrane-like lattices with different assumptions related to the mass distribution along the strings.
- In section 2 we analyse in-plane elastic vibrations of degenerate and non-degenerate bi-atomic lattice structures that exhibit phononic bandgaps.
- A general approach to spectral problems for lattice structures is presented in section 3.
- This approach is used in section 4 to design structures which possess bandgap frequencies of given magnitude. It is specifically noted that the bandgap phenomena are associated with the presence of standing waves within the structure.

1.2. A membrane-like lattice. In this section we consider illustrative examples for a lattice with the square geometry illustrated in Figure 7.3. We think of the lines of the lattice as strings with an axial force F , and a weight-per-length density ρ . The strings are attached to each other at the nodal points. We consider harmonic vibrations of this lattice with displacements of the strings

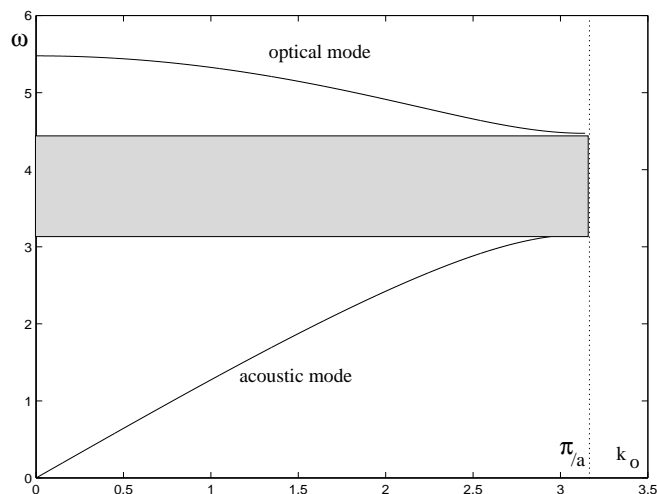


FIGURE 7.2. Acoustic and optical branches for a one-dimensional array of particles of mass $m_1 = 1$ and $m_2 = 2$ connected by springs of length $a = 1$ and stiffness $c = 10$. Along the horizontal axis we put the magnitude of the Bloch vector, and we have the radian frequency on the vertical axis.

and the nodes in the direction perpendicular to the plane of the lattice. Our goal is to determine the eigenmodes and look for bandgaps in the spectrum. We consider two different cases; first that the density is constant, second, that the string consists of two parts that each have constant density.

Homogeneous strings of constant density: Since the domain is infinite and the vibrations are quasi-periodic in space we can restrict attention to a unit cell, as illustrated in Figure 7.3. Let $u^{(j)}$, $j = 0, 1, \dots, 4$, denote the displacement of the nodes, where j is the index shown in the figure. Let $w^{(j)}(x, t)$ denote the displacement of the string connecting node 0 to node j , with $x \in (0, l)$ measured as shown in the figure and t denoting time. Then Newton's second law reads

$$F \frac{d^2 w^{(j)}}{dx^2} = \rho \frac{d^2 w^{(j)}}{dt^2}.$$

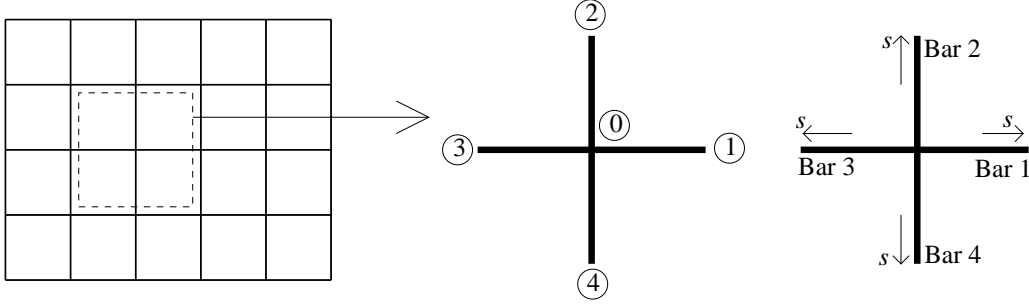


FIGURE 7.3. Square lattice with mass distributed along the bars.

Since we consider time-harmonic oscillations, say of radian frequency ω , we have $d^2 w^{(j)}/dt^2 = -\omega^2 w^{(j)}$ and obtain

$$\frac{d^2 w^{(j)}}{dx^2} + \frac{\omega^2}{v^2} w^{(j)} = 0,$$

where $v = \sqrt{\frac{F}{\rho}}$ is the internal group-velocity of the strings. The boundary conditions are $w^{(j)}(0) = u^{(0)}$ and $w^{(j)}(l) = u^{(j)}$. Considering first the case $\sin \frac{\omega l}{v} \neq 0$ we find that

$$w^{(j)}(x) = u^{(0)} \cos \frac{\omega x}{v} + \frac{u^{(j)} - u^{(0)} \cos \frac{\omega l}{v}}{\sin \frac{\omega l}{v}} \sin \frac{\omega x}{v}.$$

Equilibrium of the central node now reads

$$(1.1) \quad 0 = \sum_{n=1}^4 \left. \frac{dw^{(j)}}{dx} \right|_{x=0} = \frac{1}{\sin \frac{\omega l}{v}} \left(u^{(1)} + u^{(2)} + u^{(3)} + u^{(4)} - 4 \cos \frac{\omega l}{v} u^{(0)} \right).$$

Looking for waves with a Bloch vector $\mathbf{k} = (k_1, k_2)$ we have the quasi-periodicity conditions

$$u^{(1)} = e^{-ik_1 l} u^{(0)}, \quad u^{(2)} = e^{-ik_2 l} u^{(0)}, \quad u^{(3)} = e^{ik_1 l} u^{(0)}, \quad u^{(4)} = e^{ik_2 l} u^{(0)}.$$

Plugging this into equation (1.1) we obtain the equation

$$\cos(k_1 l) + \cos(k_2 l) - 2 \cos \frac{\omega l}{v} = 0.$$

For the case $\sin \frac{\omega l}{v} = 0$ there exist, for any \mathbf{k} , standing wave modes corresponding to internal vibrations of the strings, with no associated nodal displacements. The total dispersion equation therefore takes the form

$$\sin \frac{\omega l}{v} \left(\cos(k_1 l) + \cos(k_2 l) - 2 \cos \frac{\omega l}{v} \right) = 0.$$

Note that in the limit $k \rightarrow 0$ the dispersion equation has the asymptotic solution $|k| = \sqrt{2} \omega / v$, the same dispersion equation as that for a continuous membrane with group velocity $v/\sqrt{2}$.

Given $k \in (-\pi, \pi)^2$ the dispersion equation allows us to determine all frequencies ω such that there is a vibration mode with frequency ω and the Bloch vector k . In Figure 7.4 we plot the solutions ω versus k 's along the path shown to the right in the figure. It is clear that no complete bandgaps exist.

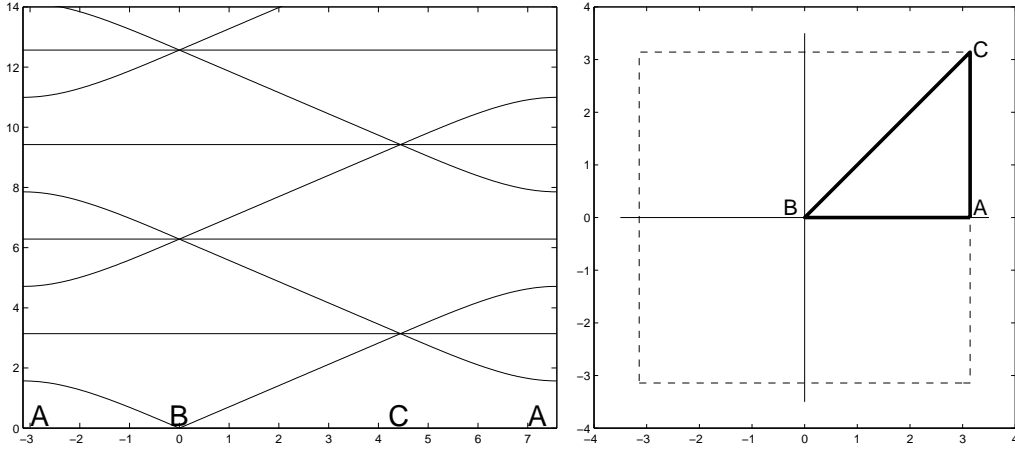


FIGURE 7.4. Dispersion diagram for the square lattice with distributed mass. The non-dimensionalized solutions $\omega l/v$ are plotted against k along the contour shown to the right.

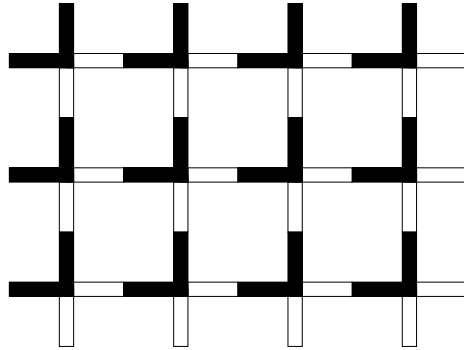


FIGURE 7.5. Lattice consisting of strings with non-constant density. The white part of the strings have density ρ , the black have density ρ/α^2 .

Inhomogeneous strings: We will next consider a structure similar to the one analysed above but where the strings are not homogeneous; the density has been changed from ρ to ρ/α^2 in half the bar, as illustrated in Figure 7.5. In this case we derive (see Appendix 1) the dispersion equation

$$(1.2) \quad \left[\cos \frac{\omega l}{2v} \sin \frac{\omega l}{2\alpha v} + \frac{1}{\alpha} \cos \frac{\omega l}{2\alpha v} \sin \frac{\omega l}{2v} \right] \\ \times \left[\frac{1}{\alpha} \left(\cos(k_1 l) + \cos(k_2 l) - 2 \cos \frac{\omega l}{2v} \cos \frac{\omega l}{2\alpha v} \right) + \left(1 + \frac{1}{\alpha^2} \right) \sin \frac{\omega l}{2v} \sin \frac{\omega l}{2\alpha v} \right] = 0.$$

One very interesting feature here is that the first factor captures exactly the eigenfrequencies of the inhomogeneous string with fixed ends. As shown in Figure 7.6, around these frequencies

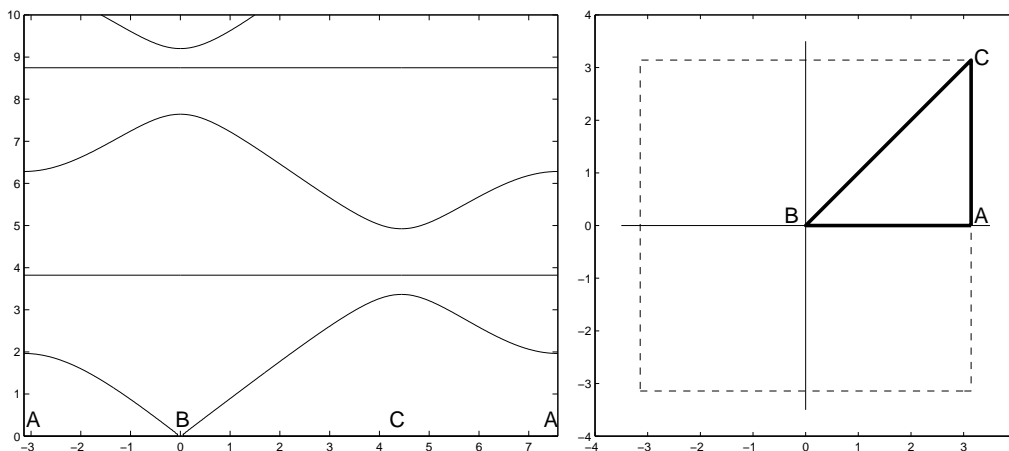


FIGURE 7.6. Dispersion diagram similar to the one shown in Figure 7.4 but for the lattice with strings of varying density, $\alpha = 2$.

there are typically complete bandgaps. This means that no waves with frequencies close to the eigenfrequencies of the composite bars can propagate through the structure.

The two elementary examples considered above provide sufficient motivation for analysis of trapped modes and phononic bandgaps in elastic structures. These vector problems are considered in the text below.

2. Two examples of mechanical lattices

Every periodic lattice is characterised by an irreducible cell and a corresponding stiffness matrix A associated with this cell. Thinking of the members of the lattice as beams we know that the matrix A splits into two components, $A = A_{\text{axial}} + A_{\text{bending}}$, with the first representing the axial stiffness of the beams and the second representing the bending stiffness. If the bars are slender we know that the axial stiffness is much higher than the bending stiffness. If A_{axial} has full rank when restricted to the translational degrees of freedom it will entirely dominate the problem and in this case we usually neglect the effect of A_{bending} and solve only for the translational degrees of freedom. We refer to these structures as *truss structures*. On the other hand, if A_{axial} does not have full rank (when restricted to the translational degree of freedom) we do need to keep A_{bending} in order to maintain structural integrity. Note that in this case A will be badly conditioned and we will expect the lattice to exhibit strongly anisotropic behaviour. Such structures we refer to as *frame structures*. In the next two subsections we will study one each of these two kinds of structures. We will try to make plausible the claim that even though bandgaps do exist in some truss structures they are more typical for the frames of the type considered in section 2.2.

2.1. A bi-atomic triangular lattice. Consider the triangular lattice illustrated in Figure 7.7. It consists of bars with an axial stiffness c connected with pin-joints. At the nodes with small dots there is a mass m_1 and at the big dots there is a mass m_2 . The lattice has an irreducible unit cell Ω whose integer translations along the lattice vectors $t^{(1)} = (2l, 0)$ and $t^{(2)} = (l/2, \sqrt{3}l/2)$ cover the whole plane, $\bigcup_{n \in \mathbb{Z}^2} (\Omega + n_1 t^{(1)} + n_2 t^{(2)}) = \mathbb{R}^2$. We identify the coordinates of the two

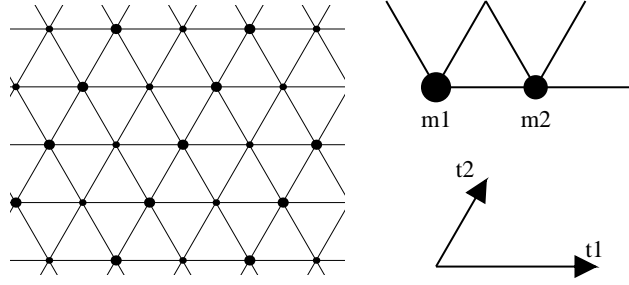


FIGURE 7.7. Triangular bi-atomic lattice. To the right we illustrate the irreducible unit cell and the lattice vectors.

nodes in Ω as $x^1 = (0, 0)$ and $x^2 = (l, 0)$, then the node $\kappa \in \{1, 2\}$ in cell $n \in \mathbb{Z}^2$ has coordinates $x^{(n, \kappa)} = x^\kappa + Tn$ where $T = [t^{(1)}, t^{(2)}]$.

We let $u^{(n, \kappa)} = (u_1^{(n, \kappa)}, u_2^{(n, \kappa)})^T$ denote the displacement of node (n, κ) . Introducing the unit vectors

$$(2.3) \quad a_j = \left(\cos \frac{2(j-1)\pi}{3}, \sin \frac{2(j-1)\pi}{3} \right)^T, \quad j = 1, 2, 3.$$

and setting $e_1 = [1, 0]^T$, $e_2 = [0, 1]^T$ we can express the equations of motion for the case of harmonic oscillations (of radian frequency ω) as

$$\begin{aligned} \omega^2 m_1 u^{(n, 1)} &= c a_1 a_1^T (2u^{(n, 1)} - u^{(n, 2)} - u^{(n-e_1, 2)}) + \\ &\quad c a_2 a_2^T (2u^{(n, 1)} - u^{(n+e_2, 1)} - u^{(n-e_2, 1)}) + \\ &\quad c a_3 a_3^T (2u^{(n, 1)} - u^{(n-e_1+e_2, 2)} - u^{(n-e_2, 2)}), \\ \omega^2 m_2 u^{(n, 2)} &= c a_1 a_1^T (2u^{(n, 2)} - u^{(n+e_1, 1)} - u^{(n, 1)}) + \\ &\quad c a_2 a_2^T (2u^{(n, 2)} - u^{(n+e_2, 2)} - u^{(n-e_2, 2)}) + \\ &\quad c a_3 a_3^T (2u^{(n, 2)} - u^{(n+e_2, 1)} - u^{(n+e_1-e_2, 1)}). \end{aligned}$$

Applying the condition of quasi-periodicity, $u^{(n+m, \kappa)} = e^{i\mathbf{k} \cdot Tm} u^{(n, \kappa)}$, we obtain

$$\begin{aligned} \omega^2 m_1 u^{(n, 1)} &= c \left[2a_1 a_1^T + 4 \sin^2 \frac{k_1 l + \sqrt{3} k_2 l}{4} a_2 a_2^T + 2a_3 a_3^T \right] u^{(n, 1)} + \\ &\quad c \left[(1 + e^{-2ik_1 l}) a_1 a_1^T + (e^{-i \frac{3k_1 l - \sqrt{3} k_2 l}{2}} + e^{-i \frac{k_2 l + \sqrt{3} k_2 l}{2}}) a_3 a_3^T \right] u^{(n, 2)} \\ \omega^2 m_2 u^{(n, 2)} &= c \left[2a_1 a_1^T + 4 \sin^2 \frac{k_1 l + \sqrt{3} k_2 l}{4} a_2 a_2^T + 2a_3 a_3^T \right] u^{(n, 1)} + \\ &\quad c \left[(1 + e^{2ik_1 l}) a_1 a_1^T + (e^{i \frac{3k_1 l - \sqrt{3} k_2 l}{2}} + e^{i \frac{k_2 l + \sqrt{3} k_2 l}{2}}) a_3 a_3^T \right] u^{(n, 2)}. \end{aligned}$$

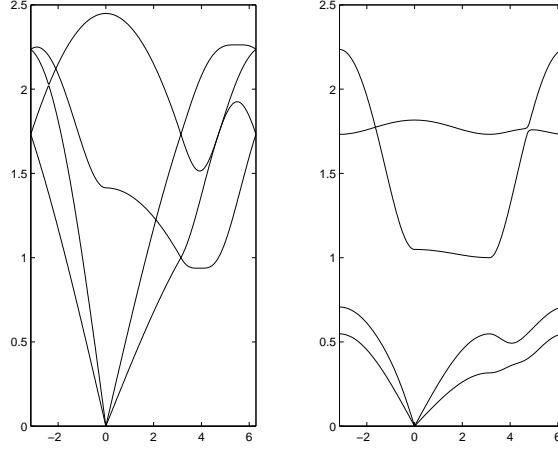


FIGURE 7.8. Eigenfrequencies for the triangular biatomic lattice with $c = 1$. In the left graph, $m_1 = m_2 = 1$, in the right, $m_1 = 1$, $m_2 = 10$.

Introducing the vector $u^{(n)} = [u^{(n,1)}, u^{(n,2)}]^T \in \mathbb{R}^4$ we write this compactly as

$$(2.4) \quad \omega^2 M u^{(n)} = \sigma(k) u^{(n)},$$

where we defined a mass matrix $M = \text{diag}\{m_1, m_1, m_2, m_2\}$ and a 4×4 stiffness matrix $\sigma(k)$. The entries of $\sigma(k)$ are given by

$$\sigma_{11}(k) = \sigma_{22}(k) = c \begin{bmatrix} \frac{5}{2} + \sin^2 \frac{k_1 l + \sqrt{3} k_2 l}{4} & -\frac{\sqrt{3}}{2} + \sqrt{3} \sin^2 \frac{k_1 l + \sqrt{3} k_2 l}{4} \\ -\frac{\sqrt{3}}{2} + \sqrt{3} \sin^2 \frac{k_1 l + \sqrt{3} k_2 l}{4} & \frac{3}{2} + 3 \sin^2 \frac{k_1 l + \sqrt{3} k_2 l}{4} \end{bmatrix},$$

$$\sigma_{12}(k) = \sigma_{21}(k)^* = c \begin{bmatrix} 1 + e^{2i k_1 l} + \frac{1}{4} e^{-i \frac{3 k_1 l - \sqrt{3} k_2 l}{2}} + \frac{1}{4} e^{-i \frac{k_1 l + \sqrt{3} k_2 l}{2}} & \frac{\sqrt{3}}{4} e^{-i \frac{3 k_1 l - \sqrt{3} k_2 l}{2}} + \frac{\sqrt{3}}{4} e^{-i \frac{k_1 l + \sqrt{3} k_2 l}{2}} \\ \frac{\sqrt{3}}{4} e^{-i \frac{3 k_1 l - \sqrt{3} k_2 l}{2}} + \frac{\sqrt{3}}{4} e^{-i \frac{k_1 l + \sqrt{3} k_2 l}{2}} & \frac{3}{4} e^{-i \frac{3 k_1 l - \sqrt{3} k_2 l}{2}} + \frac{3}{4} e^{-i \frac{k_1 l + \sqrt{3} k_2 l}{2}} \end{bmatrix}$$

Equation (2.4) has non-trivial solutions if and only if

$$(2.5) \quad \det(\sigma(k) - \omega^2 M) = 0.$$

This equation is referred to as the dispersion equation of the lattice.

The equation (2.5) has been solved numerically for some different combinations of masses (the spring constant c was set to unity). As illustrated in the left graph of Figure 7.8 there is no bandgap when $m_1 = m_2 = 1$. In this graph k follows the path illustrated in Figure 7.9. By increasing one of the masses while keeping the other one fixed we can push the “acoustic” modes down in frequency until a bandgap appears when $m_2/m_1 \approx 5$. In the right graph of Figure 7.8 we illustrate the spectrum for $m_1 = 1$, $m_2 = 10$.

2.2. A bi-atomic square lattice. Next we consider the lattice illustrated in Figure 7.10. This structure would be degenerate if bending stiffnesses were disregarded so we need to model it as a frame. To this end we endow the beams with axial stiffnesses c_j and bending stiffnesses d_j , as illustrated in the figure. There are nodes located at points $x^1 = (0, 0)$ and $x^2 = (l, 0)$ in the unit cell, these nodes have masses m_κ and polar moments of inertia J_κ , for $\kappa = 1, 2$. We use the same notation as in the previous example but note that now the lattice vectors are given by

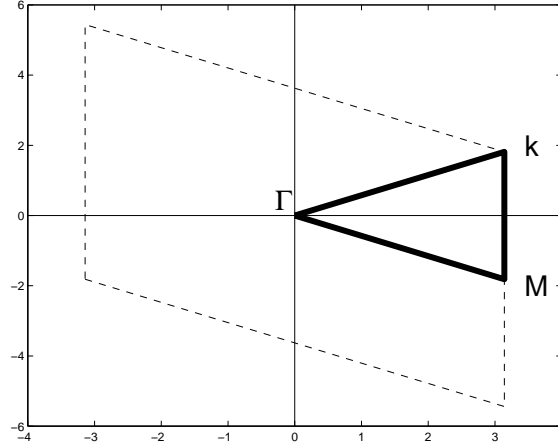


FIGURE 7.9. The reciprocal lattice is contained in the dashed parallelogram. The thick line illustrates the contour along which the eigen-frequencies are plotted.

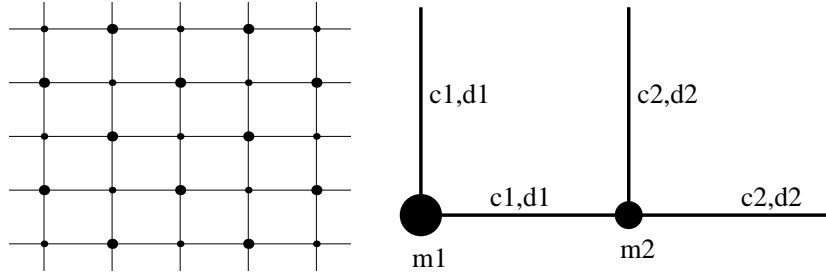


FIGURE 7.10. Square bi-atomic lattice with its irreducible unit cell to the right.

$t^{(1)} = (2l, 0)^T$ and $t^{(2)} = (l, l)^T$. We also need to include a rotational degree of freedom to the nodal displacements, $u^{(n,\kappa)} = (u_1^{(n,\kappa)}, u_2^{(n,\kappa)}, u_{\text{rot}}^{(n,\kappa)})^T$.

The equations of motion will this time constitute a set of three equations for each node, two for the components of the momentum and one for the angular momentum. The process of writing these down and combining them with the quasi-periodicity condition is straight-forward but somewhat lengthy so we leave it to Appendix 2. The end result is an equilibrium equation of the form (2.4) where now $M = \text{diag}\{m_1, m_1, J_1, m_2, m_2, J_2\}$ and the stiffness matrix $\sigma(k)$ consists of four 3×3 blocks whose entries depend on the axial and bending stiffnesses c_j and d_j .

The dispersion equation, which again takes the form (2.5), has been solved numerically, and in Figure 7.11 we show some characteristic dispersion diagrams. Note that the slope of the lowest acoustic line is far lower when going from A to B than it is when going from B to C. This is a manifestation of the strong anisotropy of this material. It is also evident from the diagram that the interval $[0.9, 1.3]$ forms a large bandgap.

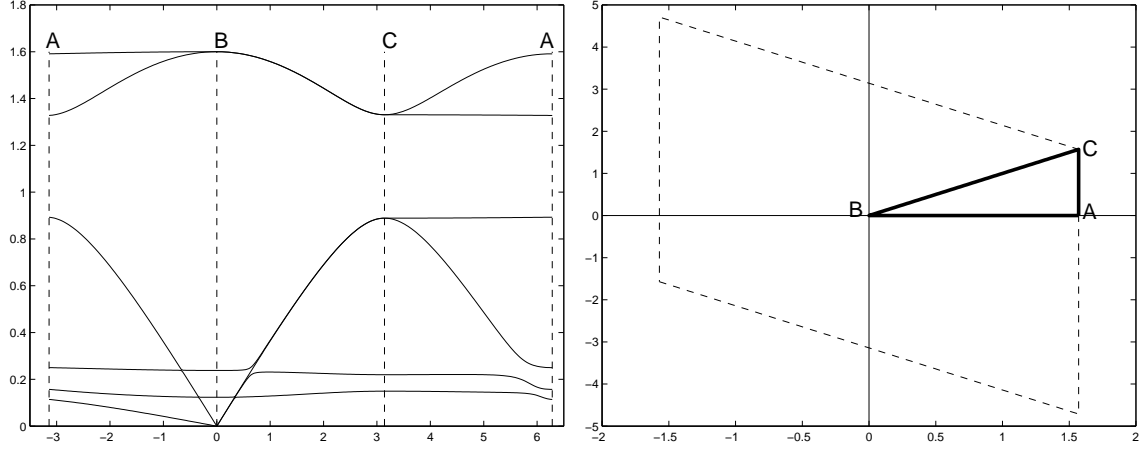


FIGURE 7.11. Dispersion curves for the square, bi-atomic lattice along the contour illustrated to the right. The constants are $c_1 = 1$, $c_2 = 2$, $d_1 = 0.002$, $d_2 = 0.004$, $m_1 = 2$, $m_2 = 3$, $J_1 = 1$, $J_2 = 2$.

3. Periodic structures of general geometry

A general lattice geometry in \mathbb{R}^d can be specified by the following objects:

Reference cell: We specify an irreducible reference cell $\Omega \subset \mathbb{R}^d$ in the form of a parallel-piped spanned by some translation vectors $t^{(i)} \in \mathbb{R}^d$, $1 \leq i \leq d$. Then its translates

$$\bigcup_{n \in \mathbb{Z}^d} \left(\Omega + \sum_{i=1}^d n_i t^{(i)} \right)$$

will form a disjoint covering of \mathbb{R}^d . We frequently collect the translation vectors in a matrix $T = [t^{(1)}, \dots, t^{(d)}]$. Then, for $n \in \mathbb{Z}^d$ label the set $\Omega^{(n)} = \Omega + Tn$ “cell n ”.

Nodes: Let $\{x^\kappa\}_{\kappa=1}^q \subset \omega$ be the nodes in the reference cell. We use the notation $x^{(n,\kappa)} = x^\kappa + Tn$ to index nodes in the lattice by giving their node number κ and the label of the cell they belong to, n .

Lattice members: Finally we specify a list of b lattice members $\{(\kappa_j, n_j, \lambda_j)\}_{j=1}^b$, where for each member we specify the node x^{κ_j} (in the reference cell) that it starts from, and the node $x^{(n_j, \lambda_j)}$ it connects to.

For convenience we define two index sets:

- $\mathbb{B}_\kappa = \{(n, \lambda)\}$ is a list of nodes (n, λ) connected to the node $(0, \kappa)$.
- $\mathbb{B}_{\kappa, \lambda} = \{n\}$ is a list of the indices n such that $(0, \kappa)$ connects to (n, λ) .

It is easy to verify that

$$(n, \lambda) \in \mathbb{B}_\kappa \Leftrightarrow n \in \mathbb{B}_{\kappa, \lambda} \Leftrightarrow -n \in \mathbb{B}_{\lambda, \kappa} \Leftrightarrow (-n, \kappa) \in \mathbb{B}_\lambda.$$

Introduce the variable $u^{(n,\kappa)}$ to denote the “displacement” of node (n, κ) . The term displacement should be interpreted in a generalized sense since depending on context it may model either the temperature at the node or translational and/or rotational degrees of freedom of a mechanical

structure. Assuming that the “load-displacement” relationship is linear for each lattice member we write equilibrium for the member of type (κ, m, λ) that connects (n, κ) to $(n + m, \lambda)$ as

$$\begin{bmatrix} f^{(1)} \\ f^{(2)} \end{bmatrix} = A^{(\kappa, m, \lambda)} \begin{bmatrix} u^{(n, \kappa)} \\ u^{(n+m, \lambda)} \end{bmatrix} = \begin{bmatrix} A_{11}^{(\kappa, m, \lambda)} & A_{12}^{(\kappa, m, \lambda)} \\ A_{21}^{(\kappa, m, \lambda)} & A_{22}^{(\kappa, m, \lambda)} \end{bmatrix} \begin{bmatrix} u^{(n, \kappa)} \\ u^{(n+m, \lambda)} \end{bmatrix},$$

where $f^{(1)}$ and $f^{(2)}$ are the (generalized) forces acting at the ends of the member. The matrices $A^{(\kappa, m, \lambda)}$ should all be non-negative and symmetric (to conform with Castigliano’s theorems). Since the lattice is periodic we must also have

$$(3.6) \quad A_{12}^{(\kappa, m, \lambda)} = (A_{12}^{(\lambda, -m, \kappa)})^T, \quad A_{11}^{(\kappa, m, \lambda)} = A_{22}^{(\lambda, -m, \kappa)}.$$

Newton’s second law for the node (n, κ) takes the form

$$f^{(n, \kappa)} = M^\kappa \ddot{u}^{(n, \kappa)} + \sum_{(m, \lambda) \in \mathbb{B}_\kappa} \left[A_{11}^{(\kappa, m, \lambda)} u^{(n, \kappa)} + A_{12}^{(\kappa, m, \lambda)} u^{(n+m, \lambda)} \right],$$

where M^κ is a mass-matrix corresponding to masses lumped at node $x^{(n, \kappa)}$. The equation is of convolution form and it is therefore easily diagonalizable by the Fourier transform

$$\mathcal{F} : u \rightarrow \tilde{u}(k) = \sum_{n \in \mathbb{Z}^d} e^{i x^{(n)} \cdot k} u^{(n)}, \quad \text{for } k \in T^{-T}[-\pi, \pi]^d,$$

where $x^{(n)} = Tn$. We find

$$\begin{aligned} \tilde{f}^\kappa(k) &= M^\kappa \partial_t^2 \tilde{u}(k) + \sum_{(m, \lambda) \in \mathbb{B}_\kappa} \left[A_{11}^{(\kappa, m, \lambda)} \tilde{u}^\kappa(k) + A_{12}^{(\kappa, m, \lambda)} e^{-i x^{(m)} \cdot k} u^\lambda(k) \right] \\ &= M^\kappa \partial_t^2 \tilde{u}(k) + \sum_{\lambda=1}^q \sum_{m \in \mathbb{B}_{\kappa\lambda}} \left[A_{11}^{(\kappa, m, \lambda)} \delta_{\kappa\lambda} + e^{-i x^{(m)} \cdot k} A_{12}^{(\kappa, m, \lambda)} \right] \tilde{u}^\lambda(k). \end{aligned}$$

Write $\tilde{u}(k) = [\tilde{u}^1(k), \dots, \tilde{u}^q(k)]^T$ and $\tilde{f}(k) = [\tilde{f}^1(k), \dots, \tilde{f}^q(k)]^T$, and introduce a matrix $\sigma(k)$ whose $\kappa\lambda$ -block is given by

$$(3.7) \quad \sigma_{\kappa\lambda}(k) = \sum_{m \in \mathbb{B}_{\kappa\lambda}} \left[A_{11}^{(\kappa, m, \lambda)} \delta_{\kappa\lambda} + e^{-i x^{(m)} \cdot k} A_{12}^{(\kappa, m, \lambda)} \right],$$

and let $M = \text{diag}\{M^\kappa\}_{\kappa=1}^q$ be the mass-matrix. Then we can write the equations compactly as

$$\tilde{f}(k) = M \partial_t^2 \tilde{u}(k) + \sigma(k) \tilde{u}(k).$$

Looking for harmonic waves we set the forcing to zero, substitute $\partial_t^2 \tilde{u}(k) \rightarrow -\omega^2 \tilde{u}(k)$ and find the eigenvalue problem

$$(3.8) \quad [\sigma(k) - \omega^2 M] \tilde{u}(k) = 0.$$

The following proposition guarantees that the solutions ω^2 are all real and non-negative.

Proposition. *The symbol $\sigma(k)$ is a Hermitian, non-negative matrix.*

Proof: Starting with equation (3.7) and using (3.6) we find

$$\begin{aligned} [\sigma_{\kappa\lambda}(k)]^* &= \sum_{m \in \mathbb{B}_{\kappa\lambda}} \left[[A_{11}^{(\kappa,m,\lambda)} \delta_{\kappa\lambda}]^T + e^{ix^{(m)} \cdot k} [A_{12}^{(\kappa,m,\lambda)}]^T \right] \\ &= \sum_{m \in \mathbb{B}_{\kappa\lambda}} \left[A_{11}^{(\kappa,m,\lambda)} \delta_{\kappa\lambda} + e^{ix^{(m)} \cdot k} A_{12}^{(\lambda,-m,\kappa)} \right] = \sigma_{\lambda\kappa}(k), \end{aligned}$$

where in the last step we used that $m \in \mathbb{B}_{\kappa\lambda} \Leftrightarrow -m \in \mathbb{B}_{\lambda\kappa}$. This proves that $\sigma(k)$ is Hermitian.

To prove the non-negativeness claim fix any test-function \tilde{u} and set $u = \mathcal{F}^{-1}[\tilde{u}]$. Then by Parseval's theorem

$$\int_{T^{-T}(-\pi,\pi)^d} (\tilde{u}(k))^* \sigma(k) \tilde{u}(k) dk = (2\pi)^d \sum_{n \in \mathbb{Z}^d} \sum_{j=1}^b \begin{bmatrix} u^{(n,\kappa_j)} \\ u^{(n+m_j,\lambda_j)} \end{bmatrix}^T A^{(\kappa_j,m_j,\lambda_j)} \begin{bmatrix} u^{(n,\kappa_j)} \\ u^{(n+m_j,\lambda_j)} \end{bmatrix} \geq 0$$

since all the local matrices are non-negative.

In the context of mechanical lattices we earlier made the distinction between truss and frame structures. For the truss structures we study only the translational degrees of freedom so that $u^{(m,\kappa)} \in \mathbb{R}^d$. The stiffness matrix of a bar with cross-section s , length l , Young's modulus E and oriented along the unit vector a will be given by

$$A = \frac{sE}{l} \begin{bmatrix} aa^T & -aa^T \\ -aa^T & aa^T \end{bmatrix}.$$

The mass of a bar is proportional to $sl\rho$ where ρ is the density of the base material. Looking at the dispersion equation (3.8) we then determine the typical frequency ω_{truss} of the eigenmodes of the truss,

$$(3.9) \quad \frac{sE}{l} \sim \omega_{\text{truss}}^2 sl\rho, \quad \Rightarrow \quad \omega_{\text{truss}} \sim \frac{1}{l} \sqrt{\frac{E}{\rho}}.$$

Recalling that elastic waves in the base material travel with a group velocity proportional to $\sqrt{E/\rho}$ we find that this frequency corresponds to waves in the base material with a wavelength equal to the cell size. Note in particular that the cross-sectional area of the bars canceled.

For frame structures the situation is somewhat more complicated, even when we restrict attention to two-dimensional structures. For a beam oriented along the x_1 -axis with cross-sectional area s and cross-sectional moment of inertia I the equilibrium equation reads

$$(3.10) \quad \begin{bmatrix} f_1^1 \\ f_2^1 \\ T^1 \\ f_1^2 \\ f_2^2 \\ T^2 \end{bmatrix} = \begin{bmatrix} \frac{sE}{l} & 0 & 0 & -\frac{sE}{l} & 0 & 0 \\ 0 & \frac{12EI}{l^3} & \frac{6EI}{l^2} & 0 & -\frac{12EI}{l^3} & \frac{6EI}{l^2} \\ 0 & \frac{6EI}{l^2} & \frac{4EI}{l} & 0 & -\frac{6EI}{l^2} & \frac{2EI}{l} \\ -\frac{sE}{l} & 0 & 0 & \frac{sE}{l} & 0 & 0 \\ 0 & -\frac{12EI}{l^3} & -\frac{6EI}{l^2} & 0 & \frac{12EI}{l^3} & -\frac{6EI}{l^2} \\ 0 & \frac{6EI}{l^2} & \frac{2EI}{l} & 0 & -\frac{6EI}{l^2} & \frac{4EI}{l} \end{bmatrix} \begin{bmatrix} u_1^1 \\ u_2^1 \\ \theta^1 \\ u_1^2 \\ u_2^2 \\ \theta^2 \end{bmatrix}.$$

Here we labeled the two ends of the beam 1 and 2 and let (f_1^j, f_2^j, T^j) denote the forces and moments acting at end j , and similarly (u_1^j, u_2^j, θ^j) denote the translational and rotational degrees

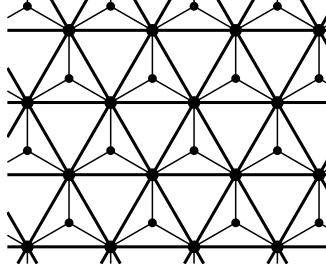


FIGURE 7.12. Triangular lattice with an oscillator.

of freedom of the displacement at end j . We commonly work with non-dimensional entities in which case the equilibrium equation takes the form (writing it only for node 1),

$$(3.11) \quad \begin{bmatrix} \frac{1}{sE} f_1^1 \\ \frac{1}{sE} f_2^1 \\ \frac{1}{slE} T^1 \end{bmatrix} = \begin{bmatrix} 1 & 0 & 0 \\ 0 & \frac{12I}{sl^2} & \frac{6I}{sl^2} \\ 0 & \frac{6I}{sl^2} & \frac{4I}{sl^2} \end{bmatrix} \begin{bmatrix} \frac{1}{l} u_1^1 \\ \frac{1}{l} u_2^1 \\ \theta^1 \end{bmatrix} + \begin{bmatrix} 1 & 0 & 0 \\ 0 & -\frac{12I}{sl^2} & \frac{6I}{sl^2} \\ 0 & -\frac{6I}{sl^2} & \frac{2I}{sl^2} \end{bmatrix} \begin{bmatrix} \frac{1}{l} u_1^2 \\ \frac{1}{l} u_2^2 \\ \theta^2 \end{bmatrix}.$$

For a solid bar of width b we have $I \sim b^2 s$ so that $I/(sl^2) \sim (b/l)^2$. For a slender bar the slenderness ratio $\varepsilon = b/l$ is small and the splitting of the stiffness matrix into one part that scales as $O(1)$ and one part that scales as $O(\varepsilon^2)$ is clear. These two parts correspond to axial and bending stiffness, respectively.

Finally we note that the polar moment of inertia of a bar will scale as $m_{\text{bar}} l^2 = \rho s l^3$. We can then estimate the typical frequency of rotational modes from equation (3.8),

$$\frac{EI}{l} \sim \omega_{\text{rot}}^2 J, \quad \Rightarrow \quad \omega_{\text{rot}} \sim \sqrt{\frac{EI}{Jl}} \sim \sqrt{\frac{Esb^2}{\rho sl^4}} \sim \frac{b}{l^2} \sqrt{\frac{E}{\rho}} = \frac{b}{l} \omega_{\text{truss}}$$

where in the last step we used equation (3.9) for ω_{truss} .

4. Designing lattices with prescribed bandgaps

In this section we will illustrate how the spectrum of an elastic lattice can be manipulated by introducing certain types of micro-structures. The idea is that the added microstructure should be such that it has its own vibrational modes corresponding to certain types of standing waves in the whole lattice.

As a first example consider a triangular truss structure with an added mass m_o at the center of every other cell, as illustrated in Figure 7.12. The mass is suspended by three bars, each with stiffness c_o . For simplicity we let the basic triangular structure (drawn with thick lines in the figure) have unit masses at the nodes and let it be connected with bars of unit stiffness. In Figure 7.13 the effect of the added micro-structure is illustrated. The left graph depicts the spectrum of the original, triangular lattice. In the middle graph the micro-structure is included, for $c_o = 1$, $m_o = 1$. The right graph shows the effect of weakening the springs to $c_o = 0.25$ and increasing the internal mass to $m_o = 4$. The interesting feature of these graphs is that the added structure clearly has introduced a bandgap in the spectrum. Interestingly, we can predict and control the location of this bandgap.

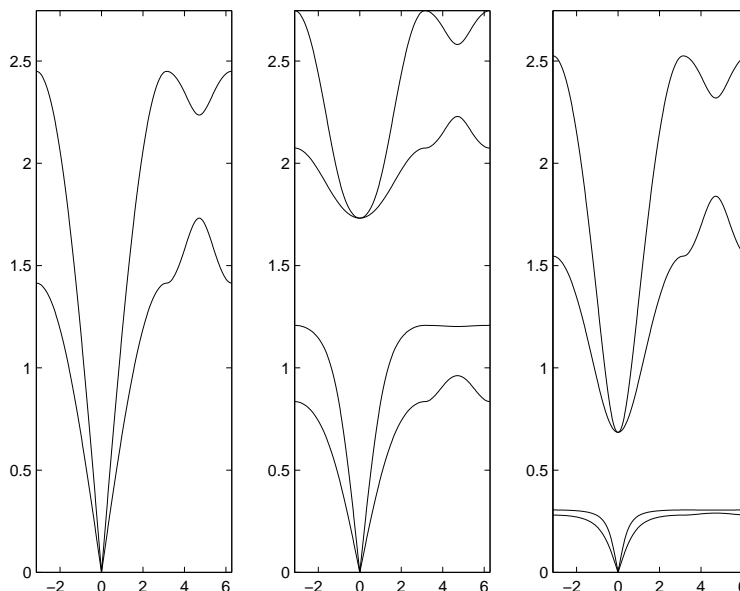


FIGURE 7.13. Spectrum for a triangular truss (left) and the same truss with a simple oscillator (middle and right).

Consider a mass m_o suspended by three springs with stiffness c_o , attached to the rigidly fixed vertices of an equilateral triangle. Using the unit vectors a_j defined in equation (2.3) and letting $u \in \mathbb{R}^2$ denote the displacement of the mass from the equilibrium point we can write

$$m_o \omega^2 u = c_o [a_1 a_1^T + a_2 a_2^T + a_3 a_3^T] u = c_o \begin{bmatrix} 3/2 & 0 \\ 0 & 3/2 \end{bmatrix} u.$$

This shows that the mass will oscillate about the equilibrium point with the frequency $\omega_o := \sqrt{\frac{3c_o}{2m_o}}$. For the examples illustrated in the graphs, $\{m_o, c_o\} = \{1, 0.2\}, \{5, 0.2\}$ we find $\omega_o = \{\sqrt{3/2}, \sqrt{3/32}\} \approx \{1.22, 0.32\}$. These values coincide to a very high degree of accuracy with the lower limits of the bandgaps observed in Figure 7.13.

Next we consider a more complex oscillator, as illustrated in Figure 7.14. In the case illustrated the small internal triangle is 0.15 times the size of the large ones. In Figure 7.15 we display the spectrum obtained if all internal nodes have mass 1 and all the internal springs have stiffness 0.2. Doing a calculation similar to the one we did for the simple oscillator in the previous paragraph, we find that the frequencies of the articulated oscillator are $\omega_o = \{0.41, 0.41, 0.55, 0.73, 0.73, 0.83\}$. These frequencies match the bands seen in Figure 7.15 very well.

Finally we will look at how an oscillator effects the spectrum of a frame structure, as illustrated in Figure 7.16. The thick lines representing the original lattice all have unit axial stiffness, a bending stiffness of 0.05 and there are unit masses at the nodes. Then we added another unit mass, $m_o = 1$, that is supported by the thin lines, which have an axial stiffness of $c_o = 0.2$ but no bending stiffness. This is the same oscillator as in the first example so we expect standing wave modes at

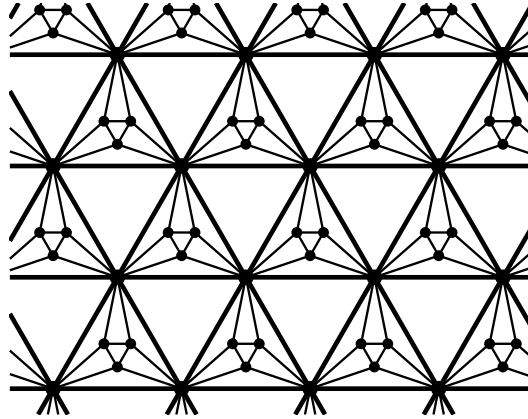


FIGURE 7.14. Triangular lattice with a complex oscillator.

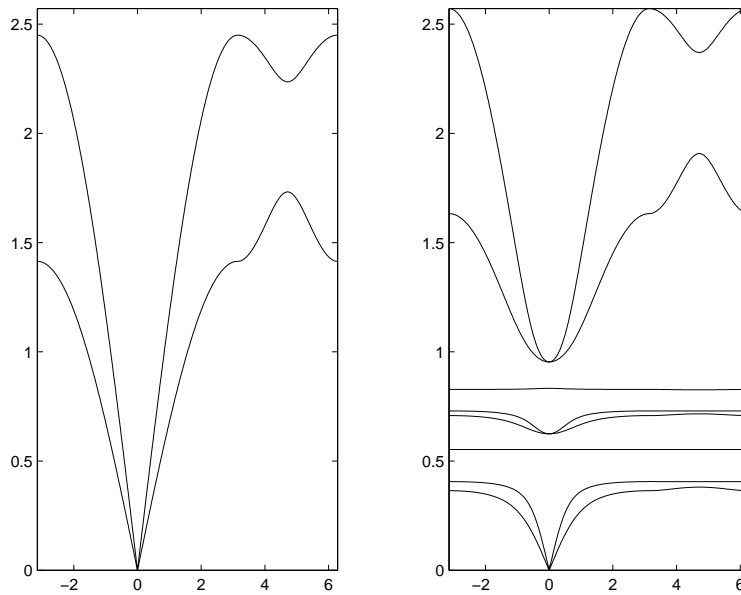


FIGURE 7.15. Spectrum for a triangular truss (left) and the same truss with a complex oscillator (right).

$\omega_o = \sqrt{(3c_o)/(2m_o)} \approx 0.55$, which corresponds exactly to where the new bandgap shows up in the right hand graph in Figure 7.17.

5. Conclusions

We have demonstrated that many mechanical lattice structures exhibit complete bandgaps, *i.e.* intervals of frequencies for which there are no propagating mechanical waves. We have provided a

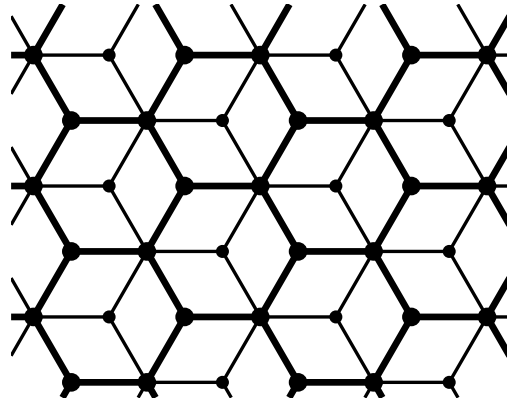


FIGURE 7.16. Honeycomb frame with an oscillator

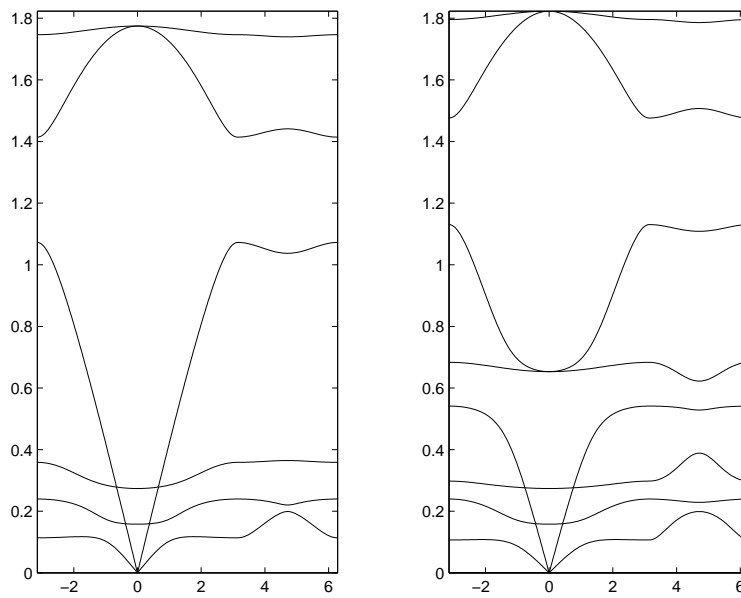


FIGURE 7.17. Spectrum for the honeycomb frame (left) and the same frame with an oscillator (right).

method for analysis that can be used to quickly determine the bandgaps, a method that is easily implemented on a computer for analysis of complicated structures. Finally we have exhibited a method by which lattices can be modified to create complete bandgaps at prescribed frequencies.

This work has a wide range of applications in the design of earthquake resistant structures, acoustic mirrors, filters and acoustic lasers.

CHAPTER 8

Concluding remarks

When the presented results are combined, they provide a powerful set of tools for solving a lattice equation defined on a very large set Ω ,

$$\begin{cases} \mathfrak{A}\mathbf{u} = \mathbf{f} & \text{on } \Omega, \\ \alpha\mathbf{u} + \beta\delta_\nu\mathbf{u} = \mathbf{g} & \text{on } \partial\Omega. \end{cases}$$

We can find a particular solution that satisfies the body load by computing the convolution $\mathfrak{G} * \mathbf{f}$ using the fast summation algorithm given in Chapter 5. In order to satisfy the boundary condition, we solve a homogeneous boundary value problem using the method given in Chapter 6. Note that a fast numerical solver for this problem again relies on the fast summation methods of Chapter 5.

The proposed method can fully resolve the problem and accurately compute \mathbf{u} at all the N nodes of Ω using $O(N)$ operations, just like other fast methods such as the FFT. However, the new method can do significantly better; taking advantage of whatever regularity happens to be present, it can use averaging in those regions where this is permissible and actually compute a solution in far less than $O(N)$ time. In essence, we embed the derivation of an averaged model directly into the fast numerical methods (FMM and BEM). This way, the resolution depth can change with spatial position and we can in a stable and systematic fashion resolve exactly those length-scales that are needed to obtain the desired level of accuracy.

Several remarks are in order:

- Short-range interactions are computed using the exact Green's function. This means that no à priori assumptions need to be made on the regularity of the problem.
- Long-range interactions are computed using the asymptotic expansion G_P of the lattice Green's function derived in Chapter 4. Note that G_P is the fundamental solution of the $O(\varepsilon^{2P+2})$ homogenized equations given in Chapter 3, which means that we are taking advantage of the very fast convergence of high-order homogenization without imposing the prohibitive regularity requirements that have heretofore been associated with such methods.
- The new method is most efficient when \mathfrak{A} is perfectly periodic but inclusions and local defects can be handled using the methods of section 3 of Chapter 6.

APPENDIX A

The stiffness matrix of a slender beam

In this appendix we describe the local stiffness matrices in the two-dimensional frame model. These results are basic strength of materials fare and are given here for reference only. For a fuller description of mechanical modelling of the kind we only touch upon here, see Przemieniecki [55].

In the frame model, a link is considered to be a slender mechanical beam. Suppose that the beam is oriented along the x_1 -axis, that its ends are displaced by the distances $U, V \in \mathbb{R}^2$ and are rotated anti-clockwise by angles $\phi, \psi \in [-\pi, \pi)$, as shown in Figure A.1. Then the forces $F, G \in \mathbb{R}^2$ and moments $M, N \in \mathbb{R}$ that are required to keep the beam in equilibrium are given by

$$(A.1) \quad \begin{bmatrix} \frac{AE}{L} & 0 & 0 & -\frac{AE}{L} & 0 & 0 \\ 0 & \frac{12EI}{L^3} & \frac{6EI}{L^2} & 0 & -\frac{12EI}{L^3} & \frac{6EI}{L^2} \\ 0 & \frac{6EI}{L^2} & \frac{4EI}{L} & 0 & -\frac{6EI}{L^2} & \frac{2EI}{L} \\ -\frac{AE}{L} & 0 & 0 & \frac{AE}{L} & 0 & 0 \\ 0 & -\frac{12EI}{L^3} & -\frac{6EI}{L^2} & 0 & \frac{12EI}{L^3} & -\frac{6EI}{L^2} \\ 0 & \frac{6EI}{L^2} & \frac{2EI}{L} & 0 & -\frac{6EI}{L^2} & \frac{4EI}{L} \end{bmatrix} \begin{bmatrix} U_1 \\ U_2 \\ \phi \\ V_1 \\ V_2 \\ \psi \end{bmatrix} = \begin{bmatrix} F_1 \\ F_2 \\ M \\ G_1 \\ G_2 \\ N \end{bmatrix}.$$

Here E is the Young's modulus, A is the cross-sectional area of the beam, L its length and I its moment of inertia. First we put (A.1) in non-dimensional form

$$\begin{bmatrix} 1 & 0 & 0 & -1 & 0 & 0 \\ 0 & \frac{12I}{AL^2} & \frac{6I}{AL} & 0 & -\frac{12I}{AL^2} & \frac{6I}{AL} \\ 0 & \frac{6I}{AL} & \frac{4I}{AL} & 0 & -\frac{6I}{AL} & \frac{2I}{AL} \\ -1 & 0 & 0 & 1 & 0 & 0 \\ 0 & -\frac{12I}{AL^2} & -\frac{6I}{AL} & 0 & \frac{12I}{AL^2} & -\frac{6I}{AL} \\ 0 & \frac{6I}{AL} & \frac{2I}{AL} & 0 & -\frac{6I}{AL} & \frac{4I}{AL} \end{bmatrix} \begin{bmatrix} U_1/L \\ U_2/L \\ \phi \\ V_1/L \\ V_2/L \\ \psi \end{bmatrix} = \begin{bmatrix} F_1/AE \\ F_2/AE \\ M/AEL \\ G_1/AE \\ G_2/AE \\ N/AEL \end{bmatrix}.$$

Next set $u = (u_1, u_2, u_3) := (U_1/L, U_2/L, \phi)$, $f = (f_1, f_2, f_3) := (F_1/AE, F_2/AE, M/AEL)$ and define v and g likewise. Then we can write (A.1) as, cf. (2.2) and (2.7),

$$\left(\begin{bmatrix} B_{\text{axial}} & -B_{\text{axial}} \\ -B_{\text{axial}} & B_{\text{axial}} \end{bmatrix} + \beta^2 \begin{bmatrix} B_{\text{bend}} & C_{\text{bend}} \\ C_{\text{bend}}^t & D_{\text{bend}} \end{bmatrix} \right) \begin{bmatrix} u \\ v \end{bmatrix} = \begin{bmatrix} f \\ g \end{bmatrix},$$

where $\beta^2 = 12I/(AL^2)$ and

$$B_{\text{axial}} = \begin{bmatrix} 1 & 0 & 0 \\ 0 & 0 & 0 \\ 0 & 0 & 0 \end{bmatrix}, \quad B_{\text{bend}} = \begin{bmatrix} 0 & 0 & 0 \\ 0 & 1 & \frac{1}{2} \\ 0 & \frac{1}{2} & \frac{1}{3} \end{bmatrix}, \quad C_{\text{bend}} = \begin{bmatrix} 0 & 0 & 0 \\ 0 & -1 & \frac{1}{2} \\ 0 & -\frac{1}{2} & \frac{1}{6} \end{bmatrix}, \quad D_{\text{bend}} = \begin{bmatrix} 0 & 0 & 0 \\ 0 & 1 & -\frac{1}{2} \\ 0 & -\frac{1}{2} & \frac{1}{3} \end{bmatrix}.$$

Note that typically $I \sim A^2$, which means that $\beta^2 \sim A/L^2 \sim (r/L)^2$, where r is the length of the cross-section of the bar. This justifies the claim made in connection with equation (2.7) that the

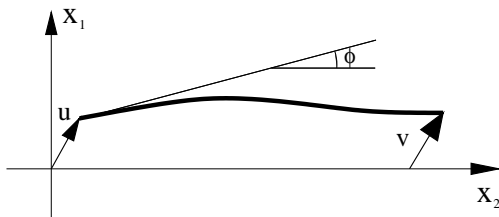


FIGURE A.1. Illustration of the coordinates in the beam model.

component of the stiffness matrix that corresponds to bending stiffness scales as the slenderness ratio squared.

It remains only to describe how to obtain the stiffness matrix for a beam that is not parallel to the x_1 -axis. Let θ be the angle that the beam forms with this axis (counted positive anti-clockwise) and define rotation matrices

$$U_\theta = \begin{bmatrix} \cos \theta & -\sin \theta & 0 \\ \sin \theta & \cos \theta & 0 \\ 0 & 0 & 1 \end{bmatrix}.$$

Then the stiffness matrix for the rotated beam is given by

$$K_\theta := \begin{bmatrix} U_\theta & 0 \\ 0 & U_\theta \end{bmatrix} \left(\begin{bmatrix} B_{\text{axial}} & -B_{\text{axial}} \\ -B_{\text{axial}} & B_{\text{axial}} \end{bmatrix} + \beta^2 \begin{bmatrix} B_{\text{bend}} & C_{\text{bend}} \\ C_{\text{bend}}^t & D_{\text{bend}} \end{bmatrix} \right) \begin{bmatrix} U_\theta^t & 0 \\ 0 & U_\theta^t \end{bmatrix}.$$

APPENDIX B

Examples of lattices

1. Introduction

In this appendix we will apply the techniques derived in the thesis to study several classical lattice geometries. For all geometries, we study the conduction problem and either the truss or the frame mechanical model, depending on whether the truss model is degenerate or not.

Given a lattice geometry and a local model, the following steps are carried out:

Step 1: Compute the symbol $\sigma(\xi)$ using (2.10) and (2.11).

Step 2: Compute the series expansion of $\sigma(\xi)$.

Step 3: Use the series expansion of Step 2 to compute the series expansion of $\sigma(\xi)^{-1}$ using Lemma 3.5.

Step 4: Read off the homogenized equations from the series expansion of $\sigma(\xi)^{-1}$.

Step 5: Compute the terms in the asymptotic expansion of the lattice Green's function using the series expansion of $\sigma(\xi)^{-1}$ combined with either Proposition 4.1 (when $d = 3$) or Propositions 4.3 and 4.4 (when $d = 2$).

While steps 2, 3 and 5 involve conceptually simple operations, they tend to require very lengthy algebraic manipulations in practice. This makes the use of symbolic algebra software indispensable. A complete suite of subroutines for dealing with arbitrary lattice geometries and the three local models studied in this thesis can be downloaded from:

http://www.ticam.utexas.edu/~pgm/Thesis/maple_program.html

2. Simple square and cubic lattices

Two-dimensional square model: The lattice is defined by

$$X(0,1) = \begin{bmatrix} 0 \\ 0 \end{bmatrix}, \quad T = \begin{bmatrix} 1 & 0 \\ 0 & 1 \end{bmatrix}, \quad \mathbb{B}_+ = \{(1, [1,0], 1), (1, [0,1], 1)\}.$$

Consider first the **conduction** problem, assuming that all bars have conductivity 1. Then

$$\sigma(\xi) = 4 \sin^2 \frac{\xi_1}{2} + 4 \sin^2 \frac{\xi_2}{2} = 2(1 - \cos \xi_1) + 2(1 - \cos \xi_2) = \sum_{j=1}^{\infty} (-1)^{j-1} \frac{2}{(2j)!} (\xi_1^{2j} + \xi_2^{2j}),$$

and

$$\begin{aligned} \frac{1}{\sigma(\xi)} &= \frac{1}{|\xi|^2} + \frac{1}{|\xi|^4} \left(\frac{\xi_1^4}{12} + \frac{\xi_2^2}{12} \right) + \frac{1}{|\xi|^6} \left(\frac{\xi_1^8}{240} - \frac{\xi_1^6 \xi_2^2}{360} + \frac{\xi_1^4 \xi_2^4}{72} - \frac{\xi_1^2 \xi_2^6}{360} + \frac{\xi_2^8}{240} \right) + \\ &\quad \frac{1}{|\xi|^8} \left(\frac{\xi_1^{12}}{6048} - \frac{11 \xi_1^{10} \xi_2^2}{30240} + \frac{\xi_1^8 \xi_2^4}{756} - \frac{\xi_1^6 \xi_2^6}{1080} + \frac{\xi_1^4 \xi_2^8}{756} - \frac{11 \xi_1^2 \xi_2^{10}}{30240} + \frac{\xi_2^{12}}{6048} \right) + O(|\xi|^6). \end{aligned}$$

We can now read off the homogenized equations, the first three read

$$\begin{aligned} (-\Delta)^1 u^{(0,\varepsilon)} &= f, \\ (-\Delta)^2 u^{(1,\varepsilon)} &= (-\Delta) f + \varepsilon^2 \left(\frac{\partial_1^4}{12} + \frac{\partial_2^4}{12} \right) f, \\ (-\Delta)^3 u^{(2,\varepsilon)} &= (-\Delta)^2 f + \varepsilon^2 \left(\frac{\partial_1^4}{12} + \frac{\partial_2^4}{12} \right) f + \varepsilon^4 \left(\frac{\partial_1^8}{240} - \frac{\partial_1^6 \partial_2^2}{360} + \frac{\partial_1^4 \partial_2^4}{72} - \frac{\partial_1^2 \partial_2^6}{360} + \frac{\partial_2^8}{240} \right) f. \end{aligned}$$

The asymptotic expansion of the lattice Green's function is

$$\begin{aligned} \mathfrak{G}(m) &= -\frac{1}{2\pi} \left(\log |m| + \gamma + \frac{\log 8}{2} \right) + \frac{1}{24\pi} \frac{m_1^4 - 6m_1^2 m_2^2 + m_2^4}{|m|^6} \\ &\quad + \frac{1}{480\pi} \frac{43m_1^8 - 772m_1^6 m_2^2 + 1570m_1^4 m_2^4 - 772m_1^2 m_2^6 + 43m_2^8}{|m|^{12}} + \dots \end{aligned}$$

In polar coordinates, $m = r(\cos \theta, \sin \theta)$, we write

$$\begin{aligned} \mathfrak{G}(m) &= -\frac{1}{2\pi} \left(\log r + \gamma + \frac{\log 8}{2} \right) + \frac{\cos(4\theta)}{24\pi r^2} + \frac{25 \cos(8\theta) + 18 \cos(4\theta)}{480\pi r^4} \\ &\quad + \frac{490 \cos(12\theta) + 459 \cos(8\theta)}{2016\pi r^6} + \frac{9625 \cos(16\theta) + 10800 \cos(12\theta) + 1302 \cos(8\theta)}{3840\pi r^8} + \dots, \end{aligned}$$

where $\gamma = 0.577206 \dots$ is the Euler constant.

Next we model the lattice as a **frame**. With γ the bending stiffness of the bars, the scaled symbol takes the form

$$\sigma^{(\varepsilon)}(\xi) = \begin{bmatrix} 4\varepsilon^{-2} \sin^2 \frac{\varepsilon \xi_1}{2} + 4\gamma \varepsilon^{-2} \sin^2 \frac{\varepsilon \xi_2}{2} & 0 & \mathbf{i} \gamma \varepsilon^{-1} \sin \varepsilon \xi_2 \\ 0 & 4\varepsilon^{-2} \sin^2 \frac{\varepsilon \xi_2}{2} + 4\gamma \varepsilon^{-2} \sin^2 \frac{\varepsilon \xi_1}{2} & -\mathbf{i} \gamma \varepsilon^{-1} \sin \varepsilon \xi_1 \\ -\mathbf{i} \gamma \varepsilon^{-1} \sin \varepsilon \xi_2 & \mathbf{i} \gamma \varepsilon^{-1} \sin \varepsilon \xi_1 & \frac{1}{3} \gamma (4 + \cos \varepsilon \xi_1 + \cos \varepsilon \xi_2) \end{bmatrix}.$$

We have

$$(B.1) \quad \sigma_H(\xi) := \left[\lim_{\varepsilon \rightarrow 0} [\sigma^{(\varepsilon)}(\xi)]^{-1} \right]^{-1} = \begin{bmatrix} \xi_1^2 + \gamma \xi_2^2 & 0 & \mathbf{i} \gamma \xi_2 \\ 0 & \gamma \xi_1^2 + \xi_2^2 & -\mathbf{i} \gamma \xi_1 \\ -\mathbf{i} \gamma \xi_2 & \mathbf{i} \gamma \xi_1 & 2\gamma \end{bmatrix},$$

from which the homogenized equations follow straight-forwardly: Letting u_1 and u_2 denote displacements and u_3 micro-rotations, we get

$$\begin{aligned} -(\partial_1^2 + \gamma \partial_2^2) u_1 + \gamma \partial_2 u_3 &= f_1, \\ -(\gamma \partial_1^2 + \partial_2^2) u_2 - \gamma \partial_1 u_3 &= f_2, \\ -\gamma \partial_2 u_1 + \gamma \partial_1 u_2 + 2\gamma u_3 &= f_3, \end{aligned}$$

where f_1 and f_2 are force loads and f_3 is the torque loading. If there is no torque load, then u_3 can be eliminated from the equations. We take the Schur complement of σ_H and obtain

$$\sigma_{H,\text{reduced}}(\xi) = \begin{bmatrix} \xi_1^2 + \gamma\xi_2^2/2 & \gamma\xi_1\xi_2/2 \\ \gamma\xi_1\xi_2/2 & \gamma\xi_1^2/2 + \xi_2^2 \end{bmatrix}.$$

This matrix equals the matrix $\sigma_0(\xi)$ provided by Lemma 2.20. It corresponds to the following equation of two-dimensional elasticity,

$$(B.2) \quad \begin{cases} -(\partial_1^2 + (\gamma/2)\partial_2^2)u_1 - (\gamma/2)\partial_1\partial_2u_2 = f_1, \\ -(\gamma/2)\partial_1\partial_2u_1 - ((\gamma/2)\partial_1^2 + \partial_2^2)u_2 = f_2. \end{cases}$$

Two-dimensional square with an appendix: Next we add a node in the center of the cell that is attached to the original node by a single link. Note that unless this node is loaded, it is “inert” in the sense that there will be no flow in the diagonal bar. The lattice is described by the parameters:

$$X(0,1) = \begin{bmatrix} 0 \\ 0 \end{bmatrix}, \quad X(0,2) = \begin{bmatrix} 1/2 \\ 1/2 \end{bmatrix}, \quad \mathbb{B} = \{(1, [1, 0], 1), (1, [0, 1], 1), (1, [0, 0], 2)\}.$$

Consider first the **conduction** problem with the diagonal bar having conductivity α and the horizontal and vertical ones conductivity 1. Then

$$\sigma(\xi) = \begin{bmatrix} 4\sin^2 \frac{\xi_1}{2} + 4\sin^2 \frac{\xi_2}{2} + \alpha & -\alpha \\ -\alpha & \alpha \end{bmatrix}.$$

We find that

$$\det \sigma(\xi) = \alpha \left(4\sin^2 \frac{\xi_1}{2} + 4\sin^2 \frac{\xi_2}{2} \right),$$

and consequently

$$\sigma^{-1}(\xi) = \frac{1}{4\sin^2 \frac{\xi_1}{2} + 4\sin^2 \frac{\xi_2}{2}} \begin{bmatrix} 1 & 1 \\ 1 & 1 + \alpha^{-1} \left(4\sin^2 \frac{\xi_1}{2} + 4\sin^2 \frac{\xi_2}{2} \right) \end{bmatrix}.$$

Note that the upper left entry exactly equals the inverse symbol for the square lattice.

Next we consider the **frame** model and assign for simplicity the diagonal bar with the same properties as the other bars. Then, *cf.* (B.1),

$$\sigma_H^{(11)}(\xi) = \begin{bmatrix} \xi_1^2 + \gamma\xi_2^2 & 0 & \mathbf{i}\gamma\xi_2 \\ 0 & \gamma\xi_1^2 + \xi_2^2 & -\mathbf{i}\gamma\xi_1 \\ -\mathbf{i}\gamma\xi_2 & \mathbf{i}\gamma\xi_1 & 2\gamma \end{bmatrix}$$

$$\sigma_H^{(12)}(\xi) = \sigma_H^{(11)}(\xi),$$

$$\sigma_H^{(22)}(\xi) = \frac{1}{1 + 12\sqrt{2}} \begin{bmatrix} (1 + 12\sqrt{2})\xi_1^2 + \gamma(1 + 6\sqrt{2})\xi_2^2 & 6\sqrt{2}\gamma\xi_1\xi_2 & \mathbf{i}\gamma\xi_2 \\ 6\sqrt{2}\gamma\xi_1\xi_2 & \gamma(1 + 6\sqrt{2})\xi_1^2 + (1 + 12\sqrt{2})\xi_2^2 & -\mathbf{i}\gamma\xi_1 \\ -\mathbf{i}\gamma\xi_2 & \mathbf{i}\gamma\xi_1 & 2\gamma \end{bmatrix}.$$

The matrix σ_0 (which again is the Schur complement of either one of the $\sigma_H^{(\kappa\lambda)}$'s) is given by

$$\sigma_0(\xi) = \begin{bmatrix} \xi_1^2 + \gamma\xi_2^2/2 & \gamma\xi_1\xi_2/2 \\ \gamma\xi_1\xi_2/2 & \gamma\xi_1^2/2 + \xi_2^2 \end{bmatrix}.$$

This expression is identical with the dominant term for lattice A, (B.2), as expected.

The cubic lattice: The analysis for the cubic lattice is a trivial analogue of the analysis for the square lattice. For reference, we give the asymptotic expansion of the lattice Green's function;

$$\begin{aligned} \mathfrak{G}(m) &= \frac{1}{4\pi|m|} + \frac{m_1^4 + m_2^4 + m_3^4 - 3m_1^2m_2^2 - 3m_1^2m_3^2 - 3m_2^2m_3^2}{16\pi|m|^7} \\ &+ \frac{1}{128\pi|m|^{13}} \left[23(m_1^8 + m_2^8 + m_3^8) - 244(m_1^6(m_2^2 + m_3^2) + m_2^6(m_1^2 + m_3^2) + m_3^6(m_1^2 + m_2^2)) \right. \\ &\quad \left. 228m_1^2m_2^2m_3^2|m|^2 + 621(m_1^4m_2^4 + m_1^4m_3^4 + m_2^4m_3^4) \right] + O(|m|^{-7}). \end{aligned}$$

3. Body-centered lattices

The two-dimensional BCC lattice: The lattice is defined by

$$X(0,1) = \begin{bmatrix} 1 \\ 0 \end{bmatrix}, \quad X(0,2) = \begin{bmatrix} 1/2 \\ 1/2 \end{bmatrix}, \quad T = \begin{bmatrix} 1 & 0 \\ 0 & 1 \end{bmatrix},$$

and

$$\mathbb{B}_+ = \{(1, [1, 0], 1), (1, [0, 1], 1), (1, [0, 0], 2), (2, [1, 0], 1), (2, [1, 1], 1), (2, [0, 1], 1)\}.$$

For the **conduction** model, let the horizontal and vertical bars have conductivity 1 and the diagonal conductivity α . Then the symbol is

$$\sigma(\xi) = \begin{bmatrix} 4\sin^2 \frac{\xi_1}{2} + 4\sin^2 \frac{\xi_2}{2} + 4\alpha & -\alpha(1 + e^{i\xi_1} + e^{i\xi_2} + e^{i(\xi_1+\xi_2)}) \\ -\alpha(1 + e^{-i\xi_1} + e^{-i\xi_2} + e^{-i(\xi_1+\xi_2)}) & 4\alpha \end{bmatrix}.$$

and its determinant is

$$\begin{aligned} \det \sigma(\xi) &= 4\alpha(1 + \alpha/2) \left(4\sin^2 \frac{\xi_1}{2} + 4\sin^2 \frac{\xi_2}{2} \right) + \alpha^2 \left(4\sin^2 \frac{(\xi_1 + \xi_2)}{2} + 4\sin^2 \frac{(\xi_1 - \xi_2)}{2} \right) \\ &= 4\alpha(1 + \alpha)|\xi|^2 + O(|\xi|^4). \end{aligned}$$

We then get the inverse symbol

$$\sigma(\xi)^{-1} = \frac{1}{\det \sigma(\xi)} \begin{bmatrix} 4\alpha & \alpha(1 + e^{i\xi_1} + e^{i\xi_2} + e^{i(\xi_1+\xi_2)}) \\ \alpha(1 + e^{-i\xi_1} + e^{-i\xi_2} + e^{-i(\xi_1+\xi_2)}) & 4\sin^2 \frac{\xi_1}{2} + 4\sin^2 \frac{\xi_2}{2} + 4\alpha \end{bmatrix}.$$

The series expansion around the origin is

$$\sigma(\xi)^{-1} = \frac{1}{(1 + \alpha)|\xi|^2} \begin{bmatrix} 1 & 1 + (1/2)\mathbf{i}(\xi_1 + \xi_2) \\ 1 - (1/2)\mathbf{i}(\xi_1 + \xi_2) & 1 \end{bmatrix} + O(1).$$

The homogenized equations follow directly,

$$\begin{cases} -(1 + \alpha)\Delta u_1^{(\varepsilon,0)} = (f_1 + f_2) + (1/2)\varepsilon(\partial_1 + \partial_2)f_2, \\ -(1 + \alpha)\Delta u_2^{(\varepsilon,0)} = (f_1 + f_2) - (1/2)\varepsilon(\partial_1 + \partial_2)f_1. \end{cases}$$

Before giving the asymptotic expansion of the lattice Green's function we recall that

$$\begin{aligned} [\mathfrak{G}(n)]_{11} &= 4\alpha\mathfrak{G}_H(n), \\ [\mathfrak{G}(n)]_{12} &= \alpha[\mathfrak{G}_H(n) + \mathfrak{G}_H(n_1 - 1, n_2) + \mathfrak{G}_H(n_1, n_2 - 1) + \mathfrak{G}_H(n_1 - 1, n_2 - 1)], \\ [\mathfrak{G}(n)]_{21} &= \alpha[\mathfrak{G}_H(n) + \mathfrak{G}_H(n_1 + 1, n_2) + \mathfrak{G}_H(n_1, n_2 + 1) + \mathfrak{G}_H(n_1 + 1, n_2 + 1)], \\ [\mathfrak{G}(n)]_{22} &= 4(1 + \alpha)\mathfrak{G}_H(n) - \alpha[\mathfrak{G}_H(n_1 - 1, n_2) + \mathfrak{G}_H(n_1 + 1, n_2) \\ &\quad + \mathfrak{G}_H(n_1, n_2 - 1) + \mathfrak{G}_H(n_1, n_2 + 1)], \end{aligned}$$

where

$$\mathfrak{G}_H(n) := \frac{1}{(2\pi)^2} \int_{(-\pi, \pi)^2} \frac{e^{-in \cdot \xi} - 1}{\det \sigma(\xi)} d\xi.$$

We then only need to give the expansion of \mathfrak{G}_H . In polar coordinates,

$$\begin{aligned} 4\alpha\mathfrak{G}_H(m) &= -\frac{\log r + C}{2\pi(1 + \alpha)} + \frac{(1 - \alpha/2) \cos(4\theta)}{24\pi(1 + \alpha)^2 r^2} \\ &\quad + \frac{25(1 - \alpha/2)^2 \cos(8\theta) + 18(1 + 2\alpha - \alpha^2/4) \cos(4\theta)}{480\pi(1 + \alpha)^3 r^4} + \dots \end{aligned}$$

where C is a constant. Note that as $\alpha \rightarrow 0$, the Green's function for the square lattice is recovered and that for $\alpha = 2$, the second term vanishes.

For the **truss** model we give the horizontal and vertical bars stiffness 1 and the diagonal ones stiffness α . Then

$$\begin{aligned} [\sigma(\xi)]_{11} &= \begin{bmatrix} 4 \sin^2 \frac{\xi_1}{2} + 2\alpha & 0 \\ 0 & 4 \sin^2 \frac{\xi_1}{2} + 2\alpha \end{bmatrix}, \\ [\sigma(\xi)]_{12} &= \begin{bmatrix} -\frac{\alpha}{2}(1 + e^{i\xi_1} + e^{i\xi_2} + e^{i(\xi_1 + \xi_2)}) & -\frac{\alpha}{2}(1 - e^{i\xi_1} - e^{i\xi_2} + e^{i(\xi_1 + \xi_2)}) \\ -\frac{\alpha}{2}(1 - e^{i\xi_1} - e^{i\xi_2} + e^{i(\xi_1 + \xi_2)}) & -\frac{\alpha}{2}(1 + e^{i\xi_1} + e^{i\xi_2} + e^{i(\xi_1 + \xi_2)}) \end{bmatrix}, \\ [\sigma(\xi)]_{22} &= \begin{bmatrix} 2\alpha & 0 \\ 0 & 2\alpha \end{bmatrix}. \end{aligned}$$

The matrix σ_0 specified in Lemma 2.16 is

$$\sigma_0(\xi) = \begin{bmatrix} (1 + \alpha/2)\xi_1^2 + (\alpha/2)\xi_2^2 & \alpha\xi_1\xi_2 \\ \alpha\xi_1\xi_2 & (\alpha/2)\xi_1^2 + (1 + \alpha/2)\xi_2^2 \end{bmatrix}.$$

The lowest order system of homogenized equations is then

$$\begin{aligned} -((1 + \alpha/2)\partial_1^2 + (\alpha/2)\partial_2^2)u_1 - (\alpha\partial_1\partial_2)u_2 &= f_1, \\ -(\alpha\partial_1\partial_2)u_1 - ((\alpha/2)\partial_1^2 + (1 + \alpha/2)\partial_2^2)u_1 &= f_2. \end{aligned}$$

These are equations of two-dimensional elasticity for any $\alpha > 0$. If $\alpha = 1$, we get the equations of an isotropic medium (in plane stress) with Young's modulus $4/3$ and Poisson's ratio $1/3$. Note that if we model an actual physical truss, the isotropic case corresponds to one where the diagonal bars have a cross-sectional area that is $\sqrt{2}$ smaller than the horizontal and vertical ones (since axial stiffness scales as area divided by length).

The three-dimensional BCC: The lattice is defined by

$$X(0,1) = \begin{bmatrix} 0 \\ 0 \\ 0 \end{bmatrix}, \quad X(0,2) = \begin{bmatrix} 1/2 \\ 1/2 \\ 1/2 \end{bmatrix}, \quad T = \begin{bmatrix} 1 & 0 & 0 \\ 0 & 1 & 0 \\ 0 & 0 & 1 \end{bmatrix}$$

$$\mathbb{B} = \{(1, [1, 0, 0], 1), (1, [0, 1, 0], 1), (1, [0, 0, 1], 1), (2, [0, 0, 0], 1), (2, [0, 0, 1], 1), (2, [0, 1, 0], 1), \\ [0, 1, 1], 1), (2, [1, 0, 0], 1), (2, [1, 0, 1], 1), (2, [1, 1, 0], 1), (2, [1, 1, 1], 1)\}.$$

For the **conduction** model we let the bars that are parallel with the coordinate axes have stiffness one and the diagonal ones stiffness α . Then

$$\begin{aligned} [\sigma(\xi)]_{11} &= 4 \sin^2 \frac{\xi_1}{2} + 4 \sin^2 \frac{\xi_2}{2} + 4 \sin^2 \frac{\xi_3}{2} + 8\alpha, \\ [\sigma(\xi)]_{12} &= -\alpha(1 + e^{i\xi_1} + e^{i\xi_2} + e^{i(\xi_1+\xi_2)} + e^{i\xi_3} + e^{i(\xi_1+\xi_3)} + e^{i(\xi_2+\xi_3)} + e^{i(\xi_1+\xi_2+\xi_3)}), \\ [\sigma(\xi)]_{22} &= 8\alpha. \end{aligned}$$

We find that $\det \sigma(\xi) = 8\alpha(1 + 2\alpha)|\xi|^2 + O(|\xi|^4)$ and so the series expansion of the inverse symbol is given by

$$\sigma(\xi)^{-1} = \frac{1}{(1 + 2\alpha)|\xi|^2} \begin{bmatrix} 1 & & 1 + (1/2)(i\xi_1 + i\xi_2 + i\xi_3) \\ & 1 - (1/2)(i\xi_1 + i\xi_2 + i\xi_3) & \\ & & 1 \end{bmatrix} + O(|\xi|^0).$$

The homogenized equations are

$$\begin{cases} (1 + 2\alpha)(-\Delta)u_1 = f_1 + f_2 + (1/2)\varepsilon(\partial_1 + \partial_2 + \partial_3)f_2, \\ (1 + 2\alpha)(-\Delta)u_2 = f_1 + f_2 - (1/2)\varepsilon(\partial_1 + \partial_2 + \partial_3)f_1. \end{cases}$$

The lattice Green's function can now be determined using the method described for lattice B. As an example, we use that $\mathfrak{G}_{11}(m) = 8\alpha\mathfrak{G}_H(m)$ and obtain

$$\mathfrak{G}_{11}(m) = \frac{1}{4\pi(1 + 2\alpha)|m|} + \frac{(1 - \alpha)(m_1^3 + m_2^4 + m_3^4 - 3m_1^2m_2^2 - 3m_1^2m_3^2 - 3m_1^2m_3^2)}{16\pi(1 + 2\alpha)^2|m|^7} + O(|m|^{-5}).$$

For $\alpha = 1$, the second term vanishes and when $\alpha \rightarrow 0$, the expansion for a cubic lattice is recovered.

For the **truss** model let the diagonal bars have stiffness α and the others stiffness 1. Then

$$\sigma_0(\xi) = \begin{bmatrix} \frac{1}{2}\xi_1^2 + \frac{\alpha}{3}|\xi|^2 & \frac{2}{3}\alpha\xi_1\xi_2 & \frac{2}{3}\alpha\xi_1\xi_3 \\ \frac{2}{3}\alpha\xi_1\xi_2 & \frac{1}{2}\xi_2^2 + \frac{\alpha}{3}|\xi|^2 & \frac{2}{3}\alpha\xi_2\xi_3 \\ \frac{2}{3}\alpha\xi_1\xi_3 & \frac{2}{3}\alpha\xi_2\xi_3 & \frac{1}{2}\xi_3^2 + \frac{\alpha}{3}|\xi|^2 \end{bmatrix}.$$

If $\alpha = 3/4$, then this corresponds to an isotropic material with Lamé constants $\lambda = \mu = 1/2$ and Poisson's ratio $\nu = 1/4$.

4. Triangular and hexagonal lattices

When we treat structures that do not have a cubic (or square) unit cell, *i.e.* $T \neq I$, we work with a modified Fourier transform,

$$\tilde{\mathbf{u}}(\xi) = \sum_{m \in \mathbb{Z}^d} e^{i(Tm) \cdot \xi} \mathbf{u}(m),$$

so that ξ truly represents inverse of physical position (the position of node m is Tm).

The triangular lattice: The lattice is defined by

$$X(0,0) = \begin{bmatrix} 0 \\ 0 \end{bmatrix}, \quad T = \begin{bmatrix} 1 & 1/2 \\ 0 & \sqrt{3}/2 \end{bmatrix}, \quad \mathbb{B}_+ = \{(1, [1, 0], 1), (1, [0, 1], 1), (1, [-1, 1], 1)\}.$$

For the **conduction** problem we let all bars have conductivity 1, whence

$$\sigma(\xi) = 4 \sin^2 \frac{\xi_1}{2} + 4 \sin^2 \frac{\xi_1 + \sqrt{3}\xi_2}{4} + 4 \sin^2 \frac{\xi_1 - \sqrt{3}\xi_2}{2},$$

which implies that

$$\frac{1}{\sigma(\xi)} = \frac{2}{3|\xi|^2} + \frac{1}{24} + \frac{23\xi_1^6 + 105\xi_1^2\xi_2^4 + 45\xi_1^2\xi_2^4 + 27\xi_2^6}{17280|\xi|^4} + \frac{5\xi_1^6 + 51\xi_1^4\xi_2^2 - 9\xi_1^2\xi_2^4 + 9\xi_2^6}{193536|\xi|^2} + \dots$$

Note in particular the cancellations that appear in this series due to the very strong symmetry properties of the lattice. When writing down the equilibrium equations that result from this expansion, we must take into account that the unit cell has area $\det T = \sqrt{3}/2$. We get

$$\begin{aligned} \sqrt{3}(-\Delta)^1 u^{(0,\varepsilon)} &= f, \\ \sqrt{3}(-\Delta)^2 u^{(1,\varepsilon)} &= (-\Delta)f + \varepsilon^2 \frac{1}{24} (-\Delta)^2 f, \\ \sqrt{3}(-\Delta)^3 u^{(2,\varepsilon)} &= (-\Delta)^2 f + \varepsilon^2 \frac{1}{24} (-\Delta)^3 f + \varepsilon^4 \frac{1}{11520} (23\partial_1^6 + 105\partial_1^4\partial_2^2 + 45\partial_1^2\partial_2^4 + 27\partial_2^6) (-\Delta)f, \\ \sqrt{3}(-\Delta)^4 u^{(3,\varepsilon)} &= (-\Delta)^3 f + \varepsilon^2 \frac{1}{24} (-\Delta)^4 f + \varepsilon^4 \frac{1}{11520} (23\partial_1^6 + 105\partial_1^4\partial_2^2 + 45\partial_1^2\partial_2^4 + 27\partial_2^6) (-\Delta)^2 f \\ &\quad + \varepsilon^6 \frac{1}{193536} (5\partial_1^6 + 51\partial_1^4\partial_2^2 - 9\partial_1^2\partial_2^4 + 9\partial_2^6) (-\Delta)^3 f. \end{aligned}$$

The asymptotic expansion of the lattice Green's function is

$$(B.3) \quad \begin{aligned} \mathfrak{G}(n) &\sim -\frac{1}{2\sqrt{3}\pi} \log r + C + \frac{1}{60\sqrt{3}\pi} \frac{\cos(6\theta)}{r^4} \\ &\quad + \frac{5}{168\sqrt{3}\pi} \frac{\cos(6\theta)}{r^6} + \frac{7}{40\sqrt{3}\pi} \frac{\cos(12\theta)}{r^8} + O(r^{-12}). \end{aligned}$$

Note again how the symmetry of the lattices kills most of the terms in the expansion. In particular, since both reflection in the origin ($\xi \mapsto -\xi$) and rotation by $\pi/6$ ($re^{i\theta} \mapsto re^{i(\theta+\pi/6)}$) leave the lattice invariant, only terms with angular dependence $\cos(6k\theta)$ for some integer k , survive. Incidentally, the error term does have the correct decay rate, the term corresponding to r^{-10} vanishes.

Next we consider the **truss** model. Letting all links have axial stiffness 1 we get

$$\sigma(\xi) = \begin{bmatrix} 4 \sin^2 \frac{\xi_1}{2} + \sin^2 \frac{\xi_1 + \sqrt{3}\xi_2}{2} + \sin^2 \frac{\xi_1 - \sqrt{3}\xi_2}{2} & \sqrt{3} \left(\sin^2 \frac{\xi_1 + \sqrt{3}\xi_2}{2} - \sin^2 \frac{\xi_1 - \sqrt{3}\xi_2}{2} \right) \\ \sqrt{3} \left(\sin^2 \frac{\xi_1 + \sqrt{3}\xi_2}{2} - \sin^2 \frac{\xi_1 - \sqrt{3}\xi_2}{2} \right) & 3 \left(\sin^2 \frac{\xi_1 + \sqrt{3}\xi_2}{2} + \sin^2 \frac{\xi_1 - \sqrt{3}\xi_2}{2} \right) \end{bmatrix}.$$

This leads to the limit symbol

$$\sigma_0(\xi) = \frac{3}{8} \begin{bmatrix} 3\xi_1^2 + \xi_2^2 & 2\xi_1\xi_2 \\ 2\xi_1\xi_2 & \xi_1^2 + 3\xi_2^2 \end{bmatrix},$$

which corresponds to a 2D isotropic material with Poisson's ratio $1/3$ and Young's modulus $2/\sqrt{3}$ (the last number is obtained after taking the scaling by $\det T = \sqrt{3}/2$ into account).

The hexagonal lattice: The lattice is defined by

$$X(0,0) = \begin{bmatrix} 1 \\ 0 \end{bmatrix}, \quad X(0,1) = \begin{bmatrix} 1/2 \\ \sqrt{3}/2 \end{bmatrix}, \quad T = \begin{bmatrix} 3/2 & 0 \\ \sqrt{3}/2 & \sqrt{3} \end{bmatrix},$$

and

$$\mathbb{B} = \{(1, [0, -1], 2), (1, [0, 0], 2), (2, [-1, 1], 1)\}.$$

For the **conduction** problem we have

$$\sigma(\xi) = \begin{bmatrix} 3 & -1 - e^{\sqrt{3}\mathbf{i}\xi_2} - e^{-3\mathbf{i}\xi_1/2 + \sqrt{3}\mathbf{i}\xi_2/2} \\ -1 - e^{-\sqrt{3}\mathbf{i}\xi_2} - e^{3\mathbf{i}\xi_1/2 - \sqrt{3}\mathbf{i}\xi_2/2} & 3 \end{bmatrix},$$

which implies that

$$S^{(\varepsilon,0)}(\xi) = \frac{2}{3|\xi|^2} \begin{bmatrix} 1 & 1 + \varepsilon(-\mathbf{i}\xi_1/3 + \mathbf{i}\xi_2/\sqrt{3}) \\ 1 + \varepsilon(\mathbf{i}\xi_1/3 - \mathbf{i}\xi_2/\sqrt{3}) & 1 \end{bmatrix}$$

and, scaling by $\det T = 3\sqrt{3}/2$, we get the homogenized equations

$$\begin{cases} -(1/\sqrt{3})\Delta u_1^{(\varepsilon,0)} = (f_1 + f_2) + \varepsilon(-\partial_1/2 + \sqrt{3}\partial_2/2)f_2, \\ -(1/\sqrt{3})\Delta u_2^{(\varepsilon,0)} = (f_1 + f_2) + \varepsilon(\partial_1/2 - \sqrt{3}\partial_2/2)f_1. \end{cases}$$

In order to compute the lattice Green's function, we start with

$$\det \sigma(\xi) = 4 \sin^2(\sqrt{3}\xi_2) + 4 \sin^2 \frac{3\xi_1 + \sqrt{3}\xi_2}{2} + 4 \sin^2 \frac{3\xi_1 - \sqrt{3}\xi_2}{2}.$$

If we let σ_{tri} denote the symbol of the triangular lattice C, then $\det \sigma(\xi_1, \xi_2) = \sigma_{\text{tri}}((2\sqrt{3})\xi_2, (2\sqrt{3})\xi_1)$. In other words, the associated mono-atomic lattice for a honeycomb lattice, is a triangular lattice, one that is enlarged by a factor $2\sqrt{3}$ and rotated 90° compared to the lattice C. Thus, the asymptotic expansion of the Green's function for the honeycomb lattice follows directly from (B.3).

We will not consider **truss** problem in detail since it is degenerate but we want to mention that is so degenerate that $\det \sigma(\xi) \equiv 0$.

For the **frame** model, we endow all bars with axial stiffness 1 and bending stiffness γ . Then

$$\begin{aligned} \sigma_{\text{H}}^{(11)}(\xi) &= \frac{\sqrt{3}}{24} \begin{bmatrix} \frac{1}{1+\gamma}(4(1+3\gamma)\xi_1^2 + \gamma(9+\gamma)\xi_2^2) & (4-\gamma)\xi_1\xi_2 & 2\gamma\mathbf{i}\xi_2 \\ (4-\gamma)\xi_1\xi_2 & \frac{1}{1+\gamma}(\gamma(9+\gamma)\xi_1^2 + 4(1+3\gamma)\xi_2^2) & -2\gamma\mathbf{i}\xi_1 \\ -2\gamma\mathbf{i}\xi_2 & 2\gamma\mathbf{i}\xi_1 & 4\gamma \end{bmatrix}, \\ \sigma_{\text{H}}^{(12)}(\xi) &= \frac{\sqrt{3}}{24} \begin{bmatrix} \frac{1}{1+\gamma}(4(1+3\gamma)\xi_1^2 + 2\gamma(3-\gamma)\xi_2^2) & (4+2\gamma)\xi_1\xi_2 & -4\gamma\mathbf{i}\xi_2 \\ (4+2\gamma)\xi_1\xi_2 & \frac{1}{1+\gamma}(2\gamma(3-\gamma)\xi_1^2 + 4(1+3\gamma)\xi_2^2) & 4\gamma\mathbf{i}\xi_1 \\ 4\gamma\mathbf{i}\xi_2 & -4\gamma\mathbf{i}\xi_1 & -8\gamma \end{bmatrix}, \\ \sigma_{\text{H}}^{(22)}(\xi) &= \sigma_{\text{H}}^{(11)}(\xi). \end{aligned}$$

As stated in section 6, Ch. 3, we have $\sigma_{\text{H}}^{(11)} \neq \sigma_{\text{H}}^{(22)}$ and thus the lowest order homogenized equations form a 6×6 system of mixed second first and zero'th order differential operators.

The dominant behavior of this model is governed by the matrix σ_0 defined in Lemma 2.20,

$$\sigma_0(\xi) = \frac{3}{4(1+\gamma)} \begin{bmatrix} (1+3\gamma)\xi_1^2 + 2\gamma\xi_2^2 & (1+\gamma)\xi_1\xi_2 \\ (1+\gamma)\xi_1\xi_2 & 2\gamma\xi_1^2 + (1+3\gamma)\xi_2^2 \end{bmatrix}.$$

It is easily verified that σ_0 is the Schur complement of either $\sigma_H^{(11)}$ or $\sigma_H^{(12)}$. This matrix corresponds to the equations of two-dimensional (plane stress) elasticity with Young's modulus and Poisson's ratio given by

$$E' = \frac{6\gamma}{1+3\gamma}, \quad \nu = \frac{1-\gamma}{1+3\gamma}.$$

Recall that in order to get the constants for the homogenized material, the Young's modulus must be divided by $\det T = 3\sqrt{3}$, which gives

$$E = \frac{2}{\sqrt{3}} \frac{\gamma}{1+3\gamma}, \quad \nu = \frac{1-\gamma}{1+3\gamma}.$$

APPENDIX C

A derivation of the multipole expansion of a poly-harmonic function using Laurent series

In this appendix, we will show that in two dimensions, the multipole expansion of a poly-harmonic kernel can be derived using complex function methods. This method is not necessarily simpler than the derivation in Chapter 5 but it has the advantage that it yields direct expressions for the expansion functions. A different derivation of essentially the same expansion was given by Vekua [64] (English translation in [65]).

We start by reviewing how analytic function methods can be used to derive the multipole expansion of the harmonic kernel in two dimensions, $G_0(x - y) = -\log|x - y|$. Setting $z = x_1 + \mathbf{i}x_2$ and $w = y_1 + \mathbf{i}y_2$, we find that

$$G_0(x - y) = \operatorname{Re}[-\log(z - w)] = \operatorname{Re}[-\log z - \log(1 - w/z)] = \operatorname{Re} \left[-\log z + \sum_{q=1}^{\infty} w^q \frac{1}{q z^q} \right].$$

We note that in polar coordinates, $x = r(\cos \theta, \sin \theta)$, $y = \rho(\cos \alpha, \sin \alpha)$, we have

$$w^q = \rho^q (\cos(q\alpha) + \mathbf{i} \sin(q\alpha)), \quad z^{-q} = r^{-q} (\cos(q\theta) - \mathbf{i} \sin(q\theta)),$$

whence the familiar expansion in real basis functions easily follows.

We will next consider a kernel of the form

$$(C.1) \quad G_P(x) = c_0^{(0)} \log|x| + \sum_{p=1}^P g_p(x),$$

where g_p are rational functions with (exact) decay rate $|x|^{-2p}$ that satisfy $(-\Delta)^{p+1}g_p = 0$ away from the origin. Due to the poly-harmonicity, each function g_p has an Almansi expansion $g_p(x) = \sum_{m=0}^p |x|^{2m} \phi_m^{(p)}(x)$ for some harmonic functions $\phi_m^{(p)}$. Since g_p is a rational function with decay rate $|x|^{-2p}$, there must exist complex constants $\{c_m^{(p)}\}_{m=0}^p$ such that

$$(C.2) \quad g_p(x) = \operatorname{Re} \left[\sum_{m=0}^p c_m^{(p)} \frac{|z|^{2m}}{z^{2p+2m}} \right] = \operatorname{Re} \left[\sum_{m=0}^p c_m^{(p)} \frac{\bar{z}^m}{z^{2p+m}} \right].$$

Example: For the Green's function for the square lattice specified in 4.14 we have

$$\begin{aligned} G_2(x) &= -\frac{1}{2\pi} \log|x| + \frac{x_1^4 - 6x_1^2x_2^2 + x_2^4}{24\pi|x|^6} + \frac{43x_1^8 - 772x_1^6x_2^2 + 1570x_1^4x_2^4 - 772x_1^2x_2^6 + 43x_2^8}{480\pi|x|^{12}} \\ &= \operatorname{Re} \left[-\frac{1}{2\pi} \log z + \frac{1}{24\pi} \frac{\bar{z}}{z^3} + \frac{1}{480\pi} \left(\frac{18}{z^4} + \frac{25\bar{z}^2}{z^6} \right) \right]. \end{aligned}$$

Thus, $c_0^{(0)} = -1/(2\pi)$, $c_0^{(1)} = 0$, $c_1^{(1)} = 1/(24\pi)$, $c_0^{(2)} = 3/(80\pi)$, $c_1^{(2)} = 0$ and $c_2^{(2)} = 5/(96\pi)$. \square

We are now prepared to derive the multipole expansion of g_p . First rewrite (C.2),

$$(C.3) \quad g_p(x-y) = \operatorname{Re} \sum_{m=0}^p c_m^{(p)} \frac{(\bar{z} - \bar{w})^m}{z^{2p+m}} \frac{1}{(1-w/z)^{2p+m}}.$$

Next use the Taylor expansion

$$(1-t)^{-k} = \sum_{q=0}^{\infty} \binom{q+k-1}{q} t^q = \sum_{q=j}^{\infty} \binom{q-j+k-1}{q-j} t^{q-j},$$

which yields, when inserted into (C.3)

$$(C.4) \quad \begin{aligned} g_p(x) &= \operatorname{Re} \sum_{m=0}^p c_m^{(p)} \frac{1}{z^{2p+m}} \left[\sum_{j=0}^m \binom{m}{j} (-1)^j \bar{z}^{m-j} \bar{w}^j \right] \left[\sum_{q=j}^{\infty} \binom{2p+m+q-j-1}{q-j} \frac{w^{q-j}}{z^{q-j}} \right] \\ &= \operatorname{Re} \sum_{q=0}^{\infty} \sum_{j=0}^{\min\{q,p\}} w^{q-j} \bar{w}^j \left[\frac{(-1)^j}{z^{2p+q}} \sum_{k=0}^{p-j} c_{j+k}^{(p)} \binom{j+k}{j} \binom{2p+k+q-1}{q-j} \frac{\bar{z}^k}{z^k} \right]. \end{aligned}$$

Setting $h_{(q,j)}(w) := w^{q-j} \bar{w}^j$, $H_{(0,0)}(z) := G_P(z)$ and for $q \geq 1$, $0 \leq j \leq \min\{P, q\}$

$$H_{(q,j)}(z) = -\delta_{j,0} \frac{c_0^{(0)}}{qz^q} + \sum_{p=\max(1,j)}^P \frac{(-1)^j}{z^{2p+q}} \sum_{k=0}^{p-j} c_{j+k}^{(p)} \binom{j+k}{j} \binom{2p+k+q-1}{q-j} \frac{\bar{z}^k}{z^k},$$

we can write (C.4) compactly as

$$G(x-y) = \operatorname{Re} \sum_{q=0}^{\infty} \sum_{j=0}^{\min\{P,q\}} h_{(q,j)}(w) H_{(q,j)}(z).$$

This is an alternative representation of (5.11). The connection with the classical multipole expansion becomes clear once we note that, with $w = \rho e^{i\alpha}$,

$$h_{(q,j)}(w) = (\rho e^{i\alpha})^{q-j} (\rho e^{-i\alpha})^j = \rho^q [\cos((q-2j)\alpha) + i \sin((q-2j)\alpha)]$$

and that the functions $H_{(q,j)}$ can be rewritten in a similar fashion.

APPENDIX D

Numerical evaluation of the lattice Green's function

The lattice Green's function for a mono-atomic lattice in two dimensions is given by

$$\mathfrak{G}(m) = \frac{1}{(2\pi)^2} \int_{I^2} \frac{e^{-im \cdot \xi} - 1}{\sigma(\xi)} d\xi.$$

This integral is absolutely convergent and standard quadrature formulæ can be used to approximate it to arbitrary accuracy. However, the integrand is both oscillatory and, worse, discontinuous, at the origin, which slows down the convergence of the quadrature. In this appendix, we will show that using residue calculus, one integration can be carried out analytically. This simplifies the approximation dramatically. We will demonstrate the procedure for the, by now familiar, square lattice Green's function

$$(D.1) \quad \mathfrak{G}(m_1, m_2) = \frac{1}{(2\pi)^2} \int_{(-\pi, \pi)^2} \frac{e^{-i(m_1 \xi_1 + m_2 \xi_2)} - 1}{4 - e^{i\xi_1} - e^{-i\xi_1} - e^{i\xi_2} - e^{-i\xi_2}} d\xi.$$

It is conceptually simple to generalize the technique to arbitrary mono-atomic lattice, and then Theorem 4.6 can be invoked to treat fully arbitrary lattices. For a general lattice, the algebra will be far more involved, and the use of symbolic computation is recommended.

We prepare the integral (D.1) for application of the residue theorem by performing some straight-forward algebraic manipulations,

$$\begin{aligned} \mathfrak{G}(m_1, m_2) &= \frac{1}{(2\pi)^2} \int_{(-\pi, \pi)^2} \frac{e^{i\xi_2 m_2} (e^{i\xi_1})^{m_1} - 1}{(2 - e^{i\xi_1} - e^{-i\xi_1}) + (2 - e^{i\xi_2} - e^{-i\xi_2})} d\xi \\ &= \frac{1}{(2\pi)^2} \int_{(-\pi, \pi)^2} \frac{\cos(\xi_2 m_2) (e^{i\xi_1})^{m_1} - 1}{(2 - e^{i\xi_1} - e^{-i\xi_1}) + 2(1 - \cos(\xi_2))} d\xi \\ &= \frac{2}{(2\pi)^2} \int_0^\pi [\cos(m_2 \xi_2) f_{m_1}(1 - \cos \xi_2) - f_0(1 - \cos \xi_2)] d\xi, \end{aligned}$$

where

$$f_k(\alpha) = \int_{-\pi}^\pi \frac{(e^{it})^k}{(2 - e^{it} - e^{-it}) + 2\alpha} dt.$$

We rewrite this last integral as a contour integral around the unit circle S_1 in \mathbb{C} by setting $z = e^{it}$. Then, with $dt = dz/(iz)$,

$$f_k(\alpha) = \int_{S_1} \frac{z^k}{2 - z - z^{-1} + 2\alpha} \frac{dz}{iz} = \mathbf{i} \int_{S_1} \frac{z^k}{z^2 - 2(1 + \alpha)z + 1} dz.$$

Now, $z^2 - 2(1 + \alpha)z + 1 = (z - z_+)(z - z_-)$ where $z_{\pm} = 1 + \alpha \pm \sqrt{\alpha^2 + 2\alpha}$. In our case, $\alpha > 0$, so the only pole inside S_1 is z_- and we find that

$$f_k(\alpha) = (2\pi\mathbf{i})\mathbf{i} \frac{z_-^k}{z_- - z_+} = \pi \frac{(1 + \alpha - \sqrt{\alpha^2 + 2\alpha})^k}{\sqrt{\alpha^2 + 2\alpha}}.$$

Note that the function $f_k(1 - \cos \xi_2)$ blows up as $\xi_2 \rightarrow 0$ but that

$$\lim_{\xi_2 \rightarrow 0} [\cos(m_2 \xi_2) f_{m_1}(1 - \cos \xi_2) - f_0(1 - \cos \xi_2)] = -\pi m_1,$$

$$\lim_{\xi_2 \rightarrow 0^{\pm}} \frac{d}{d\xi_2} [\cos(m_2 \xi_2) f_{m_1}(1 - \cos \xi_2) - f_0(1 - \cos \xi_2)] = \pm \pi \frac{1}{2} (m_2^2 - m_1^2).$$

Thus, $\mathfrak{G}(m_1, m_2)$ can be evaluated as a one-dimensional quadrature of a regular integrand.

APPENDIX E

Notes on Chapter 7

1. Derivation of the second dispersion equation in section 1.2

First consider a vibrating string, characterized by its length l and intrinsic velocity v , attached to two supports with the displacements $e^{i\omega t}u^I$ and $e^{i\omega t}u^{II}$ so that its displacement w satisfies the equation

$$\begin{aligned} w''(x) + \frac{\omega^2}{v^2}w(x) &= 0, & x \in (0, l), \\ w(0) &= u^I, & w(l) = u^{II}. \end{aligned}$$

If $\sin \frac{\omega l}{v} \neq 0$, then the solution is

$$w(x) = u^I \cos \frac{\omega x}{v} + \frac{u^{II} - u^I \cos \frac{\omega l}{v}}{\sin \frac{\omega l}{v}} \sin \frac{\omega x}{v},$$

and thus the dynamic force the string exerts at $x = 0$ equals

$$-F \frac{dw}{dx} \Big|_{x=0} = F \frac{\omega}{v} \frac{1}{\sin \frac{\omega l}{v}} \left(u^I \cos \frac{\omega l}{v} - u^{II} \right).$$

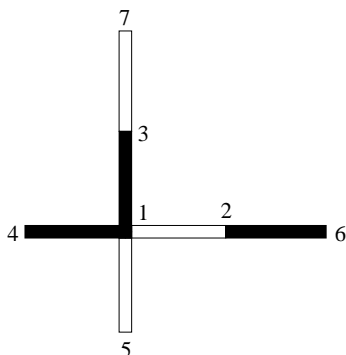


FIGURE E.1. Labeling used in Appendix 1. The white strings have wavespeed v , the black αv . The numbers refer to the nodes.

Applying the formula above to the system shown in Figure E.1 (which is a part of the big lattice shown in Figure 7.5) we get the three equilibrium equations

$$(E.1) \quad \begin{aligned} 0 &= F \frac{\omega}{2v} \frac{1}{\sin \frac{\omega l}{2v}} \left(u^{(1)} \cos \frac{\omega l}{2v} - u^{(2)} \right) + F \frac{\omega}{2\alpha v} \frac{1}{\sin \frac{\omega l}{2\alpha v}} \left(u^{(1)} \cos \frac{\omega l}{2\alpha v} - u^{(3)} \right) \\ &\quad + F \frac{\omega}{2\alpha v} \frac{1}{\sin \frac{\omega l}{2\alpha v}} \left(u^{(1)} \cos \frac{\omega l}{2\alpha v} - u^{(4)} \right) + F \frac{\omega}{2v} \frac{1}{\sin \frac{\omega l}{2v}} \left(u^{(1)} \cos \frac{\omega l}{2v} - u^{(5)} \right), \\ 0 &= F \frac{\omega}{2v} \frac{1}{\sin \frac{\omega l}{2v}} \left(u^{(2)} \cos \frac{\omega l}{2v} - u^{(1)} \right) + F \frac{\omega}{2\alpha v} \frac{1}{\sin \frac{\omega l}{2\alpha v}} \left(u^{(2)} \cos \frac{\omega l}{2\alpha v} - u^{(6)} \right) \\ 0 &= F \frac{\omega}{2\alpha v} \frac{1}{\sin \frac{\omega l}{2\alpha v}} \left(u^{(3)} \cos \frac{\omega l}{2\alpha v} - u^{(1)} \right) + F \frac{\omega}{2v} \frac{1}{\sin \frac{\omega l}{2v}} \left(u^{(3)} \cos \frac{\omega l}{2v} - u^{(7)} \right). \end{aligned}$$

We set

$$c_1 = \cos \frac{\omega l}{2v}, \quad s_1 = \sin \frac{\omega l}{2v}, \quad c_2 = \cos \frac{\omega l}{2\alpha v}, \quad s_2 = \sin \frac{\omega l}{2\alpha v},$$

and apply quasi-periodicity,

$$u^{(4)} = e^{ik_1 l} u^{(2)}, \quad u^{(5)} = e^{ik_2 l} u^{(3)}, \quad u^{(6)} = e^{-ik_1 l} u^{(1)}, \quad u^{(7)} = e^{-ik_2 l} u^{(1)},$$

to reduce the system (E.1) to

$$\begin{bmatrix} 0 \\ 0 \\ 0 \end{bmatrix} = \begin{bmatrix} \frac{2c_1}{s_1} + \frac{2c_2}{\alpha s_2} & -\frac{1}{s_1} - \frac{e^{ik_1 l}}{\alpha s_2} & -\frac{1}{\alpha s_2} - \frac{e^{ik_2 l}}{s_1} \\ -\frac{1}{s_1} - \frac{e^{-ik_1 l}}{\alpha s_2} & \frac{c_1}{s_1} + \frac{c_2}{\alpha s_2} & 0 \\ -\frac{1}{\alpha s_2} - \frac{e^{-ik_2 l}}{s_1} & 0 & \frac{c_1}{s_1} + \frac{c_2}{\alpha s_2} \end{bmatrix} \begin{bmatrix} u^{(1)} \\ u^{(2)} \\ u^{(3)} \end{bmatrix}.$$

The left hand side of the dispersion equation (1.2) is now simply the determinant of the matrix in the system above.

2. Derivation of the stiffness matrix for a square framed structure

In equation (3.10) we provided the stiffness matrix for a beam oriented along the x_1 -axis, with end-points 1 and 2 to the left and right of the beam, respectively. In the structure illustrated in Figure 7.10 there are beams of cross-sectional areas s_1 and s_2 , and with moments of inertia I_1 and I_2 . We fix a reference area s and define non-dimensional lattice variables \bar{u} and \bar{f} by

$$\begin{aligned} \bar{u}_j &= \frac{1}{l} u_j, & \bar{f}_j &= \frac{1}{sE} f_j, & j &= 1, 2, \\ \bar{u}_3 &= u_{\text{rot}}, & \bar{f}_3 &= \frac{1}{sEl} M. \end{aligned}$$

Then equilibrium for a beam of type j reads

$$\begin{bmatrix} \bar{f}_1^1 \\ \bar{f}_2^1 \\ \bar{f}_3^1 \end{bmatrix} = \underbrace{\begin{bmatrix} c_j & 0 & 0 \\ 0 & d_j & \frac{1}{2}d_j \\ 0 & \frac{1}{2}d_j & \frac{1}{3}d_j \end{bmatrix}}_{=:A_j^{0^\circ}} \begin{bmatrix} \bar{u}_1^1 \\ \bar{u}_2^1 \\ \bar{u}_3^1 \end{bmatrix} + \underbrace{\begin{bmatrix} c_j & 0 & 0 \\ 0 & -d_j & \frac{1}{2}d_j \\ 0 & -\frac{1}{2}d_j & \frac{1}{6}d_j \end{bmatrix}}_{=:B_j^{0^\circ}} \begin{bmatrix} \bar{u}_1^2 \\ \bar{u}_2^2 \\ \bar{u}_3^2 \end{bmatrix}, \quad \text{where } c_j = \frac{s_j}{s}, \quad d_j = \frac{12I_j}{sl^2}.$$

Note that if there had been bars of different lengths in the lattice one would have had to fix a reference length l to use in the non-dimensionalization.

The stiffness matrix for a bar with axial stiffness c_j and bending stiffness d_j , rotated ϕ degrees anti-clockwise from the x_1 -axis is given by

$$A_j^\phi = U^\phi A_j^{0^\circ} (U^\phi)^\text{T}, \quad B_j^\phi = U^\phi B_j^{0^\circ} (U^\phi)^\text{T}, \quad \text{where } U^\phi = \begin{bmatrix} \cos \phi & -\sin \phi & 0 \\ \sin \phi & \cos \phi & 0 \\ 0 & 0 & 1 \end{bmatrix}.$$

We are now in a position to write the equations of motion for the harmonically oscilling square bi-atomic lattice,

$$\begin{aligned} \bar{\omega}^2 \bar{M}_1 \bar{u}^{(n,1)} &= \left[A_1^{0^\circ} \bar{u}^{(n,1)} + B_1^{0^\circ} \bar{u}^{(n,2)} \right] + \left[A_1^{90^\circ} \bar{u}^{(n,1)} + B_1^{90^\circ} \bar{u}^{(n-e_1+e_2,2)} \right] \\ &\quad + \left[A_2^{180^\circ} \bar{u}^{(n,1)} + B_2^{180^\circ} \bar{u}^{(n-e_1,2)} \right] + \left[A_2^{270^\circ} \bar{u}^{(n,1)} + B_2^{270^\circ} \bar{u}^{(n-e_2,2)} \right], \\ \bar{\omega}^2 \bar{M}_2 \bar{u}^{(n,2)} &= \left[A_2^{0^\circ} \bar{u}^{(n,2)} + B_2^{0^\circ} \bar{u}^{(n+e_1,1)} \right] + \left[A_2^{90^\circ} \bar{u}^{(n,2)} + B_2^{90^\circ} \bar{u}^{(n+e_2,1)} \right] \\ &\quad + \left[A_1^{180^\circ} \bar{u}^{(n,2)} + B_1^{180^\circ} \bar{u}^{(n,1)} \right] + \left[A_1^{270^\circ} \bar{u}^{(n,2)} + B_1^{270^\circ} \bar{u}^{(n+e_1-e_2,1)} \right], \end{aligned}$$

where $\bar{M}_\kappa = \text{diag}\{m_\kappa/(\rho l s), m_\kappa/(\rho l s), J_\kappa/(\rho s l^3)\}$ and $\bar{\omega} = \omega l / \sqrt{E/\rho}$. Applying quasi-periodicity, $u^{(n+m,\kappa)} = e^{i\mathbf{k}\cdot T m} u^{(n,\kappa)}$, we obtain

$$\begin{aligned} \bar{\omega}^2 \bar{M}_1 \bar{u}^{(n,1)} &= \left[A_1^{0^\circ} + A_1^{90^\circ} + A_2^{180^\circ} + A_2^{270^\circ} \right] \bar{u}^{(n,1)} \\ &\quad + \left[B_1^{0^\circ} + e^{-i(lk_1-lk_2)} B_1^{90^\circ} + e^{-2ilk_1} B_2^{270^\circ} + e^{-i(lk_1+lk_2)} B_2^{270^\circ} \right] \bar{u}^{(n,2)}, \\ \bar{\omega}^2 \bar{M}_2 \bar{u}^{(n,2)} &= \left[A_2^{0^\circ} + A_2^{90^\circ} + A_1^{180^\circ} + A_1^{270^\circ} \right] \bar{u}^{(n,2)} \\ &\quad + \left[e^{2ilk_1} B_2^{0^\circ} + e^{-i(lk_1+lk_2)} B_2^{90^\circ} + B_1^{270^\circ} + e^{i(lk_1-lk_2)} B_1^{270^\circ} \right] \bar{u}^{(n,1)}. \end{aligned}$$

Setting $\bar{M} = \text{diag}\{\bar{M}_1, \bar{M}_2\}$ we obtain the equation

$$\sigma(k) \bar{u}^{(n)} = \bar{\omega}^2 \bar{M} \bar{u}^{(n)},$$

where the diagonal blocks of the 6×6 matrix $\sigma(k)$ are given by

$$\begin{aligned} \sigma_{11}(k) &= \begin{bmatrix} c_1 + c_2 + d_1 + d_2 & 0 & \frac{1}{2}(d_2 - d_1) \\ 0 & c_1 + c_2 + d_1 + d_2 & \frac{1}{2}(d_1 - d_2) \\ \frac{1}{2}(d_2 - d_1) & \frac{1}{2}(d_1 - d_2) & \frac{2}{3}(d_1 + d_2) \end{bmatrix}, \\ \sigma_{22}(k) &= \begin{bmatrix} c_1 + c_2 + d_1 + d_2 & 0 & \frac{1}{2}(d_1 - d_2) \\ 0 & c_1 + c_2 + d_1 + d_2 & \frac{1}{2}(d_2 - d_1) \\ \frac{1}{2}(d_1 - d_2) & \frac{1}{2}(d_2 - d_1) & \frac{2}{3}(d_1 + d_2) \end{bmatrix}, \end{aligned}$$

and the off-diagonal elements are given by

$$\begin{aligned}
 (\text{E.2}) \quad [\sigma_{12}(k)]_{11} &= -c_1 - c_2 e^{2ik_1 l} - d_1 e^{i(k_1 l - k_2 l)} - d_2 e^{i(k_1 l + k_2 l)}, \\
 [\sigma_{12}(k)]_{13} &= -\frac{1}{2} d_1 e^{i(k_1 l - k_2 l)} + \frac{1}{2} d_2 e^{i(k_1 l + k_2 l)}, \\
 [\sigma_{12}(k)]_{22} &= -c_1 e^{i(k_1 l - k_2 l)} - c_2 e^{i(k_1 l + k_2 l)} - d_1 - d_2 e^{2ik_1 l}, \\
 [\sigma_{12}(k)]_{23} &= \frac{1}{2} d_1 - \frac{1}{2} d_2 e^{2ik_1 l}, \\
 [\sigma_{12}(k)]_{31} &= \frac{1}{2} d_1 e^{i(k_1 l - k_2 l)} - \frac{1}{2} d_2 e^{i(k_1 l + k_2 l)}, \\
 [\sigma_{12}(k)]_{32} &= -\frac{1}{2} d_1 + \frac{1}{2} d_2 e^{2ik_1 l}, \\
 [\sigma_{12}(k)]_{33} &= \frac{1}{6} d_1 (1 + e^{i(k_1 l - k_2 l)}) + \frac{1}{6} d_2 (e^{2ik_1 l} + e^{i(k_1 l - k_2 l)}).
 \end{aligned}$$

Note that $\sigma_{21}(k) = \sigma_{12}(k)^*$.

In the main text, all variables are considered non-dimensionalized and the bars used in this Appendix to denote such variables have been omitted.

Bibliography

- [1] Ulf Andersson, Björn Engquist, Gunnar Ledfelt, and Olof Runborg, *A contribution to wavelet-based subgrid modeling*, Appl. Comput. Harmon. Anal. **7** (1999), no. 2, 151–164. MR **2000f**:65130
- [2] Kendall Atkinson and Weimin Han, *Theoretical numerical analysis*, Springer-Verlag, New York, 2001, A functional analysis framework. MR **2002a**:65001
- [3] Amir Averbuch, Gregory Beylkin, Ronald Coifman, and Moshe Israeli, *Multiscale inversion of elliptic operators*, Signal and image representation in combined spaces, Academic Press, San Diego, CA, 1998, pp. 341–359. MR **99a**:65162
- [4] I. Babuška, *Approximation by Hill functions*, Comment. Math. Univ. Carolinae **11** (1970), 787–811. MR 45 #1396
- [5] I. Babuška and R. C. Morgan, *Composites with a periodic structure: mathematical analysis and numerical treatment*, Comput. Math. Appl. **11** (1985), no. 10, 995–1005. MR **87b**:73040
- [6] Alain Bensoussan, Jacques-Louis Lions, and George Papanicolaou, *Asymptotic analysis for periodic structures*, North-Holland Publishing Co., Amsterdam, 1978. MR **82h**:35001
- [7] G. Beylkin, R. Coifman, and V. Rokhlin, *Wavelets in numerical analysis*, Wavelets and their applications, Jones and Bartlett, Boston, MA, 1992, pp. 181–210. MR **93j**:65215
- [8] Gregory Beylkin, *Wavelets and fast numerical algorithms*, Different perspectives on wavelets (San Antonio, TX, 1993), Amer. Math. Soc., Providence, RI, 1993, pp. 89–117. MR **95a**:65220
- [9] Éric Bonnetier, *Plane stress elasto-plastic constitutive equations obtained by homogenizing one-dimensional structures*, RAIRO Modél. Math. Anal. Numér. **29** (1995), no. 1, 23–52. MR **96d**:73005
- [10] M. E. Brewster and G. Beylkin, *A multiresolution strategy for numerical homogenization*, Appl. Comput. Harmon. Anal. **2** (1995), no. 4, 327–349. MR **96h**:65156
- [11] L. Brillouin, *Wave propagation in periodic structures. second edition*, Dover Publications, 1953.
- [12] G. Brown, M.A. Novotny, and P.A. Rokvold, *Micromagnetic simulations of thermally activated magnetization reversal of nanoscale magnets*, J. App. Ph. **87** (2000), 4792–4794.
- [13] Doina Cioranescu and Jeannine Saint Jean Paulin, *Homogenization of reticulated structures*, Springer-Verlag, New York, 1999. MR **2000d**:74064
- [14] R. Courant, K. Friedrichs, and H. Lewy, *Über die partiellen differenzgleichungen der mathematischen physik*, Mathematische Annalen **100** (1928), 32–74.
- [15] J. Cserti, *Application of the lattice Green's function for calculating the resistance of an infinite network of resistors*, Am. J. Phys. **68** (2000), no. 10, 896–906.
- [16] V.S. Deshpande, N.A. Fleck, and M.F. Ashby, *Effective properties of the octet truss material*, Tech. report, Cambridge university engineering department, 2000.
- [17] Mihai Dorobantu and Björn Engquist, *Wavelet-based numerical homogenization*, SIAM J. Numer. Anal. **35** (1998), no. 2, 540–559 (electronic). MR **99a**:65183
- [18] J.P. Dowling, H. Everitt, and E. Yablonovitch, *Photonic and sonic band-gap bibliography*, 2000, <http://home.earthlink.net/jpdowling/pbgbib.html>.
- [19] R. J. Duffin, *Discrete potential theory*, Duke Math. J. **20** (1953), 233–251. MR 16,1119d
- [20] R. J. Duffin and E. P. Shelly, *Difference equations of polyharmonic type*, Duke Math. J. **25** (1958), 209–238. MR 20 #5374
- [21] E.N. Economou, *Green's functions in quantum physics*, Springer, Berlin, 1983.
- [22] A.G. Evans, J.W. Hutchinson, and M.F. Ashby, *Multifunctionality of cellular metal systems*, Progress in Materials Science **43(3)** (1998), 171–221.

- [23] J. Fidler and T. Schrefl, *Micromagnetic modelling — the current state of the art*, J. Phys. D **33** (2000), R135–R156.
- [24] George Fix and Gilbert Strang, *Fourier analysis of the finite element method in Ritz-Galerkin theory.*, Studies in Appl. Math. **48** (1969), 265–273. MR 41 #2944
- [25] ———, *A Fourier analysis of the finite element variational method*, Constructive Aspects of Functional Analysis, Edizioni Cremonese, Rome, 1973, pp. 795–840.
- [26] Y. Fu, J. R. Overfelt, and G. J. Rodin, *Fast summation methods and integral equations*, Mathematical aspects of boundary element methods (Palaiseau, 1998), Chapman & Hall/CRC, Boca Raton, FL, 2000, pp. 128–139. MR 1 719 860
- [27] L.J. Gibson and M.F. Ashby, *Cellular solids, structure and properties*, Pergamon Press, Exeter, 1989.
- [28] A. Gilbert, *Multiresolution homogenization schemes for differential equations and applications*, Ph.D. thesis, Princeton, Dept. of Mathematics, 1997.
- [29] M. L. Glasser and J. Boersma, *Exact values for the cubic lattice Green functions*, J. Phys. A **33** (2000), no. 28, 5017–5023. MR 2001i:82022
- [30] M. Grah, K. Alzabedeh, P.Y. Sheng, M.D. Vaudin, K.J. Bowman, and M. Ostojca-Starzewski, *Brittle intergranular failure in 2d microstructures: experiments and computer simulations*, Acta Mater. **44** (1996), no. 10, 4003–4018.
- [31] Leslie Greengard, *The rapid evaluation of potential fields in particle systems*, MIT Press, Cambridge, MA, 1988. MR 89k:31008
- [32] Leslie Greengard and Vladimir Rokhlin, *A new version of the fast multipole method for the Laplace equation in three dimensions*, Acta numerica, 1997, Cambridge Univ. Press, Cambridge, 1997, pp. 229–269. MR 99c:65012
- [33] Wolfgang Hackbusch, *Integral equations*, Birkhäuser Verlag, Basel, 1995, Theory and numerical treatment, Translated and revised by the author from the 1989 German original. MR 96h:45001
- [34] Johan Helsing and Gunnar Peters, *Integral equation methods and numerical solutions of crack and inclusion problems in planar elastostatics*, SIAM J. Appl. Math. **59** (1999), no. 3, 965–982 (electronic). MR 99j:73114
- [35] Thomas Y. Hou, Xiao-Hui Wu, and Zhiqiang Cai, *Convergence of a multiscale finite element method for elliptic problems with rapidly oscillating coefficients*, Math. Comp. **68** (1999), no. 227, 913–943. MR 99i:65126
- [36] A. Hrennikoff, *Solution of problems of elasticity by the frame-work method*, ASME J. Appl. Mech. **8** (1941), A619–A715.
- [37] G. S. Joyce, *On the simple cubic lattice Green function*, Philos. Trans. Roy. Soc. London Ser. A **273** (1973), no. 1236, 583–610. MR 58 #28708
- [38] ———, *On the cubic lattice Green functions*, Proc. Roy. Soc. London Ser. A **445** (1994), no. 1924, 463–477. MR 95j:33041
- [39] ———, *Singular behaviour of the cubic lattice Green functions and associated integrals*, J. Phys. A **34** (2001), no. 18, 3831–3839. MR 1 840 848
- [40] C. Kittel, *Introduction to solid state physics. seventh edition.*, Wiley & Sons., 1996.
- [41] Ognyan Kounchev, *Multivariate polysplines: applications to numerical and wavelet analysis*, Academic Press Inc., San Diego, CA, 2001. MR 1 852 149
- [42] A. A. Maradudin, E. W. Montroll, G. H. Weiss, Robert Herman, and H. W. Milnes, *Green's functions for monatomic simple cubic lattices*, Acad. Roy. Belg. Cl. Sci. Mém. Coll. in-4 deg. (2) **14** (1960), no. 7, 176. MR 22 #7440
- [43] W.H. McCrea and F.J.W. Whipple, *Random paths in two and three dimensions*, Proc. Royal Soc. Edin. **60** (1939), 281–298.
- [44] D. McHenry, *A lattice analogy for the solution of plane stress problems*, J. Inst. Civ. Eng. **21** (1943), 59–82.
- [45] William McLean, *Strongly elliptic systems and boundary integral equations*, Cambridge University Press, Cambridge, 2000. MR 2001a:35051
- [46] R. C. Morgan and I. Babuška, *An approach for constructing families of homogenized equations for periodic media. I. An integral representation and its consequences*, SIAM J. Math. Anal. **22** (1991), no. 1, 1–15. MR 91k:35034
- [47] ———, *An approach for constructing families of homogenized equations for periodic media. II. Properties of the kernel*, SIAM J. Math. Anal. **22** (1991), no. 1, 16–33. MR 92b:35025
- [48] R.C. Morgan, *Mathematical aspects and computational considerations in the theory of homogenization*, Ph.D. thesis, University of Maryland, College Park, 1982.

- [49] A.B. Movchan, V.V. ZalipaeV, and N.V. Movchan, *Photonic band gaps for fields in continuous and lattice structures*, IUTAM Symposium on Analytical and Computational Fracture Mechanics of Non-Homogenous Materials, Cardiff, June 2001. *To appear*, 2002.
- [50] A.K. Noor, *Continuum modelling for repetitive lattice structures*, Appl. Mech. Rev. **41** (1988), no. 7, 285–296.
- [51] J.T. Oden and K. Vemaganti, *Estimation of local modeling error and goal-oriented adaptive modeling of heterogeneous materials; part i : Error estimates and adaptive algorithms*, J. Comp. Ph. **164** (2000), 22–47.
- [52] M. Ostoja-Starzewski, *Lattice models in micromechanics*, Appl. Mech. Rev. **55** (2002), no. 1, 35–60.
- [53] H.B. Phillips and N. Wiener, *Nets and the dirichlet problem*, J. of Mathematics and Physics **2** (1923), 105–124.
- [54] C.G. Poulton, A.B. Movchan, McPhedran R.C., N.A. Nicorovici, and Y.A. Antipov, *Eigenvalue problems for doubly periodic structures and phononic band gaps*, Proc. Roy. Soc. Lond. A **457** (2000), 2561 – 2568.
- [55] J.S. Przemieniecki, *Theory of matrix structural analysis*, Dover, 1985.
- [56] V. Rokhlin, *Rapid solution of integral equations of classical potential theory*, J. Comput. Phys. **60** (1985), no. 2, 187–207. MR **86k**:65120
- [57] E. Sánchez-Palencia, *Homogenization method for the study of composite media*, Asymptotic analysis, II, Springer, Berlin, 1983, pp. 192–214. MR **84m**:73060
- [58] E.N. Sigalas, M.M. & Economou, *Elastic and acoustic wave band structure*, J. Sound and Vibration **158** (1992), 377 – 382.
- [59] M.M. Sigalas and E.N. Economou, *Elastic waves in plates with periodically place inclusions*, J. Appl. Phys. **75** (1994), 2845 – 2850.
- [60] ———, *Attenuation of multiple-scattered sound*, Europhysics Let. **36** (1996), 241 – 246.
- [61] S.L. Sobolev, *Partial differential equations of mathematical physics*, Pergamon Press, Oxford, 1964.
- [62] M. Thompson and M. Renault, *Evaluation of structural porous metals*, Tech. report, United Technologies - Research Center, 1997.
- [63] S.P. Timoshenko, *History of strength of materials*, McGraw-Hill, New York, 1953.
- [64] I. N. Vekua, *Novye metody rešeniya èlliptičeskikh uravneniĭ*, OGIZ, Moscow-Leningrad, 1948. MR 11,598a
- [65] ———, *New methods for solving elliptic equations*, North-Holland Publishing Co., Amsterdam, 1967, North-Holland Series in Applied Mathematics and Mechanics, Vol. 1. MR 35 #3243
- [66] Michael Vogelius, *A homogenization result for planar, polygonal networks*, RAIRO Modél. Math. Anal. Numér. **25** (1991), no. 4, 483–514. MR **92j**:94027
- [67] J.C. Wallach and L.J. Gibson, *Mechanical behaviour of three-dimensional truss structures*, Tech. report, Department of Materials Science and Engineering, MIT, 2000.
- [68] G.N. Watson, *Three triple integrals*, Quart. J. Math. (Oxford Ser.) **10** (1939), 266–276.
- [69] N. Wicks and J.W. Hutchinson, *Optimal truss plates*, Tech. report, Div. of Eng. and Appl. Science, Harvard University, 2000.

Vita

Per-Gunnar J. Martinsson was born in Göteborg, Sweden on August 17, 1972, the son of Inger and Thomas Martinsson. After completing studies in the engineering program at the Älvekulle-gymnasiet (senior high school) in 1991, he served for fifteen months as a cipher analyst in the Swedish military intelligence service. Between August 1992 and December 1995 he earned a *Civilingenjörs examen* in Engineering Physics from the Chalmers' University of Technology and prepared a thesis entitled "Separation of Variables Techniques in Particle Simulations and Integral Equations" under the supervision of William McLean. During 1995 he was enrolled at the University of New South Wales in Sydney where he pursued studies in applied mathematics and freediving. Upon completion of his engineering studies he was employed as a research associate in the department of mathematics at the University of South Carolina in Columbia.

In September 1996 he returned to Sweden and spent the next two years earning a *Licentiat examen* in mathematics at the Chalmers University of Technology. Under the supervision of Vidar Thomée he prepared a thesis entitled "Discretisation of Certain Evolution Equations with Memory using Convolution Quadrature".

He entered the graduate school of the University of Texas at Austin in August 1998. Upon completion of his doctoral studies in computational and applied mathematics in August 2002, he will assume a Gibbs instructorship in the mathematics department at Yale university.

This thesis was typed by the author using AMS-LaTeX.

The author can be reached either at the following address, *Department of Mathematics, Yale University, 10 Hillhouse Ave, New Haven CT 06520-8283*, or by electronic mail at pgmartinsson@yahoo.com.